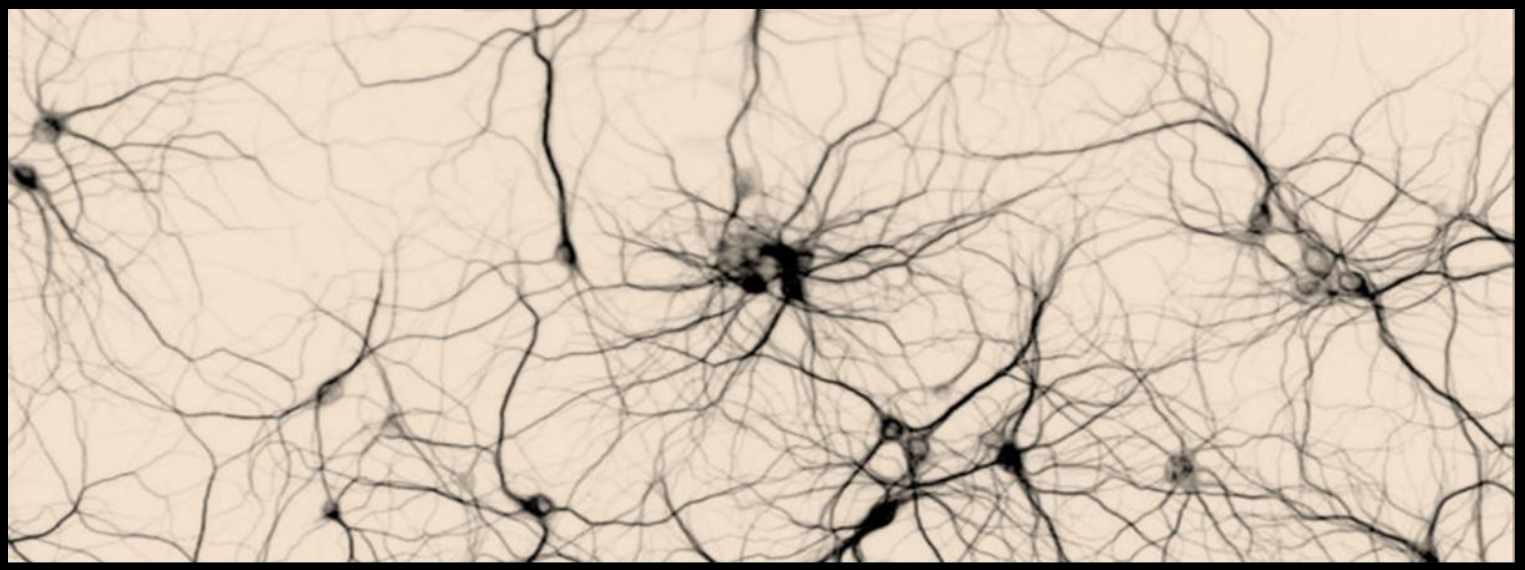

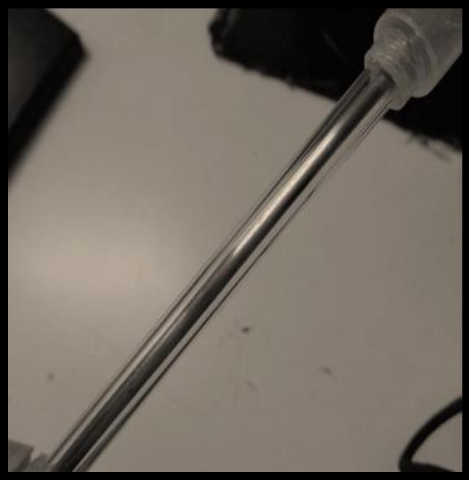

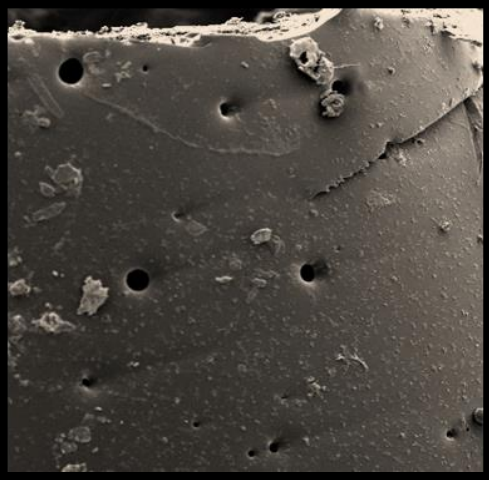

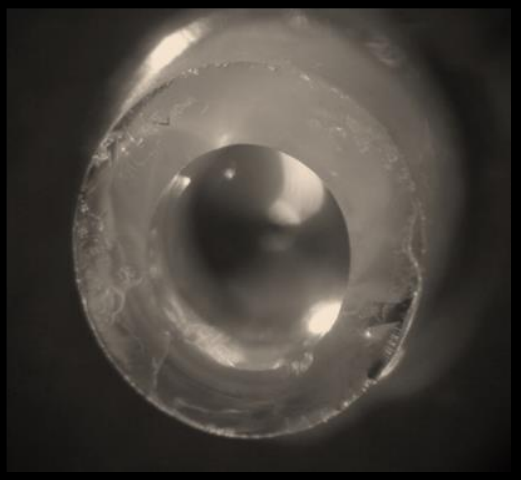

Ana Catarina da Silva Pinho

Peripheral Nerve Regeneration – Development and Evaluation of Biodegradable Polymers guide-tube

Doctoral thesis of the Doctoral Program on Advanced Materials and Processing, supervised by Professor Doctor Jorge Coelho, Professor Doctor José Domingos Santos and Professor Doctor Arménio Serra and submitted to the Department of Mechanical Engineering of the Faculty of Science and Technology of the University of Coimbra

January, 2018

· U C ·

Universidade de Coimbra

Ana Catarina da Silva Pinho

Peripheral nerve regeneration – development and evaluation of biodegradable polymers guide-tube

Thesis submitted to Faculty of Sciences and Technology, University of Coimbra to obtain the Degree of Doctor in Advanced Materials and Processing - AdvaMTech.

Coimbra

2018

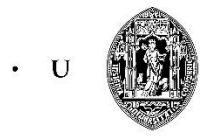

UNIVERSIDADE DE COIMBRA

Financial Support:

Ao António, à Margarida, ao Nuno e ao Eduardo…

“The mind that opens to a new idea never returns to its original size.”

Albert Einstein

ACKNOWLEDGMENTS

À Fundação para a Ciência e Tecnologia (FCT) no âmbito do programa doutoral em Materiais e Processamento Avançados (AdvaMTech), pela bolsa de doutoramento PD/BD/52626/2014.

Aos meus orientadores científicos, Professor Jorge Coelho, Professor José Domingos Santos e ao Doutor Arménio Serra, pela confiança e toda a partilha de conhecimento durante a realização deste trabalho. As vossas linhas orientadoras foram cruciais em todos os estágios deste projeto. Muito obrigada pela vossa disponibilidade e contribuição para o alcance dos objetivos a que nos propusemos com este trabalho.

À Doutora Ana Fonseca pela ajuda preciosa em todo este percurso. Obrigada por teres estado sempre lá para mim, desde o início, a partilhar o teu conhecimento comigo, mesmo quando a descrição de uma reação química era confusa. A tua calma e capacidade de trabalho são inspiradores! Estarei sempre eternamente grata pela tua paciência e carinho.

À Doutora Ana Colette Maurício por em ter aberto as portas do seu laboratório no ICBAS. Estou muito grata por me ter disponibilizado todos os meios necessários às análises biológicas deste trabalho, por me ter apresentado à sua equipa e me ter feito sentir em "casa" nas minhas excursões ao Porto. Mais importante ainda, estou muito grata por toda a disponibilidade para mim e para o meu trabalho. Muito obrigada Professora!

Ao Doutor Amílcar pela disponibilidade e realização dos testes mecânicos.

À Doutora Teresa Vieira pela excelente escola que me proporcionou. Aprendi e aprendo constantemente consigo. O meu respeito por si é enorme e sinto-me muito grata por todas as lições (não só académicas) que me ensinou.

À Doutora Paula Piedade pela realização das micrografias de SEM e não só. Muito obrigada por todo o conhecimento que partilhou comigo, por me ter ensinado a "pensar" e por ter influenciado tão positivamente o meu percurso académico. Se cheguei até aqui, a si lho devo. Agradeço também o seu inesgotável ombro amigo e por acreditar em mim, mesmo nos meus momentos de maior descrença! A sua amizade e carinho fazem de si uma espécie de "segunda mãe" para mim em Coimbra.

À Rita, Sílvia, Irina e Rui o meu muitíssimo obrigada pela realização dos testes de citotoxicidade, biocompatibilidade e avaliação funcional após neurotmese do nervo ciático do rato. Enfim, por me terem ajudado com tudo o que era biológico. Obrigada pela vossa paciência e enorme disponibilidade. Repito, a vocês, o meu muito obrigada!

Ao Engenheiro António Fonseca pela amizade e pelas intermináveis horas no SEM.

A todo o grupo de Materiais Poliméricos por toda a ajuda e amizade. Aos que riram comigo, se frustraram comigo e se desesperaram comigo, o meu muito obrigada. A vossa marca está muito presente neste percurso e neste trabalho.

À malta do costume, àqueles que estão sempre para mim e fazem parte da minha vida há tantos anos que já é difícil contar. Vocês sempre foram e continuam a ser os maiores! Um beijinho muito especial também às minhas meninas da Estudantina Feminina de Coimbra, por todo o convívio, preocupação, e importante trabalho de descompressão! A nós um FRÁ gigante!

Aos meus pais, António e Margarida por tudo. Não só por me terem concedido as condições necessárias à minha formação, bem como por acreditarem em mim e alinharem nas minhas "ideias". Muito obrigada por tudo o que me ensinaram e me ensinam todos os dias e por tudo e tudo e tudo.

Ao Nuno por ser o irmão mais velho mais fixe de sempre. A ti que acreditas mais em mim do que eu própria muito obrigada por teres feito de mim uma pessoa mais competitiva e metódica e claro, por todo o resto.

Por fim, querida agradecer ao Eduardo, por tudo e mais alguma coisa. Seria impossível enumerar tudo o que tens feito não só em prol deste trabalho, mas também em tudo o resto. Muito obrigada por teres estado sempre lá, paciente, e por me lembrares todos os dias do que era capaz. Tu és o maior e o melhor. Obrigada Lalo.

A todos vós o meu muitíssimo OBRIGADA!

ABSTRACT

The main goal of this PhD work was the development and evaluation of novel nerve guide conduits based on biocompatible and biodegradable polymers for regenerative medicine, namely peripheral nerve regeneration.

The injury of the peripheral nerves are a quite common, especially in the young male population due to accidental traumatic events. The degree of injury may vary, being the most severe cases associated with permanent disability. Since the last century, new strategies to improve peripheral nerve regeneration after injury have been studied. The first technique proposed and still nowadays showing the best results is the use of nerve autograph. Nevertheless, this technique is associated to some disadvantages, which include the need of two surgeries and site morbidity. In this sense, nerve guide conduits, which consist in hollow tubes that are sutured to both nerve ends have been proposed as alternative. These conduits should guide the newly formed axons to the opposite nerve stump while providing a suitable environment for the enhancement of axon regeneration. Among several materials tested for the preparation of these devices, polymers have presented the most promising results. However, a device, which could reproduce results comparable to nerve autograph with suitable degradation ratio *in vivo* remains to be developed.

In an attempt to overcome these limitations, the present work involved the use of the polysaccharide dextran as core material in the preparation of nerve guide conduits. The choice of this polymer relies on its well stablished biocompatibility and biodegradability. In addition, dextran is frequently reported for biomedical applications, being approved by the US Food and Drug Administration (FDA).

The initial work undertaken aimed to modify the chemical structure of dextran by the incorporation of double bonds in its chains, for further crosslinking. In this sense, dextrans with different molecular weights were modified with two different monomers, Glycidyl methacrylate (GMA) and 2-Isocyanatoethyl methacrylate (IEMA). Circular transparent membranes were prepared by ultraviolet (UV)-photocrosslinking and the physico-chemical characteristics of the resulting products were evaluated. After the washing and drying stages, the final membranes presented a fragile structure. For this reason, a poly (ε-

caprolactone) (PCL) macromonomer modified with IEMA was added to the membrane formulations. As a result, the flexibility of the membranes increased considerably. Additionally, the incorporation of PCL_IEMA did not affect the thermal-mechanical properties. On the other hand, the swelling capacity and *in vitro* degradation ratio decreased.

The work continued with the evaluation of the cytotoxicity of the most promising membranes, using human dental pulp stem cells (hDPSCs). The intracellular concentration of the calcium ion was also measured after the cell viability test. All membranes were considered suitable substrates for cell adhesion and proliferation based on their morphology and healthy calcium ion concentration, suggesting the absence of any apoptosis process. Considering the promising results obtained, the next step focused on the evaluation of the extension of immune response due to implantation of the membranes in rats dorsum. After 15 days of implantation, membranes prepared with dextran modified with GMA and PCL derivative caused an immune response that was classified as "*non-irritant*", by the scoring system of the standard ISO 10-998-6.

After the relevant results obtained for the prepared materials in a membrane shape, the next step of the work was to achieve the tube conformation. In this regard, molds composed by a quartz tube with an internal 316L stainless steel rod, and with different dimensions were prepared. In order to tailor the final dimensions of the prepared tubes, shrinkage studies were conducted. The formulation, which presented the final dimensions more similar to the commercial product Neurolac®, was then chosen for the further characterization. The structures revealed to be very compact, showing no porosity. For this reason, in order to enhance permeability, D-mannitol was added to the formulations, as porogenic agent, to create voids in the structure of the tubes. The obtained pores presented a mean size in the range between 10-20μm. Posteriorly, the physico-chemical properties of the normal tube and porous tube were evaluated. With the incorporation of D-mannitol, the swelling capacity of the tubes decreased, which may be related to a lower crosslinking density. Moreover, for the porous structure, the *in vitro* degradation ratio increased, as expected, since the contact surface area also increases. Furthermore, after six months under *in vitro* hydrolytic tests, both tube structures were able to maintain their structural integrity. The mechanical properties of the tubes were evaluated by performing tensile tests, which revealed that both tubes have the ability to support tension and elongation forces slightly

higher than the ones reported for the rat sciatic nerve. It is noteworthy to state that the tubes also were able to resist to preliminary suture tests without visible fragmentation.

Finally, nerve guide conduits were tested in the rat sciatic nerve after a neurotmesis injury, for 20 weeks. The functional evaluation results showed that the recovery percentage of motor function is similar for both tubes. In what concerns the sensorial function, the rat group, which received the porous tube revealed higher percentage of recovery. In this sense, porosity seems to induce a positive effect on nerve regeneration.

To sum up, this PhD work allowed the validation of dextran as core material for the preparation of nerve guide conduits for peripheral nerve regeneration. The obtained materials present a set of characteristics and properties, which may be relevant for the regeneration process. Furthermore, the fine-tuning of these properties can be easily achieved by changing the formulations used to prepare the tubes.

RESUMO

O principal objetivo deste trabalho de doutoramento consistiu no desenvolvimento e avaliação de novos tubos guia preparados a partir polímeros biocompatíveis e biodegradáveis, com aplicação em medicina regenerativa, nomeadamente regeneração de nervos do sistema nervoso periférico.

As lesões de nervo periférico são bastante comuns, sendo que as principais causas de incidência desta patologia estão associadas à população jovem masculina, por ocorrência de eventos traumáticos acidentais. A severidade destas lesões varia bastante, no entanto, nos casos mais graves, pode mesmo resultar em incapacidade nervosa permanente. Por este motivo, ao longo do último século têm sido estudadas novas formas de melhorar a regeneração de nervo periférico após uma lesão. A utilização da técnica do autoenxerto revelou ser apresenta resultados mais satisfatórios, provando melhorar a qualidade do nervo regenerado. Contudo, esta técnica implica o recurso a duas cirurgias. Na perspetiva de evitar esta desvantagem, surge o conceito de tubo guia que consiste num tubo oco cuja principal função é fornecer um meio adequado à regeneração do novo nervo guiando o seu crescimento até à extremidade oposta. Nos últimos anos vários materiais têm sido utilizados na preparação destes dispositivos, sendo os materiais poliméricos aqueles que melhores resultados produziram. Porém, ainda não foi desenvolvida uma solução comparável à técnica de autoenxerto com um tempo de degradação *in vivo* que acompanhe o crescimento do nervo.

No sentido de dar resposta a estas limitações, este trabalho envolve a utilização do polissacarídeo dextrano para a preparação de tubos guia. Este polímero foi escolhido como material base devido à sua biocompatibilidade e biodegradabilidade. Com efeito, o dextrano é recorrentemente reportado para aplicações biomédicas, sendo aprovado pela "*US Food and Drug Administration*" (FDA).

Numa fase inicial do trabalho pretendeu-se modificar a estrutura química do dextrano, através da incorporação de ligações duplas nas suas cadeias, para posterior reticulação. Assim, dextrano de pesos moleculares diferentes foi modificado com dois monómeros diferentes, metacrilato de glicidilo (GMA) e metacrilato de 2-isocianoetilo (IEMA). Seguidamente, membranas circulares transparentes foram preparadas através da reticulação

das cadeias dos materiais preparados, por radiação ultravioleta (UV). As suas características físico-químicas foram posteriormente avaliadas. Devido à fragilidade demonstrada por estas membranas, foi adicionado às formulações iniciais um macro monómero de base poli (ε-caprolactona) (PCL) modificado com IEMA. Como resultado, as membranas preparadas com dextrano modificado juntamente com o co monómero revelaram maior flexibilidade comparativamente às membranas previamente preparadas. Com a incorporação deste macro monómero verificou-se uma diminuição na capacidade de inchaço e da velocidade de degradação *in vitro*, não prejudicando, contudo, as propriedades térmo-mecânicas das membranas.

O trabalho prosseguiu com a avaliação da citotoxicidade das membranas que apresentaram propriedades mais apropriadas para a aplicação em questão, com recurso a células da polpa dentária humana (hDPSC). A concentração do ião cálcio intracelular foi medida para atestar a viabilidade celular das células aderidas às membranas. Todas as membranas mostraram ser substratos apropriados para a adesão e proliferação celular, sugerindo a ausência de início do processo apoptótico. Seguidamente foi avaliada a extensão da reação imunológica provocada pela implantação subcutânea destas membranas no dorso de ratos. Neste caso, as membranas preparadas com dextrano modificado com GMA, e com a adição de PCL modificado com IEMA provocaram uma resposta imunológica, ao fim de 15 dias, que foi classificada de "não irritante", através do sistema de pontuação proposto pela norma ISO 10-998-6.

Face aos resultados relevantes, a etapa seguinte do trabalho consistiu na preparação de um tubo, utilizando as melhoras formulações de membranas. Neste sentido, foi preparado um molde de quartzo com uma vara de aço inoxidável 316L por forma a criar tubos ocos. Os moldes foram preparados com vista à obtenção de dimensões finais semelhantes às do produto comercial Neurolac®. Foram conduzidos estudos para avaliar o encolhimento das estruturas tubulares, permitindo assim a escolha da formulação mais adequada. Através de microscopia electrónica de varrimento (SEM) foi possível avaliação a superfície dos tubos, que se revelou ser bastante compacta. Neste sentido, foi adicionado D-Mannitol como agente porogénico, de modo que aumentar a permeabilidade dos tubos, por meio de indução de porosidade. Com recurso a esta técnica foi possível obter porosidade com tamanho médio compreendido entre 10-20µm. Posteriormente foi feito um estudo comparativo das propriedades físico-químicas do tubo sem porosidade e com porosidade. Com a introdução

do D-mannitol, a capacidade de inchamento dos tubos diminuiu, o que pode denotar uma estrutura com menor densidade de reticulação. No entanto, com a porosidade, a velocidade de degradação dos tubos aumentou, como seria de esperar, visto que a superfície de contacto com o meio também é superior. Contudo, ao fim de seis meses, em solução de PBS os dois tubos mantiveram a sua integridade estrutural. As propriedades mecânicas destes tubos foram também avaliadas através de ensaios de tração uniaxial. Estes testes revelaram que os tubos têm capacidade de resistir a forças de tensão e elongação ligeiramente superiores às do nervo ciático de rato. De notar que estes tubos revelaram ser resistentes a testes preliminares de perfuração com sutura, sem fragmentação visível.

Finalmente, os tubos guia foram testados em nervos ciáticos de ratos, após uma lesão de neurotmese induzida. Ao longo de 20 semanas os resultados da avaliação funcional do nervo lesionado mostram que em termos de função motora, a recuperação é semelhante para o tubo não poroso e para o tubo poroso. No que concerne a função sensorial, o grupo de ratos que recebeu o tubo poroso mostrou maior índice de recuperação. Assim, a porosidade aparenta ter um efeito positivo na regeneração do nervo.

Este trabalho permitiu validar o dextrano como material base para a preparação de tubos-guia para a regeneração de nervo periférico. Os materiais obtidos apresentam um conjunto de características e propriedades relevantes para o processo regenerativo. Com efeito, estas podem ainda ser facilmente adaptadas através da alteração das formulações utilizadas para preparar os tubos.

LIST OF PUBLICATIONS

Published papers:

Pinho, A. C.; Fonseca, A. C.; Serra, A. C.; Santos, J. D.; Coelho, J. F. F., Peripheral Nerve Regeneration: Current Status and New Strategies Using Polymeric Materials. *Advanced Healthcare Materials* **2016**, 5 (21), 2732-2744. DOI: 10.1002/adhm.201600236 (Chapter 1).

Papers in preparation:

Pinho, A.C.; Fonseca, A. C.; Caseiro, A. R.; Maurício, A. C.; Serra, A. C.; Santos, J. D.; Coelho, J. F. J., Preparation and Evaluation of novel dextran based materials for regenerative medicine. (Chapter 2).

Pinho, A.C.; Fonseca, A. C.; Caseiro, A. R.; Amorim, I.; Maurício, A. C.; Serra, A. C.; Santos, J. D.; Coelho, J. F. J., *In vitro* and *in vivo* testing of dextran based membranes for regenerative medicine. (Chapter 3).

Pinho, A. C.; Fonseca, A. C.; Serra, A. C.; Santos, J. D.; Coelho, J. F. J, Preparation and characterization of dextran based nerve guide conduits for peripheral nerve regeneration. (Chapter 4).

Pinho, A.C.; Fonseca, A. C.; Caseiro, A. R.; Pedrosa, S. S.; Alvites, R. D.; Maurício, A. C.; Serra, A. C.; Santos, J. D.; Coelho, J. F. J., Novel dextran-based tube-guides for the regeneration of the rat sciatic nerve after neurotmesis injury. (Chapter 5).

THESIS OUTLINE

The main goal of this PhD work was the preparation, development and evaluation of novel biocompatible and biodegradable nerve guide conduits for peripheral nerve regeneration. The adopted approach relies on the use of dextran as core material due to its excellent biocompatibility characteristics. Dextran derivatives were photocrosslinked in a tube shape originating a material with suitable mechanical properties. The PhD thesis is organized in six chapters:

- Chapter 1 presents an overview on the nervous system and its divisions, with special attention to peripheral nervous system. The nerve degeneration after lesion and regeneration process are also described. Furthermore, a state of the art concerning the techniques used for enhancement of peripheral nerve regeneration are also described, with special focus on the nerve guide conduits prepared with polymeric materials.

- Chapter 2 describes the chemical modifications performed in dextran and PCL structure and the main physico-chemical characteristics of the resulting materials. In addition, the preparation and characterization of membranes using several formulations of these materials by UV-photocrosslinking was carried out. The influence of the ratio of precursors on the final properties of the membranes is discussed.

- Chapter 3 presents the *in vitro* essays performed in the membranes that showed the most promising characteristics. The subsequent part of this chapter is dedicated to the description and discussion of the results obtained by preliminary *in vivo* tests, consisting on the implantation of the membranes in the subcutaneous tissue of rats.

- Chapter 4 discusses the fabrication of tubes starting using the best formulations developed in chapter 3. Different tubes were prepared with different molds until the desired dimensions are achieved. The influence of the porogenic agent addition in the final properties of the tubes were evaluated.

- Chapter 5 reports the *in vivo* tests performed using a neurotmesis of the sciatic nerve model in rats. The regeneration of the nerve was assessed through the evaluation of the mobility of the rats.

- Chapter 6 presents the most relevant conclusions from this PhD research, along with further recommendations on future work.

LIST OF ACRONYMS

AM: acetoxymethyl

ANOVA: analysis of variance

CNS: central nervous system

DMAP: dimethylaminopyridine

DMSO: dimethyl sulfoxide

DMTA: differential mechanical thermal analysis

DPSCs: human dental pulp stem cells

DSC: differential scanning calorimetry

EDS: energy dispersive spectrometry

EPT: extensor postural thrust

ePTFE: expanded poly(tetrafluorethylene)

FBS: fetal bovine serum

FDA: US food and drug administration

FGF: fibroblast growth factor

G: α-L-guluronic acid

GDNF: glial cell-derived neurotrophic factor

GGF: glial growth factor

GMA: glycidyl methacrylate

H&E: hematoxylin-eosin

hMSCs: human mesenchymal stem cells

ICBAS-UP: institute of biomedical science Abel Salazar, University of Porto

IEMA: 2-Isocyanoethylmethacrylate

ISO: international organization of standardization

M: β-D-mannuronic acid

MSCs: mesenchymal stem cells

MWCNT: multi-wall carbon nanotubes

NGC: nerve guide conduits

NGF: nerve growth factor

NVP: N-vinylpyrrolidone

OECD: organization for economic co-operation and development

P(DLLA-*co*-CL): poly(D,L-lactic acid-*co*-ε-caprolactone)

PBS: phosphate buffered saline

PCL: poly(caprolactone)

PDLA: poly(D-lactic acid)

PDLLA: poly(D,L-lactic acid)

PGA: poly(glycolic acid)

PHB: poly-3-hydroxbutyrate

PHBV: poly(3-hydroxybutyrate-*co*-hydroxyvalerate)

PLA: poly(lactic acid)

PLGA: poly(lactic acid-*co*-glycolic acid)

PNS: peripheral nervous system

Ppy: polypyrrole

PVA: poly(vinyl alcohol)

RGD: arginine-glycine-aspartate

SD: standard deviation

SEM: scanning electron microscopy

SEM: standard error mean

SFI: sciatic functional index

SIS: small intestine submucosa

SSI: static sciatic index

TEA: triethylamine

TGA: thermogravimetric analysis

THF: tetrahydrofuran

UV: ultraviolet

WRL: withdrawal reflex latency

NOMENCLATURE

T_c: crystallization temperature, ºC

T_g: glass transition temperature, ºC

T_m: melting temperature, ºC

T_{on}: temperature of onset, ºC

$T_{5\%}$: Temperature to which corresponds 5% of weight loss, ºC

$T_{10\%}$: Temperature to which corresponds 10% of weight loss, ºC

T_p: peak temperature, ºC

T_α: α transition, ºC

CONTENTS

LIST OF FIGURES

LIST OF TABLES

MOTIVATION AND OBJECTIVES

Peripheral nerve injuries may cause severe impairment in the quality of life of patients since it can cause a permanent disability. Usually, young adults compose the population where a major incidence of this problem can be observed. This fact derives from the most common causes of this problem, which are related to industrial accidents, motor vehicle accidents, tumor damage, side effects of neurosurgery and even viral infections. It is also important to refer that 60% of the patients that suffer from peripheral nerve injury have also traumatic brain injury. In this sense, the degeneration and regeneration of the nerve processes have been subject of study over the past century.

The peripheral nerve system has the ability to regenerate by itself. However, the recovery of nerve function is often suboptimal, especially in the cases of motor nerves. For this reason, it is well established that the regeneration process may benefit from surgical intervention. For small gaps, (<10mm) direct repair, consisting in the suturing of both nerve stumps, revealed to be sufficient for achieving satisfying results. On the other hand, for longer gaps, this technique may cause extensive tension between the nerve stumps, which may jeopardize the regeneration process. In these cases, nerve autograph and allograph were proposed as standard technique to connect nerve stumps. Nevertheless, the application of these techniques has many disadvantages and limitations including among others, site morbidity and need of immunosuppression treatments.

To overcome these limitations, the tubulization technique has been developed. The concept behind this technique relies on the use of a hollow tube (nerve guide conduit), which could be sutured to both nerve stumps. This tube should provide a guide path for newly grown axons reestablishing the nerve connection more efficiently.

Several materials have been proposed for the preparation of such biomedical devices. Due to the possibility of tailoring their properties, polymeric materials have received special attention. However, limitations concerning the degradation ratio, release of acidic degradation products and ability to maintain the structural integrity due to unsuitable mechanical properties are still observed. In an attempt to overcome these limitations, recent approaches report the combination of natural and synthetic polymers with stem cells and growth factors. Yet, an economic solution with the ability to regenerate larger gaps with suitable degradation ratio and mechanical properties was still not reported.

In this sense, this PhD work looks towards the development of novel biocompatible and biodegradable dextran based hollow tubes prepared by a UV-photocrosslinking technique that could be suitable for regenerative medicine applications, namely, peripheral nerve regeneration.

Chapter 1. **REVIEW OF LITERATURE**

1.1 ABSTRACT

Since the end of the XIX century, experiments concerning peripheral nerve regeneration have been reported. The need to implement an effective surgical procedure in terms of functional recovery resulted in the appearance of several approaches to solve this problem. Nerve autograft was the first studied approach and is still considered the "gold standard". Since autografts require donor harvesting, other strategies involving the use of natural materials have been studied. Nevertheless, the results were not very encouraging and attention has moved towards the use of nerve conduits made from polymers, whose properties can be easily tailor made. Also, the polymer based nerve conduits can be easily processed in a variety of shapes and forms. Some of these materials are already approved by Food and Drug Administration (FDA). Very recently, polymers with electro conductive properties have been subject of intensive study in this field since it is believed that such properties have a positive influence in the regeneration of the new axons. This chapter intends to give a global view of the mechanisms involved in peripheral nerve regeneration and the main strategies used to recover motor and sensorial function of injured nerves.

1.2 INTRODUCTION

Peripheral nerve injuries represent a common disability around the world.[1] Indeed, annually more than one million people suffer from this kind of injury, being 300,000 of these cases only in Europe.[2]

Injuries in the peripheral nervous system can result from working accidents, motor vehicle accidents, tumor damage, side effects of neurosurgery and even viral infections.[1,3] For this reason, the development of suitable methods to properly regenerate these injuries is mandatory and represents a worldwide social need.

For the last 100 years, examples of degeneration and regeneration of the nervous system have been described in literature.[4] However, during the first 40 years of investigation, the regeneration process was not completely known. During that period, nerve autografts and allografts were the standard techniques used to treat the transected nerves. Unfortunately, these techniques present several disadvantages, being the worst ones related to high morbidity and the need of immunosuppression treatments. Since the peripheral nervous system has the ability of regeneration, new approaches using nerve guide tubes, also known

as nerve guide conduits (NGC), have been studied. A NGC can be defined as a tube that is sutured or fixed to the two stumps of the injured nerve and provides an adequate environment for the nerve regeneration.

Nowadays, it is well established that nerve conduits have a key role in guiding axon migration, maintaining the nerve growth factors in the space between distal and proximal stumps, and preventing the wound healing space from being invaded by scar tissue and cells that could compromise the nerve recovery process.[5]

Nerve conduits made of several kinds of materials have been tested throughout the years. Among such materials, natural and synthetic polymers have been the most used and several nerve conduits based polymers are already commercially available.

1.3 NERVOUS SYSTEM

The nervous system controls the fast activities of the body as contraction of the skeletal muscles, contraction of the smooth muscles of the internal organs, secretion of exocrine and endocrine glands, visceral events and even secretion of some endocrine glandules.[6] It receives literally millions of signals sent from the different sensorial organs and then integrates them, in order to determine the proper answer that should be given by the body. Structurally, the nervous system is divided in two parts: central nervous system (CNS) which is composed by the brain and spinal cord, and the peripheral nervous system (PNS) composed by cranial, spinal, and autonomic nerves that connect to the CNS.[7,8] The main function of the PNS is to establish the connection between the CNS and the environment. CNS and PNS are composed by two types of cells: neurons or nerve cells and supporting cells, which are called neuroglia, or simply, glia.[9] The main function of the neurons is related to electrical signaling, while glia cells are involved in the development of the adult brain.[9] The glial cells of the CNS are astrocytes, microglia, and oligodendrocytes[10]. In the case of PNS, its glial cells are known as Schwann cells.[11]

1.3.1 Neuron

The functional unit cell of the nervous system is called neuron, as aforementioned, and it is estimated that an adult has around 100 billion of these cells. Briefly, the main function of the neuron is to transmit nervous pulses, which are modifications of electric or chemical energy.

Neurons are composed by three components: cell body or soma, dendrites and axon, which are represented in Figure 1.1.

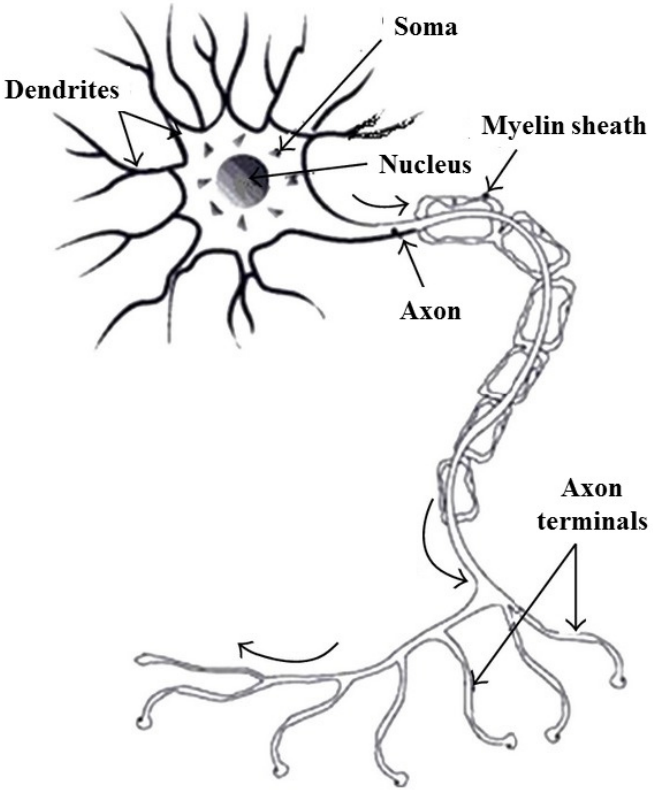

Figure 1.1 Structure of a typical neuron. The direction of the impulse is represented by the curve arrows. (adapted)[12]

Inside of the cell body there is the cellular nucleus that contains all the genetic material of the cell. The cell body also present extensions called dendrites. Their function is to receive chemical messages from other neurons and transmit them to the cell body. Finally, the axon, that usually represents the longer extension that comes from the cell body, transmits an electro-chemical signal to other neurons. This signal is going to be converted into a chemical message at the end of the axon and then travel to the next neuron. The direction

of the transmitted signals is always made from the dendrite to the axon and never from the axon to the dendrite. Some axons are also covered by a myelin sheath, which provides a faster transmittance of the signals.[7]

According to their function, neurons can be classified in three different categories: sensory, motor and interneurons. The sensory neurons are responsible for collecting stimuli from the exterior and transmit them to the spinal cord and brain. The motor neurons transmit the information from the central nervous system to muscle cells in order to answer to the previous stimuli. The interneurons are the ones that interpret the stimuli collected by sensory neurons and elaborate a proper reaction to be transmitted to motor neurons.[7]

1.4 PERIPHERAL NERVOUS SYSTEM

In PNS, the neuron cell bodies accumulate forming structures called ganglia. On the other hand, the axons derived from those cell bodies are organized differently. Firstly, some neuron axons are surrounded by the glial cells of PNS, known as Schwann cells.[9] These cells are responsible for the formation of a structure based on concentric layers around the axons, named myelin sheath (Figure 1.1). The function of this layer is to increase the speed of propagation of an impulse along the axon.[13] Also, it prevents the electrical current to leave the axon. The segments of myelin sheath are called internodes. In turn, the connection points between internodes are called nodes of Ranvier.[14]
The system formed by the axon, myelin sheath and the surround Schwann cells is called a nerve fiber.

1.4.1 Structure of the Peripheric Nerve

Apart from the myelin sheath and Schwann cells, nerve fibers are surrounded by more layers of tissue. Together, all these tissues form a structure which is called nerve. Figure 1.2 presents the structure of a nerve.

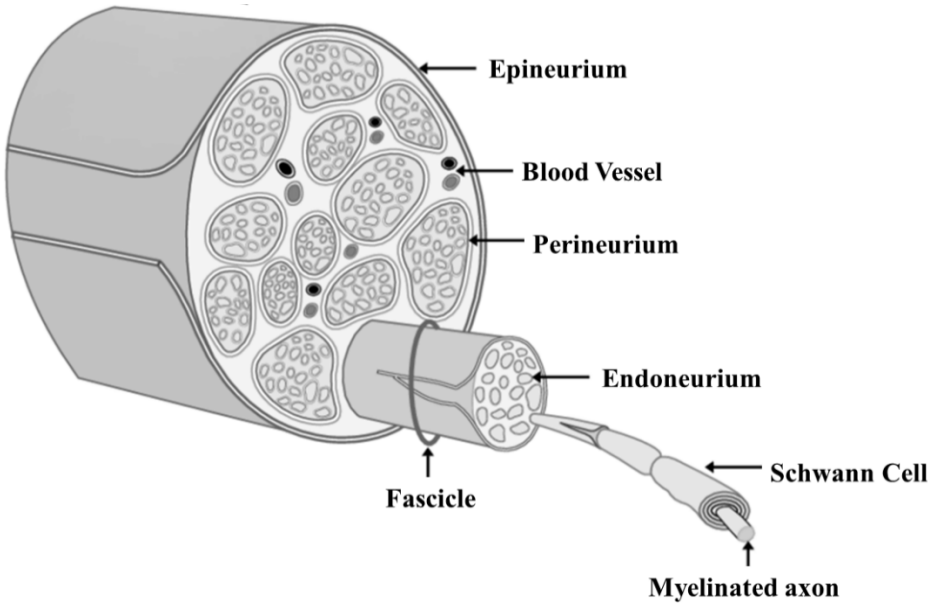

Figure 1.2 Structure of a nerve.[15] (Adapted)

As observed on Figure 1.2, the endoneurium is the tissue that surrounds the nerve fiber. This tissue is formed by Type III collagen and fibroblasts.[16]

Then, nerve fibers gather in different dimensions, number and pattern forming groups (fascicles). These fascicles are delimited by the perineurium, a fibroblasts based layer, which functions as a protective diffusion barrier against the passage of macromolecules.[17]

All these structures, including blood vessels, are finally hold by an external fibrous layer called epineurium. This tissue wraps all nerve and is constituted by Type I collagen and fibroblasts.[18]

1.4.2 Peripheric Nerve Classification

Based on their function, peripheric nerves can be classified as sensory (afferent) and motor (efferent). Briefly, sensory nerves transport information from the environment and internal organs towards the brain and spinal cord.[19] In turn, the motor nerves transport the information from the brain and spinal cord towards the related organs and muscles. Furthermore, there are mixed nerves which contain both types of nerve fibers.[16]

1.4.3 Peripheric Nerve Degeneration and Regeneration

After an injury, axons derived by CNS and from peripheral PNS have different behavior. The regeneration of CNS system is much more limited than the PNS and can affect functions such as cognition, memory, voluntary movement and language.[8] This fact is related to the nature of the axons of these systems, because while the axons from PNS can re-extend and re-innervate its extremities, a lesion to the CNS results in the formation of extensive scar tissue at the lesion site inhibiting the regeneration.[20,21]

After a peripheral nerve injury, a series of cellular and molecular events occurring in the distal portion of the injured nerve are triggered.[22] These events are called Wallerian degeneration, and were described, for the first time, by August Waller in 1850.[23]
Briefly, the myelin sheath is degraded and several axon ends are sealed which results in the disintegration of neurofilaments and microtubes, being the regeneration process activated.[24,25] Also, the metabolism of proteins is altered resulting in the increasing of production of regenerative materials while the production of neurotransmitters decreases. After 48 hours, the myelin sheath is reduced to a short segment. In the following days, macrophages and monocytes are recruited to the site of the injury to begin the removal of myelin and axon debris by phagocytosis. During these processes, Schwann cell proliferation is stimulated. These cells start forming structures with a tube shape, bands of Büngner, in order to provide guidance for axon regeneration. SCs produce extracellular matrix molecules and neurotrophic factors that have a positive influence in the sprouting of new axons from the proximal portion of injured nerves. These new axons usually arise at the terminal nodes of Ranvier and the remyelination process also performed by SCs starts.[24,25] Although the regeneration of PNS axons, fully recovery of the function is very unusual and unsatisfactory, especially for large gaps.

1.4.4 Classification of PNS injuries

As aforementioned, when an injury of the peripheral nervous system occurs, a sequence of events called Wallerian degeneration is triggered leading to a sequence of events towards nerve regeneration. Although peripheral nervous system (PNS) axons can be fully regenerated, the recovery of the function is very unusual and unsatisfactory, especially for large gaps. Due to this fact, microsurgical techniques were introduced by Millesi in the 1960s in order to improve the healing of this kind of injuries.[26] The first attempts consisted

on simply suture the nerve stumps (neurorhaphy). However, excessive tension between the two stumps can be harmful[27], leading to unsatisfactory results, as functional recovery could not be achieved. Therefore, a total understanding of the nerve topography of motor and sensory neurons as well as the type of injuries and their consequences was urgently needed.[28]

It is also important to stress that some factors as the elapsed time, patient age, associated soft tissue or vascular injuries and proximity of the lesion to distal targets directly influence the recovery and regeneration of a nerve injury.[29]

Currently, to classify PNS injuries there are two different models: Seddon and Sunderland.[30,31] The description of each approach is described in Table 1.1.

Table 1.1 Classification of PNS injuries by Seddon and Sunderland (adapted)[1,28,30,31]

Seddon classification	Sunderland classification	Pathology	Prognosis
Neurapraxia	**First degree**	No axon loss	Spontaneous recovery time between hours up to a few months
Axonotmesis	**Second degree**	Axon loss	Spontaneous recovery can be achieved without surgery depending on the distance to muscle
	Third degree	2nd degree + Disruption of the endoneurial tubes	Spontaneous recovery is poor due to axonal misdirection. Surgical intervention may be required
	Fourth degree	3rd degree + Disruption of the perineurium	Spontaneous recovery is worse than 3rd degree. Surgery is more often required.
Neurotmesis	**Fifth degree**	Entire nerve disruption. Connective tissue components of the nerve severed.	Recovery depends on surgical intervention

In the most severe cases, as shown in Table 1.1, surgery is needed for the reconstruction of the nerve. Many approaches have appeared, being nerve autographing the most popular. Briefly, nerve autographing consists in harvesting a nerve segment from another site in the body to gather the stumps of the injured nerve. However, nerve autographing presents several disadvantages such as tissue availability, differences in tissue size and structure, and donor site morbidity.[32] In order to overcome these disadvantages, the NGC approach has started to be used.

1.5 IDEAL NERVE GUIDE CONDUIT PROPERTIES

In 1882, a NGC was successfully tested for the first time in a dog nerve gap with 30mm, bridged by a hollow bone tube.[33] Since then, many attempts to produce the ideal NGC have been reported and some of them were used in clinical trials in humans. The concept behind the NGC is to create a tubular structure that could bridge the two sections of the previously injured axon, providing guidance for the new axons and protect them from the scarred tissue that is formed within just a few days.[34] The main aim of this strategy is to increase the probability of axon regeneration as well as their length and growth speed. Nowadays, it is believed that NGC should be capable of providing mechanical support for the new fibers, guide the regenerated axons from the proximal to distal nerve stump, avoid scarred tissue infiltration and behave like a channel that allows the diffusion of neurotropic and neurotrophic factors secreted by the nerve stumps.[35] Basically, these structures should provide an adequate microenvironment for nerve regeneration. Figure 1.3 represents the steps that occur when regeneration of a nerve includes a tube guide.

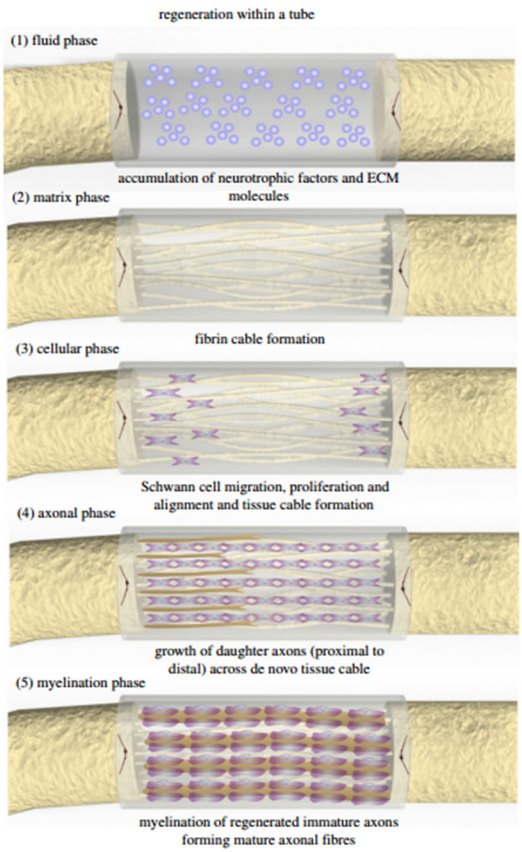

Figure 1.3 Nerve regeneration within a hollow NGC. Reproduced with permission.[36] Copyright 2012, The Royal Society.

Among the advantages of these 3D structures, in comparison to the old method of suturing the two stumps, is the possibility of stressing the reduction in neuroma, scar formation and collateral sprouting of the new axons.[36] Furthermore, as the neurotrophic factors secreted by the stumps become trapped inside the conduit, an accumulation occurs resulting in a higher concentration of such molecules that favor nerve regeneration. Their ability to provide a pathway for the new fibers to achieve the distal stump makes them a suitable choice for the regeneration of the nerve and recovery of its functionality.

Regarding the main properties that these devices must have, the most important are: biocompatibility, biodegradability, permeability, biomechanical properties, surface properties, custom dimension and interaction with neurotrophic factors.[37-40]

The biocompatibility of NGC is evaluated considering three aspects: blood compatibility, histocompatibility and mechanical compatibility. The first one requires that blood should not undergo hemolysis or damage of its components that could result in coagulation and formation of thrombus, when in contact with the NGC. The second aspect demands that no toxic side effects should arise from the device that could contaminate surrounding tissue. The last one concerns the mechanical properties of the NGC that should match the same properties of nerve tissue.[41]

As referred above, NGC should provide a pathway for nerve regeneration, resist to tear from sutures and provide a mechanically stable architecture for the new tissue.[42] Therefore, it should remain intact during the first stages of regeneration. The degradation should start after some time, depending on the size and type of injury, in a very slow way with no swelling, constriction and foreign body response.[24]

The NGC should be semi-permeable to allow the diffusion of nutrients, oxygen, growth factors to the inside of the tube and, at the same time, it should allow the exclusion of waste products to the outside of the tube.[36,43,44] Some researchers assume that the material used has to be permeable to a molecular weight of up to 50kDa.[36] Other aspects that have to be considered are both the diffusion of inflammatory cells to the inside of the tube, that has to be avoided, and the diffusion of growth factors to the outside of the tube. Since the permeability of the material is directly related to the porosity, it is reported that ideally the pore size should be between 5-30μm, with preferred values in the range of 10-20μm.[45] With pores smaller than 5μm, cells and new tissue are unable to cross, and above 30μm the

material is too permeable to inflammatory cells, which may compromise nerve regeneration.[41] It is important to mention that some of the fluid inside the tube should diffuse to the outside, in order to avoid a pressure increase inside the conduit due to fluid retention.

Since the main function of the NGC is to provide a pathway for nerve regeneration, it has to present proper biomechanical properties for this application.[46] NGC should be smooth and flexible to avoid new fiber compression, but at the same time, it is also required some stiffness as the conduit has to be resistant to bending without the risk of collapsing with shape loss.[38,43] Nevertheless, a conduit that is too stiff can easily cause distortion and a too flexible one can fail to support regeneration.[24] Due to these facts, the fine balance between these two properties is required. The Young modulus of NGC should also be similar to those of the nerves, in order to ensure the necessary resistance to the common *in vivo* physiological loads (65-155N for ulnar and 73-220N for median nerves).[24] These properties are mostly dependent on the chosen material, dimensions, thickness, diameter of the lumen and lumen fibers, as will be described in the following sections.

The surface properties of the tubes need to be evaluated, since during the formation of the new tissue, this will interact with the surface of the conduit. A longitudinal texture has been reported as ideal to help the alignment of the Schwann cells.[47] As nerve gaps differ in size and neurons have different diameters and sizes, the length and lumen dimensions of a NGC should be easily adjustable to the specific nerve type to be recovered.

Another approach that has been used in the design of NGC is the incorporation of luminal fillers, either growth factors or accessory cells, in the tube as a means of improving the efficiency of reconstruction for both small and large gaps. Table 1.2 shows the most common growth factors and their functions in nerve regeneration.

Table 1.2 Most common growth factors used in nerve guide conduits.[34,45,48]

Growth Factor	Function
Nerve growth factor (NGF)	Involved in the survival of the sensory nerve cell bodies and outgrowth of their neurites.
Glial Growth factor (GGF)	Induces Schwann cell motility and proliferation. Helps improving the survival of motor/sensory neurons.
Fibroblast growth factor (FGF)	Stimulates mitogenesis which increases cell growth and regeneration.
Glial cell-derived neurotrophic factor (GDNF)	Improve motor/sensory neuron survival, neurite outgrowth and schwann cell migration.
Neurotrophin - 3	Restoration of sensory/motor conduction velocity

Schwann cells also represent an attractive class of luminal fillers due to their key role in the nerve regeneration process. Nevertheless, other accessory cells like bone-marrow stromal cells, ectomesenchymal stem cells and fibroblasts can be used to enhance the nerve regeneration process.[25] The incorporation of these cells and growth factors in nerve guide conduits can be performed in different ways, namely: (i) use of a matrix for the delivery of growth factors or accessory cells. This matrix will provide support and guidance for regenerating axons, control the release of growth factors avoiding an enzymatic breakdown and growth of supportive cells. However, these growth factors and/or accessory cells are incorporated in a hydrogel that can be too dense enabling cell growth.; (ii) use of an affinity-based system for the delivery of growth factors or accessory cells; (iii) impregnating the NGC wall with accessory cells or growth factors via crosslinking or immobilization (diffusion-based systems). By crosslinking the growth factors, there is no need to use hydrogels, but not all crosslinking preparations are biodegradable. Crosslinking of different types of growth factors is also possible; (iv) direct culturing of accessory cells on the NGC wall which results in empty lumens not compromising the growth of new axons. Unfortunately, the absence of supportive cells at the surface of the lumen can be a disadvantage; (v) using microspheres to delivery growth factors or accessory cells to the NGC lumen providing multiple unit dosage but there are many limitations in what concerns the microencapsulation technology and growth factor stability. Other strategies involve the use of genetically modified cells which arises safety issues due to viral vectors or the

application of mechanical devices that allow the delivery of multiple proteins simultaneously. However, non-biodegradable systems imply further surgical removal.[25,49,50]

Also, there are some technical requirements that should be taken into account when preparing a NGC. It should be able to be sutured onto the nerve stumps and it should be able to bear surgical handling. NGC should exhibit a long-term storage and has to be sterilizable, as all medical devices that are created for implantation purposes.[51] Also, to facilitate its implantation, transparent NGC are preferred.

1.6 PERIPHERAL NERVE REGENERATION: STRATEGIES

In the search for an efficient method to bridge nerve gaps with success, a vast portfolio of materials and different approaches has been proposed. In this section, the most common ones, as well as their advantages and disadvantages are going to be discussed.

1.6.1 Nerve Autograft

For the last 50 years, nerve autograft has been considered the "gold standard" for bridging nerve gaps.[36] Autografting was reported for the first time between 1870 and 1900, and Millesi was the first researcher demonstrating the benefits of this technique using animal studies.[43] The technique consists in harvesting a nerve from another site of the body, which is then used to connect the two nerve stumps and align the fibers to allow functional recovery of the injured nerve. The most common nerve used in this approach is the sural nerve, taken from the back outer ankle.[28,43] The factors that affect the choice of the most suitable nerve to harvest is related to the location of the nerve to be repaired, size and diameter of the nerve gap and associated donor-site morbidity.[29]

The use of nerve autografts bring some advantages because they act like immunogenically inert scaffolds that have the ability to provide the appropriate neurotrophic factors and Schwann cells.[29,43,52] However, this technique also has many disadvantages, such as: donor site morbidity due to harvesting; donor site mismatch; limited supply; requirement of a second surgery; possibility of painful neuroma formation and scarring; and loss of function,

especially in injuries of the motor nerves.[36,38,43,52,53] Additionally, the use of nerve autografts is limited to nerve gaps with lengths of approximately 5 cm.

1.6.2 Nerve Allograft

The use of nerve allografts in the regeneration of nerves was reported for the first time in 1885, by Albert Einige. This technique consists of harvesting the missing nerve material from humans cadavers, followed by the implantation and suture to the injured nerve.[54] Nowadays, allografts are mostly used for segmental nerve injuries.[28] They can be used fresh, or pretreated by techniques such as freezing, freeze-drying, freeze-thawing, pre-degeneration and chemical treatments with or without immunosuppressants.[52]

The choice of using a nerve allograft always comes after some limitation (*e.g.*, length) of nerve autografts. One of the advantages of using these materials is related to the fact that there is an abundant supply of donor nerves.[29]

However, many disadvantages are also associated to this technique, being the most important the occurrence of an undesirable immune response, and the need for systemic immunosuppression to prevent rejection and potential immunogenicity.[55] At the same time, the patient is really prone to infections, disease transmission risk and in the most severe cases, even tumor formation.[28] Immunosuppression can be avoided when nerve allografts are decellularised.[56] A commercial product with these characteristics has already been commercialized under the tradename of AxoGen®. This device acts as a scaffold whose structure is provided by the extracellular matrix.[28]

FDA approved a commercial product called Avance®, made of cadaveric material, which does not need immunosuppression.[51] This material has all the advantages associated with the nerve allografts, and allows the choice of the type of nerve needed. However, over time, immunosuppression may be required.[51]

Due to the problems listed above concerning nerve autografts and allografts, new alternatives using different materials need to be investigated. Natural materials, biopolymers and synthetic polymers have been used to produce NGC and tested in order to enhance nerve regeneration. The following sections describe the materials that have been used, their structure, formulations and clinical trials results.

1.6.3 Natural Materials

Blood Vessels

Blood vessels, such as arteries and veins, have been used to bridge nerve gaps since the first years of the 19th century. The use of arteries was first reported in 1891 with good results, but the lack of suitable donor vessels made this technique fall into unpopularity and its clinical implementation has never occurred.[56]

Veins began being used in 1909, and since then many experiments were carried out. One of the most interesting conclusions was that the application of veins as NGC was more successful when nerve slices were used to seed its lumen.[56] This interposition was considered a practical and reliable procedure for nerve gaps between 2 and 4.5 cm.[56]

One of the main advantages in using veins is that they are extremely abundant and induce less donor-site morbidity.[52] However, the possibility of collapsing due to their thin walls, turn veins a non-recommended tissue for gap bridging.[57]

Muscle

Skeletal muscle in nerve repair applications was first reported in 1940.[58] Studies demonstrated that fresh and denatured conduits made from muscle could lead to regeneration of nervous tissue. One of the main advantages of its use is the fact that it has extracellular matrix components and longitudinally oriented basal lamina. These factors are extremely useful for enhancing nerve regeneration as this microenvironment helps to promote cell adhesion.[52] Also, it can be noted that there are numerous donor sites from which muscle tissue can be harvested.[56] However, this fact represents a disadvantage because a harvesting procedure has to be performed. Moreover, using muscle has its risks, as some nerve fibers may grow out of the muscle tissue while the regeneration process is occurring.[56]

Tendon

Tendon from rat tail has already been used for nerve regeneration. In the most known experiment, a 10 mm nerve gap was bridged.[59] As the rat tail tendon has extracellular matrix components and also a longitudinal arrangement of collagen, it constitutes a good path for cells to adhere to during nerve regeneration.[56] In terms of morphometric and functional

evaluation, the results obtained by autografting are quite similar to muscle graft. Unlimited source of graft material, as well as limited loss of function, are the main advantages of these tissues for nerve bridging.[52]

Reports concerning the use of natural materials in nerve regeneration are summarized in Table 1.3.

Table 1.3 Summary of the natural materials used in NGC, and main results obtained.

Year	Material	Nerve	Gap (mm)	Animal	Results	Ref
1982	Vein	Sciatic	10	Rat	Conduction restored after 4 months of surgery	60
1984	Vein	Sciatic	25	Rat	Satisfactory results with minimal scar tissue formation	61
1986	Artery	Peroneal	5	Rat	Growth of a minority of axons	62
1986	Muscle	Sciatic	40	Rat and Rabbit	Satisfactory limb function recovery	63
1986	Vein	Femoral	14 and 2	Rabbit	Smaller gap had better remyelination comparing with the longer one	64
1988	Vein	Sciatic	5	Rat	Nerve vein graft conduction velocity similar to autogenous nerve graft	65
1989	Vein	Peroneal	10	Rat	Vein graft showed similar pattern of nerve regeneration as nerve graft	66
1992	Aortic	Tibial	10	Rat	Preferential growth toward the distal nerve was observed	67
1992	Muscle	Peroneal	50	Rat	Muscle graft did not lead to reliable recovery	68
1993	Vein	Sciatic	10	Rat	Compared with polyethylene nerve conduit, vein graft showed accelerated rate of nerve regeneration and earlier myelination.	69
1994	Vein	Sciatic	10	Rat	Small regenerated axons	70
2007	Muscle+ Vein	Median	10	Dog	Fresh and predegenerated skeletal muscle present similar results after 1 month regarding to integrity	71

1.6.4 Natural polymers

Following nerve allografts, natural polymers were seen as reliable alternative materials to construct nerve autografts.[44] The most common naturally-derived polymers used in nerve regeneration are collagen, chitosan and alginate.

Collagen

Collagen is a structural protein of connective tissues in humans and animals and the major component of extracellular matrix (Figure 1.4).

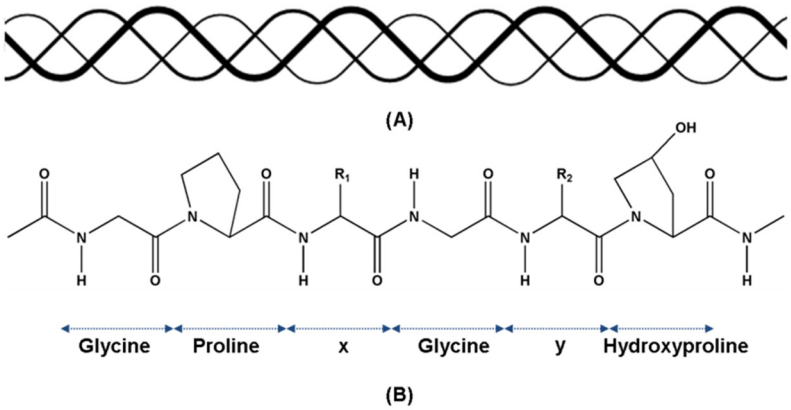

Figure 1.4 Chemical structure of collagen type I. (A) secondary left handed helix and tertiary right handed triple-helix structure, (B) primary amino acid sequence.[72]

Due to this fact, it has been used in implants as wound dressings and artificial skin.[24] It is a natural biodegradable material with high biocompatibility, low antigenicity, which is known to promote neurite outgrowth, nerve regeneration and helps to maintain biological functions of the cells.[24,44,73,74]

This material has been used as NGC since 1990s, adopting different forms. These include fibers inserted inside the conduit's lumen to function as fillers and hydrogel formulations to deliver cells, drugs or growth factors.[24]

Some studies have also shown that collagen filaments incorporated in NGC made with biodegradable materials, help to guide the new nerve fibers as they improve permeability and surface area exposed to the surrounding tissue.[73]

As collagen is a natural polymer, it presents poor mechanical strength, high water uptake and fast degradation, which are undesirable characteristics in nerve regeneration. Indeed,

the structural integrity is compromised and the swelling can compress the new nerve tissue as it is growing.[44] To overcome such disadvantages, some techniques, like solution casting and freeze-drying, are being performed to achieve the required mechanical strength and high porosity (70-90%).[44] The mechanical strength can also be improved by crosslinking collagen between amine groups, which provides structural stability to the NGC.[2] Among the techniques used for preparation of collagen nerve conduits, the most reported ones include injection molding and dip-coating, extrusion, electrospinning, freeze drying followed by lyophilization and crosslinking due to microwave radiation.[2,42] Table 1.4 presents some of the works where collagen was used as NGC.

Table 1.4 NGC made with collagen submitted to *in vivo* tests.

Year	Material	Nerve	Gap (mm)	Animal	Results	Ref
1983	Collagen	Radial	8	Cat	Reinnervation of sensory structures	75
1990	Collagen-PGA	Peroneal	0.5	Rat	Axonal regeneration equal to sutured autografts	76
1991	Collagen	Sciatic	4	Rat	Nerve regeneration similar to nerve autograft	77
2009	Collagen	Peroneal	10	Rat	Regeneration of motor axons with no noticeable foreign body reaction	73
2010	Collagen	Peroneal	30	Dog	Functional recovery of the regenerated nerve	78
2013	Collagen	Median	10-20	Human	8 in 9 patients achieved functional recovery	79
2013	Collagen	Digital	≤ 26	Human	Useful to span digital nerve defects up to 2.6 cm	80
2014	Collagen-Collagen fibers	Sciatic	---	Rat	Nerve regeneration similar to nerve autograft	74
2014	Collagen	Sciatic	10	Rat	Study of the influence of the conduit diameter for motor recovery.	81
2016	Collagen	Sciatic	20	Rat	Functional recovery similar to autograft but thinner myelin sheaths.	82
2016	Silk fibroin /Collagen	Sciatic	10	Rat	When seeded with SCs, similar results to autograft	83
2017	Collagen	Sciatic	15	Rat	Regeneration of myelinated fibers after 8 weeks	84

Chitosan

Chitosan (Figure 1.5) is a cationic biopolymer obtained from the alkaline deacetylation of chitin, which is the most abundant natural polymer after cellulose.[2,85]

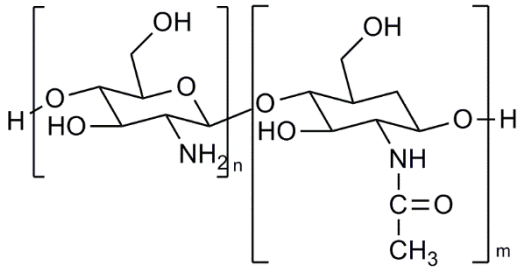

Figure 1.5 Chitosan structure.

Over the years, chitosan has been widely used in several biomedical applications,[86-91] mainly because of its promising intrinsic properties. Among them, it is possible to mention: biocompatibility,[53,91,92] biodegradability,[85,91] low toxicity and non-immunogenicity,[85,91,92] low cost and large availability.[91,92]

Very recently, chitosan started to be used in the fabrication of NGC for peripheral nerve regeneration, with some success.[90] The good results obtained might be due to the favorable interaction of chitosan with biological environments, namely the promotion of cell attachment, adhesion, differentiation, and survival, ability to create a good pathway for neurite outgrowth and ability to inhibit the scarred tissue formation.[53,91,93]

Unfortunately, some structural properties of this biopolymer are not suitable for the construction of NGC, being its mechanical strength being the most critical issue. As it presents low mechanical strength under physiological conditions, the capability to maintain a certain structure, needed to guide the new fibers, is seriously compromised.[87,89,91] To compensate the lack of mechanical strength, chitosan is subjected to a crosslinking reaction with, for instance, genipin[94]. This formulation was already tested in many biomedical applications such as drug carriers and in the encapsulation of biological products and living cells.[94] The addition of chitin powder to chitosan solution has also been tested to increase mechanical strength.[95]

Along with mechanical strength, porosity is also a property which has to be optimized[94] and is related to the fabrication procedure of the material to be implanted. The most

common techniques used are cast molding, and knitting techniques combined with lyophilization.[53,91,95]

Table 1.5 presents some studies regarding the use of chitosan in nerve regeneration, as well as their main results, performed since the middle 2000s.

Table 1.5 Chitosan membranes and NGC tested for nerve regeneration *in vivo.*

Year	Material	Nerve	Gap(mm)	Animal	Resultados	Ref
2004	Chitosan-chitin powder	Sciatic	8	Rat	Compatible with the surround tissue *in vivo*	95
2005	Chitosan-neurosteroids	Facial	10	Rabbit	Regeneration of the nerve fibers. Faster regeneration when using the neurosteroids *in vivo*	96
2005	Chitosan-Filaments of PGA	Sciatic	30	Dog	Restoration of nerve continuity and functional recovery.	53
2009	Chitosan-GDNF	Sciatic	10	Rat	Axon area and myelination higher than chitosan tube (control)	85
2010	Cross-linked carboxymethyl chitosan	Sciatic	10	Rat	Myelin sheath similar to nerve autografts and higher fiber density compared to chitosan tube	86
2013	Chitosan with varying degrees of acetylation	Sciatic	10	Rat	Poor mechanical properties and low stability	89
2013	Collagen-Chitosan with RGD	Sciatic	15	Rat	Faster regeneration with RGD compared with collagen-chitosan tubes	97
2015	Chitosan	Phrenic	15	Dog	Functional recovery was not totally achieved	98
2016	Chitosan/NVR with SCs	Sciatic	15	Rat	Axonal growth was impaired by NVP with SCs	99
2016	Chitosan	Sciatic	10	Rat	Similar results to autograft	100
2017	Chitosan+ simvastatin/ Pluronic F-127 hydrogel	Sciatic	10	Rat	Improvements in functional recovery and myelin sheath thickness after ten weeks	101

Poly(3-hydroxy butyrate) (PHB) and Poly(3-hydroxybutyrate-co-hydroxyvalerate) (PHBV)

Poly-3-hydroxbutyrate (PHB) is a bio-absorbable polymeric material that is synthesized by microorganisms as an energy-storage medium.[102] It can be produced from fermentation followed by solvent extraction from bacterial cultures and carbon substrates.[103] *In vivo*, it degrades by hydrolytic and enzymatic action.[104] Its copolymer with 3-hydroxyvalerate, poly(3-hydroxybutyrate-co-hydroxyvalerate) (PHBV), is more flexible and easier to process when compared with PHB. PHB is usually molded into a sheet made with aligned fibers. At the end of the 1990's, the first attempts in using this material for peripheral nerve regeneration were reported showing effect on helping regeneration of axons.[105] PHB is non-antigenic and presents good tensile strength, but its degradation lasts at least 24 to 30 months until all polymer is resorbed.[103] A comparative study between the performance of PHB with epineural suturing was carried out in the median and/or ulnar nerve at the wrist/forearm level. The results suggested better recovery with PHB than with epineural suturing.[102] The effect of blending PHB and PHBV has also been studied. After the blending, scaffolds were obtained by electrospinning. Satisfactory results were observed for Schwann cells proliferation, which increased with the addition of collagen to the scaffold.[106] More recently, Biazar *et al.* performed studies using PHBV as the unique material for the preparation of nerve guide tubes, achieving interesting results in what concerns mechanical properties. Also, as the nerve guide was micro patterned, improvement in adhesion of Schwann cells was observed.[107] Later, the same group, crosslinked PHBV with gelatin, and the resulting material showed improved cellular adhesion in comparison with PHBV alone. The tube was used to bridge a gap with 30mm in the sciatic nerve of a rat. After four months, restoration of the nerve and myelated nerve fibers were observed.[107]

Recently a study has been reported where PHBV was crosslinked with laminin, proving that cell adhesion on its surface was improved compared with the neat PHBV.[108] Furthermore, the incorporation of chitosan in a nanofibrous PHBV conduit was studied concerning its ability to promote cell proliferation. Crosslinked structures presented better results in comparison with the blend based structures.[109] Different formulations of PHBV/collagen blends were also used in the prepared of nerve conduits using the electrospinning technique. Blends with 50:50% of both materials showed higher cell proliferation, in comparison with other formulations, revealing a cell elongated

morphology with bipolar neurite extensions favorable to nerve regeneration.[110] All these results show that PHBV is a promising material for peripheral nerve regeneration due to good mechanical properties, cellular interaction, and also the possibility to control the degradation rate of its constructs.

Alginate

Alginate is a linear polysaccharide copolymer of (1-4)-linked β-D-mannuronic acid (M) and α-L-guluronic acid (G), extracted from brown seaweed.[4] It is biocompatible, biodegradable, sterilizable without degradation, and, very importantly, its physical and rheological properties can be easily modified by varying the monomers (G and M) ratio and molecular weight of the polymer chain.[4,111] Since the past decade, the interest in alginate for biomedical applications has increased significantly due to its good cell compatibility.[112] Alginate based hydrogels have been used as covers for diabetes treatment and hemophilia, detoxification, transplanted pancreas or liver cells, and as bridging materials for both spinal cord and nerve repair.[4,113] In what concerns the nerve regeneration, the compatibility of this biopolymer with Schwann cells, neurotrophic factors and stem cells is a very interesting and the most decisive characteristic.[4,113,114]

In peripheral nerve regeneration, alginate is not reported as main component of nerve guide tubes. Instead, is it usually used as a gel, which is inserted in the conduit lumen to guide the new nerve fibers. However, it is reported in literature that the regeneration of nerve tissue requires that some amount of gel has to degrade, in order to open space in the lumen.[114] This gel usually results from the crosslinking of alginate with calcium ions.[114] The gel degradation starts with the diffusion on the calcium ions from alginate, allowing the slow loss of crosslinking of the alginate gel. The resulting products are immunologically inert and are not digested by mammalian cells.[113]

Alginate gels have been tested both *in vitro* and *in vivo* for peripheral nerve regeneration purposes, but contradictory results were obtained. *In vitro* tests showed a negative influence of alginate on cell proliferation. Unexpectedly, *in vivo* tests showed the opposite. A sciatic nerve gap with 7 mm in rats and a sciatic nerve gap with 50 mm in cats were successfully bridged with alginate foams, leading to promising results.[24] Because of this paradox, and due to ethical issues, alginates are not widely used materials for peripheral nerve regeneration. More recently, the attempt to crosslink alginate with chitosan has been

reported, and interesting results were achieved.[112] In another approach, Shahriani *et al* tested a high-purity alginate scaffold for spinal cord repair in rats.[115] After 14 days, the scaffolds revealed a degradation ratio not compatible with the regeneration of the axons.[115]

Other Natural polymers

Other materials such as hyaluronic acid, natural silk, silk fibroin and keratin have also been tested, but not as intensively as the former ones. These materials lack some important properties, namely mechanical stability. Consequently, the only way to use them is by chemical modifications via crosslinking or by incorporation in other natural or synthetic polymers.[24]

1.6.5 Synthetic polymers

During the last years, enormous efforts have been made to create NGC based on synthetic polymers. Typically, these materials can be classified as non-degradable and degradable.

Non-biodegradable synthetic polymers

While trying natural polymers, researchers also focused their interest on non-biodegradable polymeric materials to be used in nerve regeneration due to their superior mechanical properties. Good results were achieved for small gaps, but in many cases the conduits had to be removed due to immunologic response. The next topic presents the most used non-degradable polymeric materials for nerve regeneration purposes and also the new trends in using these materials.

Silicone

Since 1960s, silicone has been studied as material for NGC in peripheral nerve regeneration. It was one of the first synthetic materials to be used in these applications due to its elastic properties and inertness.[24] It is non-biodegradable and non- permeable to large molecules.

The first researcher to present a successful case of recovery from an injury using silicone was Merle.[116] Some years later, Chen, doped silicone tubes with laminin, collagen and fibronectin gels, concluding that better results than the non-doped silicone tube can be achieved.[117] Lundborg, in turn, concluded that silicone tubes gave better regeneration results in gaps smaller than 5mm.[118-121] This result was confirmed after another study where a 8mm gap in the peroneal nerve of the rat was bridged with a silicone tube showing the presence of new axons, although some of them not myelinated.[122] However, many works in rats also reported the formation of scarred tissue, compression of the new axons or even no regeneration at all.[123-125]

Moreover, researchers also refer that in some patients, silicone tubes had to be removed because of loss of nerve function due to irritation at the implantation site. As this material is non-biodegradable, a chronic inflammation associated to excessive scarred tissue formation can occur during time, in some cases, after one week.[39] Contradictory results have been more recently reported in histomorphometrical and immunohistochemical assessments, which supported that no excess of scarred tissue was formed and axons can regenerate within a silicone tube.[126] Ikeguchi *et al.* treated the inner surface of a silicone tube with negative-charged carbon ions, claiming that axonal regeneration was improved.[127] Unfortunately, none of these recent works gives further information concerning the consequences that this type of conduits could evoke a long time after implantation.

Expanded poly(tetrafluorethylene) (ePTFE)

ePTFE was discovered in the 1970s and it's chemically identical to PTFE but, after processing, it presents small pores. This porous structure cannot be obtained without the use of soluble fillers, foaming agents or other chemical additives.[128]

It is used to make lightweight, waterproof and breathable fabrics, micro-porous membranes, microwave carriers, industrial sealants and high-tensile fabrics and cords and medical tubes and implants.[128]

For peripheral nerve regeneration, a product made from ePTFE is commercialized under the tradename of Gore-Tex®. The main conclusions taken from *in vivo* trials in humans were that small gaps in the lower arm (15-40mm) were successfully bridged, but longer

defects (till 60mm) could not recover and useful reinnervation was only verified in 13,3% from a population of 43 patients.[43]

In another trial, Gore-Tex® was used in seven patients with nerve defects (<3 mm) in the inferior alveolar nerve, and only two of them revealed some return of sensation.[128] Also, this product causes an excess of scarred tissue formation, compression of the new fibers and severe immunologic responses from the host body. Nowadays, and for these reasons, these materials are lacking the interest from the medical field.

Polypyrrole (Ppy)

Ppy is a conductive polymer which is commonly used in advanced materials such as sensors, solar cells, water treatment materials, among others.[129] It has been object of interest for peripheral nerve regeneration in recent years due to the positive responses induced in cells by electric stimulation.[130,131] Among the many advantages of using this material there is the fact that it can support cell adhesion and has a good biocompatibility and no evidence of toxicity.[132] In 1997 was the first time that neurite outgrowth from PC12 cells in contact with a film of Ppy was reported, proving that conductive polymers could be useful for nerve regeneration applications.[133] After these findings, researchers have tried to incorporate new features to Ppy based NGC, such as the incorporation of adhesive cells. Also, changing the topography of these materials help the regeneration of new axons due to guidance providence.[134] Unfortunately, the use of Ppy brings some disadvantages, namely those related with its slow degradation rate and poor solubility.[135] For that reason, Ppy has been incorporated in composite materials as a way to overcome its drawbacks. Using emulsion polymerization, Xu et al. prepared Ppy/PDLLA conductive composites and it was found that the materials were able to support neurite regrowth in a similar way to that of autologous grafting.[135] More recently, nerve guide tubes based on PVA/Ppy were also studied. The tubes were prepared using a casting technique and molded in a silicone tube. A satisfactory number of regenerated nerve fibers was achieved although better results were obtained by a conduit based on PVA loaded with multi-wall carbon nanotubes (MWCNT) seeded with Mesenchymal stem cells (MSCs).[136] In conclusion, conductive polymers have demonstrated to be promising materials for peripheral nerve regeneration, when blended with other polymers with more desirable solubility, mechanical and degradation properties.

Biodegradable synthetic polymers

Due to the problems caused by non-biodegradable polymers, their biodegradable counterparts started to be more popular for peripheral nerve regeneration. These materials have the ability to fully degrade *in vivo* which leads to a new approach for this application: by the end of the regeneration, the conduit should be gone completely and with that avoid immune response from the body. Many biodegradable materials were tested, but in this section only poly(glycolic acid) (PGA), poly(lactic acid-co-glycolic acid) (PLGA), poly(ε-caprolactone) (PCL), and poly(DL-lactic acid –co-ε-caprolactone) (P(DLLA-co-CL)) will be presented, as they are those with more clinical trials and with FDA approved products.

PGA

PGA is an aliphatic polyester known in the biomedical field as a suture material for wound closure. It has been used for a long time in this application because it can be absorbed by the human body within 90 days after implantation, through an hydrolysis mechanism.[137] Due to its good biological properties, the interest in producing NGC from this material has increased substantially.

PGA was first used as a NGC in 1990, by Mackinnon and Dellon, and the results were similar to those obtained from nerve autografting.[138]

Although several works report good results, others refer that PGA alone has a too fast degradation rate, which can be undesirable for larger nerve gaps. Another problem concerns the technique used to fabricate the conduit. When extrusion was used, the surface of PGA conduits presented poor quality.[56] Moreover, while it degrades, the products that are released have an acidic nature, leading to the decrease of the pH at the site of implantation that can trigger the immune response.

A new approach was then adopted and involved the use of PGA, not as the core material of the nerve conduit, but as filler.[139] The promising results led researchers to conclude that PGA is a good material for nerve regeneration, especially when combined with other materials, of which, chitosan and collagen are examples.[140-143]

PLGA

PLGA is an aliphatic copolyester made from glycolic and lactic acid that has FDA approval and has been used as a suture material throughout the years (Polyglactin 10®).[144] Different ratios of the two monomers allow the tailoring of the polymer properties (e.g., thermomechanical, wettability, swelling and degradation), which is an advantage of PLGA over PGA.[144] The ability to manipulate the degradation ratio, which allows tailoring the material for different types and sizes of nerve gaps, turns PLGA a very attractive material for peripheral nerve regeneration.

PLGA is biodegradable, and releases acidic products during degradation, which presents the deleterious effect described above.

In NGC production, PLGA has been tested as the core material of the conduit and also in combination with others (e.g., collagen). When used alone, in order to turn it permeable and with an adequate porosity, some approaches have been tested, namely the addition of a porogenic agent.[145] and preparation of hollow fiber membranes using a phase-inversion process.[146] In both works, interesting mechanical properties and degradation profiles were achieved. In a more recent study, a PLGA based catheter was prepared.[147] This catheter comprises an outer tube, which has a scaffold inside. This scaffold has many tube shaped structures in order to correctly guide the new nerve fibers. The outside tube provides the mechanical support required for nerve regeneration. As a result, fibroblast growth was facilitated across the inner scaffold and also the outer structure showed good capacity to overcome compression.[147] PLGA had also been electrospun and then coated with a conductive polymer, Ppy. An *in vitro* assessment with PC12 rat cells showed the formation of longer neuritis compared with the control.[148] In another approach, PLGA conduits were coated with nanosilver to benefit from silver's antimicrobial effect which resulted in an increase of infection resistance of the conduit.[149] A combination of electrospun PCL with nanospheric PLGA was also tested with PC12 rat cells, revealing long and guided neuritis due to the alignment provided by the scaffold.[150]

Neurotrophic factors, as well as Schwann cells, have also been incorporated in PLGA matrices leading to good results, but only in small gaps. Nevertheless, PLGA does not represent an universal solution for peripheral nerve regeneration in general, as only some specific cases can be treated with this polymer. Table 1.6 shows the main conclusions of the works reported in literature that used this polymer in nerve regeneration.

Table 1.6 PLGA based NGCs tested *in vivo.*

Year	Material	Nerve	Gap (mm)	Animal	Results	Ref
2004	PLGA(85:15)+ Schwann cells	sciatic	10	Rat	Ultrasonic stimulation has a positive effect on seeded Schwann cells within PLGA conduit	151
2006	PLGA(75:25)+ collagen	peroneal	15	Rabbit	PLGA-coated collagen tube showed better regeneration comparing to vein grafts	144
2006	PLGA(85:15)	sciatic	10	Rat	Asymmetric structure enhance the removal of drained waste	150
2007	PLGA (90:10; 50:50)+ Schwann cells	sciatic	10	Rat	Directional permeability has a positive effect in nerve regeneration through PLGA conduits	5
2007	PLGA (90:10)	sciatic	10	Rat	Axon regeneration similar to Neurolac®	152
2008	PLGA/Pluronic F127	sciatic	10	Rat	Regeneration achieved due to good mechanical properties, permeability and prevention of scar tissue invasion.	153
2010	PLGA/ Chitosan+CNTF	tibial	25	Dog	Favorable conduit for Schwann cell migration and axonal regeneration	154
2017	PLGA+ SDS/SCs	Sciatic	12	Rat	Functional improvements after 12 weeks of implantation	155
2017	PLGA pre-coated with NECL1	Sciatic	15	Rat	Enhanced functional recovery comparing with the control (PLGA)	156

PCL and P(DLLA-co-CL)

PCL is a bioresorbable, hydrophobic and semi-crystalline polyester.[157] Its tailorable degradation and mechanical properties, along with its good compatibility, have made this polymer very attractive to the biomedical field since the 1970s. During this time, it was used in various drug delivery systems, but as its degradation rate was slow, other resorbable polymers as PGA and poly(D,L-lactide) (PDLA) were preferred.[158] However, since the 2000s, as tissue engineering arose, PCLs has been extensively tested both *in vitro* and *in vivo* revealing good results in terms of biocompatibility. As a result, FDA approved its use in tissue engineering applications.[159]

For peripheral nerve regeneration, this polymer, like other bioabsorbable polymers, has been tested in conduits alone mixed with other polymers and seeded with both cells and nerve growth factors. Improvement of the motor function of the sciatic nerve was achieved

with a PCL conduit seeded with MSCs.[160] In a study of the topography of the surface and mechanical properties, NGC based on PCL-PVA were prepared by solvent casting.[38] The presence of a grooved improves mechanical properties of the material, approaching to the ones of the healthy nerve. Another study evaluated the effect of encapsulated neurotrophic factor derived from glial cell (GDNF) embedded in a nerve conduit made with PCL.[161] The bioactivity of GDNF was confirmed and also the sterilization technique proved to be suitable for this material, as it did not alter its structure or porosity percentage. More recently, works including the use of peptides as RGD with PCL based surfaces have also been reported, and promising results were obtained.[162] Table 1.7 shows the main conclusions of the works reported in literature that used this polymer in nerve regeneration.

Table 1.7 Recent PCL NGCs tested *in vivo.*

Year	Material	Nerve	Gap (mm)	Animal	Results	Ref
2012	PCL+MSCs	sciatic	3	rat	Gastrocnemius muscle was restored while motor function was improved.	160
2013	PCL/Pluronic F127	sciatic	10	rat	The double stimulation of nerve growth factor (NGF) and low-intensity pulse ultrasound (US) were more effective in nerve regeneration than single stimulation.	163
2014	PCL/gelatin+ stem cells (SHED)	Sciatic	10	Rat	Improved nerve regrowth across the SHED seeded conduit.	164
2014	PCL/gelatin	Sciatic	5	Rat	Electrospun PCL is more suitable for *in vivo* implantation than PCL/gelatin due to poor histology and electrophysiology.	165
2014	PCL+Schwann cells	Sciatic	14	Rat	Electrospun bilayered seeded conduits improve the sprouting of nerve fibers and motor recovery.	166
2016	PCL	Sciatic	10	Rat	Successful nerve growth after 14 weeks of implantation	167
2017	PCL+agarose scaffold	Sciatic	10	Rat	SCs adhesion and robust axon ingress into the tube	168

P(DLLA-co-CL) is a polyester made from D,L-lactic acid and ε-caprolactone that has attracted the interest of the researchers for peripheral nerve regeneration. It should be

mentioned that problems derived from its degradation *in vivo* lead to less damage of the surrounding tissue, in comparison with materials as PGA or PLGA. This fact is related with the slower degradation ratio of P(DLLA-co-CL), which results in a dilatory release of degradation products, avoiding higher concentrations of the resulting acidic products. Due to its degradation rate, the local pH is not so negatively affected as verified for PGA or PLGA.[152]

Moreover, compared with the other biodegradable materials, P(DLLA-co-CL) is more hydrophobic, which can lead to higher degradation times, extending the life time of the conduit in the body. Moreover, in some cases, even after the nerve is regenerated and functional activity is restored, there still small fragments of the nerve conduits standing by the new nerve.[51] FDA gave approval to a commercial product made from this copolyester known as Neurolac®. This conduit has a diameter of 1.5-10 mm and length of 3 cm. In terms of degradation, it only degrades completely after 16 months.[51]

1.7 FDA APPROVED DEVICES FOR PERIPHERAL NERVE REGENERATION

As aforementioned, the preparation of a device able to improve the recovery ratios after peripheral nerve injury still remains a clinical challenge. After mid-1980s, some devices received FDA approval, which include devices made of natural and synthetic polymers. These devices can be in a nerve conduit structure or in a wrap structure and are presented in the Table 1.8 and Table 1.9.[51]

Table 1.8 Available FDA approved nerve guide devices (adapted).[51]

FDA clearance date	Product name	Material	Degradation (months)	Diameter	Length
22nd March, 1999/1995	Neurotube®	PGA	3	2.3-8 mm	2-4 cm
22nd June, 2001	NeuraGen®	Type I collagen	36-48	1.5-7 mm	2-3 cm
21st September, 2001	Neuroflex™	Type I collagen	4-8	2-6 mm	2.5 cm
21st September, 2001	NeuroMatrix™	Type I collagen	4-8	2-6 mm	2.5 cm
15th May, 2003	AxoGuard™ Nerve Connector	Porcine small intestinal submucosa (SIS)	3	1.5-7 mm	10 mm
10th October, 2003/ 4th May, 2005	Neurolac®	P(DLLA-co-CL)	16	1.5-10 mm	3 cm
5th August, 2010	SaluTunnel™ Nerve Protector™	Polyvinyl alcohol (PVA)	Non-absorbable	2-10 mm	6.35 cm

The majority of devices approved are based on Type I Collagen. Nevertheless, limitations concerning their degradation ratio need to be considered. On the other hand, Neurolac® presents a degradation ratio that seems to match the regeneration of the nerve. However, its structure is highly compact, showing no porosity, which may jeopardize the regeneration process.

Table 1.9 Available FDA approved absorbable nerve cuff/protectant wrap devices.

FDA clearance date	Product name	Material	Degradation	Diameter	Length
24th November, 2000/2001	Salubridge™	Polyvinyl alcohol (PVA)	Non-absorbable	2-10 mm	6.35 cm
15th May, 2003	AxoGuard™ Nerve Protector	Porcine SIS	3 months	2- 10 mm	2-4 cm
16th July, 2004	NeuraWrap™	Type I Collagen	36-48 months	3-10 mm	2-4 cm
14th July, 2006	NeuroMend™	Type I Collagen	4-8 months	4-12 mm	2.5-5 cm

Unfortunately, despite the offer of approved devices, none of them has all the characteristics that would be desired for achieving better results, as they present limited repair for gaps longer than 30 mm.[73]

1.8 OUTLOOK AND CONCLUSIONS

Peripheral nerve injury is a serious problem affecting millions of people all around the world, with consequences that can lead to irreversible disability. The preparation of a device able to improve the recovery ratios after peripheral nerve injury still remains a clinical challenge. Some devices based on natural and synthetic polymers have already received the approval of FDA and are commercially available. It is believed that the trend of peripheral nerve regeneration is to create devices, which can be adapted to different gap lengths and degradation rates. Also, the inclusion of exogenous cells to enhance the recovery of the nerve has received considerable interest in the last years showing promising results.

The use of non-biodegradable materials in this application, as mentioned in this chapter, can be seen as a disadvantage as the material may constrict the new nerve fibers and a second surgical intervention may be needed for its removal.

To sum up, in the authors' opinion, polymeric materials seem to be a reliable solution to prepare such nerve conduits, since their properties can be easily modulated and also allow the easy incorporation of nerve growth factors and accessory cells, which play an important role in successful regeneration of the injured nerve.

1.9 REFERENCES

1. Robinson, L. R., Traumatic injury to peripheral nerves. *Muscle & Nerve* **2000,** *23*, 863-873.

2. Wang, S. F.; Cai, L., Polymers for Fabricating Nerve Conduits. *International Journal of Polymer Science* **2010**, 20.

3. Schlosshauer, B.; Muller, E.; Schroder, B.; Planck, H.; Muller, H. W., Rat Schwann cells in bioresorbable nerve guides to promote and accelerate axonal regeneration. *Brain Research* **2003,** *963*, 321-326.

4. Szarek, D.; Marycz, K.; Bednarz, P.; Tabakow, P.; Jarmundowicz, W.; Laska, J., Influence of calcium alginate on peripheral nerve regeneration: *In vivo* study. *Biotechnology and Applied Biochemistry* **2013,** *60*, 547-556.

5. Chang, C. J.; Hsu, S. H.; Yen, H. J.; Chang, H.; Hsu, S. K., Effects of unidirectional permeability in asymmetric poly(DL-lactic acid-co-glycolic acid) conduits on peripheral nerve regeneration: An *in vitro* and *in vivo* study. *Journal of Biomedical Materials Research Part B-Applied Biomaterials* **2007,** *83B*, 206-215.

6. Guyton, A. C.; Hall, J. E., *Human Physiology and Mechanisms of Disease, 6th edition*. Saunders Company: **1997**.

7. Noback, C. R.; Strominger, N. L.; Demarest, R. J.; Ruggiero, D. A., *The human nervous system : Structure and function*. Humana Press Inc.: **2005**; Vol. sixth edition.

8. Zhang, N.; Yan, H.; Wen, X., Tissue-engineering approaches for axonal guidance. *Brain Research Reviews* **2005,** *49*, 48-64.

9. Purves, D. E.; Augustine, G. J.; Fitzpatrick, D. E.; Katz, L. C., *Neuroscience*. Sinauer Associates: **1997**.

10. Jäkel, S.; Dimou, L., Glial Cells and Their Function in the Adult Brain: A Journey through the History of Their Ablation. *Frontiers in Cellular Neuroscience* **2017,** *11*, 24.

11. Lutz, A. B.; Chung, W.-S.; Sloan, S. A.; Carson, G. A.; Zhou, L.; Lovelett, E.; Posada, S.; Zuchero, J. B.; Barres, B. A., Schwann cells use TAM receptor-mediated phagocytosis in addition to autophagy to clear myelin in a mouse model of nerve injury. *Proceedings of the National Academy of Sciences* **2017**, 201710566.

12. Koo, C. L.; Liew, M. J.; Mohamad, M. S.; Mohamed Salleh, A. H., A review for detecting gene-gene interactions using machine learning methods in genetic epidemiology. *BioMed research international* **2013,** *2013*.

13. Birchmeier, C.; Bennett, D. L., Chapter Four-Neuregulin/ErbB Signaling in Developmental Myelin Formation and Nerve Repair. *Current Topics in Developmental Biology* **2016,** *116*, 45-64.

14. Saifetiarova, J.; Taylor, A. M.; Bhat, M. A., Early and late loss of the cytoskeletal scaffolding protein, ankyrin G reveals its role in maturation and maintenance of nodes of Ranvier in myelinated axons. *Journal of Neuroscience* **2017,** *37*, 2524-2538.

15. Mira, P. K. U., *Life Sciences, Fundamentals and Practise, Part II*. 5th ed.; Pathfinder Publication: New Delhi, India, **2016**.

16. Junqueira, L.; Carneiro, J., *Tecido nervoso*. 12th ed.; Texto & Atlas: Rio de Janeiro, **2013**; p 149-175.

17. Duhan, A.; Rana, P.; Beniwal, K.; Parihar, D., Perineurioma of scalp in an infant: A case report with short review of literature. *Asian Journal of Neurosurgery* **2016,** *11*, 70-71.

18. Rigoard, P., The Normal Nerve. In *Atlas of Anatomy of the Peripheral Nerves*, Springer: 2017; pp 2-13.

19. Ghalib, N.; Houšt'ava, L.; Haninec, P.; Dubový, P., Morphometric analysis of early regeneration of motor axons through motor and cutaneous nerve grafts. *Annals of Anatomy - Anatomischer Anzeiger* **2001,** *183*, 363-368.

20. Geuna, S.; Perroteau, I.; Tos, P.; Battiston, B., *International Review of Neurobiology. Tissue Engineering of the Peripheral Nerve: Stem Cells and Regeneration Promoting Factors*. Academic Press: **2013**; Vol. 108.

21. Smith, G. M.; Onifer, S. M., Construction of pathways to promote axon growth within the adult central nervous system. *Brain Research Bullets* **2011,** *84*, 300-305.

22. Mietto, B. S.; Mostacada, K.; Martinez, A. M. B., Neurotrauma and Inflammation: CNS and PNS Responses. *Mediators of Inflammation* **2015,** *2015*, 14.

23. Gong, L. L.; Zhu, Y.; Xu, X.; Li, H. Q.; Guo, W. M.; Zhao, Q.; Yao, D. B., The effects of claudin 14 during early Wallerian degeneration after sciatic nerve injury. *Neural Regeneration Research* **2014,** *9*, 2151-2158.

24. Gu, X.; Ding, F.; Yang, Y.; Liu, J., Construction of tissue engineered nerve grafts and their application in peripheral nerve regeneration. *Progress in Neurobiology* **2011,** *93*, 204-230.

25. Pabari, A.; Yang, S. Y.; Mosahebi, A.; Seifalian, A. M., Recent advances in artificial nerve conduit design: Strategies for the delivery of luminal fillers. *Journal of Controlled Release* **2011,** *156*, 2-10.

26. Millesi, H., Microsurgery of peripheral nerves. *The Hand* **1973,** *5*, 157-160.

27. Weber, R. V.; Mackinnon, S. E., Bridging the Neural Gap. *Clinics in Plastic Surgery* **2005,** *32*, 605-616.

28. Pabari, A.; Yang, S. Y.; Seifalian, A. M.; Mosahebi, A., Modern surgical management of peripheral nerve gap. *Journal of Plastic Reconstruction & Aesthetic Surgery* **2010,** *63*, 1941-1948.

29. Ray, W. Z.; Mackinnon, S. E., Management of nerve gaps: autografts, allografts, nerve transfers, and end-to-side neurorrhaphy. *Experimental Neurology* **2010,** *223*, 77-85.

30. Kaya, Y.; Sarikcioglu, L., Sir Herbert Seddon (1903–1977) and his classification scheme for peripheral nerve injury. *Child's Nervous System* **2015,** *31*, 177-180.

31. S, S., A classification of peripheral nerve injuries producing loss of function. *Brain* **1951,** *74*, 491-516.

32. Demir, Y., Epineural Sheath Grafts for Nerve Regeneration. In *Plastic and Reconstructive Surgery*, Siemionow, M. Z., Ed. Springer London: 2015; pp 455-464.

33. Vanlair, C., De la régénération des nerfs périphériques par le procédé de la suture tubulaire. *Archives de Biologie* **1882a,** *3*, 379-496.

34. Faroni, A.; Mobasseri, S. A.; Kingham, P. J.; Reid, A. J., Peripheral nerve regeneration: Experimental strategies and future perspectives. *Advanced Drug Delivery Reviews* **2015,** *82–83*, 160-167.

35. de Ruiter, G. C.; Malessy, M. J.; Yaszemski, M. J.; Windebank, A. J.; Spinner, R. J., Designing ideal conduits for peripheral nerve repair. *Neurosurg Focus* **2009,** *26*, E5.

36. Daly, W.; Yao, L.; Zeugolis, D.; Windebank, A.; Pandit, A., A biomaterials approach to peripheral nerve regeneration: bridging the peripheral nerve gap and enhancing functional recovery. *Journal of The Royal Society Interface* **2012,** *9*, 202-221.

37. Owens, C. M.; Marga, F.; Forgacs, G.; Heesch, C. M., Biofabrication and testing of a fully cellular nerve graft. *Biofabrication* **2013,** *5*, 045007.

38. Mobasseri, S. A.; Terenghi, G.; Downes, S., Micro-structural geometry of thin films intended for the inner lumen of nerve conduits affects nerve repair. *Journal of Material Science Materials in Medicine* **2013,** *24*, 1639-1647.

39. Luo, L.; Gan, L.; Liu, Y.; Tian, W.; Tong, Z.; Wang, X.; Huselstein, C.; Chen, Y., Construction of nerve guide conduits from cellulose/soy protein composite membranes combined with Schwann cells and pyrroloquinoline quinone for the repair of peripheral nerve defect. *Biochemical and Biophysical Research Communications* **2015,** *457*, 507-513.

40. Ren, T.; Yu, S.; Mao, Z.; Gao, C., A complementary density gradient of zwitterionic polymer brushes and NCAM peptides for selectively controlling directional migration of Schwann cells. *Biomaterials* **2015,** *56*, 58-67.

41. Chiono, V.; Tonda-Turo, C., Trends in the design of nerve guidance channels in peripheral nerve tissue engineering. *Progress in Neurobiology* **2015,** *131*, 87-104.

42. Diban, N.; Stamatialis, D., Polymeric hollow fiber membranes for bioartificial organs and tissue engineering applications. *Journal of Chemical Technology & Biotechnology* **2014,** *89*, 633-643.

43. Ichihara, S.; Inada, Y.; Nakamura, T., Artificial nerve tubes and their application for repair of peripheral nerve injury: an update of current concepts. *Injury* **2008,** *39 Suppl 4*, 29-39.

44. Xiangmei, W.; Jing, Z.; Hao, C.; Qingrui, W., Preparation and characterization of collagen-based composite conduit for peripheral nerve regeneration. *Journal of Applied Polymer Science* **2009,** *112*, 3652-3662.

45. Jiang, X.; Lim, S. H.; Mao, H.-Q.; Chew, S. Y., Current applications and future perspectives of artificial nerve conduits. *Experimental Neurology* **2010,** *223*, 86-101.

46. Wang, G.-W.; Yang, H.; Wu, W.-F.; Zhang, P.; Wang, J.-Y., Design and optimization of a biodegradable porous zein conduit using microtubes as a guide for rat sciatic nerve defect repair. *Biomaterials* **2017,** *131*, 145-159.

47. Spivey, E. C.; Khaing, Z. Z.; Shear, J. B.; Schmidt, C. E., The fundamental role of subcellular topography in peripheral nerve repair therapies. *Biomaterials* **2012,** *33*, 4264-4276.

48. Goraltchouk, A.; Scanga, V.; Morshead, C. M.; Shoichet, M. S., Incorporation of protein-eluting microspheres into biodegradable nerve guidance channels for controlled release. *Journal of Controlled Release* **2006,** *110*, 400-407.

49. Wood, M. D.; Moore, A. M.; Hunter, D. A.; Tuffaha, S.; Borschel, G. H.; Mackinnon, S. E.; Sakiyama-Elbert, S. E., Affinity-based release of glial-derived neurotrophic factor from fibrin matrices enhances sciatic nerve regeneration. *Acta Biomaterialia* **2009,** *5*, 959-968.

50. Wood, M. D.; MacEwan, M. R.; French, A. R.; Moore, A. M.; Hunter, D. A.; Mackinnon, S. E.; Moran, D. W.; Borschel, G. H.; Sakiyama-Elbert, S. E., Fibrin Matrices With Affinity-Based Delivery Systems and Neurotrophic Factors Promote Functional Nerve Regeneration. *Biotechnology and Bioengineering* **2010,** *106*, 970-979.

51. Kehoe, S.; Zhang, X.; Boyd, D., FDA approved guidance conduits and wraps for peripheral nerve injury: a review of materials and efficacy. *Injury* **2012,** *43*, 553-572.

52. Siemionow, M.; Bozkurt, M.; Zor, F., Regeneration and repair of peripheral nerves with different biomaterials: review. *Microsurgery* **2010,** *30*, 574-588.

53. Wang, X.; Hu, W.; Cao, Y.; Yao, J.; Wu, J.; Gu, X., Dog sciatic nerve regeneration across a 30-mm defect bridged by a chitosan/PGA artificial nerve graft. *Brain* **2005,** *128*, 1897-1910.

54. Einige, A. E., Operationen an Nerven. *Wien Med. Presse* **1885,** *26*, 1285-1289.

55. Biazar, E.; Keshel, S. H.; Sahebalzamani, A.; Heidari, M., Design of oriented porous PHBV scaffold as a neural guide. *International Journal of Polymeric Materials and Polymeric Biomaterials* **2014,** *63*, 753-757.

56. Konofaos, P.; Ver Halen, J. P., Nerve Repair by Means of Tubulization: Past, Present, Future. *Journal of Reconstruction Microsurgery* **2013,** *29*, 149-164.

57. Tang, J. B.; Gu, Y. Q.; Song, Y. S., Repair of digital nerve defect with autogenous vein graft during flexor tendon surgery in zone 2. *Journal of Hand Surgery Br* **1993,** *18*, 449-453.

58. Kraus, H.; Reisner, H., Behandlungsergenisse von Verletungen pripherer Nerven mit besonderer Berücksichtigung der Schussverletzungen del Jahre 1919, 1927, und 1934. *Arch Klin Chir* **1940,** *199*, 318-336.

59. Brandt, J.; Dahlin, L. B.; Lundborg, G., Autologous tendons used as grafts for bridging peripheral nerve defects. *Journal of Hand Surgery-British and European Volume* **1999,** *24B*, 284-290.

60. Chiu, D. T. W.; Janecka, I.; Krizek, T. J.; Wolff, M.; Lovelace, R. E., Autogenous vein graft as a conduit for nerve regeneration. *Surgery* **1982,** *91*, 226-233.

61. Rice, D. H.; Berstein, F. D., The use of autogenous vein for nerve grafting. *Otolaryngology-Head and Neck Surgery* **1984,** *92*, 410-412.

62. Anderson, P. N.; Turmaine, M., Axonal regeneration through arterial grafts. *Journal of Anatomy* **1986,** *147*, 73-82.

63. Fawcett, J. W.; Keynes, R. J., Muscle basal lamina - a new graft material for peripheral-nerve repair. *Journal of Neurosurgery* **1986,** *65*, 354-363.

64. Smahel, J.; Jentsch, B., Stimulation of peripheral-nerve regeneration by an isolated nerve segment. *Annals of Plastic Surgery* **1986,** *16*, 494-501.

65. Chiu, D. T.; Lovelace, R. E.; Yu, L. T.; Wolff, M.; Stengel, S.; Middleton, L.; Janecka, I. P.; Krizek, T. J., Comparative electrophysiologic evaluation of nerve grafts and autogenous vein grafts as nerve conduits: an experimental study. *Journal of Reconstructive Microsurgery* **1988,** *4*, 303-309, 311-302.

66. Risitano, G.; Cavallaro, G.; Lentini, M., Autogenous vein and nerve grafts - a comparative-study of nerve regeneration in the rat. *Journal of Hand Surgery-British and European Volume* **1989,** *14B*, 102-104.

67. Ochi, M.; Ikuta, Y.; Miyamoto, Y.; Takeno, S., Experimental-evidence of selective axonal regeneration in allogenic and isogenic y-chambers. *Experimental Neurology* **1992,** *115*, 260-265.

68. Hems, T. E. J.; Glasby, M. A., Comparison of different methods of repair of long peripheral-nerve defects - an experimental-study. *British Journal of Plastic Surgery* **1992,** *45*, 497-502.

69. Wang, K. K.; Costas, P. D.; Bryan, D. J.; Jones, D. S.; Seckel, B. R., Inside-out vein graft promotes improved nerve regeneration in rats. *Microsurgery* **1993,** *14*, 608-618.

70. Benito-ruiz, J.; Navarro-monzonis, A.; Piqueras, A.; Baenamontilla, P., Invaginated vein graft as nerve conduit - an experimental-study. *Microsurgery* **1994,** *15*, 105-115.

71. Tos, P.; Battiston, B.; Nicolino, S.; Raimondo, S.; Fornaro, M.; Lee, J. M.; Chirila, L.; Geuna, S.; Perroteau, I., Comparison of fresh and predegenerated muscle-vein-combined guides for the repair of rat median nerve. *Microsurgery* **2007,** *27*, 48-55.

72. Fonseca, A. C.; Ferreira, P.; Cordeiro, R. A.; Mendonça, P. V.; Góis, J. R.; Gil, M. H.; Coelho, J. F. J., Drug delivery systems for predictive medicine: polymers as tools for

advanced applications. In *New Strategies to Advance Pre/Diabetes Care: Integrative Approach by PPPM*, Springer: 2011; pp 399-455.

73. Alluin, O.; Wittmann, C.; Marqueste, T.; Chabas, J.-F.; Garcia, S.; Lavaut, M.-N.; Guinard, D.; Feron, F.; Decherchi, P., Functional recovery after peripheral nerve injury and implantation of a collagen guide. *Biomaterials* **2009,** *30*, 363-373.

74. F. Ma, Z. X., D. Meng, X. Hou, J. Zhu, J. Dai, R. Xu, Use of Natural Neural Scaffolds Consisting of Engineered Vascular Endothelial Growth Factor Immobilized on Ordered Collagen Fibers Filled in a Collagen Tube for Peripheral Nerve Regeneration in Rats. *International Journal of Molecular Sciences* **2014,** *15*, 18593-18609.

75. Gibby, W. A.; Koerber, H. R.; Horch, K. W., A quantitative-evaluation of suture and tubulization nerve repair techniques. *Journal of Neurosurgery* **1983,** *58*, 574-579.

76. Rosen, J. M.; Padilla, J. A.; Nguyen, K. D.; Padilla, M. A.; Sabelman, E. E.; Pham, H. N., Artificial nerve graft using collagen as an extracellular-matrix for nerve repair compared with sutured autograft in a rat model. *Annals of Plastic Surgery* **1990,** *25*, 375-387.

77. Archibald, S. J.; Krarup, C.; Shefner, J.; Li, S. T.; Madison, R. D., A collagen-based nerve guide conduit for peripheral-nerve repair - an electrophysiological study of nerve regeneration in rodents and nonhuman-primates. *Journal of Comparative Neurology* **1991,** *306*, 685-696.

78. Okamoto, H.; Hata, K.; Kagami, H.; Okada, K.; Ito, Y.; Narita, Y.; Hirata, H.; Sekiya, I.; Otsuka, T.; Ueda, M., Recovery process of sciatic nerve defect with novel bioabsorbable collagen tubes packed with collagen filaments in dogs. *Journal of Biomedical Materials Research Part A* **2010,** *92*, 859-868.

79. Dienstknecht, T.; Klein, S.; Vykoukal, J.; Gehmert, S.; Koller, M.; Gosau, M.; Prantl, L., Type I Collagen Nerve Conduits for Median Nerve Repairs in the Forearm. *The Journal of Hand Surgery* **2013,** *38*, 1119-1124.

80. Haug, A.; Bartels, A.; Kotas, J.; Kunesch, E., Sensory Recovery 1 Year After Bridging Digital Nerve Defects With Collagen Tubes. *The Journal of Hand Surgery* **2013,** *38*, 90-97.

81. Giusti, G.; Shin, R. H.; Lee, J.-Y.; Mattar, T. G.; Bishop, A. T.; Shin, A. Y., The influence of nerve conduits diameter in motor nerve recovery after segmental nerve repair. *Microsurgery* **2014,** *34*, 646-652.

82. Bozkurt, A.; Boecker, A.; Tank, J.; Altinova, H.; Deumens, R.; Dabhi, C.; Tolba, R.; Weis, J.; Brook, G. A.; Pallua, N.; van Neerven, S. G. A., Efficient bridging of 20 mm rat sciatic nerve lesions with a longitudinally micro-structured collagen scaffold. *Biomaterials* **2016,** *75*, 112-122.

83. Xu, Y.; Zhang, Z.; Chen, X.; Li, R.; Li, D.; Feng, S., A silk fibroin/collagen nerve scaffold seeded with a co-culture of Schwann cells and adipose-derived stem cells for sciatic nerve regeneration. *PLoS ONE* **2016,** *11*, e0147184.

84. Fujimaki, H.; Uchida, K.; Inoue, G.; Miyagi, M.; Nemoto, N.; Saku, T.; Isobe, Y.; Inage, K.; Matsushita, O.; Yagishita, S.; Sato, J.; Takano, S.; Sakuma, Y.; Ohtori, S.; Takahashi, K.; Takaso, M., Oriented collagen tubes combined with basic fibroblast growth factor promote peripheral nerve regeneration in a 15 mm sciatic nerve defect rat model. *Journal of Biomedical Materials Research Part A* **2017,** *105*, 8-14.

85. Patel, M.; Mao, L.; Wu, B.; VandeVord, P., GDNF blended chitosan nerve guides: an *in vivo* study. *Journal of Biomedical Materials Research Part A* **2009,** *90*, 154-165.

86. Wang, G.; Lu, G.; Ao, Q.; Gong, Y.; Zhang, X., Preparation of cross-linked carboxymethyl chitosan for repairing sciatic nerve injury in rats. *Biotechnology Letters* **2010,** *32*, 59-66.

87. Freier, T.; Montenegro, R.; Shan Koh, H.; Shoichet, M. S., Chitin-based tubes for tissue engineering in the nervous system. *Biomaterials* **2005,** *26*, 4624-4632.

88. Zhang, L.; Ao, Q.; Wang, A.; Lu, G.; Kong, L.; Gong, Y.; Zhao, N.; Zhang, X., A sandwich tubular scaffold derived from chitosan for blood vessel tissue engineering. *Journal of Biomedical Materials Research Part A* **2006,** *77*, 277-284.

89. Haastert-Talini, K.; Geuna, S.; Dahlin, L. B.; Meyer, C.; Stenberg, L.; Freier, T.; Heimann, C.; Barwig, C.; Pinto, L. F.; Raimondo, S.; Gambarotta, G.; Samy, S. R.; Sousa, N.; Salgado, A. J.; Ratzka, A.; Wrobel, S.; Grothe, C., Chitosan tubes of varying degrees of acetylation for bridging peripheral nerve defects. *Biomaterials* **2013,** *34*, 9886-9904.

90. Yang, Y.; Zhao, W.; He, J.; Zhao, Y.; Ding, F.; Gu, X., Nerve conduits based on immobilization of nerve growth factor onto modified chitosan by using genipin as a crosslinking agent. *European Journal of Pharmaceutics and Biopharmaceutics* **2011,** *79*, 519-525.

91. Wang, A.; Ao, Q.; Cao, W.; Yu, M.; He, Q.; Kong, L.; Zhang, L.; Gong, Y.; Zhang, X., Porous chitosan tubular scaffolds with knitted outer wall and controllable inner structure for nerve tissue engineering. *Journal of Biomedical Materials Research Part A* **2006,** *79*, 36-46.

92. Li, G.; Zhang, L.; Wang, C.; Zhao, X.; Zhu, C.; Zheng, Y.; Wang, Y.; Zhao, Y.; Yang, Y., Effect of silanization on chitosan porous scaffolds for peripheral nerve regeneration. *Carbohydrate Polymers* **2014,** *101*, 718-726.

93. Yuan, Y.; Zhang, P.; Yang, Y.; Wang, X.; Gu, X., The interaction of Schwann cells with chitosan membranes and fibers *in vitro*. *Biomaterials* **2004,** *25*, 4273-4278.

94. Zhu, J.; Xiong, Y.; Zeng, C.; Qiang, N.; Quan, D.; Wan, J., Elastic chitosan conduits with multiple channels and well defined microstructure. *International Journal of Biological Macromolecules* **2012,** *51*, 105-112.

95. Yang, Y. M.; Gu, X. S.; Tan, R. X.; Hu, W.; Hu, W.; Wang, X. D.; Zhang, P. Y.; Zhang, T. Y., Fabrication and properties of a porous chitin/chitosan conduit for nerve regeneration. *Biotechnology Letters* **2004,** *26*, 1793-1797.

96. Chavez-Delgado, M. E.; Gomez-Pinedo, U.; Feria-Velasco, A.; Huerta-Viera, M.; Castaneda, S. C.; Toral, F. A.; Parducz, A.; Anda, S. L.; Mora-Galindo, J.; Garcia-Estrada, J., Ultrastructural analysis of guided nerve regeneration using progesterone- and pregnenolone-loaded chitosan prostheses. *Journal of Biomedical Materials Research Part B: Applied Biomaterials* **2005,** *74*, 589-600.

97. Xiao, W.; Hu, X. Y.; Zeng, W.; Huang, J. H.; Zhang, Y. G.; Luo, Z. J., Rapid sciatic nerve regeneration of rats by a surface modified collagen-chitosan scaffold. *Injury* **2013,** *44*, 941-946.

98. Tanaka, N.; Matsumoto, I.; Suzuki, M.; Kaneko, M.; Nitta, K.; Seguchi, R.; Ooi, A.; Takemura, H., Chitosan tubes can restore the function of resected phrenic nerves. *Interactive CardioVascular and Thoracic Surgery* **2015**.

99. Meyer, C.; Wrobel, S.; Raimondo, S.; Rochkind, S.; Heimann, C.; Shahar, A.; Ziv-Polat, O.; Geuna, S.; Grothe, C.; Haastert-Talini, K., Peripheral nerve regeneration through hydrogel-enriched chitosan conduits containing engineered schwann cells for drug delivery. *Cell transplantation* **2016,** *25*, 159-182.

100. Shapira, Y.; Tolmasov, M.; Nissan, M.; Reider, E.; Koren, A.; Biron, T.; Bitan, Y.; Livnat, M.; Ronchi, G.; Geuna, S.; Rochkind, S., Comparison of results between chitosan hollow tube and autologous nerve graft in reconstruction of peripheral nerve defect: An experimental study. *Microsurgery* **2016,** *36*, 664-671.

101. Guo, Q.; Liu, C.; Hai, B.; Ma, T.; Zhang, W.; Tan, J.; Fu, X.; Wang, H.; Xu, Y.; Song, C., Chitosan conduits filled with simvastatin/Pluronic F-127 hydrogel promote peripheral nerve regeneration in rats. *Journal of Biomedical Materials Research Part B: Applied Biomaterials* **2017**, n/a-n/a.

102. Aberg, M.; Ljungberg, C.; Edin, E.; Millqvist, H.; Nordh, E.; Theorin, A.; Terenghi, G.; Wiberg, M., Clinical evaluation of a resorbable wrap-around implant as an alternative to nerve repair: a prospective, assessor-blinded, randomised clinical study of sensory, motor and functional recovery after peripheral nerve repair. *Journal of Plastic, Reconstructive & Aesthetic Surgery* **2009,** *62*, 1503-1509.

103. Hazari, A.; Johansson-Ruden, G.; Junemo-Bostrom, K.; Ljungberg, C.; Terenghi, G.; Green, C.; Wiberg, M., A new resorbable wrap-around implant as an alternative nerve repair technique. *Journal of Hand Surgery Br* **1999,** *24*, 291-295.

104. Saito, T.; Tomita, K.; Juni, K.; Ooba, K., *In vivo* and *in vitro* degradation of poly (3-hydroxybutyrate) in pat. *Biomaterials* **1991,** *12*, 309-312.

105. Arslantunali, D.; Dursun, T.; Yucel, D.; Hasirci, N.; Hasirci, V., Peripheral nerve conduits: technology update. *Medical Devices (Auckland, N.Z.)* **2014,** *7*, 405-424.

106. Masaeli, E.; Morshed, M.; Nasr-Esfahani, M. H.; Sadri, S.; Hilderink, J.; van Apeldoorn, A.; van Blitterswijk, C. A.; Moroni, L., Fabrication, Characterization and

Cellular Compatibility of Poly(Hydroxy Alkanoate) Composite Nanofibrous Scaffolds for Nerve Tissue Engineering. *PLoS ONE* **2013,** *8*, e57157.

107. E. Bialzar, S. H. K., A. Sahebalzamani, M. Heidari, Design of oriented porous PHBV scaffold as a neural guide. *International Journal of Polymeric Materials and Polymeric Biomaterials* **2014,** *63*, 753-757.

108. Sahebalzamani, M.; Biazar, E.; Shahrezaei, M.; Hosseinkazemi, H.; Rahiminavaie, H., Surface Modification of PHBV Nanofibrous Mat by Laminin Protein and Its Cellular Study. *International Journal of Polymeric Materials and Polymeric Biomaterials* **2015,** *64*, 149-154.

109. Biazar, E.; Heidari Keshel, S., Development of chitosan-crosslinked nanofibrous PHBV guide for repair of nerve defects. *Artificial cells, nanomedicine, and biotechnology* **2014,** *42*, 385-391.

110. Prabhakaran, M. P.; Vatankhah, E.; Ramakrishna, S., Electrospun aligned PHBV/collagen nanofibers as substrates for nerve tissue engineering. *Biotechnology and Bioengineering* **2013,** *110*, 2775-2784.

111. Drury, J. L.; Mooney, D. J., Hydrogels for tissue engineering: scaffold design variables and applications. *Biomaterials* **2003,** *24*, 4337-4351.

112. J. Chaw, H. L., Y. Shih, C. Huang, New designed nerve conduits with a porous ionic cross-linked alginate/chitisan structure for nerve regeneration. *Bio-Medical Materials and Engineering* **2015,** *26*, 95-102.

113. Novikova, L. N.; Mosahebi, A.; Wiberg, M.; Terenghi, G.; Kellerth, J. O.; Novikov, L. N., Alginate hydrogel and matrigel as potential cell carriers for neurotransplantation. *Journal of Biomedical Materials Research Part A* **2006,** *77*, 242-252.

114. Pfister, L. A.; Papaloizos, M.; Merkle, H. P.; Gander, B., Hydrogel nerve conduits produced from alginate/chitosan complexes. *Journal of Biomedical Materials Research Part A* **2007,** *80*, 932-937.

115. Shahriari, D.; Koffler, J.; Lynam, D. A.; Tuszynski, M. H.; Sakamoto, J. S., Characterizing the degradation of alginate hydrogel for use in multilumen scaffolds for spinal cord repair. *Journal of Biomedical Materials Research Part A* **2016,** *104*, 611-619.

116. Merle, M.; Dellon, A.; Campbell, J.; Chang, P., Complications from silicon-polymer intubulation of nerves. *Microsurgery* **1989,** *10*, 130-133.

117. Chen, Y. S.; Hsieh, C. L.; Tsai, C. C.; Chen, T. H.; Cheng, W. C.; Hu, C. L.; Yao, C. H., Peripheral nerve regeneration using silicone rubber chambers filled with collagen, laminin and fibronectin. *Biomaterials* **2000,** *21*, 1541-1547.

118. Lundborg, G.; Dahlin, L.; danielsen, N., Ulnar nerve repair by the silicone chamber technique. Case report. *Scandinavian Journal of Plastic and Reconstructive Surgery and Hand Surgery* **1991,** *25*, 79-82.

119. Lundborg, G.; Rosén, B.; Dahlin, L.; Danielsen, N.; Holmberg, J., Tubular versus conventional repair of median and ulnar nerves in the human forearm: early results from a prospective, randomized, clinical study. *Journal of Hand Surgery-American Volume* **1997,** *22*, 99-106.

120. Lundborg, G.; Rosén, B.; Abrahamson, S.; Dahlin, L.; Danielsen, N., Tubular repair of the median nerve in the human forearm. Preliminary findings. *Journal of Hand Surgery* **1994,** *19*, 273-276.

121. Lundborg, G.; Dahlin, L. B.; Danielsen, N.; Gelberman, R. H.; Longo, F. M.; Powell, H. C.; Varon, S., Nerve regeneration in silicone chambers - influence of gap length and of distal stump components. *Experimental Neurology* **1982,** *76*, 361-375.

122. Ochi, M., Experimental-study on orientation of regenerating fibers in the severed peripheral-nerve. *Hiroshima Journal of Medical Sciences* **1983,** *32*, 389-406.

123. Williams, L. R.; Powell, H. C.; Lundborg, G.; Varon, S., Competence of nerve-tissue as distal insert promoting nerve regeneration in a silicone chamber. *Brain Research* **1984,** *293*, 201-211.

124. Gibson, K. L.; Daniloff, J. K., Comparison of sciatic-nerve regeneration through silicone tubes and nerve allografts. *Microsurgery* **1989,** *10*, 126-129.

125. Francel, P. C.; Francel, T. J.; Mackinnon, S. E.; Hertl, C., Enhancing nerve regeneration across a silicone tube conduit by using interposed short-segment nerve grafts. *Journal of Neurosurgery* **1997,** *87*, 887-892.

126. Azizi, S.; Mohammadi, R.; Amini, K.; Fallah, R.; Karegar, K., Bridging Small-Gap Peripheral Nerve Defect Using Silicone Rubber Chamber in the Rat Sciatic Nerve Transection Model. *Veterinary Research Forum* **2012,** *1*, 107-115.

127. Ikeguchi, R.; Kakinoki, R.; Tsuji, H.; Yasuda, T.; Matsuda, S., Peripheral nerve regeneration through a silicone chamber implanted with negative carbon ions: Possibility to clinical application. *Applied Surface Science* **2014,** *310*, 19-23.

128. Pitta, M.; Wolford, L.; Mehra, P.; Hopkin, J., Use of Gore-Tex tubing as a conduit for inferior alveolar and lingual nerve repair: experience with 6 cases. *Journal of Oral and Maxillofacial Surgery* **2001,** *59*, 493-496.

129. Shi, Z.; Gao, H.; Feng, J.; Ding, B.; Cao, X.; Kuga, S.; Wang, Y.; Zhang, L.; Cai, J., In Situ Synthesis of Robust Conductive Cellulose/Polypyrrole Composite Aerogels and Their Potential Application in Nerve Regeneration. *Angewandte Chemie International Edition* **2014,** *53*, 5380-5384.

130. Caseiro, A. R.; Pereira, T.; Ivanova, G.; Luís, A. L.; Maurício, A. C., Neuromuscular regeneration: perspective on the application of mesenchymal stem cells and their secretion products. *Stem cells international* **2016,** *2016*.

131. Thompson, B. C.; Moulton, S. E.; Richardson, R. T.; Wallace, G. G., Effect of the dopant anion in polypyrrole on nerve growth and release of a neurotrophic protein. *Biomaterials* **2011,** *32*, 3822-3831.

132. Ai, J.; Kiasat-Dolatabadi, A.; Ebrahimi-Barough, S.; Ai, A.; Lotfibakhshaiesh, N.; Norouzi-Javidan, A.; Saberi, H.; Arjmand, B.; Aghayan, H. R., Polymeric Scaffolds in Neural Tissue Engineering: A Review. *Archives of Neuroscience* **2014,** *1*, 15-20.

133. Schmidt, C. E.; Shastri, V. R.; Vacanti, J. P.; Langer, R., Stimulation of neurite outgrowth using an electrically conducting polymer. *Proceedings of the National Academy of Sciences* **1997,** *94*, 8948-8953.

134. Gomez, N.; Lee, J. Y.; Nickels, J. D.; Schmidt, C. E., Micropatterned Polypyrrole: A Combination of Electrical and Topographical Characteristics for the Stimulation of Cells. *Advanced Functional Materials* **2007,** *17*, 1645-1653.

135. Xu, H.; Holzwarth, J. M.; Yan, Y.; Xu, P.; Zheng, H.; Yin, Y.; Li, S.; Ma, P. X., Conductive PPY/PDLLA conduit for peripheral nerve regeneration. *Biomaterials* **2014,** *35*, 225-235.

136. Ribeiro, J.; Pereira, T.; Caseiro, A. R.; Armada-da-Silva, P.; Pires, I.; Prada, J.; Amorim, I.; Amado, S.; França, M.; Gonçalves, C.; Lopes, M. A.; Santos, J. D.; Silva, D. M.; Geuna, S.; Luís, A. L.; Maurício, A. C., Evaluation of biodegradable electric conductive tube-guides and mesenchymal stem cells. *World Journal of Stem Cells* **2015,** *7*, 956-975.

137. Yang, F.; Murugan, R.; Ramakrishna, S.; Wang, X.; Ma, Y.; Wang, S., Fabrication of nano-structured porous PLLA scaffold intended for nerve tissue engineering. *Biomaterials* **2004,** *25*, 1891-1900.

138. Mackinnon, S.; Dellon, A., Clinical nerve reconstruction with a bioabsorbable polyglycolic acid tube. *Plastic and Reconstructive Surgery* **1990,** *85*, 419-424.

139. Hu, W.; Gu, J.; Deng, A.; Gu, X., Polyglycolic acid filaments guide Schwann cell migration *in vitro* and *in vivo*. *Biotechnology Letters* **2008,** *30*, 1937-1942.

140. Kiyotani, T.; Nakamura, T.; Shimizu, Y.; Endo, K., Experimental study of nerve regeneration in a biodegradable tube made from collagen and polyglycolic acid. *Asaio Journal* **1995,** *41*, M657-M661.

141. Matsumoto, K.; Ohnishi, K.; Kiyotani, T.; Sekine, T.; Ueda, H.; Nakamura, T.; Endo, K.; Shimizu, Y., Peripheral nerve regeneration across an 80-mm gap bridged by a polyglycolic acid (PGA)-collagen tube filled with laminin-coated collagen fibers: a histological and electrophysiological evaluation of regenerated nerves. *Brain Research* **2000,** *868*, 315-328.

142. Waitayawinyu, T.; Parisi, D. M.; Miller, B.; Luria, S.; Morton, H. J.; Chin, S. H.; Trumble, T. E., A comparison of polyglycolic acid versus type 1 collagen bioabsorbable

nerve conduits in a rat model: An alternative to autografting. *Journal of Hand Surgery-American Volume* **2007,** *32A*, 1521-1529.

143. Nakamura, T.; Inada, Y.; Fukuda, S.; Yoshitani, M.; Nakada, A.; Itoi, S.; Kanemaru, S.; Endo, K.; Shimizu, Y., Experimental study on the regeneration of peripheral nerve gaps through a polyglycolic acid-collagen (PGA-collagen) tube. *Brain Research* **2004,** *1027*, 18-29.

144. Lee, D. Y.; Choi, B. H.; Park, J. H.; Zhu, S. J.; Kim, B. Y.; Huh, J. Y.; Lee, S. H.; Jung, J. H.; Kim, S. H., Nerve regeneration with the use of a poly(l-lactide-co-glycolic acid)-coated collagen tube filled with collagen gel. *Journal of Craniomaxillofacial Surgery* **2006,** *34*, 50-56.

145. Yang, Y.; De Laporte, L.; Rives, C. B.; Jang, J.-H.; Lin, W.-C.; Shull, K. R.; Shea, L. D., Neurotrophin releasing single and multiple lumen nerve conduits. *Journal of Controlled Release* **2005,** *104*, 433-446.

146. Wen, X.; Tresco, P. A., Fabrication and characterization of permeable degradable poly(dl-lactide-co-glycolide) (PLGA) hollow fiber phase inversion membranes for use as nerve tract guidance channels. *Biomaterials* **2006,** *27*, 3800-3809.

147. Wang, B.; Zhang, P.; Song, W.; Zhao, L.; He, C., Design and properties of a new braided poly lactic-co-glycolic acid catheter for peripheral nerve regeneration. *Textile Research Journal* **2015,** *85*, 51-61.

148. Lee, J. Y.; Bashur, C. A.; Goldstein, A. S.; Schmidt, C. E., Polypyrrole-coated electrospun PLGA nanofibers for neural tissue applications. *Biomaterials* **2009,** *30*, 4325-4335.

149. Doubra, N.; Amiri, A.; Koudehi, M. F.; Jamalpoor, Z.; Fooladi, A. A. I.; Reza, N. M., Fabrication of PLGA conduit for peripheral nerve regeneration. *Journal of Applied Tissue Engineering* **2014,** *1*, 13-19.

150. Zhu, W.; Masood, F.; O'Brien, J.; Zhang, L. G., Highly aligned nanocomposite scaffolds by electrospinning and electrospraying for neural tissue regeneration. *Nanomedicine: Nanotechnology, Biology and Medicine* **2015,** *11*, 693-704.

151. Chang, C. J.; Hsu, S. H., The effects of low-intensity ultrasound on peripheral nerve regeneration in poly(DL-lactic acid-co-glycolic acid) conduits seeded with Schwann cells. *Ultrasound in Medicine & Biology* **2004,** *30*, 1079-1084.

152. Luis, A. L.; Rodrigues, J. M.; Amado, S.; Veloso, A. P.; Armada-Da-Silva, P. A. S.; Raimondo, S.; Fregnan, F.; Ferreira, A. J.; Lopes, M. A.; Santos, J. D.; Geuna, S.; Varejao, A. S. P.; Mauricio, A. C., PLGA 90/10 and caprolactione biodegradable nerve guides for the reconstruction of the rat sciatic nerve. *Microsurgery* **2007,** *27*, 125-137.

153. Oh, S. H.; Kim, J. H.; Song, K. S.; Jeon, B. H.; Yoon, J. H.; Seo, T. B.; Namgung, U.; Lee, I. W.; Lee, J. H., Peripheral nerve regeneration within an asymmetrically porous PLGA/Pluronic F127 nerve guide conduit. *Biomaterials* **2008,** *29*, 1601-1609.

154. Shen, H.; Shen, Z.-L.; Zhang, P.-H.; Chen, N.-L.; Wang, Y.-C.; Zhang, Z.-F.; Jin, Y.-Q., Ciliary neurotrophic factor-coated polylactic-polyglycolic acid chitosan nerve conduit promotes peripheral nerve regeneration in canine tibial nerve defect repair. *Journal of Biomedical Materials Research Part B: Applied Biomaterials* **2010,** *95B*, 161-170.

155. Liu, H.; Lv, P.; Zhu, Y.; Wu, H.; Zhang, K.; Xu, F.; Zheng, L.; Zhao, J., Salidroside promotes peripheral nerve regeneration based on tissue engineering strategy using Schwann cells and PLGA: *in vitro* and *in vivo*. *Scientific Reports* **2017,** *7*, 39869.

156. Xu, F.; Zhang, K.; Lv, P.; Lu, R.; Zheng, L.; Zhao, J., NECL1 coated PLGA as favorable conduits for repair of injured peripheral nerve. *Materials Science and Engineering: C* **2017,** *70*, 1132-1140.

157. Williams, J. M.; Adewunmi, A.; Schek, R. M.; Flanagan, C. L.; Krebsbach, P. H.; Feinberg, S. E.; Hollister, S. J.; Das, S., Bone tissue engineering using polycaprolactone scaffolds fabricated via selective laser sintering. *Biomaterials* **2005,** *26*, 4817-4827.

158. Woodruff, M. A.; Hutmacher, D. W., The return of a forgotten polymer—Polycaprolactone in the 21st century. *Progress in Polymer Science* **2010,** *35*, 1217-1256.

159. Hutmacher, D. W.; Schantz, T.; Zein, I.; Ng, K. W.; Teoh, S. H.; Tan, K. C., Mechanical properties and cell cultural response of polycaprolactone scaffolds designed and fabricated via fused deposition modeling. *Journal of Biomedical Materials Research* **2001,** *55*, 203-216.

160. Frattini, F.; Lopes, F. R. P.; Almeida, F. M.; Rodrigues, R. F.; Boldrini, L. C.; Tomaz, M. A.; Baptista, A. F.; Melo, P. A.; Martinez, A. M. B., Mesenchymal Stem Cells in a Polycaprolactone Conduit Promote Sciatic Nerve Regeneration and Sensory Neuron Survival after Nerve Injury. *Tissue Engineering Part A* **2012,** *18*, 2030-2039.

161. Bliley, J. M.; Sivak, W. N.; Minteer, D. M.; Tompkins-Rhoades, C.; Day, J.; Williamson, G.; Liao, H. T.; Marra, K. G., Ethylene Oxide Sterilization Preserves Bioactivity and Attenuates Burst Release of Encapsulated Glial Cell Line Derived Neurotrophic Factor from Tissue Engineered Nerve Guides For Long Gap Peripheral Nerve Repair. *ACS Biomaterials Science & Engineering* **2015,** *1*, 504-512.

162. Sedaghati, T.; Jell, G.; Seifalian, A., Investigation of Schwann cell behaviour on RGD-functionalised bioabsorbable nanocomposite for peripheral nerve regeneration. *New Biotechnology* **2014,** *31*, 203-213.

163. Kim, J. R.; Oh, S. H.; Kwon, G. B.; Namgung, U.; Song, K. S.; Jeon, B. H.; Lee, J. H., Acceleration of Peripheral Nerve Regeneration Through Asymmetrically Porous Nerve Guide Conduit Applied with Biological/Physical Stimulation. *Tissue Engineering Part A* **2013,** *19*, 2674-2685.

164. Beigi, M.-H.; Ghasemi-Mobarakeh, L.; Prabhakaran, M. P.; Karbalaie, K.; Azadeh, H.; Ramakrishna, S.; Baharvand, H.; Nasr-Esfahani, M.-H., *In vivo* integration of poly(ε-caprolactone)/gelatin nanofibrous nerve guide seeded with teeth derived stem cells for peripheral nerve regeneration. *Journal of Biomedical Materials Research Part A* **2014,** *102*, 4554-4567.

165. Cirillo, V.; Clements, B. A.; Guarino, V.; Bushman, J.; Kohn, J.; Ambrosio, L., A comparison of the performance of mono- and bi-component electrospun conduits in a rat sciatic model. *Biomaterials* **2014,** *35*, 8970-8982.

166. Xie, J.; MacEwan, M. R.; Liu, W.; Jesuraj, N.; Li, X.; Hunter, D.; Xia, Y., Nerve Guidance Conduits Based on Double-Layered Scaffolds of Electrospun Nanofibers for Repairing the Peripheral Nervous System. *ACS Applied Materials & Interfaces* **2014,** *6*, 9472-9480.

167. Pixley, S. K.; Hopkins, T. M.; Little, K. J.; Hom, D. B., Evaluation of peripheral nerve regeneration through biomaterial conduits via micro-CT imaging. *Laryngoscope Investigative Otolaryngology* **2016,** *1*, 185-190.

168. Shahriari, D.; Shibayama, M.; Lynam, D. A.; Wolf, K. J.; Kubota, G.; Koffler, J. Y.; Tuszynski, M. H.; Campana, W. M.; Sakamoto, J. S., Peripheral nerve growth within a hydrogel microchannel scaffold supported by a kink-resistant conduit. *Journal of Biomedical Materials Research Part A* **2017,** *105*, 3392-3399.

Chapter 2. **PREPARATION OF NOVEL DEXTRAN BASED MEMBRANES FOR APPLICATION IN REGENERATIVE MEDICINE**

2.1 ABSTRACT

For the past years, many studies have been conducted proposing new materials for the preparation of scaffolds to improve peripheral nerve regeneration. Despite this fact, nerve autograph is still considered to be the "gold standard" nowadays. The goal of this work is prepare a suitable alternative to autograph, using dextran based materials. For this purpose, dextran, a biocompatible and biodegradable polysaccharide, was modified with glycidyl methacrylate (GMA) and with 2-isocyanoethymethacrylate (IEMA) aiming to prepare transparent membranes via a photocrosslinking process.[1,2] Additionally, poly(ε-caprolactone) (PCL) was modified with 2-isocyanoethymethacrylate (IEMA) to tailor the final flexibility of the dextran based membranes. The thermal properties of the membranes prepared using different formulations were characterized by TGA, DSC and DMTA techniques. The results show that the membranes are thermally stable up to temperatures around 300ºC. Moreover, T_g values decrease with the increase content of the added PCL_IEMA. The swelling capacity and degradation ratio were also evaluated. The former showed values between 50-200%. In what concerns to hydrolytic degradation *in vitro*, the membranes proved to be able to maintain their structural integrity for more than 30 days, losing only around 8-12% of their mass.

These results show that the envisaged membranes fulfill a list of important requirements, particularly transparency and low degradability, to be used as materials for nerve regeneration.

2.2 INTRODUCTION

Nowadays, peripheral nerve injury is considered to be a common health problem in the world, being the number of new patients close to 300.000 only in Europe.[3] This condition is quite worrying as it can result in severe loss of quality of life.[4]

Direct neurorrhaphy was the first technique to be proposed for the cases in which spontaneous regeneration was not sufficient for the recovery of nerve function. Unfortunately, for gaps longer than 5mm, the tension created by the direct suturing of the nerve stumps can be excessive jeopardizing the recovery process.[5,6] For this reason, nerve autographs were proposed to bridge longer nerve gaps.[7,8] However, several disadvantages arise from this procedure, being site morbidity one of the most significant. To circumvent

the aforementioned issues, studies have been conducted to propose feasible strategies that allow the nerve reinnervation.

Biomedical devices, as scaffolds, have been receiving important attention. These devices should provide a proper environment for the growing of new axons and reach the distal nerve stump.

In this context, polymeric membranes were considered to be candidates as they can be wrapped and sutured to both ends of the injured nerve. Natural and synthetic polymers have been used with this approach.

In what concerns natural polymers, chitosan is one of the most studied, being already been proposed as base material for the preparation of membranes.[9,10] Some studies regarding the use of chitosan based membranes demonstrated their ability to promote cell adhesion, proliferation and differentiation.[11,12] Additionally, the bridge of the two nerve stumps with nerve fiber regeneration and functional recovery was also reported.[11] In fact, hybrid chitosan membranes used to bridge a rat sciatic after crushing, revealed enhanced axon number and myelin thickness affecting positively the recovery of the functionality of the nerve.[13]

Regarding synthetic polymers, membranes prepared with polycaprolactone (PCL), polyurethane (PU) and poly(dimethylsiloxane) (PDMS) have been studied and tested *in vitro* with encouraging results.[14] Also, published studies show that poly(DL-lactide-ε-caprolactone) (PLA-co-CL) membranes promote the differentiation of human mesenquimal stem cells into neuroglial-like cells.[15] These membranes were also tested in a neurotmesis of the rat sciatic nerve model, during a period of time of 20 weeks showing promising results specially regarding the recovery of motor function.[15]

Nevertheless, the major disadvantages concerning the use of both natural and synthetic polymers are the fragility during suturing and inappropriate *in vivo* degradation rate.

Some membranes or wraps using natural and synthetic polymers were already approved by FDA and are available under the commercial name of: Salubridge™ (poly(vinyl alcohol) (PVA)); AxoGuard™ Nerve Protector (Porcine small intestine submucosa (SIS)); NeuraWrap™ (Type I Collagen) and NeuroMend™ (Type I Collagen).[16]

Despite the extensive studies, none of the listed materials present a performance comparable to those obtained with nerve autograft. The main disadvantages are related to the degradation rate *in vitro*, which can be too long (48 months for NeuraWrap™), or too fast (8 months for NeuroMend™ and AxoGuard™).[16] Also, for the non resorbable product

Salubridge™, high compression and tension in the suture lines are the major disadvantages.[16]

The present work intends to prepare dextran based materials as potential candidates for peripheral nerve regeneration.

Dextran is a polysaccharide well known as a biocompatible material.[17,18] It is already used in many biomedical applications such as drug delivery systems and wound dressings.[19-25] This polymer is also biodegradable and its degradation products are non-toxic. The degradation occurs through the action of the dextranase enzyme in organs such as liver, spleen, kidneys and colon.[26] However, albeit its interesting advantages, dextran presents poor mechanical properties,[27,28] and hence its modification is often needed.[27,29,30]

In this work, dextran was modified with incorporation of double bonds by its reaction with glycidyl methacrylate (GMA) or 2-isocyanatoethyl methacrylate (IEMA). Membranes using methacrylated dextrans were prepared, and in order to fine tune their properties a co-macromonomer, PCL dimethacrylate, was added to the formulation. The PCL dimethacrylate was obtained from the reaction of PCL with hydroxyl terminal groups with IEMA (PCL-IEMA). Transparent membranes were obtained upon the photocrosslinking reaction of the modified dextran with the PCL dimethacrylate, in the presence of Irgacure 2959® as the photoinitiator. Photocrosslinking technique brings advantages since there is no need of high temperatures (70-80ºC in the case of thermal polymerization), which avoids the occurance of undesirable side reactions that could alter the final structure of the polymer.[31,32] In addition, this technique requires small quantities of photoinitiator.[31] The photoinitiator - Irgacure 2959®, is a safe product presenting biocompatibility in the presence of different cell lines.[33]

The membranes were characterized regarding their thermal stability, thermomechanical properties, swelling capacity and *in vitro* hydrolytic degradation behavior.

2.3 EXPERIMENTAL SECTION

2.3.1 Materials

Dextran (Mw=70000 g/mol and Mw=200000 g/mol) and phosphate buffered saline (PBS) tablets were purchased from Sigma Aldrich (St. Louis, Missouri, USA). Glycidyl methacrylate (GMA) was purchased from Acros Organics (Geel, Belgium). 4-

Dimethylaminopyridine (DMAP), 2-Isocyanatoethyl methacrylate (IEMA) were acquired from TCI Europe (Zwijndrecht, Bélgica) and dimethyl sulfoxide (DMSO) was purchased from Fisher Scientific (Hampton, New Hampshire, EUA). Dibutyltin dilaurate was obtained from Fluka (St. Louis, Missouri, USA). Tetrahydrofuran (THF) was obtained from VWR (Radnor, Pensilvânia, EUA) and *n*-hexane was obtained from José Manuel Gomes dos Santos, Lda (Odivelas, Portugal). Poly(ε-caprolactone)-diol (PCL-diol Capa ™2054; Mw=550 g/mol) was a gift from Perstorp(Warrington, UK). Irgacure 2959® was gently supplied by Ciba Specialty Chemicals (Basel, Switzerland). D_2O and DMSO-d_6 were acquired from Euriso-Top (Saint-Aubin, France). Sodium azide was purchased from Panreac (Barcelona, Spain).

2.3.2 Synthesis and Procedures

Modification of Dextran with GMA

The modification of low molecular weight dextran (70.000 g/mol) (P_LMW) and high molecular weight dextran (200,000 g/mol) (P_HMW) with GMA (Figure 2.1) was adapted from elsewhere.[34] First, 2.5g (1.54×10^{-2} mol) of dextran were dissolved in 22.5mL of DMSO in a round bottom flask. The flask was immersed in a water bath at 30ºC. After the complete solubilization of dextran, 0.5g (4.09×10^{-3} mol) of DMAP was dissolved in the solution and 2.05mL (1.54×10^{-2} mol) of GMA was added. The reaction proceeded for 8h or 24h, under nitrogen atmosphere. After this time, to neutralize the solution, 0.33mL of HCl 37% (w/w) was added. The product of the reaction was then dialyzed against water. The product was freeze dried, leading to a sponge-like product. Four products were synthesized: P_LMW_GMA8 corresponding to 8h of reaction; P_LMW_GMA24 referring to 24h of reaction; P_HMW_GMA8 (8h reaction) and P_HMW_GMA24 (24h reaction).

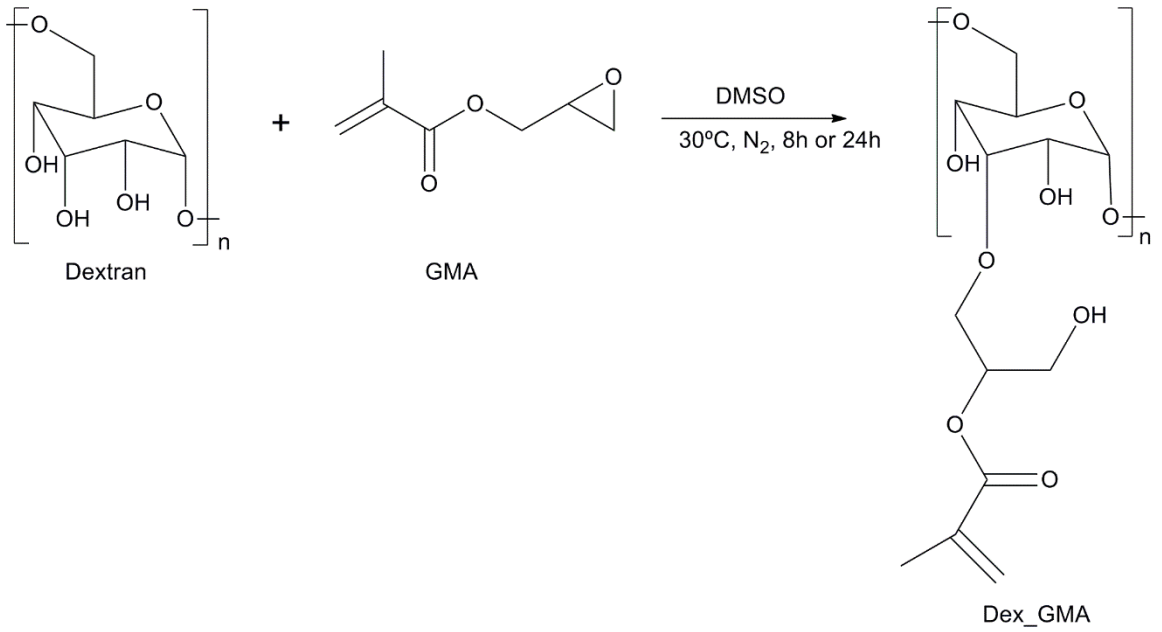

Figure 2.1 Scheme of the reaction between dextran and GMA.

Modification of Dextran with IEMA

The modification of low molecular weight dextran (P_LMW) and dextran of high molecular weight (P_HMW) with IEMA (Figure 2.2) was adapted from elsewhere.[35] Briefly, 2.5g (3.57×10^{-5} and 1.25×10^{-5} mol) of dextran were dissolved in 22.5mL of DMSO by stirring in a round bottom flask, under nitrogen atmosphere. The vessel was placed in a water bath at 60ºC. After the dextran dissolution, 6.54mL (0.0463 mol) of IEMA were added. The reaction was allowed to proceed during 24h. The product of the reaction was recovered from precipitation in distilled water, followed by drying under vacuum, at 40 ºC, until constant weight (yield=80%, ≈ 2 g).

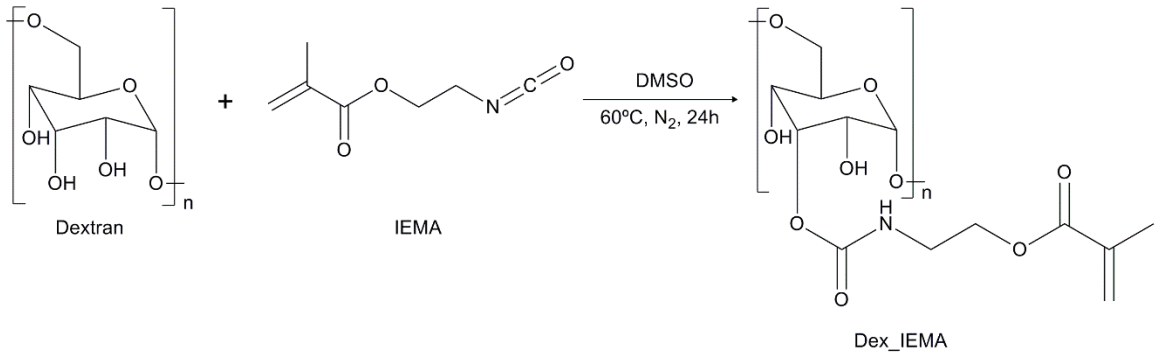

Figure 2.2 Schematic representation of dextran modification with IEMA.

Modification of PCL-diol with IEMA

The modification of PCL-diol with IEMA (Figure 2.3) was adapted from elsewhere.[36] In a round bottom flask placed in a water bath at 40ºC, 2.2g (4 mmol) of PCL-diol was dissolved in 30mL of THF, under nitrogen atmosphere. After PCL-diol solubilization, 1.27g (8.2 mmol) of IEMA and 150 mg dibutyltin dilaurate (3 drops) were added to the reaction mixture. The reaction was allowed to proceed for 24h. The product was recovered by precipitation in *n*-hexane and dried under vacuum, until constant weight, at room temperature (yield=90%, ≈2 g). The scheme of the reaction is presented in Figure 2.3.

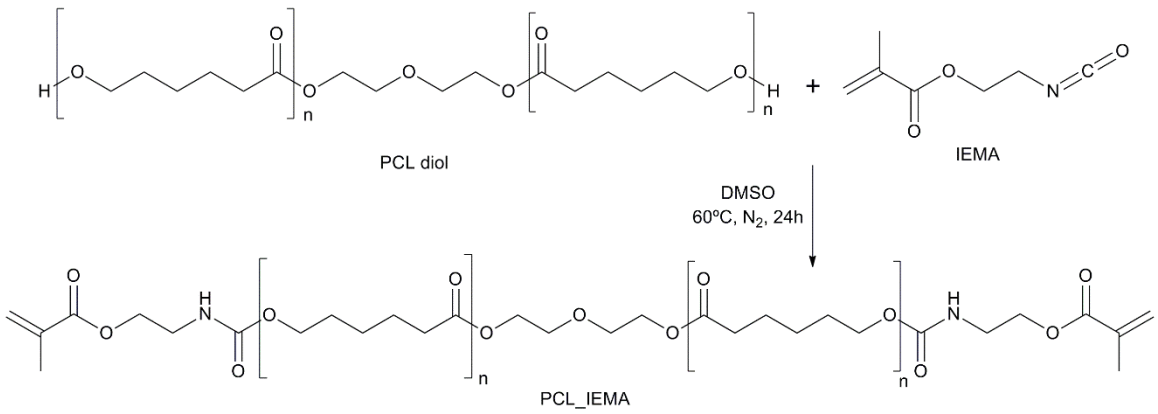

Figure 2.3 Schematic representation of the modification of PCL with IEMA.

Preparation of the Membranes

Modified dextran and/or PCL-dimethacrylate were dissolved in 2mL of DMSO, according to Table 2.1. After the dissolution of the components, a biocompatible photoinitiator Irgacure 2959® was added in a concentration of 0.1/ w/v ($1.11x10^{-2}$ mmol).[37,38] The solution was then placed in a Petri dish and left to photocrosslink in a UV chamber (Model BS-02, from Dr. Gröbel, UV-Electronik GmbH), with light with a wavelength of 280 nm, for 2 hours, to yield transparent membranes. The membranes were then washed with distilled water during 7 days. After the washing process, the membranes were cut in circles with a diameter of 1cm and dried under vacuum, at room temperature, in a desiccator.

Table 2.1 Amounts of modified dextran and PCL-IEMA used in the preparation of the membranes.

Designation	Modified dextran	PCL-IEMA
M_LMW_GMA8(0.5)_PCL(0)	0.5g P_LMW_GMA8	--------
M_LMW_GMA8(0.2)_PCL(0.2)	0.2g P_LMW_GMA8	0.2g
M_LMW_GMA8(0.1)_PCL(0.3)	0.1g P_LMW_GMA8	0.3g
M_LMW_GMA24(0.2)_PCL(2)	0.2g P_LMW_GMA24	0.2g
M_LMW_GMA24(0.1)_PCL(0.3)	0.1g P_LMW_GMA24	0.3g
M_HMW_GMA8(0.5)_PCL(0)	0.5g P_HMW_GMA8	--------
M_HMW_GMA8(0.2)_PCL(0.2)	0.2g P_HMW_GMA8	0.2g
M_HMW_GMA8(0.1)_PCL(0.3)	0.1g P_HMW_GMA8	0.3g
M_HMW_GMA24(0.2)_PCL(0.2)	0.2g P_HMW_GMA24	0.2g
M_HMW_GMA24(0.1)_PCL(0.3)	0.1g P_HMW_GMA24	0.3g
M_LMW_IEMA(0.5)_PCL(0)	0.5g P_LMW_IEMA	--------
M_LMW_IEMA(0.2)_PCL(0.2)	0.2g P_LMW_IEMA	0.2g
M_LMW_IEMA(0.1)_PCL(0.3)	0.1g P_LMW_IEMA	0.3g

2.3.3 Characterization Techniques

Chemical Structure Identification

FTIR spectra were obtained using a Jasco FT/IR-4200 spectrometer with ATR mode, at room temperature. Data were collected in the range 4000-500 cm^{-1} with 4 cm^{-1} spectral resolution and 64 accumulations.

The ^{1}H NMR spectra were obtained at 25ºC on a Bruker Avance III 400MH spectrometer using a triple detection TIX 5mm probe. For dextran and modification products, the solvent used was D_2O and specific conditions were used, as described elsewhere.[34] Briefly, a pulse angle of 87.7º was used with a relaxation delay of 30s. The water signal at 4.8 ppm was eliminated by solvent suppression with decoupling. The decoupling power was adjusted to a level at which the intensity of the anomeric proton signal was not affected. For PCL-diol and PCL-dimethacrylate, the solvent used was DMSO-d_6. TMS was used as the internal standard.

Thermogravimetric Analysis

The thermal stability of the materials was evaluated by thermogravimetric analysis (TGA) using a TA Instruments Q500 equipment. The range of temperatures between 25ºC and 600ºC was used. The heating rate of 10ºC.min^{-1} and the analysis was performed under nitrogen atmosphere.

Differential Scanning Calorimetry and Dynamic Mechanical Thermal Analysis

The thermal behavior of the materials before degradation was evaluated by Differential Scanning Calorimetry (DSC). The equipment used is a TA Instruments Q100, equipped with a RSC90 cooling unit. The modified dextran and the membranes were first heated from 25ºC to 250ºC, followed by a cooling cycle from 250 ºC to -80ºC in order to eliminate their thermal history. The samples were then submitted to a second heating cycle from -80 ºC to 250 ºC.

In the case of PCL-diol and PCL-IEMA, the first heating cycle was performed from 25ºC to 150 ºC, followed by a cooling cycle until -80 ºC. The second heating cycle was performed from -80ºC to 150 ºC.

The heating rate was 10 ºC.min^{-1} and the analysis was done under N_2 atmosphere (50 mL.min^{-1}). The mass of the samples was between 7 mg and 9 mg were used.

The Dynamic Mechanical Thermal Analysis (DMTA) of the samples was conducted in a Tritec2000DMA. The samples were placed in stainless steel material pockets and analyzed in single cantilever mode. The tests were carried out in a temperature range from -150ºC to 300ºC, with a heating rate of 10ºC.min^{-1}, in multifrequency mode. The T_g was determined from the peak of tan δ curve, at 1Hz.

Swelling Capacity

The swelling capacity of circular membranes with 1cm diameter was measured in PBS (pH=7.4, 0.01M). Dried samples with a known dried weight were immersed in 5mL of PBS, at 37ºC, until a swelling equilibrium was achieved. At predetermined times, the samples were taken out from the PBS, and the surface water gently blotted by filter paper. The swollen samples were then weighted and the swelling capacity was calculated using the equation 2.1

$$Swelling\ Capacity\ (\%) = \frac{W_s - W_d}{W_d} \times 100 \qquad \text{eq } \mathbf{2.1}$$

Where W_s is the weight of the swollen samples and W_d is the weight of the dried samples before the immersion in PBS. The measurements were conducted in triplicate.

In vitro hydrolytic degradation

In vitro hydrolytic degradation tests were performed in PBS (pH=7.4, 0.01M). Dried circular membranes with 1cm diameter and with known weight were immersed in PBS, at 37ºC, during 30 days. At predetermined times, the membranes were removed from PBS,

rinsed with distilled water and dried. The drying process was accomplished in two phases: first, the samples were dried under vacuum at room temperature for a week, and then dried at 50ºC until the stabilization of their weight. The estimation of the degree of degradation was made through the calculation of the weight loss after incubation, according to the equation 2.2

$$Weight\ Loss\ (\%) = \frac{W_0 - W_t}{W_0} \times 100 \qquad \text{eq. } \mathbf{2.2}$$

Where W_0 is the initial weight of the dry sample before being immersed and W_t is the weight of the dry sample after being immersed in PBS and dried. The measurements were conducted in triplicate.

2.4 RESULTS AND DISCUSSION

As mentioned before, the aim of this work was the development of dextran based materials to be further tested in peripheral nerve regeneration process. In order to improve mechanical properties, the dextran was modified with double bonds, which were photocrosslinked to yield transparent membranes. In addition to the modified dextran, a PCL based macromonomer (PCL-IEMA) was added to formulation, in different amounts, in order to tune some of the properties of the membranes (e.g., balance between hydrophobic and hydrophilic character, swelling capacity, *in vitro* hydrolytic degradation, thermomechanical properties). PCL was chosen as core material of the co-macromonomer because it has been extensively used in applications in the biomedical field.[39] Besides the amount of macromonomer, the influence of the dextran molecular weight, the influence of the hydroxyl groups of dextran, the influence of the monomer used to perform the modification (ether bond, in the case of GMA or urethane bond, in the case of IEMA), and the influence of dextran's degree of modification in the final properties of the membranes were also assessed.

This section is divided in two parts: the first part describes the synthesis and characterization of the precursors of the membranes (modified dextran and PCL-IEMA) and the second part is devoted to the preparation and characterization of the membranes.

2.4.1 Synthesis of the precursors and their chemical structure identification

Modification of Dextran with GMA and IEMA

In order to introduce unsaturations in the dextran backbone GMA and IEMA monomers were incorporated into dextran structure. As the degree of substitution may depend on the reaction time two derivatives were prepared one with 8 h of reaction and the other with 24 h reaction. For dextran modification with IEMA only the 24 h reaction was tested.
Figure 2.4 presents the FTIR spectra of pristine dextran and dextran after being modified with GMA or IEMA.

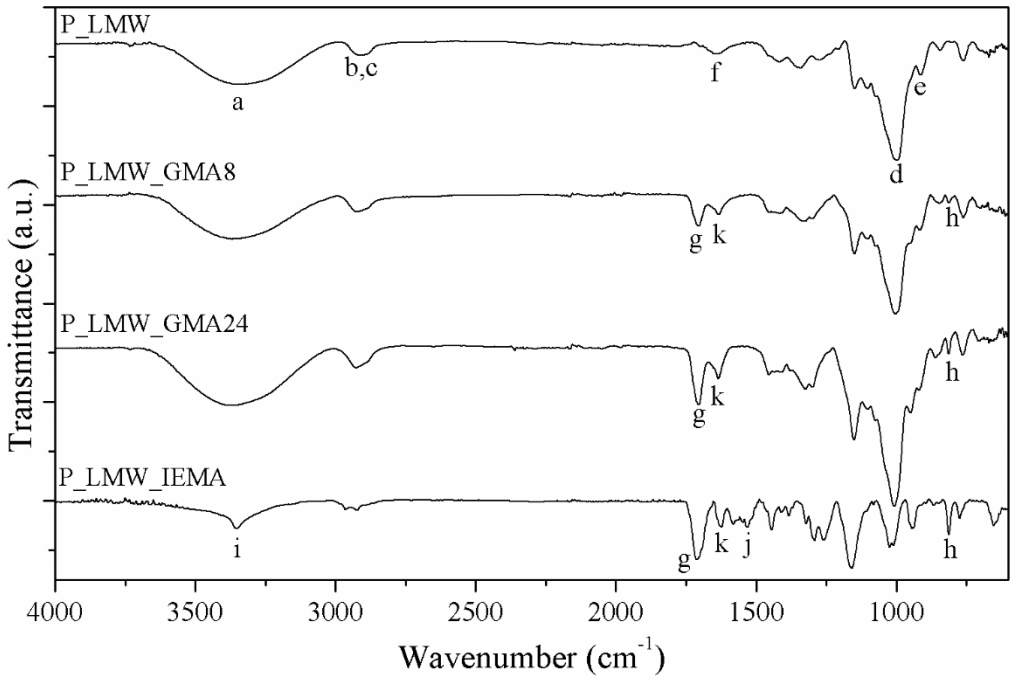

Figure 2.4 FTIR spectra of dextran and respective products of modification.

In the dextran spectrum it is possible to identify the typical bands found in this polysacharide, namely the stretching vibration of -OH groups (a) which can be observed at 3300cm^{-1}.[40] At 2910cm^{-1} it is possible to observe the bands corresponding to the stretching vibration of both CH and CH_2 groups (b and c, respectively).[41,42] Between 1000-1100cm^{-1}, there are the bands corresponding to the stretching vibration of ether linkages[43] (d) and at

914cm^{-1} it is the band ascribed to the vibration of the α-glycosidic bond (e).[44] At 1636cm^{-1}, it is possible to observe the band that corresponds to the bending of bound water (f).[45]
Regarding the spectra of the products of modification of dextran with GMA (P_LMW_GMA8 and P_LMW_GMA24), it is possible to observe some differences in relation to the spectra of pristine dextran. A new band at *ca.* 1710cm^{-1} (g) corresponds to the stretching vibration of the carbonyl group of the ester linkage (present in GMA).[34] The bending vibration of the methacrylate group can be seen in both spectra at 813cm^{-1} (h).[34] The stretching vibration of the double bond can be seen at 1650 cm^{-1} (k).
In what concerns the modification of dextran with IEMA, it is possible to observe the appearance of a set of new bands, namely at *ca.* 3352cm^{-1}, which corresponds to the stretching vibration of the -NH bond (i). The band at *ca.* 1531cm^{-1} is ascribed to the stretching and bending vibrations of C-N and N-H linkages (j).[35] At 812cm^{-1} is present band that corresponds to the bending of CH_3 (h), at *ca.* 1710 cm^{-1} (g) corresponds to the stretching vibration of the carbonyl group present in the urethane linkage and at 1650 cm^{-1} (k) there is the stretching vibration of the C=C bonds.
The FTIR spectra obtained for the modifications of P_HMW are similar to those of the modifications of P_LMW, and are presented in Figure A.1.

The products of modification of P_LMW were also analysed by ^{1}H NMR spectroscopy. Figure 2.5 presents the spectra of pristine dextran and dextran modified with GMA for 24h (P_LMW_GMA24). The spectrum of the product of modification of dextran with GMA for 8h (P_LMW_GMA8) are in Figure A.2. The spectrum of P_HMW, P_HMW_GMA8 and P_HMW_GMA24 are shown in Figure A.3.

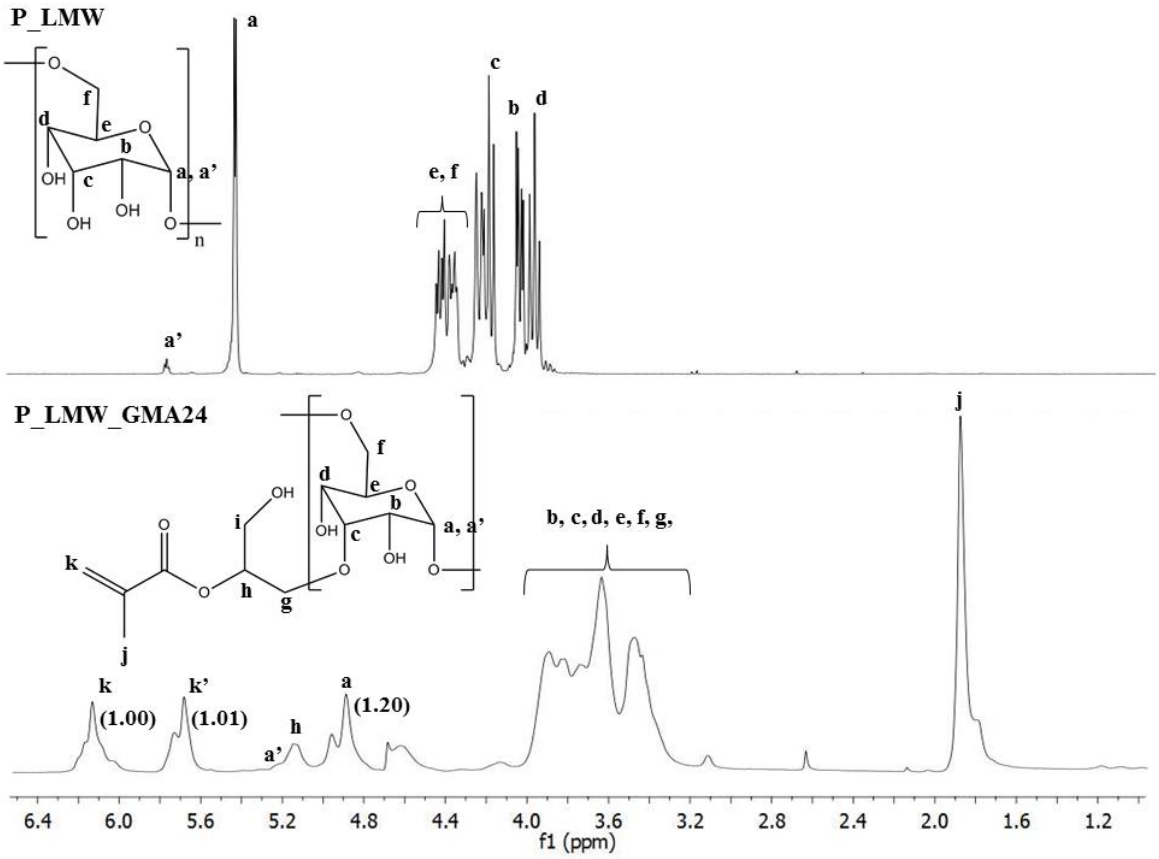

Figure 2.5 ^{1}H NMR spectra of P_LMW and P_LMW_GMA24 (in brackets are indicated the values of the relative integrals used in DS calculation).

In the ^{1}H NMR spectrum of P_LMW in D_2O, it can be observed the typical peaks of dextran polymer, which are the multiplet peaks in the range from 4.0ppm and 3.3ppm and the anomeric proton peak that is visible at around 5.3 ppm(a').[34]

The spectrum of P_LMW_GMA24 shows additional ressonances at *ca.* 6.1 and 5.7 ppm (k), ascribed to the protons of the double bonds, and at *ca.* 1.9 ppm (j), corresponding to the protons of the $–CH_3$ group belonging to the methacrylate group. The percentage of modification of dextran was calculated from the relation between the integrals values of the signals corresponding to dextran and to the double bond of GMA. The calculation of the degree of modification of dextran was carried out using Equation A.1. As expected, the P_LMW_GMA8 present a lower degree of substitution (average 31-34%) compared with the P_LMW_GMA24 (average 44-48%).

In what concerns the modification of P_LMW with IEMA, the ^{1}H NMR spectrum is presented in Figure 2.6. The spectrum of the modification of P_HMW with IEMA is showed in Figure A.4.

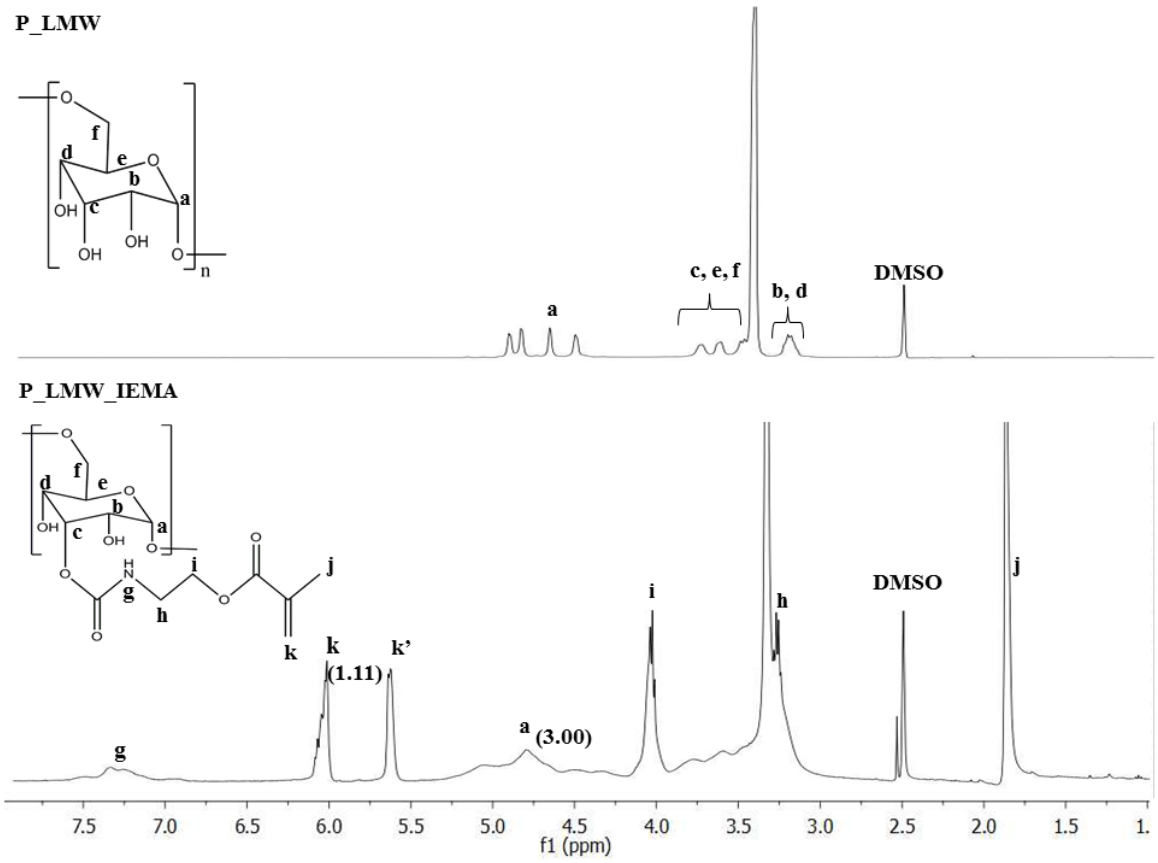

Figure 2.6 ^{1}H NMR spectra of P_LMW and P_LMW_IEMA (in brackets are indicated the values of the integrals of the peaks).

Although the use of a different solvent (DMSO-*d6*), the spectrum of pristine dextran presents the characteristic peaks discussed above. At 4.7 ppm, it is possible to see the peak of the anomeric proton.[46] The other signals at this zone 4.5-5.0 corresponds to the hydrogen of OH groups.[47] The multiplet (*ca.* 3.7-3.0 ppm) is divided into 2 multiplets corresponding to the protons of the glycosidic ring.

Relatively to the spectrum of P_LMW_IEMA signals relatively to double bonds is clearly visible at 5.6 and 6.1ppm. At *ca.* 7.3 ppm appears a new peak which corresponds to the proton of the NH group, belonging to the urethane linkage. At 1.8 ppm the signal corresponds to the hydrogens of methyl group. This peak and the multiple peaks of the glucopyranosyl ring are also present in the spectrum of the P_LMW_GMA.

Similarly, to P_LMW_GMA, the percentage of modification of P_LMW_IEMA was determined from the relation between the integrals values of the peaks corresponding to

dextran and to IEMA. The calculated modification percentage was *ca.* 45-50% for P_LMW_IEMA, and *ca.* 50-55% for P_HMW_IEMA.

Modification of PCL with IEMA

PCL-diol was modified with IEMA (Figure 2.7) in order to prepare a PCL-dimethacrylate that was used as co-macromonomer in the formulation of the membranes. Figure 2.7 presents the FT-IR spectra of neat PCL-diol and PCL modified with IEMA (PCL-IEMA).

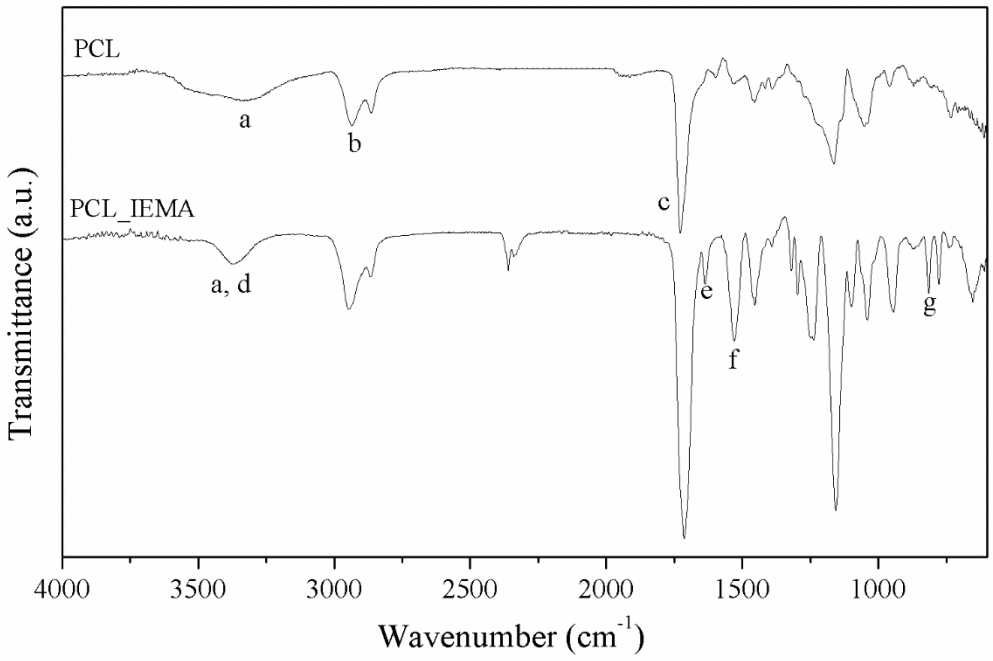

Figure 2.7 FTIR spectra of PCL-diol and PCL_IEMA.

In the PCL-diol spectrum, it is possible to identify the following bands: (a) 3340cm^{-1}, corresponding to the vibration of –OH groups, (b) 2940cm^{-1} and 2865cm^{-1}, corresponding to asymmetric and symmetric stretching of CH_2, respectively. The peak at (c) 1730cm^{-1} is ascribed to the stretching vibration of the –C=O group of the ester linkage.[48,49]

In the spectrum of PCL_IEMA, it is possible to identify the characteristic bands of the urethane linkage, confirming the successful modification of the PCL-diol structure. The first of these bands is at (d) 1720cm^{-1}, corresponding to the stretching vibration of the carbonyl group of the ester from PCL-diol, which is overlapped with the carbonyl group belonging to the urethane linkage. Then, at (e) 1630cm^{-1} is ascribed to the stretching vibration of the C=C group. Furthermore, at (f) 1566cm^{-1} the bands corresponding to the

bending vibration of N-H and stretching vibration of C-N groups can also be observed.[50] Additionally, it is noted the disappearance of the broad band corresponding to the –OH groups, and the appearance of a more sharp band characteristic of the stretching vibration of the –NH group. At (g) 817cm^{-1} appears the band corresponding to the bending vibration of the double bonds of methacrylate group. The strong band characteristic of isocyanate group (2270cm^{-1}) is not visible. This indicates that all the isocyanate groups were consumed during the modification.[36]

The ^{1}H NMR spectra of PCL-diol (Mw=550) and PCL-IEMA are presented in Figure 2.8.

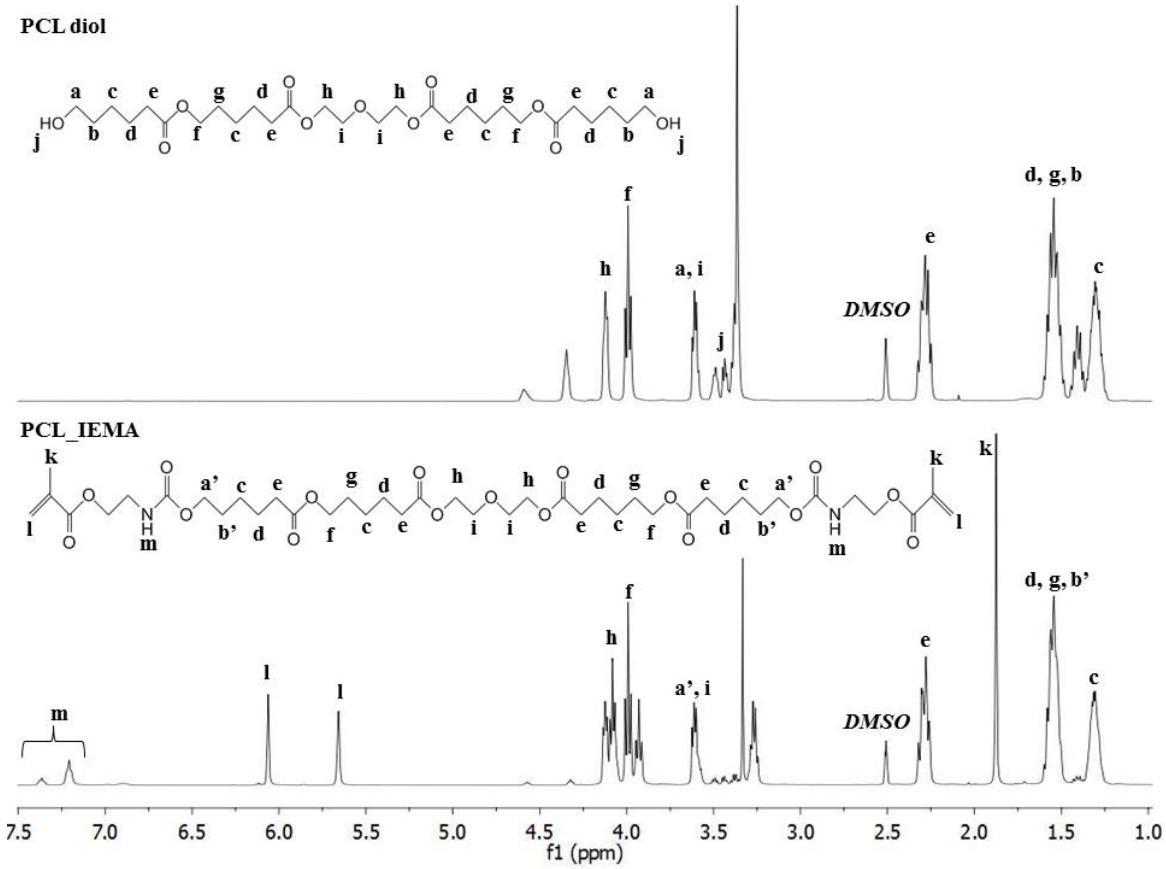

Figure 2.8 ^{1}H NMR spectra of PCL diol and PCL_IEMA.

The ^{1}H NMR spectrum of PCL-diol presents the typical resonances of PCL.[51,52] In the case of PCL_IEMA's ^{1}H NMR spectrum, it is shown clearly the resonance corresponding to the –NH group (m) of the urethane linkage, at 7.2-7.4 ppm. It is also possible to identify the peaks corresponding to the protons of the double bonds (l), at 5.6 and 6.1 ppm, and the peaks of the protons of the –CH_3 groups (k), at 1.8 ppm. Moreover, it is possible to see that

the resonances corresponding to the protons of the terminal groups in PCL-diol (j) disappeared in the spectrum of PCL_IEMA.

2.4.2 Thermal Properties of the precursors

Thermal properties of dextran and respective products of modification

The thermal stability of dextran and products of modification was evaluated by TGA, in a temperature range from 25 to 600ºC, under nitrogen atmosphere. The thermoanalytical curves are shown in Figure 2.9.

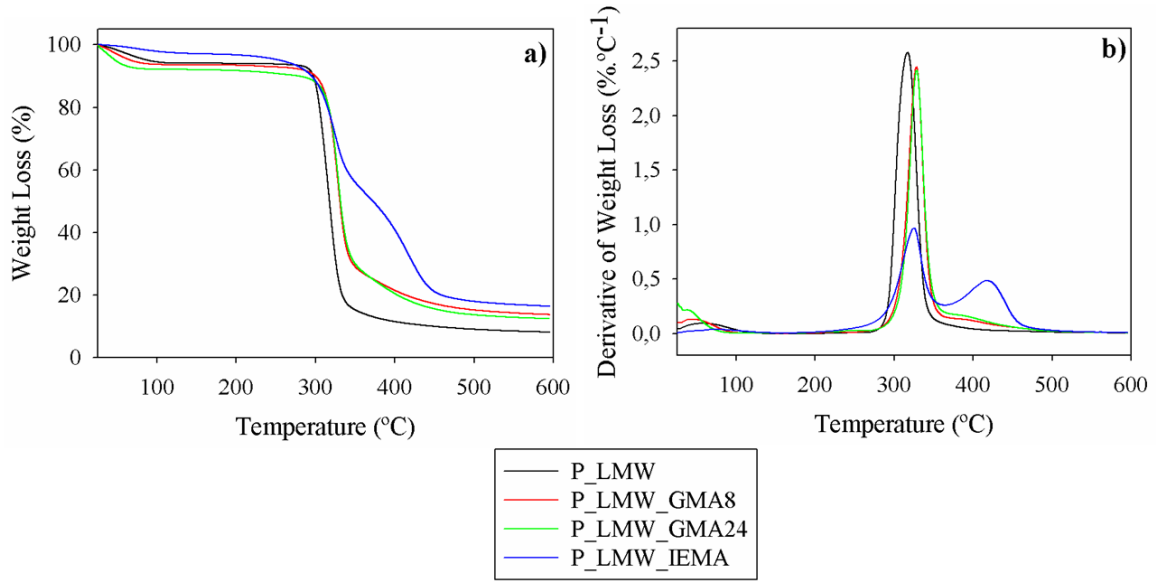

Figure 2.9 Thermoanalytical curves of dextran, P_LMW_GMA and P_LMW_IEMA: a) TG, and b) DTG.

The thermoanalytical curve of dextran presents two stages of weight loss. For dextran modified with GMA and IEMA, three stages of weight loss can be identified. The first stage of weight loss, between 25 to 150ºC, is common to all samples, can be attributed to the loss of residual moisture.[53] The second stage of decomposition, between 270-370ºC, refers to the degradation of the polysaccharide dextran chains.[54] This stage of weight loss is also present in all curves. The additional stages of weight loss observed for P_LMW_GMA8, P_LMW_GMA24 and P_LMW_IEMA can be ascribed to the degradation of the modified

part of dextran. In the case of the modifications with GMA, the temperature at which appears the third of weight loss is still in the range of the decomposition of pristine dextran (270ºC-370ºC). These data suggest that the thermal stability of dextran is not affected by the modification with GMA. On the other hand, for the modification with IEMA, the decomposition stages are more distinguished. The mass loss observed at 400-600ºC could be ascribed to decomposition of the urethane groups but also to the decomposition of allophanates, carbodiimides, isocyanurates, ureas and biuret that can be formed as side reaction of the isocyanite groups.[55,56] Those reactions can occur during the reaction between dextran and IEMA, or during the product precipitation in water.[55] Furthermore, the decomposition of P_LMW_IEMA originates 8% of residual char that may came from the complex pattern of decomposition.[56] This may justify the difference in the mass at the final of the test between both pristine and modified dextran (around 8% of mass). The thermoanalytical curves of the products of modification of P_HMW present similar profiles and can be found in Figure A.5.

The relevant temperatures obtained from the thermoanalytical curves are summarized in Table 2.2.

Table 2.2 Characteristic temperatures obtained by TGA.

	T_{on} (ºC)	$T_{5\%}$ (ºC)	$T_{10\%}$ (ºC)	$T_{p,1}$ (ºC)	$T_{p,2}$ (ºC)
P_LMW	300.80	297.85	302.93	316.68	----
P_LMW_GMA8	313.74	304.82	313.90	328.08	393.87
P_LMW_GMA24	314.90	299.26	313.31	328.64	387.63
P_LMW_IEMA	298.96	280.55	301.67	325.19	417.35
P_HMW	297.44	295.20	299.38	312.94	----
P_HMW_GMA8	310.54	303.69	311.06	324.67	400.11
P_HMW_GM24	314.13	305.25	314.92	328.64	387.63
P_HMW_IEMA	308.34	301.42	312.76	328.08	412.02

T_{on}: Temperature of onset; $T_{5\%}$: Temperature to which corresponds 5% of weight loss; $T_{10\%}$: Temperature to which corresponds 10% of weight loss; T_p: peak temperature.

The temperatures presented in Table 2.2 allow concluding that all materials are thermally stable until temperatures around 300 ºC. Regarding the values of T_{on}, $T_{5\%}$ and $T_{10\%,}$ all samples present similar values, indicating that the modifications carried out did not have any deleterious effect in the thermal stability of the materials.

The thermal events of dextran and modified dextran below the degradation temperature were studied by DSC and DMTA. The heat flow curves are presented in Figure 2.10.

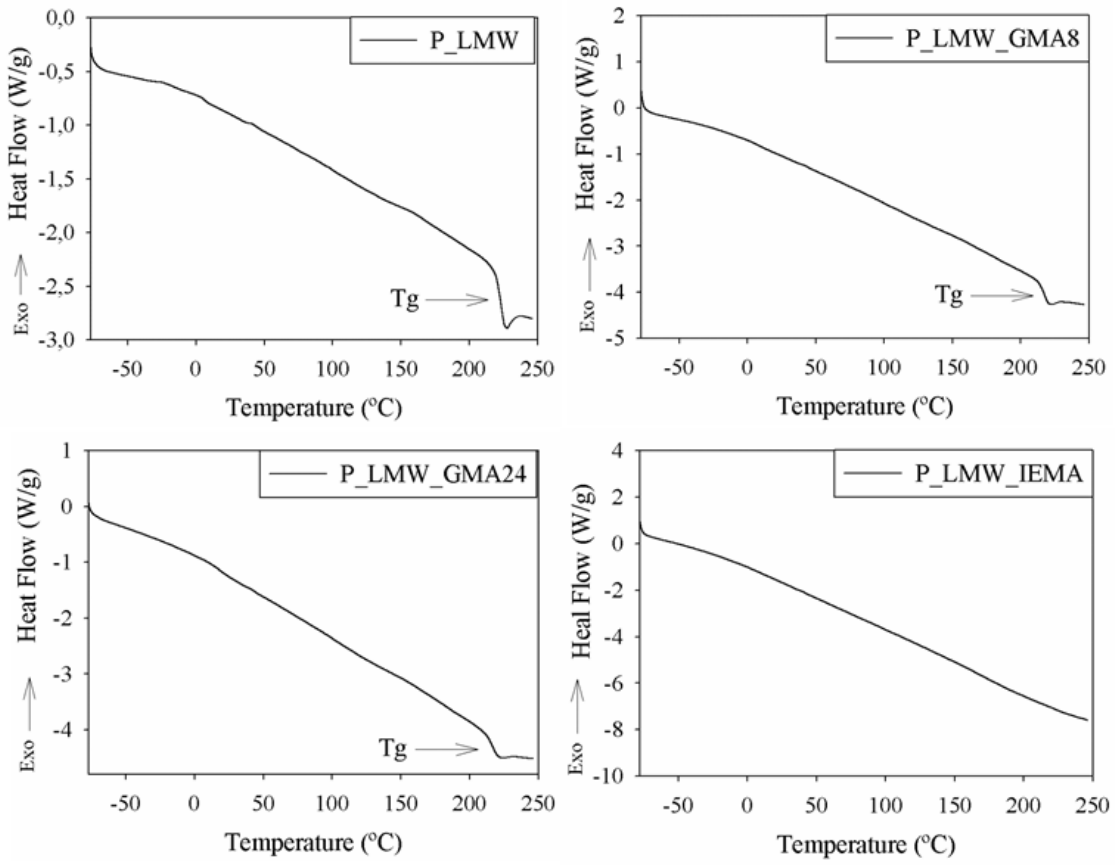

Figure 2.10 Heat flow curves of dextran and modified dextran.

In the heat flow curves of the materials under study the only thermal event that can be identified is the T_g, indicating that these materials, as expected, are totally amorphous (Table 2.3). As reported in the literature, the T_g value of unmodified dextran is *ca.* 220ºC.[57] In the case of P_LMW_IEMA and P_HMW_IEMA (Figure A.6), it was not possible to identify the T_g.

The DMTA traces in multifrequency of pristine dextran (P_HMW) are presented in Figure 2.11.

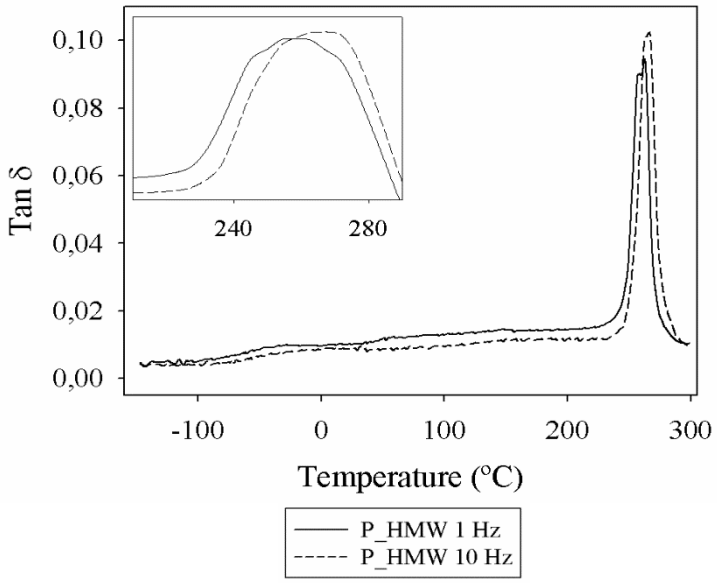

Figure 2.11 DMTA traces of P_HMW.

DMTA traces of dextran show a peak at ≈ 260ºC. This peak can be attributed to a T_α transition, which refers to the glass transition (T_g) of the material and can be seen for both frequencies, with a slight deviation. This confirms the presence of a T_g as it is known to be a frequency dependent process.[58]

DMTA analysis was also performed for modified dextran. However, the traces obtained for P_LMW_IEMA were not clear and well defined. Consequently, two consecutive runs were conducted in an attempt to remove residual water and solvent. Figure 2.12 shows the DMTA traces of P_LMW_IEMA for both runs.

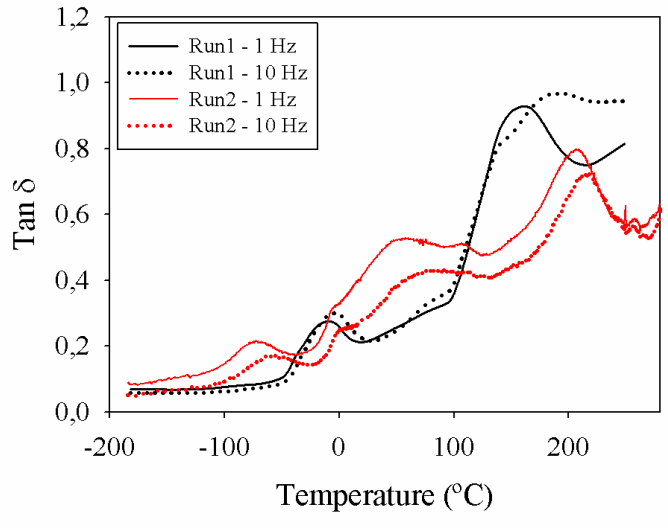

Figure 2.12 DMTA traces (run1 and run2) of P_LMW_IEMA.

The DMTA traces of the first run reveal the main thermal event between 100-200ºC. The second run of the same sample reveals a similar thermal event at around 200ºC. Since both events are dependent on the frequency, they correspond to the T_g ion of the material. However, in the first run, this transition occurs for a lower temperature, due to the presence of water that can provide a plasticizing effect of the structure. Consequently, during the second run, the absence of water turns this transition to a higher temperature. For this reason, in the following discussion, for the samples of P_LMW_IEMA only the second run traces will be considered.

DMTA traces of pristine dextran and modified dextrans are presented in Figuren 2.13.

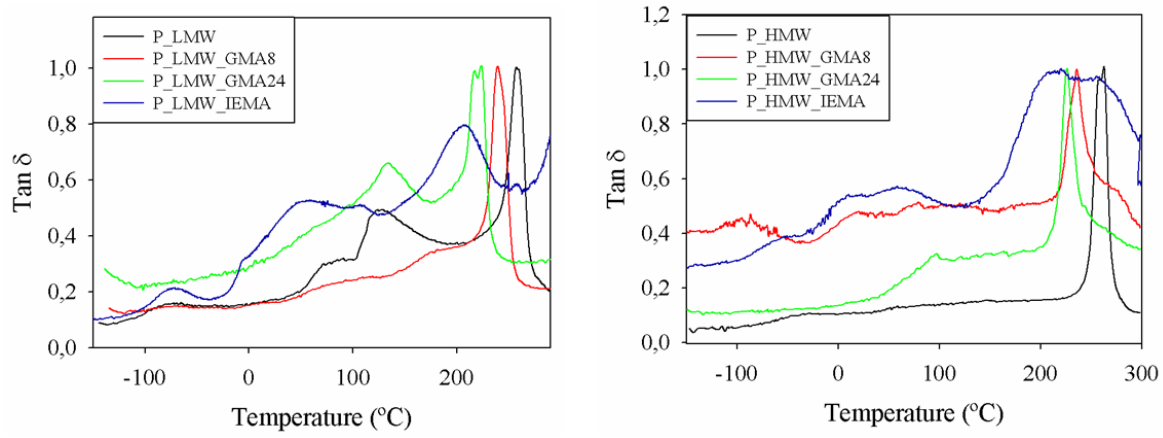

Figure 2.13 DMTA traces of dextran and modified dextrans.

DMTA traces show that all precursors have a peak corresponding to the T_g, which is in the same region of the pristine dextran. No relevant reduction of the T_g was observed after modification. This can be confirmed in the multifrequency DMTA traces shown in Figure A.7. Table 2.3 summarizes the T_g values of the samples determined both by DSC and DMTA.

Table 2.3 T_g values of dextran and modified dextran evaluated by DSC and DMTA.

	$T_{g\,DSC}$ (°C)	$T_{g\,DMTA}$ (°C)
P_LMW	223.44	256.6
P_LMW_GMA8	217.85	240.2
P_LMW_GMA24	217.7	219.9
P_LMW_IEMA	----	205.6
P_HMW	223.86	261.2
P_HMW_GMA8	219.62	230.6
P_HMW_GMA24	217.43	226.7
P_HMW_IEMA	----	220.6

The differences observed in the values of T_g for the different techniques are due to the differences on the principles used to determine the T_g.[59] Nevertheless, the same trend in terms of T_g values is observed in both DSC and DMTA

The modified dextran, with GMA or IEMA, presented lower T_g when compared with pristine dextran. A plausible reason would be the increase of the free volume between the polysaccharide chains.[60] The dextran modified with IEMA (P_LMW_IEMA and P_HMW_IEMA) has a lower T_g when compared with the dextran modified with GMA (P_LMW_GMA and P_HMW_GMA).

Thermal Properties of PCL and respective product of modification

The thermogravimetric analysis of PCL and PCL_IEMA was performed between 25-600ºC, under nitrogen atmosphere. The thermoanalytical curves are shown in Figure 2.14.

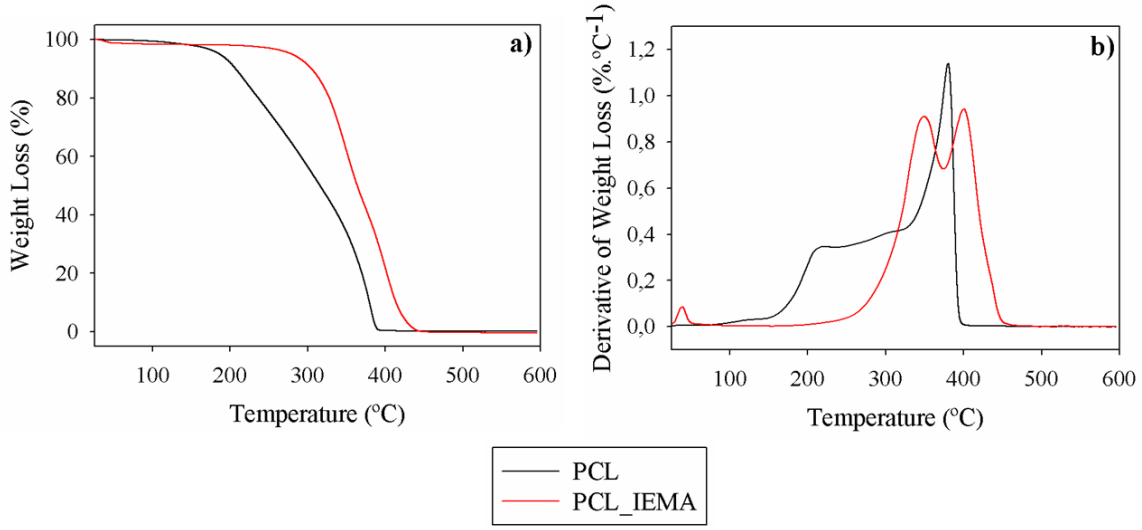

Figure 2.14 Thermoanalytical curves of PCL and PCL_IEMA: a) TG, and b) DTG.

The decomposition of PCL-diol occurs in two stages. This can be due to the early degradation of smaller chains present within the PCL-diol matrix. In what concerns PCL_IEMA, it presents also two main stages of weight loss. The first stage (345-350ºC) can be attributed to the decomposition of the urethane bonds, followed by a second stage (378-443ºC) attributed to the degradation of the ester bonds.[61] Also, it can be confirmed, that the sample are free of unreacted IEMA, as there is no peak near its boiling point, 211ºC.[36] The characteristic temperatures obtained by this technique are presented in Table 2.4.

Table 2.4 Characteristic temperatures obtained by TGA.

	T_{on} (ºC)	$T_{5\%}$ (ºC)	$T_{10\%}$ (ºC)	$T_{p,1}$ (ºC)	$T_{p,2}$ (ºC)	$T_{p,3}$ (ºC)
PCL	180.57	185.18	206.75	----	215.77	380.26
PCL_IEMA	310.59	291.19	310.28	25-50	348.49	400.11

T_{on}: Temperature of onset; $T_{5\%}$: Temperature to which corresponds 5% of weight loss; $T_{10\%}$: Temperature to which corresponds 10% of weight loss; T_p: peak temperature.

The thermal stability of PCL increases substancially upon the modification with IEMA. The explanation of this behavour may be based on the different terminal groups of the polymer chains. Foremost, PCL-diol has two OH terminal groups while PCL_IEMA does not. The degradation of PCL-diol starts from the degradation of these terminal OH groups which, in turn, hydrolyze the polyester chains.[62] Consequently, carboxylic acid and new terminal OH groups are generated [61,62] Furthermore, the increase of COOH and OH groups have an enhancement effect on the hydrolysis rate of PCL-diol. As the polymer degradation proceeds, some chains can degrade to a point where their mass is so low that its volatization occurs.[63] This can be observed in the DTG curve of PCL-diol as a peak appears at 200ºC, and continues to increase until 340ºC. After surpassing this temperature, all chains start to degrade, reaching to another peak around 360ºC. On the other hand, in the structure of PCL_IEMA, since there are no OH terminal groups, the degradation of the polymer starts with the degradation of the urethane bonds (T=345-350ºC). Therefore, the structure of PCL_IEMA presents higher thermal stability when compared with PCL-diol.

PCL-diol and PCL_IEMA thermal events were studied by DSC and DMTA. The heat flux curves obtained by DSC and thermograms obtained by DMTA are presented in Figure 2.15.

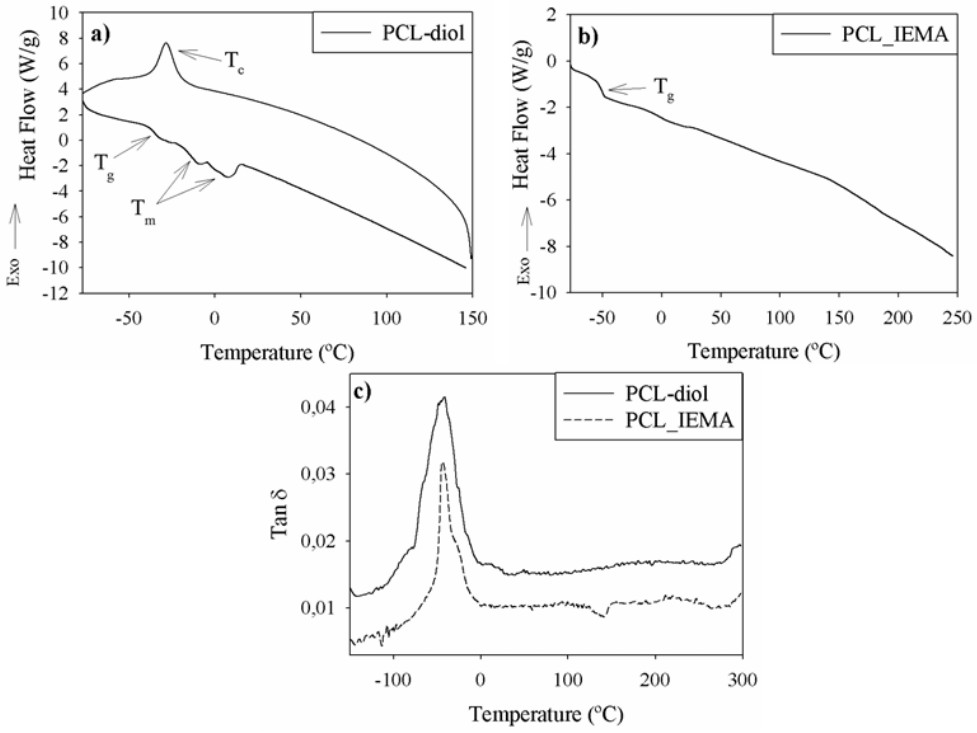

Figure 2.15 (a) Heat flow curves of PCL-diol, (b) Heat flow curves of PCL-IEMA, and (c) DMTA traces of PCL-diol and PCL-IEMA.

The heat flow curves of PCL-diol show one thermal event at -41.0ºC, which corresponds to its glass T_g. Moreover, two other thermal events are present that correspond to the melting (T_m) of the material (-9.0ºC and 7.5ºC) and, in the cooling cycle, to a crystallization (T_c) (-28.6ºC). This fact confirms that PCL-diol is a semi-crystalline polymer.[64] Upon the modification with IEMA, PCL-diol loses its structural order, leading to an amorphous material. In addition, a small decrease in the T_g value is observed (-42.9ºC). The inclusion of IEMA in the PCL-diol structure contributes to an augment in the free volume between the backbone polymeric chains, justifying the observed decrease in the T_g.

2.4.3 Preparation and Characterization of the Membranes

The different precursors were used to prepare membranes by using a photocrosslinking technique. For comparison purposes, blank membranes (prepared only with modified dextran) and membranes with different ratios of modified dextran and PCL_IEMA, were prepared.

For the blank membranes 0.5g of modified dextran was used. In this case, this amount was found to be the suitable since it was possible to prepare membranes that maintained their structural integrity upon the drying process. For the case of the membranes containing both modified dextran and PCL_IEMA, the use of 0.5 g of each precursors in the formulation showed to be unsuitable since very thick membranes were obtained. In this sense, the total amount of precursors was reduced for 0.4 g and the membranes presented a thickness similar to the blank membranes (approximately 0.33-0.38 mm).

However, for precursor P_LMW_GMA24 (higher modification degree), it was not possible to prepare blank membranes as they were not able to maintain their structural integrity during the drying step. For this reason, with this precursor, only formulations including PCL_IEMA were characterized.

Unfortunately, it was not possible to prepare membranes using the precursor P_HMW_IEMA due to solubility problems with the amount of DMSO used. For this reason, for the modification of dextran with IEMA, only the precursor P_LMW_IEMA was used to prepare membranes.

The time of photocrosslinking required was evaluated, being the optimal expose to radiation approximately 2h. Also, the distance to UV light was established to be between 22-23 cm. Figure 2.16 presents the membranes after photocrosslinking and after the drying stage.

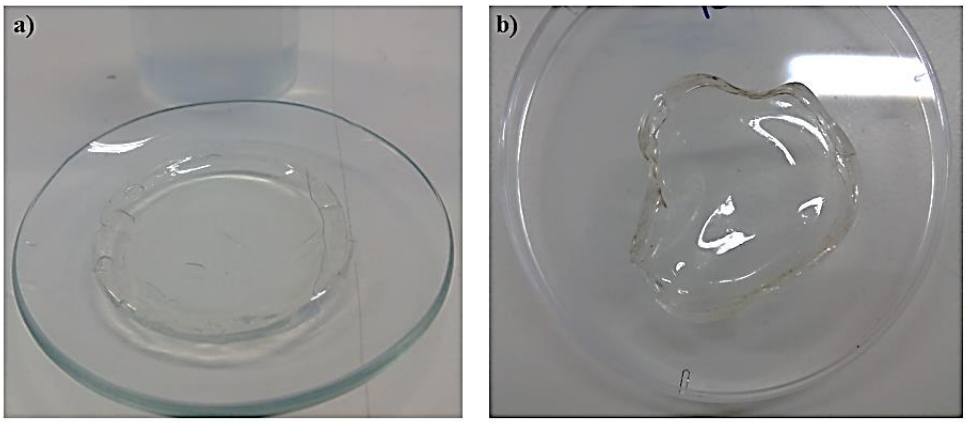

Figure 2.16 Final aspect of prepared membranes: a) after photocrosslinking; b) after drying stage.

Thermal Properties of the membranes

The thermogravimetric analysis of the membranes was performed in a range of temperatures from 25ºC to 600ºC. The thermoanalytical curves obtained by this technique are presented in Figure 2.16, 2.17 and 2.18.

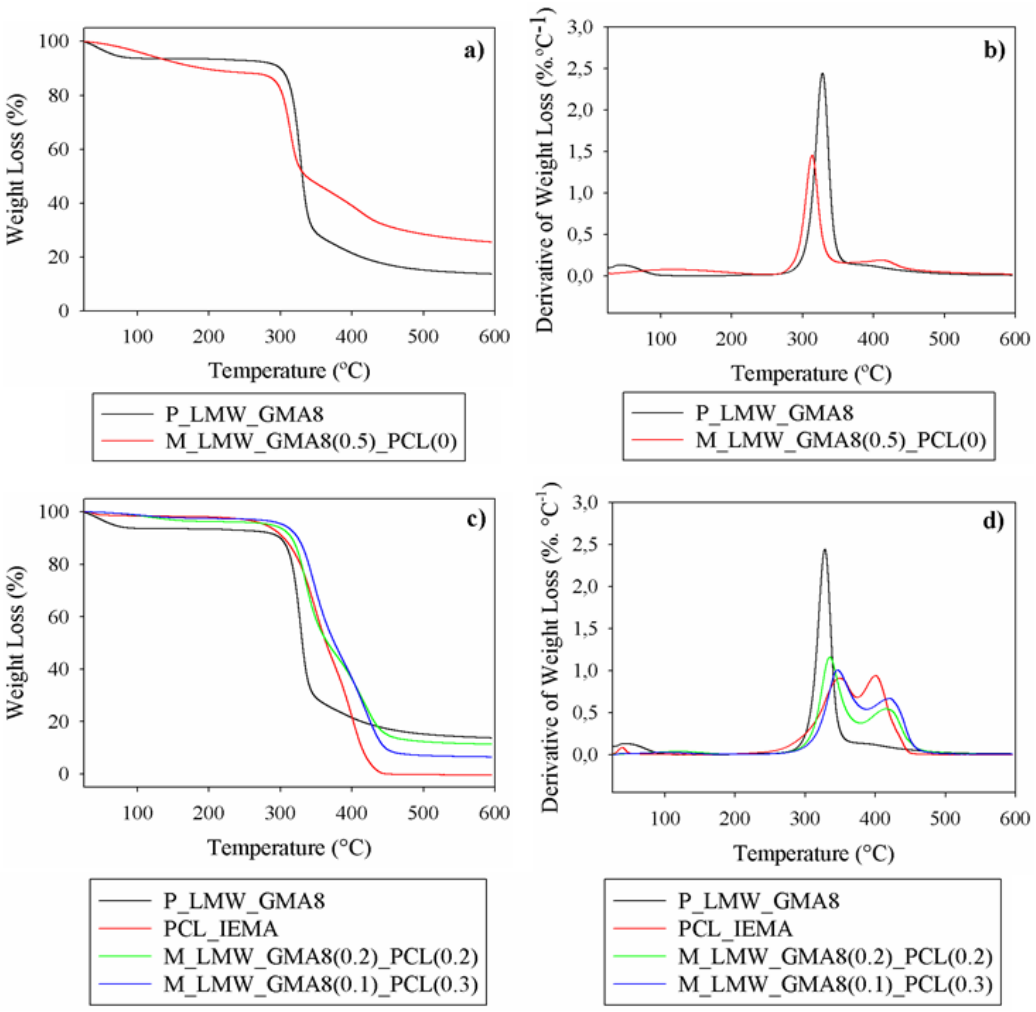

Figure 2.17 Thermogravimetric curves of membranes prepared with P_LMW_GMA8: a)M_LMW_GMA8(0.5)_PCL(0); b)M_LMW_GMA8(0.2)_PCL(2); c)M_LMW_GMA8(0.1)_PCL(0.3).

The thermogravimetric analysis of the P_LMW_GMA8 based membranes show clearly two stages of weight loss, despite their different compositions.

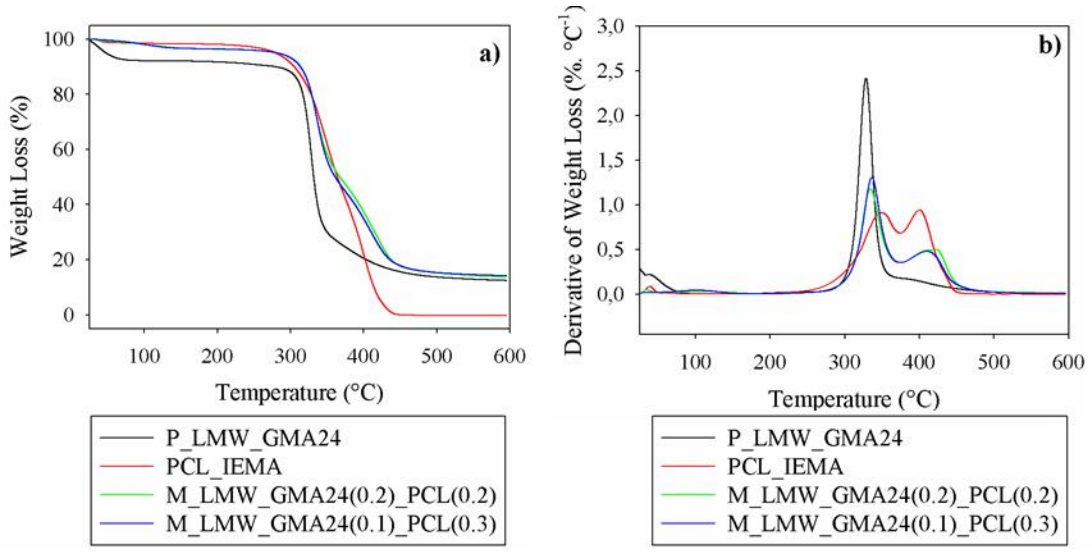

Figure 2.18 Thermogravimetric curves of membranes prepared with P_LMW_GMA24: a) M_LMW_GMA24(0.2)_PCL(2); b) M_LMW_GMA24(0.1)_PCL(0.3).

Similarly, to the weight loss profile observed in Figure 2.17, P_LMW_GMA24 based membranes present two well defined stages of weight loss. Furthermore, a resemblance in the range of the peak temperatures is also observed.

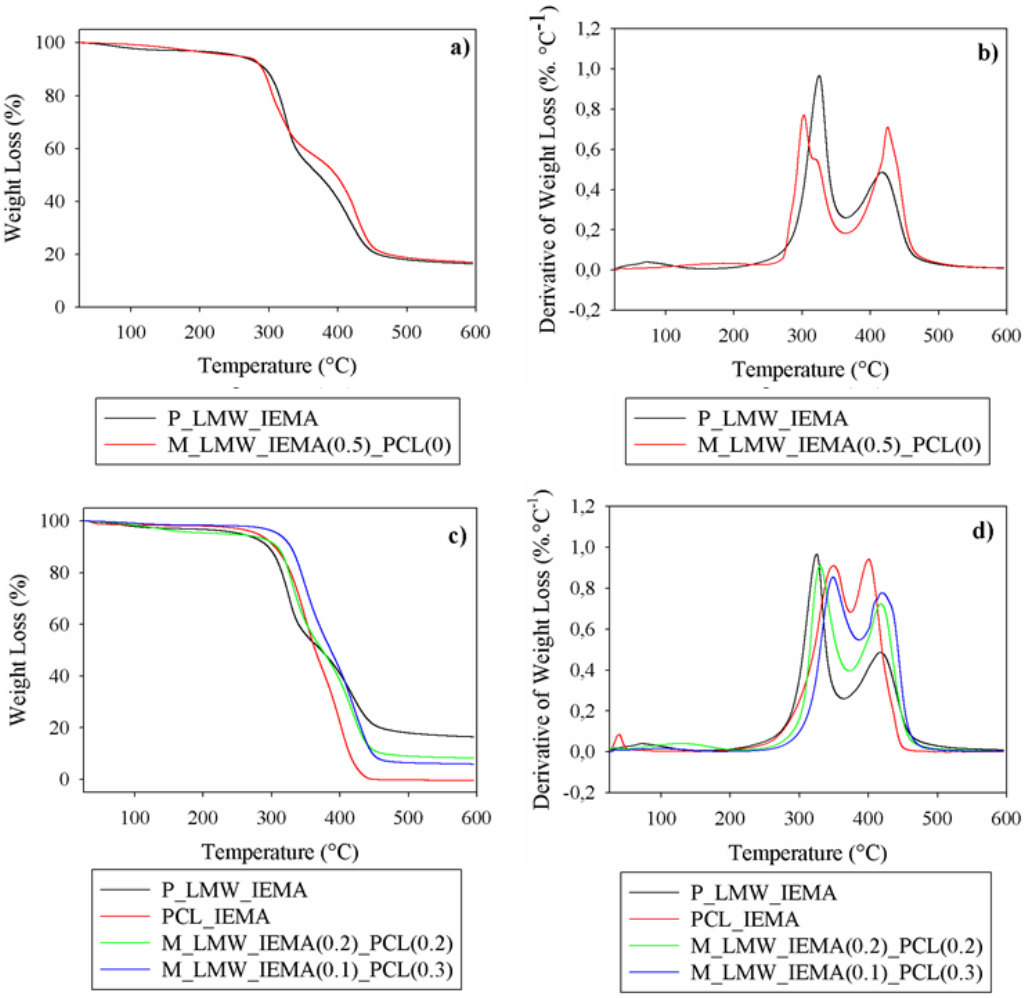

Figure 2.19 Thermogravimetric curves of membranes prepared with P_LMW_IEMA: a) M_LMW_IEMA(0.5)_PCL(0); b)M_LMW_IEMA(0.2)_PCL(2); c) M_LMW_IEMA(0.1)_PCL(0.3).

The thermogravimetric curves observed in figure 2.19, despite the slightly different profile comparing to the P_LMW_GMA8/24 based membranes, shows similar weight loss peaks, in the same range of temperatures. The first stage of degradation can be attributed to the degradation of unmodified dextran, which has no crosslinking points, whereas the second stage can be ascribed to the degradation of the tridimensional network.[65,66]

The membranes prepared with high molecular weight dextran (P_HMW) have similar weight loss profiles and their thermoanalytical curves are presented in Figure A.8.

Table 2.5 summarizes the temperatures of interest taken from the thermogravimetric curves.

Table 2.5 Characteristic temperatures obtained by TGA. T_{on}: Temperature of onset; $T_{5\%}$: Temperature to which corresponds 5% of weight loss; $T_{10\%}$: Temperature to which corresponds 10% of weight loss; T_p: peak temperature

	T_{on} (ºC)	$T_{5\%}$ (ºC)	$T_{10\%}$ (ºC)	$T_{p,1}$ (ºC)	$T_{p,2}$ (ºC)
M_LMW_GMA8(0.5)_PCL(0)	300.0	296.9	305.4	313.3	415.8
M_LMW_GMA8(0.2)_PCL(2)	317.2	312.2	323.0	335.5	416.6
M_LMW_GMA8(0.1)_PCL(0.3)	324.4	314.5	327.5	345.7	420.5
M_LMW_GMA24(0.2)_PCL(2)	317.1	307.7	321.3	336.0	411.5
M_LMW_GMA24(0.1)_PCL(0.3)	320.1	310.5	325.8	346.2	406.4
M_LMW_IEMA(0.5)_PCL(0)	279.1	283.3	290.6	292.3 (312.8)*	423.9
M_LMW_IEMA(0.2)_PCL(0.2)	310.3	307.7	319.0	329.8	418.3
M_LMW_IEMA(0.1)_PCL(0.3)	322.5	316.2	331.5	348.5	420.0
M_HMW_GMA8(0.5)_PCL(0)	299.9	295.8	304.3	313.3	414.3
M_HMW_GMA8(0.2)_PCL(0.2)	318.3	311.1	321.3	334.9	416.0
M_HMW_GMA8(0.1)_PCL(0.3)	321.1	312.2	326.9	347.4	417.7
M_HMW_GMA24(0.2)_PCL(0.2)	312.6	304.8	317.3	331.5	404.6
M_HMW_GMA24(0.1)_PCL(0.3)	319.1	312.2	325.8	347.4	412.0

All membranes were found to be thermally stable until temperatures of *ca.* 300ºC. Also, the different membranes present similar characteristic temperatures, specially the membranes prepared with GMA modified dextran regardless the molecular weight and different degrees of modification used. In what concerns, the membranes prepared with only modified dextran, M_LMW_GMA8(0.5)_PCL(0) and

M_LMW_IEMA(0.5)_PCL(0), the thermal stability is higher when compared with the corresponding precursors, which is explained by their crosslinked structure.[67]
On the other hand, with the introduction of PCL_IEMA in the formulations, thermal stability increases, suggesting that PCL_IEMA has a positive influence on thermal stability. The membranes with higher content (0.3 g) of PCL_IEMA are consistently more stable compared with the ones with lower content (0.2 g). This behavior may be ascribed to the increasing crosslinking of a the final materials.[68]

The T_g of membranes was evaluated by DMTA. Figure 2.20, 2.21 and 2.22 presents the DMTA traces of the membranes prepared with P_LMW. The DMTA traces of the membranes prepared with the P_HMW are presented in Figure A.9. Generally, it was observed that the DMTA traces of the membranes presents signals with higher uncertainty compared with the DMTA of the precursors. However, the analysis carried out with a different frequency allows us to detect the T_g of the materials.

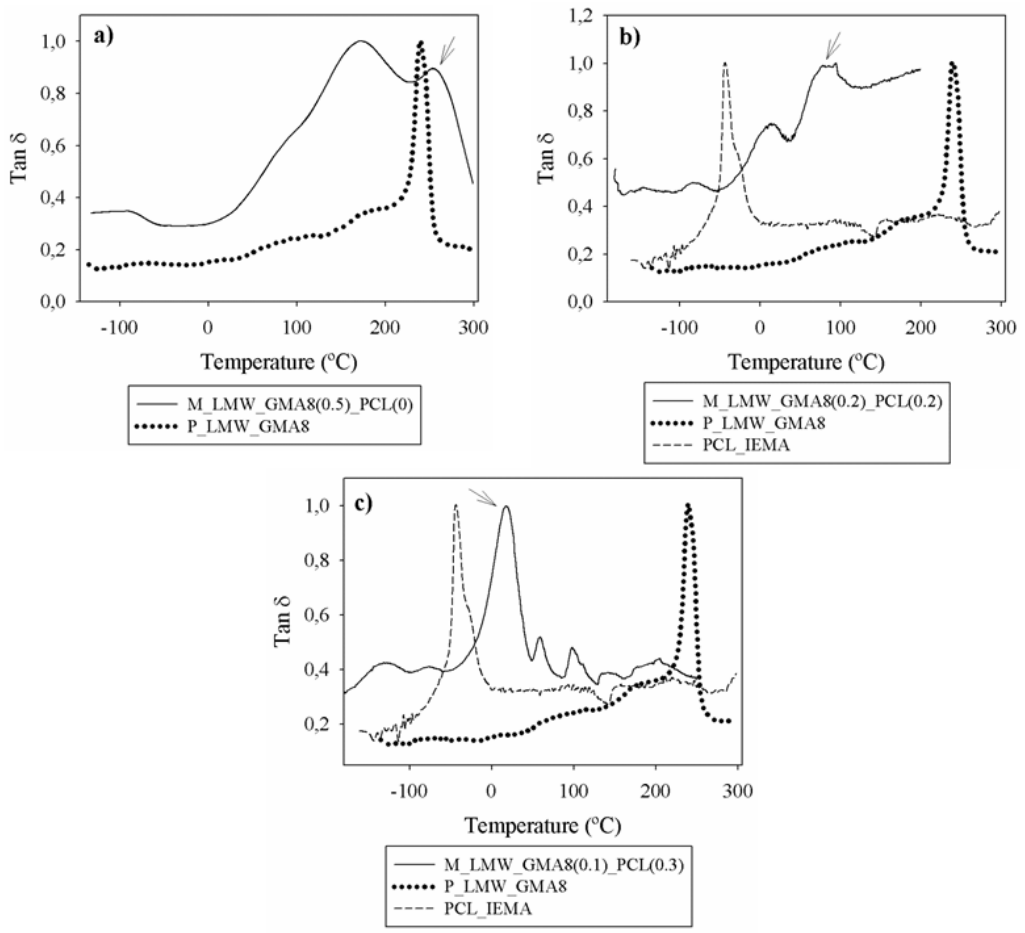

Figure 2.20 DMTA traces of the membranes prepared with P_LMW_GMA8: a)M_LMW_GMA8(0.5)_PCL(0); b)M_LMW_GMA8(0.2)_PCL(0.2); c)M_LMW_GMA8(0.1)_PCL(0.3). The arrows indicate the peak corresponding to the T_g of the membranes.

The glass transition for M_LMW_GMA8(0.5)_PCL(0) is higher than the precursor, as expected, due to the establishment of a crosslinked network. The presence of PCL_IEMA originates membranes with a glass transition that is located between the values of the precursors meaning that after crosslinking, the polymeric chains with some degree of freedom show a mobility higher that of PCL_IEMA but less than M_LMW_GMA8(0.5). DMTA traces of membranes prepared with P_LMW_GMA8 reveal a decrease in their T_g with the increasing content of PCL_IEMA.

In the DMTA trace of M_LMW_GMA8(0.5)_PCL(0), two transitions can be observed. The first one is non-frequency dependent and might correspond to the evaporation of residual solvent (DMSO). In fact, a closer look to the thermogravimetric curves of this

membrane (see Figure 2.17) shows an initial weight loss (100ºC-200ºC), suggesting the presence of residual DMSO. The present of remaining solvent in membranes although not desired, does not interfere with biological media as cells. For this reason, for low concentrations of DMSO, it is not toxic.[69]

The second transition is sensitive to frequency, and corresponds to the T_g of the material (259.9ºC). As expected, this value is higher than the one obtained for the precursor. M_LMW_GMA8(0.2)_PCL(2) presents not only a shoulder between 90-100ºC, but also a broad peak sensitive to frequency. These peaks corresponds to the T_g of the membranes. The T_g value decreased significantly (from 259.9ºC to 94.3ºC) when compared with M_LMW_GMA8(0.5)_PCL(0). It seems that the PCL-IEMA acted as a plasticizer contributing to a decrease in the value of the T_g. In turn, in the DMTA curve of M_LMW_GMA8(0.1)_PCL(0.3), a main peak corresponding to the T_g is observed at 17.3ºC. For this membrane the T_g value is lower than that observed for M_LMW_GMA8(0.1)_PCL(0.3), due to the use of a higher amount of PCL-IEMA in the formulation of the membranes. This results consubstantiates the fact PCL-IEMA acts as a plasticizer of the membranes. It should be pointed out that for M_LMW_GMA8(0.2)_PCL(0.2) and M_LMW_GMA8(0.1)_PCL(0.3), a single T_g peak is observed, indicating that the two components of the membrane are miscible.

Figure 2.21 plots the DMTA traces obtained for the membranes prepared with P_LMW_GMA24.

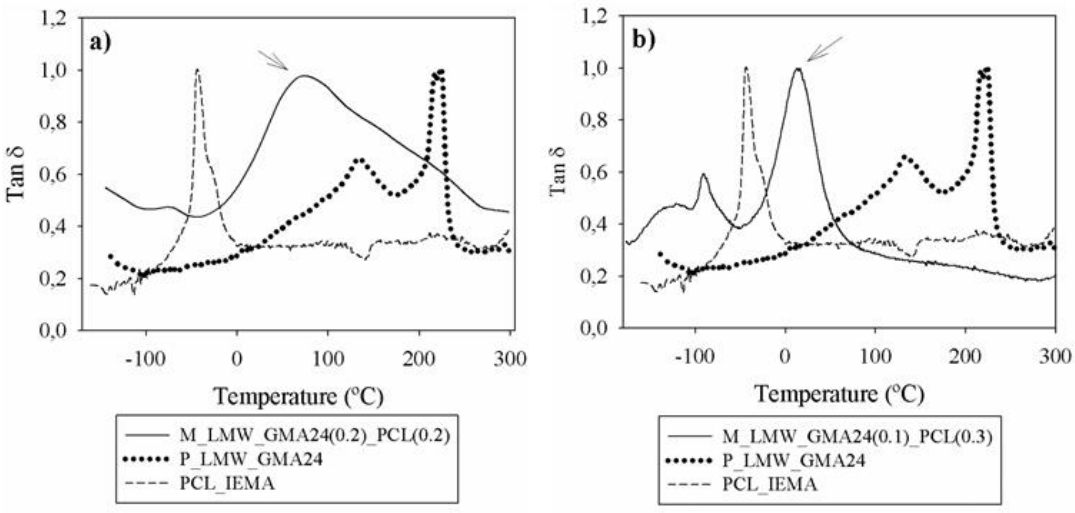

Figure 2.21 DMTA traces of the membranes prepared with P_LMW_GMA24: a)M_LMW_GMA8(0.2)_PCL(0.2); b)M_LMW_GMA8(0.1)_PCL(0.3). The arrows indicate the peak corresponding to the T_g of the membranes.

The T_g of both membranes prepared with P_LMW_GMA24 are located between the T_g of the two precursors. Similarly, to what was observed for P_LMW_GMA8, with the increased content of PCL_IEMA in the membranes' formulation, a decrease of the T_g is verified. This fact was already expected since the only different between the precursors of these membranes is the degree of modification of dextran.

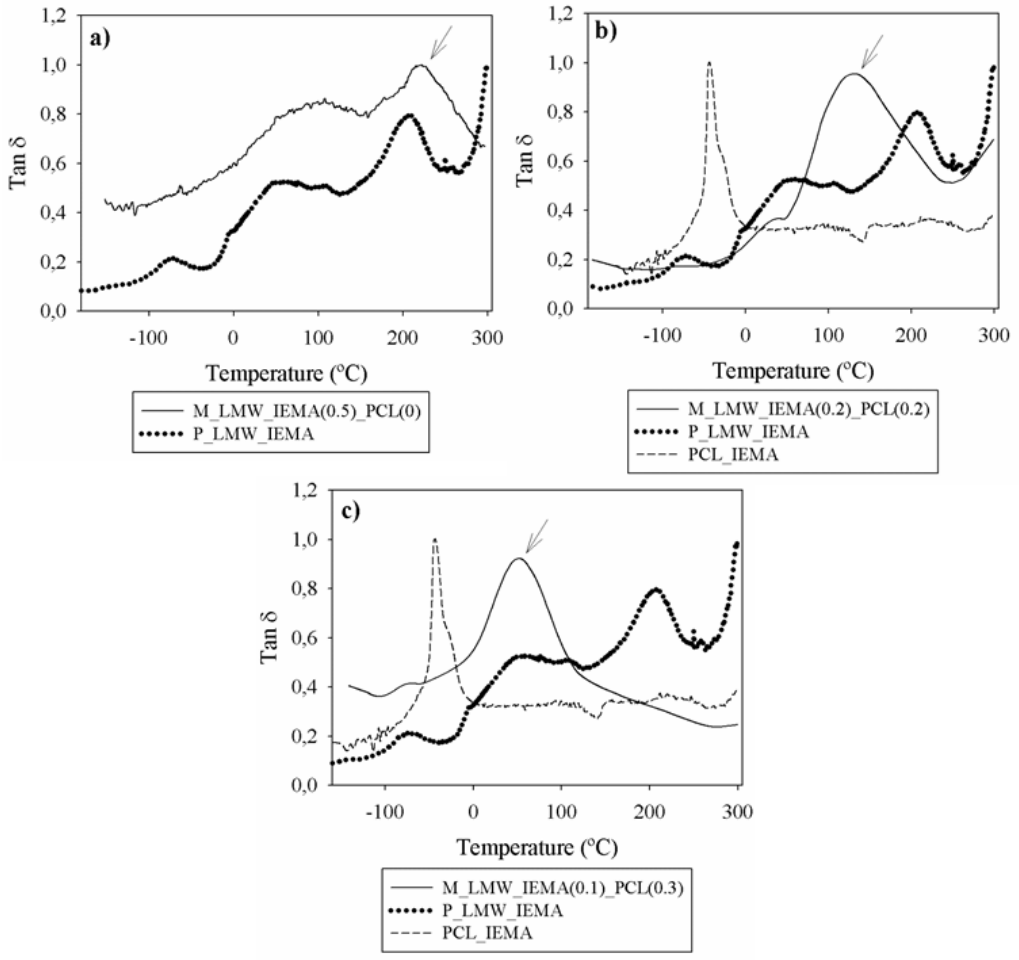

Figure 2.22 DMTA traces of the membranes prepared with P_LMW_IEMA: a)M_LMW_IEMA(0.5)_PCL(0); b)M_LMW_IEMA(0.2)_PCL(0.2); c)M_LMW_IEMA(0.1)_PCL(0.3).

Membranes prepared with P_LMW_IEMA also present a decrease in their T_g with the increase of content of PCL_IEMA. However, this decrease is not so pronounced, especially for M_LMW_IEMA(0.2)_PCL(0.2). In addition, as expected, M_LMW_IEMA(0.5)_PCL(0) presents higher T_g than the precursor.

Regarding M_LMW_IEMA(0.5)_PCL(0), two peaks can be distinguished in the tan δ curve. The first peak is non-frequency dependent and might correspond to the evaporation of residual DMSO, the second peak, in turn, is sensitive to frequency and is ascribed to the T_g of the material. The T_g value (221.4ºC) is higher than the T_g (73.7ºC) obtained for P_LMW_IEMA, most probably due to the crosslinked nature of the membrane. Both P_LMW_IEMA(0.2)_PCL(0.2) and M_LMW_IEMA(0.1)_PCL(0.3) present broad, but defined T_g peaks (129.8ºC and 51.9ºC). The T_g values of these membranes are lower than

that obtained for M_LMW_IEMA(0.5)_PCL(0), due to the inclusion of PCL_IEMA. As already observed for the P_LMW_GMA membranes, PCL-IEMA acts as a plasticizer, decreasing the values of T_g.

DMTA traces of most of the membranes present a "shoulder" at *ca.* -100ºC - -90ºC. This peak corresponds to a secondary relaxation due absorbed water.[23] It is quite common to appear in hydrophilic polymers due to their affinity with water. When this peak is very pronounced, it can be said that this specific water has a sort of plasticizing effect, which results in more conformational freedom of polymer chains.[70]
Table 2.6 presents the T_g values of the membranes under study.

Table 2.6 T_g values of prepared membranes, obtained by DMTA.

	$T_{g\ DMTA}$ ºC
M_LMW_GMA8(0.5)_PCL(0)	259.9
M_LMW_GMA8(0.2)_PCL(2)	94.3
M_LMW_GMA8(0.1)_PCL(0.3)	17.3
M_LMW_GMA24(0.2)_PCL(2)	79.8
M_LMW_GMA24(0.1)_PCL(0.3)	12.8
M_LMW_IEMA(0.5)_PCL(0)	221.4
M_LMW_IEMA(0.2)_PCL(0.2)	130.4
M_LMW_IEMA(0.1)_PCL(0.3)	58.0
M_HMW_GMA8(0.5)_PCL(0)	262.2
M_HMW_GMA8(0.2)_PCL(0.2)	21.7
M_HMW_GMA8(0.1)_PCL(0.3)	12.0
M_HMW_GMA24(0.2)_PCL(0.2)	69.3
M_HMW_GMA24(0.1)_PCL(0.3)	-8.8

The DMTA traces obtained for the membranes prepared with P_HMW_GMA present the same tendency observed for the membranes prepared with P_LMW_GMA.

2.4.4 Swelling Capacity of membranes

The swelling capacity of the membranes was evaluated in PBS (pH=7.4), at 37ºC. This parameter is extremely important when the final application of the materials involve their implantation *in vivo*, requiring dimensional stability. Knowing the swelling capacity of the materials is possible to predict changes in the final dimensions caused by water uptake, which is crucial for the mold design.

Figure 2.23 presents the data of swelling capacity *vs* time for the membranes under study.

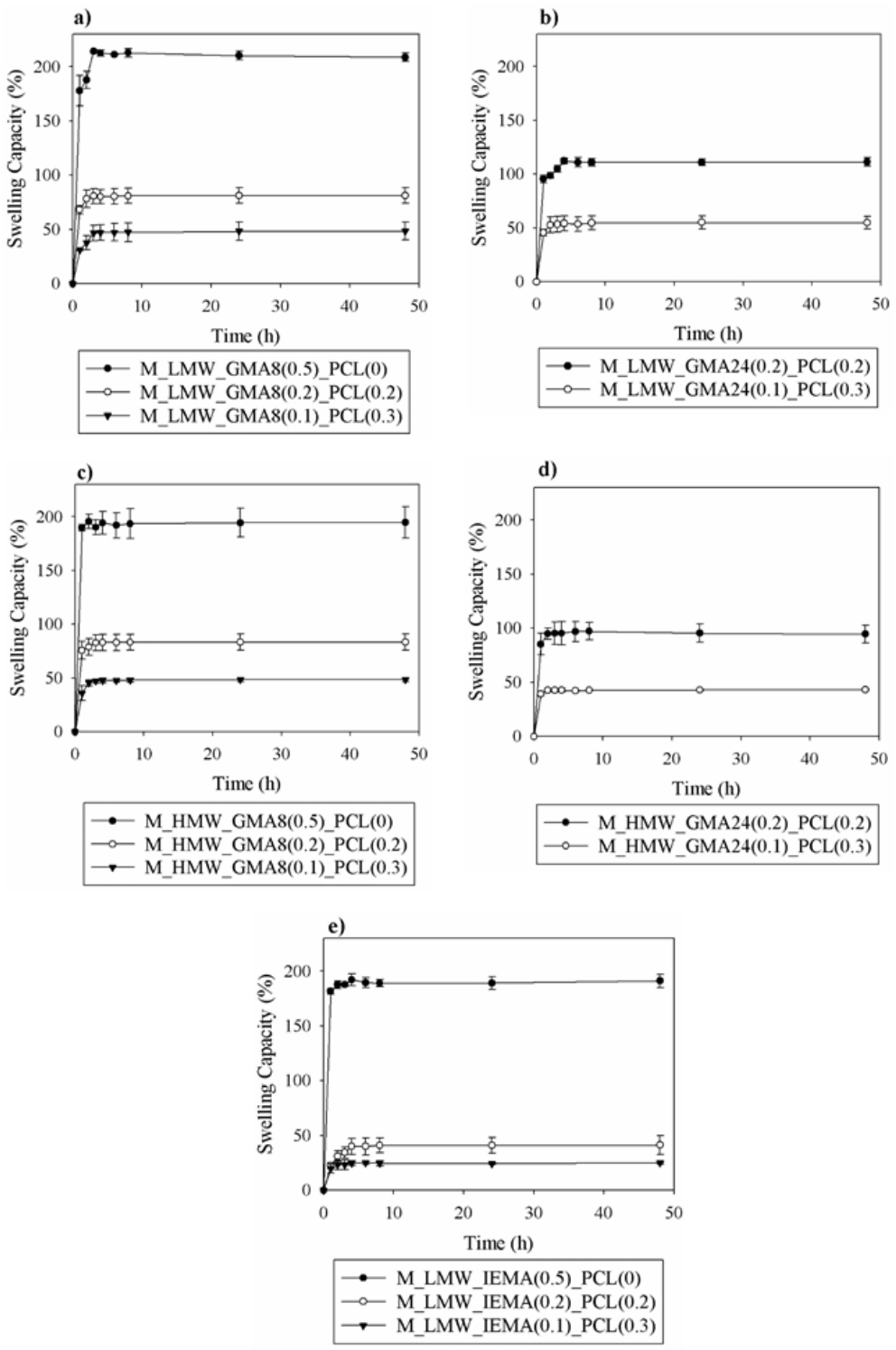

Figure 2.23 Swelling Capacity of membranes prepared with: a) P_LMW_GMA8; b) P_LMW_GMA24; c) P_HMW_GMA8; d) P_HMW_GMA24; e) P_LMW_IEMA.

The results show that all membranes stabilized their swelling capacity after approximately 2-3 hours. Dextran with different molecular weights, and modified with the same monomer show similar behavior.

Dextran is well known for its high affinity with water, which results in high swelling capacity ratios (400%).[57] This is in agreement with the results obtained for the membranes prepared only with modified dextran (M_LMW_GMA8(0.5)_PCL(0), M_HMW_GMA8(0.5)_PCL(0), M_LMW_IEMA8(0.5)_PCL(0)), which present the higher swelling capacity ratios (between 190-212%).

In turn, PCL is known for its hydrophobicity, which means that this material has low affinity with water. As a consequence, has low swelling capacity. Due to these facts, it was expected that membranes which had modified PCL in their composition suffered a decrease in their swelling capacity. It was verified that with the increase of the hydrophobic PCL_IEMA content in the formulation of the membranes, the swelling capacity decreases (from *ca.* 200% to 100-50% approximately).

The membranes M_LMW_IEMA(0.2)_PCL(0.2) and M_LMW_IEMA(0.1)_PCL(0.3) have a lower swelling capacity than those prepared with dextran modified with GMA. This might indicate that these membranes have higher crosslinking, hindering the water penetration.[71] In fact, looking at the values of T_g (Table 2.6) of the above mentioned membranes it is possible to see that those obtained from the P_LMW_IEMA have higher T_g, which is indicative of a more closely packed network.

For the final application of this work, it is important that membranes have the ability to swell as it affects positively the cell attachment and growth.[72] However, swelling capacity values around 200% hinders the prediction of the final dimension of the membrane. For this reason, membranes containing PCL_IEMA with low swelling in their structure are considered to be more suitable for the final application of this work.

Swelling capacity also helps in the prediction of the final dimension that membranes will have *in vivo*, which is very important to avoid future nerve constriction. In this study, the diameter and thickness of the membranes were measured before and after the swelling capacity evaluation. The percentages of increase of dimensions are presented in table 2.7.

Table 2.7 Percentage of dimension increase after swelling capacity tests.

	Dimension increase after swelling	
Membrane	**Diameter (%)**	**Thickness (%)**
M_GMA8(0.5)_PCL(0)	71.1	27.2
M_GMA8(0.2)_PCL(0.2)	12.7	19.4
M_GMA8(0.1)_PCL(0.3)	10.6	2.9
M_GMA24(0.2)_PCL(0.2)	25.6	13.2
M_GMA24(0.1)_PCL(0.3)	10.5	4.0
M_IEMA(0.5)_PCL(0)	42.5	104.8
M_IEMA(0.2)_PCL(0.2)	16.7	31.7
M_IEMA(0.1)_PCL(0.3)	8.8	3.75

As expected, the membranes with higher contents of PCL_IEMA (0.3), which presented lower swelling capacity, also have lower dimension increase after swelling. To avoid nerve constriction, the most important measure is the thickness of the membrane. For this reason, for the desired application, M_GMA8(0.1)_PCL(0.3), M_GMA24(0.1)_PCL(0.3) and M_IEMA(0.1)_PCL(0.3) are the most appropriate membranes due to their low thickness increase (*ca.* 3-4%).

2.4.5 *In vitro* hydrolytic degradation of membranes

The *in vitro* hydrolytic degradation of the membranes under simulated physiological conditions (PBS, pH=7.4, 37ºC) was studied. The weight loss profiles are presented in Figure 2.24.

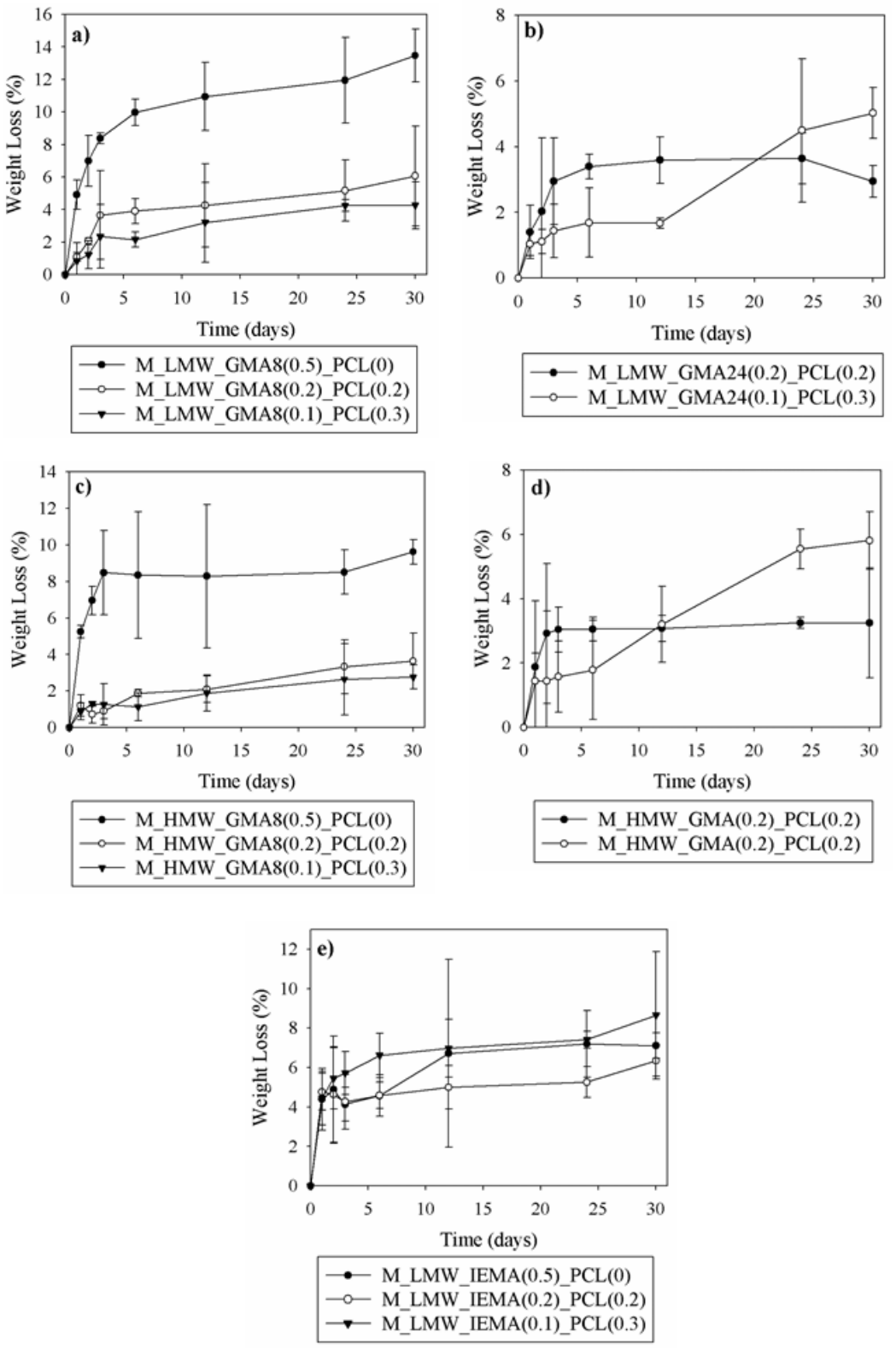

Figure 2.24 Weight loss *vs* time profiles of the membranes prepared with: a) P_LMW_GMA8; b) P_LMW_GMA24; c) P_HMW_GMA8; d) P_HMW_GMA24; e) P_LMW_IEMA.

The degradation profiles of membranes prepared with dextran modified with GMA are quite similar with a slightly lower weight loss for the ones prepared with P_HMW_GMA8 and P_HMW_GMA24. This can be explained by the fact that the higher the molecular weight, the slower is the degradation rate, as polymer chains are longer, and the structure is denser. Regarding the membranes prepared from P_LMW_GMA8 or P_HMW_GMA8, it is possible to observe that those prepared only from modified dextran and those with the highest values of swelling capacity have the highest weight loss values (9-13%, after 30 days). This fact could be attributed to more easy penetration of the medium in the crosslinked network. Upon the incorporation of PCL_IEMA, a decrease in the weight loss is observed. The hydrophobic nature of PCL_IEMA does not allow the degradation medium to easily penetrate in the crosslinked network, leading to a decrease in the weight loss values.

Concerning the membranes prepared with P_LMW_IEMA, it is observed that their weight loss profile is quite similar. It was expected that M_LMW_IEMA(0.5)_PCL(0) had loss more weight than M_LMW_IEMA(0.2)_PCL(0.2) or M_LMW_IEMA(0.1)_PCL(0.3), as its swelling degree is higher although the fact that that in certain measurements, a very high standard deviation was observed.

Nevertheless, all the membranes showed interesting weight loss profiles for the desired application (between 10-20%).[73] After 30 days of immersion in the degradation medium, all of them maintained their structural integrity, which is a very important characteristic.

2.5 CONCLUSIONS

The aim of this part of the work was to prepare and characterize dextran based membranes prepared by a photocrosslinking process. The membranes were prepared using formulations of methacrylated dextran and a PCL acrylated macromonomer, using Irgacure®2959 as the photoinitiator. The membranes were transparent and their thermal-mechanical properties showed to be dependent on the ratio of the precursors in the formulations, and on the molecular weight of dextran. With the increase of the content of PCL_IEMA, the swelling capacity of the membranes decreased, as expected due to the hydrophobic character of PCL. Furthermore, membranes with higher contents of PCL_IEMA presented lower percentage of dimension increase after swelling tests.

In vitro hydrolytic degradation tests show that during 30 days, the membranes lose around 8-12% of their total mass. In addition, membranes are able to maintain their structural integrity during this period of time.

In conclusion, the new dextran-based membranes prepared in this work showed promising results for the use in peripheral nerve regeneration. For this reason, they can be considered good candidates to be tested *in vitro*, in order to evaluate their interaction with biological material.

2.6 REFERENCES

1. Wei, X.; Xiong, H.; He, S.; Wang, Y.; Zhou, D.; Jing, X.; Huang, Y., A facile way to prepare functionalized dextran nanogels for conjugation of hemoglobin. *Colloids and Surfaces B: Biointerfaces* **2017,** *155*, 440-448.

2. Bahremand, A. H.; Mousavi, S. M.; Ahmadpour, A.; Taherian, M., Biodegradable blend membranes of poly (butylene succinate)/cellulose acetate/dextran: Preparation, characterization and performance. *Carbohydrate Polymers* **2017,** *173*, 497-507.

3. Jacchetti, E.; Tonazzini, I.; Meucci, S.; Beltram, F.; Cecchini, M., Microstructured polydimethylsiloxane membranes for peripheral nerve regeneration. *Microelectronic Engineering* **2014,** *124*, 26-29.

4. Taylor, C. A.; Braza, D.; Rice, J. B.; Dillingham, T., The Incidence of Peripheral Nerve Injury in Extremity Trauma. *American Journal of Physical Medicine & Rehabilitation* **2008,** *87*, 381-385.

5. Daly, W.; Yao, L.; Zeugolis, D.; Windebank, A.; Pandit, A., A biomaterials approach to peripheral nerve regeneration: bridging the peripheral nerve gap and enhancing functional recovery. *Journal of the Royal Society Interface* **2012,** *9*, 202-221.

6. Johnson, E. O.; Soucacos, P. N., Nerve repair: experimental and clinical evaluation of biodegradable artificial nerve guides. *Injury* **2008,** *39 Suppl 3*, S30-36.

7. Ichihara, S.; Inada, Y.; Nakamura, T., Artificial nerve tubes and their application for repair of peripheral nerve injury: an update of current concepts. *Injury* **2008,** *39 Suppl 4*, 29-39.

8. Gerth, D. J.; Tashiro, J.; Thaller, S. R., Clinical outcomes for Conduits and Scaffolds in peripheral nerve repair. *World Journal of Clinical Cases : WJCC* **2015,** *3*, 141-147.

9. Li, G.; Zhang, L.; Wang, C.; Zhao, X.; Zhu, C.; Zheng, Y.; Wang, Y.; Zhao, Y.; Yang, Y., Effect of silanization on chitosan porous scaffolds for peripheral nerve regeneration. *Carbohydrate Polymers* **2014,** *101*, 718-726.

10. Yuan, Y.; Zhang, P.; Yang, Y.; Wang, X.; Gu, X., The interaction of Schwann cells with chitosan membranes and fibers *in vitro*. *Biomaterials* **2004,** *25*, 4273-4278.

11. Fregnan, F.; Ciglieri, E.; Tos, P.; Crosio, A.; Ciardelli, G.; Ruini, F.; Tonda-Turo, C.; Geuna, S.; Raimondo, S., Chitosan crosslinked flat scaffolds for peripheral nerve regeneration. *Biomedical Materials* **2016,** *11*, 045010.

12. Simoes, M. J.; Gartner, A.; Shirosaki, Y.; Gil da Costa, R. M.; Cortez, P. P.; Gartner, F.; Santos, J. D.; Lopes, M. A.; Geuna, S.; Varejao, A. S.; Mauricio, A. C., *In vitro* and *in vivo* chitosan membranes testing for peripheral nerve reconstruction. *Acta Medica Portuguesa* **2011,** *24*, 43-52.

13. Amado, S.; Simoes, M.; da Silva, P. A.; Luís, A.; Shirosaki, Y.; Lopes, M.; Santos, J.; Fregnan, F.; Gambarotta, G.; Raimondo, S., Use of hybrid chitosan membranes and N1E-115 cells for promoting nerve regeneration in an axonotmesis rat model. *Biomaterials* **2008,** *29*, 4409-4419.

14. Morelli, S.; Piscioneri, A.; Messina, A.; Salerno, S.; Al-Fageeh, M. B.; Drioli, E.; De Bartolo, L., Biodegradable Membranes for Neuronal Growth and Differentiation. *Procedia Engineering* **2012,** *44*, 363-366.

15. Pereira, T.; Gartner, A.; Amorim, I.; Almeida, A.; Caseiro, A. R.; Armada-da-Silva, P. A. S.; Amado, S.; Fregnan, F.; Varejão; o, A. S. P.; Santos, J. D.; Bartolo, P. J.; Geuna, S.; Lu; s, A. L.; Mauricio, A. C., Promoting Nerve Regeneration in a Neurotmesis Rat Model Using Poly(DL-lactide--caprolactone) Membranes and Mesenchymal Stem Cells

from the Wharton's Jelly: *In Vitro* and *In Vivo* Analysis. *BioMed Research International* **2014,** *2014*, 17.

16. Kehoe, S.; Zhang, X. F.; Boyd, D., FDA approved guidance conduits and wraps for peripheral nerve injury: a review of materials and efficacy. *Injury* **2012,** *43*, 553-572.

17. Remya, N. S.; Syama, S.; Sabareeswaran, A.; Mohanan, P. V., Toxicity, toxicokinetics and biodistribution of dextran stabilized Iron oxide Nanoparticles for biomedical applications. *International Journal of Pharmaceutics* **2016,** *511*, 586-598.

18. Icoz, D. Z.; Moraru, C. I.; Kokini, J. L., Polymer–polymer interactions in dextran systems using thermal analysis. *Carbohydrate Polymers* **2005,** *62*, 120-129.

19. Maia, J.; Carvalho, R. A.; Coelho, J. F. J.; Simões, P. N.; Gil, M. H., Insight on the periodate oxidation of dextran and its structural vicissitudes. *Polymer* **2011,** *52*, 258-265.

20. Ghica, M.; Albu Kaya, M.; Dinu-Pîrvu, C.-E.; Lupuleasa, D.; Udeanu, D., Development, Optimization and *In Vitro/In Vivo* Characterization of Collagen-Dextran Spongious Wound Dressings Loaded with Flufenamic Acid. *Molecules* **2017,** *22*, 1552.

21. Bajpai, S. K.; Chand, N.; Tiwari, S.; Soni, S., Swelling behavior of cross-linked dextran hydrogels and preliminary Gliclazide release behavior. *International Journal of Biological Macromolecules* **2016,** *93*, 978-987.

22. Ivanovic, J.; Knauer, S.; Fanovich, A.; Milovanovic, S.; Stamenic, M.; Jaeger, P.; Zizovic, I.; Eggers, R., Supercritical CO2 sorption kinetics and thymol impregnation of PCL and PCL-HA. *The Journal of Supercritical Fluids* **2016,** *107*, 486-498.

23. Hoffman, A. S., Hydrogels for biomedical applications. *Advanced Drug Delivery Reviews* **2012,** *64*, 18-23.

24. Yucel Falco, C.; Falkman, P.; Risbo, J.; Cárdenas, M.; Medronho, B., Chitosan-dextran sulfate hydrogels as a potential carrier for probiotics. *Carbohydrate Polymers* **2017,** *172*, 175-183.

25. Hussain, Z.; Thu, H. E.; Shuid, A. N.; Katas, H.; Hussain, F., Recent advances in polymer-based wound dressings for the treatment of diabetic foot ulcer: an overview of state-of-the-art. *Curr Drug Targets* **2017**.

26. Kaneo, Y.; Uemura, T.; Tanaka, T.; KANOH, S., Polysaccharides as drug carriers: biodisposition of fluorescein-labeled dextrans in mice. *Biological and Pharmaceutical Bulletin* **1997,** *20*, 181-187.

27. Pan, J.-f.; Yuan, L.; Guo, C.-a.; Geng, X.-h.; Fei, T.; Fan, W.-s.; Li, S.; Yuan, H.-f.; Yan, Z.-q.; Mo, X.-m., Fabrication of modified dextran-gelatin in situ forming hydrogel and application in cartilage tissue engineering. *Journal of Materials Chemistry B* **2014,** *2*, 8346-8360.

28. Pinho, A. C.; Fonseca, A. C.; Serra, A. C.; Santos, J. D.; Coelho, J. F. J., Peripheral Nerve Regeneration: Current Status and New Strategies Using Polymeric Materials. *Advanced Healthcare Materials* **2016,** *5*, 2732-2744.

29. Yin, R.; Wang, K.; Han, J.; Nie, J., Photo-crosslinked glucose-sensitive hydrogels based on methacrylate modified dextran–concanavalin A and PEG dimethacrylate. *Carbohydrate Polymers* **2010,** *82*, 412-418.

30. Jalaja, K.; Kumar, P. R. A.; Dey, T.; Kundu, S. C.; James, N. R., Modified dextran cross-linked electrospun gelatin nanofibres for biomedical applications. *Carbohydrate Polymers* **2014,** *114*, 467-475.

31. Elisseeff, J.; Anseth, K.; Langer, R.; Hrkach, J. S., Synthesis and Characterization of Photo-Cross-Linked Polymers Based on Poly(l-lactic acid-co-l-aspartic acid). *Macromolecules* **1997,** *30*, 2182-2184.

32. Kim, S. H.; Won, C. Y.; Chu, C. C., Synthesis and characterization of dextran-based hydrogel prepared by photocrosslinking. *Carbohydrate Polymers* **1999,** *40*, 183-190.

33. Williams, C. G.; Malik, A. N.; Kim, T. K.; Manson, P. N.; Elisseeff, J. H., Variable cytocompatibility of six cell lines with photoinitiators used for polymerizing hydrogels and cell encapsulation. *Biomaterials* **2005,** *26*, 1211-1218.

34. van Dijk-Wolthuis, W. N. E.; Franssen, O.; Talsma, H.; van Steenbergen, M. J.; Kettenes-van den Bosch, J. J.; Hennink, W. E., Synthesis, Characterization, and Polymerization of Glycidyl Methacrylate Derivatized Dextran. *Macromolecules* **1995,** *28*, 6317-6322.

35. Almeida, J. F.; Ferreira, P.; Lopes, A.; Gil, M. H., Photocrosslinkable biodegradable responsive hydrogels as drug delivery systems. *International Journal of Biological Macromolecules* **2011,** *49*, 948-954.

36. Ferreira, P.; Coelho, J. F. J.; Gil, M. H., Development of a new photocrosslinkable biodegradable bioadhesive. *International Journal of Pharmaceutics* **2008,** *352*, 172-181.

37. Pabari, A.; Yang, S. Y.; Seifalian, A. M.; Mosahebi, A., Modern surgical management of peripheral nerve gap. *Journal of Plastic Reconstruction & Aesthetic Surgery* **2010,** *63*, 1941-1948.

38. Bahney, C. S.; Lujan, T. J.; Hsu, C. W.; Bottlang, M.; West, J. L.; Johnstone, B., Visible light photoinitiation of mesenchymal stem cell-laden bioresponsive hydrogels. *European Cell Materials* **2011,** *22*, 43-55; discussion 55.

39. Ceylan, M.; Yang, S.-Y.; Asmatulu, R., Effects of gentamicin-loaded PCL nanofibers on growth of Gram positive and Gram negative bacteria. *International Journal of Applied Microbiology and Biotechnology Research* **2017,** *5*, 40-51.

40. Fiege, K.; Lünsdorf, H.; Atarijabarzadeh, S.; Mischnick, P., Cyanoethylation of the glucans dextran and pullulan: Substitution pattern and formation of nanostructures and entrapment of magnetic nanoparticles. *Beilstein Journal of Organic Chemistry* **2012,** *8*, 551-566.

41. Dou, H.; Tang, M.; Sun, K., A Facile One-Pot Synthesis to Dextran-Based Nanoparticles with Carboxy Functional Groups. *Macromolecular Chemistry and Physics* **2005,** *206*, 2177-2181.

42. Varshosaz, J.; Hassanzadeh, F.; Sadeghi Aliabadi, H.; Nayebsadrian, M.; Banitalebi, M.; Rostami, M., Synthesis and Characterization of Folate-Targeted Dextran/Retinoic Acid Micelles for Doxorubicin Delivery in Acute Leukemia. *BioMed Research International* **2014,** *2014*, 14.

43. Zhou, S.; Dou, H.; Zhang, Z.; Sun, K.; Jin, Y.; Dai, T.; Zhou, G.; Shen, Z., Fluorescent dextran-based nanogels: efficient imaging nanoprobes for adipose-derived stem cells. *Polymer Chemistry* **2013,** *4*, 4103-4112.

44. Vettori, M. H. P. B.; Franchetti, S. M. M.; Contiero, J., Structural characterization of a new dextran with a low degree of branching produced by Leuconostoc mesenteroides FT045B dextransucrase. *Carbohydrate Polymers* **2012,** *88*, 1440-1444.

45. Velazquez, G.; Herrera-Gómez, A.; Martín-Polo, M. O., Identification of bound water through infrared spectroscopy in methylcellulose. *Journal of Food Engineering* **2003,** *59*, 79-84.

46. Kuang, H.; Wu, Y.; Zhang, Z.; Li, J.; Chen, X.; Xie, Z.; Jing, X.; Huang, Y., Double pH-responsive supramolecular copolymer micelles based on the complementary multiple hydrogen bonds of nucleobases and acetalated dextran for drug delivery. *Polymer Chemistry* **2015,** *6*, 3625-3633.

47. Wang, T.; Nie, J.; Yang, D., Dextran and gelatin based photocrosslinkable tissue adhesive. *Carbohydrate Polymers* **2012,** *90*, 1428-1436.

48. Elzein, T.; Nasser-Eddine, M.; Delaite, C.; Bistac, S.; Dumas, P., FTIR study of polycaprolactone chain organization at interfaces. *Journal of Colloid and Interface Science* **2004,** *273*, 381-387.

49. Benkaddour, A.; Jradi, K.; Robert, S.; Daneault, C., Grafting of Polycaprolactone on Oxidized Nanocelluloses by Click Chemistry. *Nanomaterials* **2013,** *3*, 141-157.

50. Chiono, V.; Mozetic, P.; Boffito, M.; Sartori, S.; Gioffredi, E.; Silvestri, A.; Rainer, A.; Giannitelli, S. M.; Trombetta, M.; Nurzynska, D.; Di Meglio, F.; Castaldo, C.; Miraglia, R.; Montagnani, S.; Ciardelli, G., Polyurethane-based scaffolds for myocardial tissue engineering. *Interface Focus* **2014,** *4*.

51. Fernández, M. J.; Fernández, M. D.; Cobos, M., Synthesis, characterization and properties of telechelic hybrid biodegradable polymers containing polyhedral oligomeric silsesquioxane (POSS). *RSC Advances* **2014,** *4*, 21435-21449.

52. Ikpo, N.; Flogeras, J. C.; Kerton, F. M., Aluminium coordination complexes in copolymerization reactions of carbon dioxide and epoxides. *Dalton Transactions* **2013,** *42*, 8998-9006.

53. Stenekes, R. J. H.; Talsma, H.; Hennink, W. E., Formation of dextran hydrogels by crystallization. *Biomaterials* **2001,** *22*, 1891-1898.

54. Juríková, A.; Csach, K.; Miškuf, J.; Koneracká, M.; Závišová, V.; Kubovčíková, M.; Kopčanský, P., Thermal analysis of magnetic nanoparticles modified with dextran. *Acta Physica Polonica-Series A General Physics* **2012,** *121*, 1296.

55. Lapprand, A.; Boisson, F.; Delolme, F.; Méchin, F.; Pascault, J. P., Reactivity of isocyanates with urethanes: Conditions for allophanate formation. *Polymer Degradation and Stability* **2005,** *90*, 363-373.

56. Semsarzadeh, M. A.; Navarchian, A. H., Effects of NCO/OH ratio and catalyst concentration on structure, thermal stability, and crosslink density of poly(urethane-isocyanurate). *Journal of Applied Polymer Science* **2003,** *90*, 963-972.

57. Campos, F. d. S.; Cassimiro, D. L.; Crespi, M. S.; Almeida, A. E.; Gremião, M. P. D., Preparation and characterisation of Dextran-70 hydrogel for controlled release of praziquantel. *Brazilian Journal of Pharmaceutical Sciences* **2013,** *49*, 75-83.

58. Ferreira, P.; Pereira, R.; Coelho, J. F. J.; Silva, A. F. M.; Gil, M. H., Modification of the biopolymer castor oil with free isocyanate groups to be applied as bioadhesive. *International Journal of Biological Macromolecules* **2007,** *40*, 144-152.

59. Bandzierz, K.; Reuvekamp, L.; Dryzek, J.; Dierkes, W.; Blume, A.; Bielinski, D., Influence of Network Structure on Glass Transition Temperature of Elastomers. *Materials* **2016,** *9*, 607.

60. Kwei, T. K., The effect of hydrogen bonding on the glass transition temperatures of polymer mixtures. *Journal of Polymer Science: Polymer Letters Edition* **1984,** *22*, 307-313.

61. Trovati, G.; Sanches, E. A.; Neto, S. C.; Mascarenhas, Y. P.; Chierice, G. O., Characterization of polyurethane resins by FTIR, TGA, and XRD. *Journal of Applied Polymer Science* **2010,** *115*, 263-268.

62. Wunderlich, B., *Thermal analysis of polymeric materials*. Springer Science & Business Media: **2005**.

63. Persenaire, O.; Alexandre, M.; Degée, P.; Dubois, P., Mechanisms and Kinetics of Thermal Degradation of Poly(ε-caprolactone). *Biomacromolecules* **2001,** *2*, 288-294.

64. Jenkins, M. J.; Harrison, K. L.; Silva, M. M. C. G.; Whitaker, M. J.; Shakesheff, K. M.; Howdle, S. M., Characterisation of microcellular foams produced from semi-crystalline PCL using supercritical carbon dioxide. *European Polymer Journal* **2006,** *42*, 3145-3151.

65. İmren, D.; Gümüşderelioğlu, M.; Güner, A., Synthesis and characterization of dextran hydrogels prepared with chlor- and nitrogen-containing crosslinkers. *Journal of Applied Polymer Science* **2006,** *102*, 4213-4221.

66. Kenari, H. S.; Imani, M.; Nodehi, A., Full factorial design-of-experiments for preparation of crosslinked dextran microspheres. *Journal of Applied Polymer Science* **2013,** *127*, 3712-3724.

67. Charulatha, V.; Rajaram, A., Influence of different crosslinking treatments on the physical properties of collagen membranes. *Biomaterials* **2003,** *24*, 759-767.

68. Park, S.-J.; Cho, K.-S., Filler–elastomer interactions: influence of silane coupling agent on crosslink density and thermal stability of silica/rubber composites. *Journal of Colloid and Interface Science* **2003,** *267*, 86-91.

69. Windrum, P.; Morris, T.; Drake, M.; Niederwieser, D.; Ruutu, T., Variation in dimethyl sulfoxide use in stem cell transplantation: a survey of EBMT centres. *Bone marrow transplantation* **2005,** *36*, 601-603.

70. Scandola, M.; Ceccorulli, G.; Pizzoli, M., Molecular motions of polysaccharides in the solid state: dextran, pullulan and amylose. *International Journal of Biological Macromolecules* **1991,** *13*, 254-260.

71. Ruini, F.; Tonda-Turo, C.; Chiono, V.; Ciardelli, G., Chitosan membranes for tissue engineering: comparison of different crosslinkers. *Biomedical Materials* **2015,** *10*, 065002.

72. Shanmugasundaram, N.; Ravichandran, P.; Neelakanta Reddy, P.; Ramamurty, N.; Pal, S.; Panduranga Rao, K., Collagen–chitosan polymeric scaffolds for the *in vitro* culture of human epidermoid carcinoma cells. *Biomaterials* **2001,** *22*, 1943-1951.

73. Lu, G.; Kong, L.; Sheng, B.; Wang, G.; Gong, Y.; Zhang, X., Degradation of covalently cross-linked carboxymethyl chitosan and its potential application for peripheral nerve regeneration. *European Polymer Journal* **2007,** *43*, 3807-3818.

Chapter 3. **CYTOCOMPATIBILITY EVALUATION USING HDPSCS AND BIOCOMPATIBILITY EVALUATION BY ISO 10-998-6 SCORE – MEMBRANES**

3.1 ABSTRACT

The peripheral nerve system has the ability to self-regenerate after nerve injury.[1] In this sense, studies have been carried out in order to evaluate the regeneration process within a closed environment provided by a nerve guide conduit.[2]

The aim of this part of the work was to evaluate the cytocompatibility of the dextran-based membranes by measuring *in vitro* viability of cells in contact with these previously prepared biomaterials. In addition, the membranes showing the most promising results were subcutaneously implanted in rats' dorsum, to assess the extension of the host inflammatory response in order to evaluate the biocompatibility using ISO 10998-6 score.

The cell viability essays show that, in general, all the membranes are adequate substrates for cell growth and proliferation. From the dextran-based membranes tested, the ones with the co-macromonomer PCL_IEMA in their formulation revealed the best results. M_GMA(0.5)_PCL(0), M_GMA(0.2)_PCL(0.2) and M_GMA(0.1)_PCL(0.3) samples were tested in an animal model. According to the ISO 10993-6:2016 classification, after 15 days M_GMA(0.5)_PCL(0) was considered to be "*slight-irritant*". Moreover, M_GMA(0.2)_PCL(0.2) and M_GMA(0.1)_PCL(0.3) were classified as "*non-irritant*". Histological analysis were also conducted in main tissue organs, showing no signs of fibrosis or necrosis in order to ensure that the by-products resulting from absorption of these materials were not systemic toxic and do not accumulate in the main organs. Modified dextran-based membranes can be considered promising candidates for the preparation of medical devices involved in peripheral nerve regeneration / reconstruction.

3.2 INTRODUCTION

Despite the intrinsic nature of peripheral nerves to regenerate by themselves[3], functional recovery is often poor, leading to drastic changes in the life quality of patients.[4,5] In the cases where the injury involves substantial tissue loss, nerve autograph is still the most common technique used, despite the disadvantages associated to this procedure.[6,7] To overcome these limitations, different techniques, including the use of polymeric materials to build structures (nerve tube-guides for example), which could support the growth of newly formed axons and support glial cells involved in the regeneration process, have been studied.

Among the classes of polymeric materials reported, namely natural and synthetic, the first ones have shown the most promising results.[8] In this sense, dextran, a bacterially derived polysaccharide, which is biocompatible and biodegradable in physiological environment, arises as a good candidate for the preparation of devices suitable for this application.[9,10] Moreover, this natural polymer has been widely used in the biomedical field, as core material of surgical adhesives[11] and hydrogels[9] for tissue regeneration purpose.

Since the aim of the preparation of materials for peripheral nerve regeneration enhancement, the material characterization upon implantation needs to be assessed.[12] Before the use of animal models, *in vitro* tests should be performed to evaluate the cytocompatibility, allowing the evaluation of the interaction between the biomaterial and cell lines. [13] In this regard, Human mesenchymal stem cells (hMSCs) from the Wharton's jelly umbilical cord have been used for this propose. These cells are considered to be very interesting for research and therapeutic applications due to their high capacity for self-renewal, multi-lineage differentiation and growth factors production.[14] Additionally, their collection is easy[15] and they can be cryogenically stored and finally expanded for therapeutic purposes.[16] More recently, Human dental pulp stem cells (hDPSCs) have been also used in these studies, due to their feasibility and biological properties.[17] These cells are considered to be also highly proliferative which increased its use for the scaffolds seeding in regenerative medicine.[18]

In what concerns to the study of the biocompatibility of a material in *in vivo* models, a common approach for preliminary studies is the subcutaneous implantation of the material in rats. This approach has been reported for several medical devices used in peripheral nerve and bone regeneration to evaluate the extent of host inflammatory response and the occurrence of revascularization.[19-22] In addition, from histological analysis of tissues and organs it is possible to evaluate if the material and the by-products resulting from the absorption of these materials are accumulated in the main organs and have a systemic negative effect.

This part of the work corresponds to the evaluation of the *in vitro* and *in vivo* performance of dextran-based membranes. These membranes were prepared with dextran modified with two different monomers: glycidyl methacrylate (GMA) or 2-isocyanoethylmethacrylate (IEMA) following a photocrosslinking step (see Chapter 2). In addition, to enhance flexibility, a poly(ε-caprolactone) (PCL) based co-macromonomer was added to the formulations. The cell viability / apoptosis essay was assessed using an *in vitro* model based on hDPSCs. After this test, the intracellular ionic calcium concentration ($[Ca^{2+}]_i$) of the adherent cells was measured by an

epifluorescence technique to evaluate if cells were viable or initiating the apoptosis process. After this initial screening, membrane samples were implanted subcutaneously in rats' dorsum. The inflammatory response / cell counting on the site of implantation was assessed and compared with a control rat with no biomaterial implanted. The histological analysis of tissue surrounding the implants and from organs was also performed. The results obtained correspond to healthy tissue with no signs of fibrosis or necrosis.

3.3 EXPERIMENTAL SECTION

3.3.1 Materials

Dextran (Mw=70000 g/mol) was purchased from Sigma Aldrich (St. Louis, Missouri, USA). Glycidyl methacrylate (GMA) was purchased from Acros Organics (Geel, Belgium). 4-Dimethylaminopyridine (DMAP), 2-Isocyanatoethyl methacrylate (IEMA) were acquired from TCI Europe (Zwijndrecht, Bélgica) and dimethyl sulfoxide (DMSO) was purchased from Fisher Scientific (Hampton, New Hampshire, EUA). Dibutyltin dilaurate was obtained from Fluka (St. Louis, Missouri, USA). Tetrahydrofuran (THF) was obtained from VWR (Radnor, Pensilvânia, EUA) and *n*-hexane was obtained from José Manuel Gomes dos Santos, Lda (Odivelas, Portugal). Poly(ε-caprolactone)-diol (PCL-diol Capa ™2054; Mw=550 g/mol) was a gift from Perstorp (Warrington, UK). Irgacure 2959® was gently supplied by Ciba Specialty Chemicals (Basel, Switzerland). D_2O and DMSO-d_6 were acquired from Euriso-Top (Saint-Aubin, France). Sodium azide was purchased from Panreac (Barcelona, Spain). Human Dental Pulp stem cells (DPSCs) were obtained from AllCells, LLC (Cat. DP0037F, Lot No. DPSC090411-01). MEM α, GlutaMAX™ Supplement, no nucleosides, Streptomycin, Amphotericin B and HEPES Buffer solution were purchased from Gibco, with catalog's number of 32561029, 15140122, 15290026 and 15630122, respectively. Also, Phosphate buffer solution (PBS) was obtained from Gibco, Life Technologies. Fetal Bovine Serum (FBS) was acquired from BI, Biological Industries (BI LTD, Certified FBS, ref#04-400-1A). Presto Blue cell viability reagent was purchased from Invitrogen (A13262).

3.3.2 Procedures and Methods

Preparation of Membranes

The preparation of the membranes was already described in section 2.3.2 of Chapter 2.

Table 3.1 resumes the composition and nomenclature of the membranes used in this Chapter.

Table 3.1 Composition of the membranes[1].

Membranes	Composition	
Designation	**Modified dextran**	**PCL-IEMA**
M_GMA(0.5)_PCL(0)	0.5g P_LMW_GMA8*	--------
M_GMA(0.2)_PCL(0.2)	0.2g P_LMW_GMA24**	0.2g
M_GMA(0.1)_PCL(0.3)	0.1g P_LMW_GMA24	0.3g
M_IEMA(0.5)_PCL(0)	0.5g P_LMW_IEMA	--------
M_IEMA(0.2)_PCL(0.2)	0.2g P_LMW_IEMA	0.2g
M_IEMA(0.1)_PCL(0.3)	0.1g P_LMW_IEMA	0.3g

* 8 - corresponds to 8h – time of reaction between dextran and GMA
** 24 – corresponds to 24h - time of reaction between dextran and GMA

***In vitro* validation – Cell viability assessment**

Sample preparation

All membranes were sterilized by UV irradiation of 3 sets of 30 minute periods.

[1] Since only P_LMW was used in this chapter, the nomenclature of membranes was shortened. However, as can be observed in Table 3.1, the formulations used remain as previously reported in Chapter 2.

Cell culture and maintenance

DPSCs were maintained in MEM α, GlutaMAX™ supplement, no nucleosides, supplemented with 10% (v/v) FBS, 100 IU/mL penicillin, 0.1 mg/mL streptomycin, 2.05 µg/mL amphotericin B and 10mM HEPES buffer solution. FBS is heat inactivated, sterile-filtered, and according to the manufacturer information, presents hemoglobin in a concentration ≤25 mg/dL, and ≤10 EU/mL endotoxin. All cells were maintained at 37ºC and 95% humidified atmosphere with 5% CO^2, environment.

Presto Blue® Cell Viability Protocol

The Presto Blue® assay is a commercially available, ready-to-use, water-soluble preparation. Cell viability assessment is based on a cell permeable resarzurin-based solution that functions as a cell viability indicator by using the reducing power of living cells to quantitatively measure the proliferation of cells.

M_GMA(0.5)_PCL(0), M_GMA(0.2)_PCL(0.2), M_GMA(0.1)_PCL(0.3), M_IEMA(0.5)_PCL(0), M_IEMA(0.2)_PCL(0.2) and M_IEMA(0.1)_PCL(0.3) implants were fixed to each well in a 24-well cell culture plate, and relevant controls were prepared with the fixation agent alone and implants without cells. Implants were seeded at $4x10^4$ cells/well density. Cells were left adhering in 0.5 mL of complete culture medium overnight.

At every time point [24 hours (1 day), 72 hours (3 days), 120 hours (5 days) and 168 hours (7 days)] culture medium was removed from each well and fresh complete medium was added to each well, with 10% (v/v) of 10x Presto Blue® cell viability reagent.

Cells were incubated for 1 hour at 37ºC, 5% CO_2, changes in cell viability were detected by absorption spectroscopy in a Thermo Scientific Multiskan FC. Supernatant was collected and transferred to a 96-well plate and absorbance was read at 570 nm and 595 nm. After, cells were washed with PBS to remove any Presto Blue® residues and fresh culture medium is reset to each well. Presto Blue® excitation wavelength is 570 nm, and emission is at 595 nm. For each well, the absorbance at 595 nm (normalization wavelength) was subtracted to the absorbance at 570 nm (experimental result). Corrected absorbance is obtained by the subtraction of average of the control wells to each experimental well.

Cell viability assessment statistical analysis

Statistical analysis was performed using the GraphPad Prism version 6.00 for Mac OS X, GraphPad Software, La Jolla California USA. The experiments were performed in quadruplicates and the results were presented as Mean ± Standard Deviation (SD). Analysis was performed by one-way ANOVA test followed by Tukey multiple comparisons test. Differences were considered statistically significant at $P \leq 0.05$. Results significance are presented through the symbol (*). Significance results are also indicated according to P values with one, two, three or four of the symbols (*) corresponding to 0.01<p 0.05, 0.001<p 0.01, 0.0001<p 0.001 e p 0.0001, respectively.

Epifluorescence technique

$[Ca^{2+}]_i$ was measured in Fura-2-AM-loaded cells by using dual wavelength spectrofluorometry as previously described[23].

Ca^{2+} indicator Fura-2/AM loading

DPSCs cells (cultured on and around the following membranes: M_GMA(0.5)_PCL(0), M_GMA(0.2)_PCL(0.2), M_GMA(0.1)_PCL(0.3), M_IEMA(0.5)_PCL(0), M_IEMA(0.2)_PCL(0.2), M_IEMA(0.1)_PCL(0.3), were loaded with Ca^{2+} indicator by incubation in 2.5 mM fura-2 acetoxymethyl ester (Fura-2-AM, Molecular Probes) and 0.03% pluronic (Molecular Probe) in a Ringer solution with the following composition: 121 mM NaCl, 5.4 mM KCl, 9 mM D-glucose, 1.5 mM $MgCl_2$, 1.8 mM $CaCl_2$, 6 mM $NaHCO_3$, and 25 mM HEPES, with a pH of 7.4; at 37◦C in darkness for 120 minutes.

Measurement of intracellular Ca^{2+} in DPSCs

After loading Fura-2-AM, DPSCs cells were washed in Ringer Solution (121 mM NaCl, 5.4 mM KCl, 9 mM D-glucose, 1.5 mM $MgCl_2$, 1.8 mM $CaCl_2$, 6 mM $NaHCO_3$, and 25 mM HEPES, with a pH 7.4). The wells that presented adhering hDPCSs cells on M_GMA(0.5)_PCL(0), M_GMA(0.2)_PCL(0.2), M_GMA(0.1)_PCL(0.3), M_IEMA(0.5)_PCL(0), M_IEMA(0.2)_PCL(0.2) and M_IEMA(0.1)_PCL(0.3) were transferred to a glass chamber containing 100 µl of the Ringer Solution. The chamber was placed in a well on the stage of an epifluorescence microscope (Zeiss, Germany). Fluorescence

measurements were performed in each individual cell. The emitted fluorescence intensities at 510 nm were acquired by computer software, which registered the number of photons emitted per second, during 30 s for each 340 nm and 380 nm excitation wavelengths. The $[Ca^{2+}]_i$ was estimated from the equation proposed by Grynkiewiez.[24] For determination background fluorescence, cells were incubated in 2.5 mM 4-br-A23186 (Molecular Probe) and 10 mM $MnCl_2$ in 100 µl of Ringer solution at room temperature in darkness for 10 minutes. The $[Ca^{2+}]_i$ measurements considered for these results were the ones which background signal was inferior to 20% of the total emitted fluorescence.

All data were presented as mean ± SEM, where N is the number of cells where the $[Ca^{2+}]_i$ was measured by the epifluorescence technique. All statistical tests were Student's t test.[25] The given P values correspond to errors of the second kind ($P < 0.05$). For each experimental condition M_GMA(0.5)_PCL(0), M_GMA(0.2)_PCL(0.2), M_GMA(0.1)_PCL(0.3), M_IEMA(0.5)_PCL(0), M_IEMA(0.2)_PCL(0.2) and M_IEMA(0.1)_PCL(0.3), 25 DPSCs cells were analyzed.

In vivo **biocompatibility studies of implantable devices in subcutaneous tissue [ISO 10993-6:2016]**

Surgical Procedure

Implants of M_GMA(0.5)_PCL(0), M_GMA(0.2)_PCL(0.2) and M_GMA(0.1)_PCL(0.3) were tested in adult male Sasco Sprague-Dawley rats (Charles River, Barcelona, Spain) weighing 250-300 g. All animals were housed in a temperature and humidity controlled room with 12-12 hours light/dark cycles, two animals per cage and are allowed normal cage activities under standard laboratory conditions. The animals were fed with standard chow and water *ad libitum*. For the biomaterial implantation, anesthesia was administered intraperitoneally Xylazine/Ketamin (Rompun®/Imalgène 1000®; 1,25mg/ 9mg per 100 g b.w., intraperitoneally), and the skin prepared for surgical access. Up to three 15-20 mm long linear incisions were made paired along the dorsum. After blunt dissection towards the ventral aspect of the body, a portion of biomaterial was implanted subcutaneously. Skin and subcutaneous tissues were sutured, and animals recovered and returned to their housing groups. At 3, 7 and 15 days after surgery, after deep anesthesia, the rats were then euthanized, by lethal intra-cardiac injection (Eutasil® 200 mg/ml, 200 mg/kg b.w.). Skin and subcutaneous tissues from the implant area were collected and fixed in with 4% -formaldehyde. All the animal testing procedures were in

conformity with the Directive 2010/63/EU of the European Parliament and the Portuguese DL 113/2013. All the procedures are approved by the ICBAS-UP Animal Welfare Organism of the Ethics Committee and by the Veterinary Authorities of Portugal (DGAV). Humane end points will be followed in accordance to the OECD Guidelines (2000).

Histological evaluation

Samples were routinely processed for histopathological analysis, and 3µm-thin sequential sections were stained with hematoxylin-Eosin (H&E) for accurate evaluation using a Nikon microscope (Nikon Eclipse E600) equipped with ×2, ×4, ×10 and ×40 objectives and coupled with a photo camera (Nikon Digital Sight DS-5M) equipped with a lens (Nikon PLAN UW 2X/0.06). Preparations were assessed for inflammatory infiltrate, fibrosis, angiogenesis and/or necrosis surrounding the implants according to the annex E from ISO-10993-6 by experienced veterinary pathologist.

The ISO-10998-6 standard focus on the identification and grading of the inflammatory cells populations surrounding the implanted biomaterial, as well as evaluating concurrent events, such as the presence of giant cells, necrosis, fibrosis, and local vascularization. Individual scores are attributed to each parameter according to the ISO's proposed system. The scoring system proposed is presented in Table 3.2 and Table 3.3.

Table 3.2 Key parameters and scoring system used for the histological evaluation system – cell type/response.

Cell type/response	**Score**				
	0	**1**	**2**	**3**	**4**
Polymorphonuclear cells	0	Rare, 1-5/phf*	5-10/phf*	Heavy infiltrate	Packed
Lymphocytes	0	Rare, 1-5/phf*	5-10/phf*	Heavy infiltrate	Packed
Plasma cells	0	Rare, 1-5/phf*	5-10/phf*	Heavy infiltrate	Packed
Macrophages	0	Rare, 1-5/phf*	5-10/phf*	Heavy infiltrate	Packed
Giant cells	0	Rare, 1-2/phf*	3-5/phf*	Heavy infiltrate	Sheets
Necrosis	0	Minimal	Mild	Moderate	Severe

*phf – per high powered (400x) field.

Table 3.3 Key parameters and scoring system used for the histological evaluation system – response.

Response	Score				
	0	**1**	**2**	**3**	**4**
Neovascularisation	0	Minimal capillary proliferation, focal, 1-3buds	Groups of 4-7 capillaries, with supporting fibroblastic structures	Broad band of capillaries with supporting structures	Extensive band of capillaries with supporting fibroblastic structures
Fibrosis	0	Narrow band	Moderately thick bands	Thick band	Extensive band
Fatty infiltrate	0	Minimal amount of fat associated with fibrosis	Several layers of fat and fibrosis	Elongated and broad accumulation of fat cells about the implant site	Extensive fat completely surrounding the implant

This system enables the semi-quantitative classification of the implants as *"non-irritant"* (score 0,0 up to 2,9), *"slight irritant"* (score 3,0 up to 8,9), *"moderate irritant"* (score 9,0 up to 15,0) or *"severe irritant"* (score> 15).

Statistical Analysis

Statistical analysis was performed using the GraphPad Prism version 6.00 for Mac OS X, GraphPad Software, La Jolla California USA. The experiments were performed in quadruplicates and the results were presented as Mean ± Standard Error Mean (SEM). Analysis was performed by one-way ANOVA test followed by Tukey multiple comparisons test. Differences were considered statistically significant at $P \leq 0.05$. Results significance are presented as compared to sham through the symbol (*). Significance results are also indicated according to P values with one, two, three or four of the symbols (*) corresponding to 0.01<p 0.05, 0.001<p 0.01, 0.0001<p 0.001 e p 0.0001, respectively.

3.3.3 Morphological characterization by *Scanning Electron Microscopy*

Scanning electron micrographies (SEM) of the surface and transversal cut of the prepared tubes were obtained using a *JOEL XL30* equipment, with Energy Dispersive Spectometry system (EDS) from *EDAX*. The observations were conducted with a beam acceleration voltage of 10kV.

Sample Preparation: After the *in vitro* assessment, all samples were kept in a plate with 24 wells. The samples were then rinsed three times with 1mL of phosphate buffer solution (PBS). After complete removal of PBS, 1mL of a solution of glutaraldehyde 5% (v/v) was inserted into the wells. This solution was kept in contact with the samples for 15 minutes. During this time, the aldehyde groups of the solution bonded with the amine groups of the proteins, establishing crosslinking points, which helped in the maintenance of the cytoskeletal of the cells during the dehydration process. After this process, the samples were washed one time with 1mL of the PBS solution. For the dehydration process, four solutions with different concentrations of ethanol were prepared. The first solution had a concentration of 25% of ethanol, the second had 50%, followed by the third with 75% and finally, the last one, was 100% ethanol. To begin the dehydration process, the 1mL of the first ethanol solution was added to each well and kept for 10 minutes. Then, this solution was removed and the next solution (50% concentration) was added and kept in the well for the same time as the first one. This process was performed consecutively until the last solution (100%) was finally removed from the well. Posteriorly, the samples were completely dried. Since the samples are non-conductive, they were coated with a thin layer of gold, using the sputtering technique. The equipment used was from Edwards EXC 120 with a Huttinger PFG 1500 DC power source. Samples were coated for 1min with P=0.11kW, V=1000V and I=1.83A. After this stage, the samples were ready for the study with SEM.

3.4 RESULTS AND DISCUSSION

According to the results reported in the previous chapter, the differences in structural characteristics between membranes prepared with P_LMW and P_HMW were not significant. In this sense, in the present work, the membranes tested (Table 3.1) were all prepared based on P_LMW.

Regarding the membranes prepared with dextran modified with GMA (Table 3.1), two different precursors were used: P_LMW_GMA8 and P_LMW_GMA24. The difference between these two precursors is the degree of substitution (DS) of dextran, which is higher for P_LMW_GMA24.

3.4.1 Cytocompatibility assessment

The studies of cell viability were performed in the following membranes: M_GMA(0.5)_PCL(0), M_GMA(0.2)_PCL(0.2), M_GMA(0.1)_PCL(0.3), M_IEMA(0.5)_PCL(0), M_IEMA(0.2)_PCL(0.2), and M_IEMA(0.1)_PCL(0.3), during 24 hours (1 day), 72 hours (3 days), 120 hours (5 days) and 168 hours (7 days) time points. Table 3.4 presents the absorbance values obtained by Presto Blue® viability assay.

Table 3.4 Absorbance assessed by Presto Blue® viability assay of hMSCs seeded in membranes for up to 7 days.

Sample	Day 1	Day 3	Day 5	Day 7
Ct	0.1876 ± 0.0129	0.3304 ± 0.0096	0.6234 ± 0.0256	0.4563 ± 0.0134
Ct SG	0.1639 ± 0.0047	0.3654 ± 0.0539	0.6293 ± 0.0065	0.4341 ± 0.0107
M_GMA(0.5)_PCL(0)	0.0959 ± 0.0142	0.2874 ± 0.0338	0.4594 ± 0.0681	0.3656 ± 0.0566
M_GMA(0.2)_PCL(0.2)	0.0846 ± 0.0058	0.3024 ± 0.0031	0.4669 ± 0.0097	0.3824 ± 0.0162
M_GMA(0.1)_PCL(0.3)	0.1129 ± 0.0052	0.2900 ± 0.0207	0.5629 ± 0.0208	0.4428 ± 0.0239
M_IEMA(0.5)_PCL(0)	0.0806 ± 0.0059	0.2337 ± 0.0071	0.3638 ± 0.0178	0.2559 ± 0.0110
M_IEMA(0.2)_PCL(0.2)	0.1202 ± 0.0034	0.3905 ± 0.0200	0.5486 ± 0.0291	0.4849 ± 0.0085
M_IEMA(0.1)_PCL(0.3)	0.1371 ± 0.0028	0.4045 ± 0.0077	0.5897 ± 0.0222	0.4875 ± 0.0283

Results presented as Mean ± SD. Ct stands for to the Control, which corresponds to the well filled only with the culture media. Ct SG stands for Control with super glue (fixation agent), which corresponds to a well with super glue on it, immersed in culture media.

Results show that fixation agent used to fix the membranes to the cell culture plate does not significantly affect cell adhesion and cell metabolism as compared to the control at any time point. This can be observed by the similarity of absorbance values obtained for the control (Ct) with the values obtained for the control with the fixation agent (Ct SG).

Presto Blue® is a resazurin-based solution, which is cell permeable. When in contact with cells, the viable ones have the ability to metabolize this reagent, which results into a change of color from blue to red. After this modification, the reagent becomes highly fluorescent. This color change can be detected using absorbance (technique used in this work) or fluorescence. With the information given by this technique, it is not possible to know how many cells adhere to a substrate, or even the percentage of surface covered. However, before measuring, both wells and samples are washed in order to assure that the signals measured are referred to the adherent cells. Additionally, the absorbance of the well itself (595 nm – normalization wavelength) is also subtracted to the final signal (570 nm – experimental result). Considering these procedures, it is considered that higher absorbance values are related to higher number of cells adhered to the surface.

It is noteworthy the fact that cell adhesion to the membranes upon seeding is significantly inferior to the control and to the fixation agent control. This may be due to the adjustment of cells to the architecture of the membranes that are bend and not flat, which can hinder the process of cell adhesion.

In general M_IEMA(0.2)_PCL(0.2) and M_IEMA(0.1)_PCL(0.3) membranes showed enhanced cell adhesion, viability and metabolic rates at all time points, and especially after 3 days incubation. In fact, the absorbance is significantly superior to the control. At later incubation time (at 5 and 7 days) M_GMA(0.1)_PCL(0.3) membranes follow M_IEMA(0.2)_PCL(0.2) and M_IEMA(0.1)_PCL(0.3) performances and show improved cell viability and metabolic activity as compared to the control. The significance of the results of absorbance obtained (Table 3.4) is shown in Figure 3.1.

Day 1

Groups	Ct	Ct SG	M_GMA(0.5)_PCL(0)	M_GMA(0.2)_PCL(0.2)	M_GMA(0.1)_PCL(0.3)	M_GMA(0.5)_PCL(0)	M_IEMA(0.2)_PCL(0.2)	M_IEMA(0.1)_PCL(0.3)
Ct								
Ct SG	*							
M_GMA(0.5)_PCL(0)	****	****						
M_GMA(0.2)_PCL(0.2)	****	****	ns					
M_GMA(0.1)_PCL(0.3)	****	****	**	****				
M_IEMA(0.5)_PCL(0)	****	****	*	*	****			
M_IEMA(0.2)_PCL(0.2)	****	****	**	****	*	****		
M_GMA(0.1)_PCL(0.3)	****	****	***	****	****	****	****	

Day 3

Groups	Ct	Ct SG	M_GMA(0.5)_PCL(0)	M_GMA(0.2)_PCL(0.2)	M_GMA(0.1)_PCL(0.3)	M_GMA(0.5)_PCL(0)	M_IEMA(0.2)_PCL(0.2)	M_IEMA(0.1)_PCL(0.3)
Ct								
Ct SG	ns							
M_GMA(0.5)_PCL(0)	ns	ns						
M_GMA(0.2)_PCL(0.2)	**	ns	ns					
M_GMA(0.1)_PCL(0.3)	*	**	ns	ns				
M_IEMA(0.5)_PCL(0)	****	**	**	****	**			
M_IEMA(0.2)_PCL(0.2)	***	ns	****	****	****	****		
M_GMA(0.1)_PCL(0.3)	****	ns	****	****	****	****	ns	

Day 5

Groups	Ct	Ct SG	M_GMA(0.5)_PCL(0)	M_GMA(0.2)_PCL(0.2)	M_GMA(0.1)_PCL(0.3)	M_GMA(0.5)_PCL(0)	M_IEMA(0.2)_PCL(0.2)	M_IEMA(0.1)_PCL(0.3)
Ct								
Ct SG	ns							
M_GMA(0.5)_PCL(0)	***	***						
M_GMA(0.2)_PCL(0.2)	****	****	ns					
M_GMA(0.1)_PCL(0.3)	*	***	ns	***				
M_IEMA(0.5)_PCL(0)	****	****	**	****	***			
M_IEMA(0.2)_PCL(0.2)	*	***	ns	**	ns	****		
M_GMA(0.1)_PCL(0.3)	ns	*	*	****	*	****	*	

Day 7

Groups	Ct	Ct SG	M_GMA(0.5)_PCL(0)	M_GMA(0.2)_PCL(0.2)	M_GMA(0.1)_PCL(0.3)	M_GMA(0.5)_PCL(0)	M_IEMA(0.2)_PCL(0.2)	M_IEMA(0.1)_PCL(0.3)
Ct								
Ct SG	ns							
M_GMA(0.5)_PCL(0)	**	ns						
M_GMA(0.2)_PCL(0.2)	***	**	ns					
M_GMA(0.1)_PCL(0.3)	ns	ns	ns	**				
M_IEMA(0.5)_PCL(0)	****	****	*	****	****			
M_IEMA(0.2)_PCL(0.2)	**	***	**	****	*	****		
M_GMA(0.1)_PCL(0.3)	ns	***	*	***	****	****	ns	

Figure 3.1 Absorbance assessed by Presto Blue® viability assay of hMSCs seeded in membranes. Results presented as Mean ± SD. Aborbance Results (Table 3.4) significance is represented with the symbol (*), indicated according to P values with one, and two (*) corresponding to 0.01<p 0.05, 0.001<p 0.01, respectively.

It is important to address the swelling capacity of the M_GMA(0.1)_PCL(0.3), M_IEMA(0.2)_PCL(0.2) and M_IEMA(0.1)_PCL(0.3) membranes. As mentioned in the previous chapter, these membranes have the lowest swelling capacity, which may correspond to higher crosslinking density. These structural facts, along with the presence of PCL_IEMA, seem to be beneficial for the viability of hDPSCs.

The membrane that showed consistently lower cell adhesion and cell viability rates at all time points was M_IEMA(0.5)_PCL(0). Figure 3.2 plots the correlated absorbance obtained for the tested membranes.

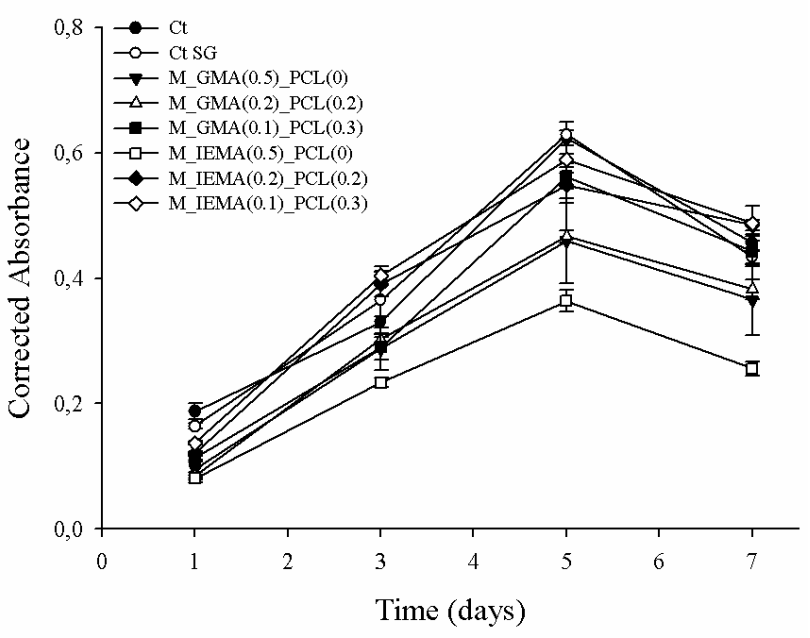

Figure 3.2 Absorbance assessed by Presto Blue® viability assay of hMSCs seeded in M_GMA(0.5)_PCL(0), M_GMA(0.2)_PCL(0.2), M_GMA(0.1)_PCL(0.3), M_IEMA(0.5)_PCL(0), M_IEMA(0.2)_PCL(0.2) and M_IEMA(0.1)_PCL(0.3) membranes for up to 7 days

At 5 days incubation, it was reached the maximum absorbance and cell metabolic activity measure. This is due to the fact that cells reached their confluency between 5 and 7 days period leading to an arrest on cell metabolic activity due to the lack of available surface space.

It is important to address that the macroscopic differences, resistance and friability of the membranes were different upon hydration. For instance, M_IEMA(0.5)_PCL(0), M_IEMA(0.2)_PCL(0.2), and M_IEMA(0.1)_PCL(0.3) membranes in general were rigid, with low pliability and glassier like. Yet, M_GMA(0.2)_PCL(0.2), and M_GMA(0.1)_PCL(0.3) membranes were flexible and with adequate resistance upon handling. Nevertheless, M_GMA(0.5)_PCL(0), although flexible was very friable and brittle when hydrated and manipulated. This behavior is in agreement with the discussion of the previous chapter.

3.4.2 Measurement of intracellular Ca^{2+} in hDPSCs

The ionic intracellular calcium is involved in several intracellular events, such as neurite outgrowth and differentiation.[26-28] Furthermore, deregulations in the mechanisms that control the concentration of intracellular calcium ions, can interfere with the normal homeostasis of cells, leading to cellular changes.[29] Also, if the calcium concentration reaches values above 105 nM, it can result in cell death.[30]

To correlate the hDPSCs ability to expand and survival capacity in the presence of the developed implants, the $[Ca^{2+}]_i$ of undifferentiated DPSCs was determined by the epifluorescence technique using the Fura-2AM probe. Fura-2, a pentacarboxylate calcium indicator, is commonly used to measure the intracellular calcium concentrations. However, Fura-2 cannot cross lipid bilayer membranes and therefore is not cell permeant. To overcome this limitation, cells are incubated in the acetoxymethyl (AM) ester form of Fura-2 (Fura-2-AM), which is uncharged and hydrophobic. During incubation, Fura-2-AM can successfully cross cell membranes. Then, inside of the cell, the AM group is hydrolyzed and removed by esterase enzymes, regenerating the Fura-2 indicator.

In this study, $[Ca2+]_i$ was measured by an epifluorescence technique, using the Fura-2-AM probe in non-differentiated DPSCs cells, after 7 days of cell culture in presence of the M_GMA(0.5)_PCL(0), M_GMA(0.2)_PCL(0.2), M_GMA(0.1)_PCL(0.3), M_IEMA(0.5)_PCL(0), M_IEMA(0.2)_PCL(0.2) and M_IEMA(0.1)_PCL(0.3) membranes. The values of $[Ca^{2+}]_i$ were obtained from cells that did not begin the apoptosis process after 7 days in culture. Table 3.5 shows the measured $[Ca2+]_i$ values.

Table 3.5 $[Ca2+]_i$ values measured by the epifluorescence technique. Results are presented as mean and standard error of the mean (SEM). N corresponds to the number of DPSCs cells analyzed per experimental well. All statistical tests were Student's t test. The P values given correspond to errors of the second kind ($P < 0.05$).

Membranes	$[Ca^{2+}]_i$ in nM
M_GMA(0.5)_PCL(0)	53,9±3,8 (N=25)
M_GMA(0.2)_PCL(0.2)	51,3±6,4 (N=25)
M_GMA(0.1)_PCL(0.3)	46,4±2,3 (N=25)
M_IEMA(0.5)_PCL(0)	69,2±7,5 (N=25)
M_IEMA(0.2)_PCL(0.2)	42,1±3,2 (N=25)
M_IEMA(0.1)_PCL(0.3)	43,2±4,1 (N=25)

The membranes proved to be adequate to be used as scaffold associated with DPSCs, since the $[Ca^{2+}]_i$ values are in the range of the normal intracellular concentration for viable mammals cells (between 40-70nM) after 7 days of *in vitro* culture in the presence of the tested membranes (Table 3.1). Additionally, during this analysis, it was possible to see that the undifferentiated hDPSCs cultured in the presence of M_GMA(0.5)_PCL(0), M_GMA(0.2)_PCL(0.2), M_GMA(0.1)_PCL(0.3), M_IEMA(0.5)_PCL(0), M_IEMA(0.2)_PCL(0.2) and M_IEMA(0.1)_PCL(0.3) membranes reached 70-90% confluence and exhibited a normal star-like shape with a flat morphology in culture. According to these results, it is possible to conclude that the membranes are a viable substrate for undifferentiated hDPSCs adhesion, and multiplication. Also, since the results obtained correspond to normal values, it can be concluded that the fixation agent (super glue) used to fix the tested membranes to the well is not toxic for hDPSCs.

3.4.3 Morphology of membranes' surface after cell viability tests

The morphology of the samples after the cell viability tests were assessed by SEM. Before the scanning, all samples were immersed in a glutaraldehyde solution and then dried with ethanol. Following this methodology, it was possible to maintain the structure of cells during the drying

stage. Then, samples were coated with a thin layer of gold to allow the observation through SEM. The images obtained are presented in Figure 3.3.

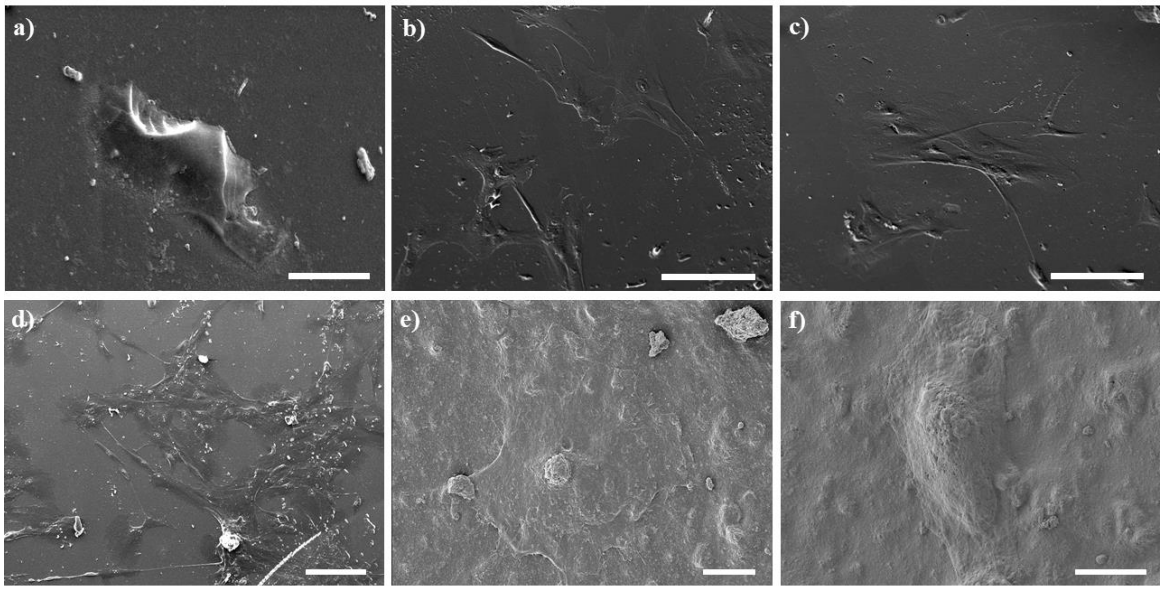

Figure 3.3 Surface SEM images of: a) M_GMA(0.5)_PCL(0), b) M_GMA(0.2)_PCL(0.2), c) M_GMA(0.1)_PCL(0.3), d) M_IEMA(0.5)_PCL(0), e) M_IEMA(0.2)_PCL(0.2), f) M_GMA(0.1)_PCL(0.3). Scale bar of a), e) and f) = 10µm. Scale bar of b), c) and d) = 100µm.

SEM images show the adhesion of the cells on the surface of the studied membranes. In general, all cells presented a flat morphology, with a well spread cytoplasm on the surfaces, exhibiting a star-like shape. In addition, the nucleus of the cells is well defined. This is indicative of the presence of healthy cells.[31] However, for a) M_GMA(0.5)_PCL(0), the cell body of the cell represented seems to be detaching from the surface. This may be related with some changes in the cell metabolism, which may result in deficient adhesion to the surface and posterior detachment.

Accordingly, to the cell viability and measurement of $[Ca^{2+}]_i$ results, all samples can be considered good substrates for cell adhesion and proliferation. The results obtained for samples with PCL_IEMA stood out, leading to the conclusion that this co-macromonomer has a positive effect in the whole performance of the membranes *in vitro*.

3.4.4 *In vivo* biocompatibility studied of implantable devices in subcutaneous tissue [ISO 10993-6:2016]

The validation of the produced biomaterials regarding their biological interactions with host organisms, *in vivo* biocompatibility was assessed accordingly the ISO 10993-6:2016 guidelines.

Following *in vivo* biological validation of the produced biomaterials, we meant to relate the interaction of the obtained biomaterials in subcutaneous tissue, proceeded by histological analysis, to comply with applicable normative requirements for the 'Biological evaluation of medical devices' of the ISO 10993-6:2016 (ISO 10993-6:2016 Part 6: Tests for local effects after implantation). Using the proposed protocols, it is possible to obtain data concerning biocompatibility, inflammatory reaction to the biomaterial, biomaterial biodegradation and fibrosis. [32]

Taking into consideration all membranes evaluated that are suitable for *in vivo* testing, the most promising ones, in what concerns structural properties, are M_GMA(0.5)_PCL(0), M_GMA(0.2)_PCL(0.2) and M_GMA(0.1)_PCL(0.3). The P_LMW_IEMA based membranes presented a stiffer behavior, which would require more effort for their animal implantation. For that reason, they were not tested.

Upon euthanasia, observation of the dorsum presented no abnormalities, with the incision/suture area presenting expected healing progress, with no observable differences from the Sham incision. Figure 3.4 shows the incisions at the implantation day, and after 15 days.

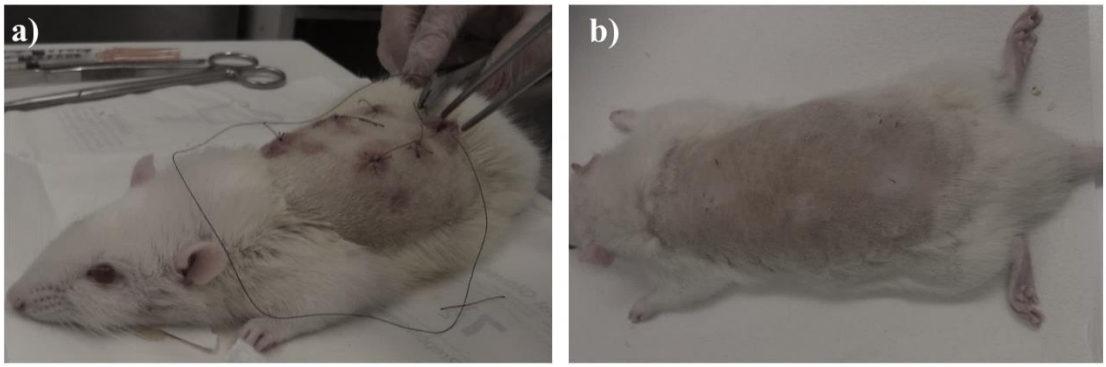

Figure 3.4 Dorsum incisions at a) implantation day; and b) after 15 days.

Exposed subcutaneous tissue presented smooth, with no visible signs of hemorrhage or inflammation. In all groups, implants were involved by a thin, transparent capsule of subcutaneous tissue (Figure 3.5).

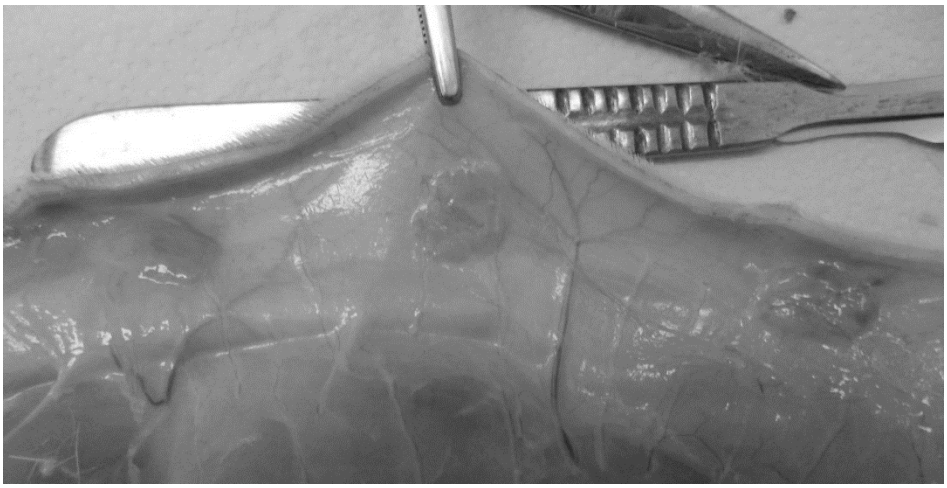

Figure 3.5 Subcutaneous tissue with implants, at day 15.

Microscopically, at 3 days after implantation, a mixed cellular infiltrate was observed in all groups. However, at this time point, a predominance of mononuclear inflammatory cells, such as macrophages and lymphocytes, was present in both sham (control - incision without implant), M_GMA(0.5)_PCL(0), M_GMA(0.2)_PCL(0.2), M_GMA(0.1)_PCL(0.3) samples. Minimal necrosis events were observable in all groups (Sham: 0,139; M_GMA(0.5)_PCL(0): 0,563; M_GMA(0.2)_PCL(0.2): 0,389, and M_GMA(0.1)_PCL(0.3): 0,045 mean score out of a maximum 4 score). Regarding fibrosis, all groups, including Sham, scored under 1.4 out of 4 mean scores (Table 3.2 and 3.3).

At 7 days implantation, an acute inflammatory response is still detectable with continuing dominance of mononuclear cells. Necrosis findings decrease significantly in almost all samples and sham, except for M_GMA(0.1)_PCL(0.3) membranes, in which values reach 0.450, out of 4 mean scores. Regarding fibrosis, all samples and sham maintain the scores of the 3 days group analysis.

After 15 days implantation, an expected decrease in polymorphonuclear leukocytes was observed in almost all groups except M_GMA(0.5)_PCL(0) membranes. In addition, a moderate chronic response mainly constituted by lymphocytic aggregates is still detectable in all groups tested. At this time, no necrosis is observed in M_GMA(0.5)_PCL(0) and M_GMA(0.1)_PCL(0.3) samples (0.00 mean scores), although M_GMA(0.2)_PCL(0.2) reveal residual necrosis score values (0.059), lower than the observed in sham (0.091).

Fibrosis remained under 1.9 with in all groups. A slight increase in vascularization was observed in M_GMA(0.1)_PCL(0.3), and a slight decrease was recorded for M_GMA(0.5)_PCL(0).

Globally, ISO 10998-6 scores attributed are presented in Table 3.4 and plotted in Figure 3.6. The detailed cell count after 3, 7 and 15 days can be found in Table B.1.

Table 3.6 Global histological scores of subcutaneous implantation of M_GMA(0.5)_PCL(0), M_GMA(0.2)_PCL(0.2) and M_GMA(0.1)_PCL(0.3) membranes. Individual results presented in MEAN ± SEM; global scores presented in absolute values.

	SHAM	**M_GMA(0.5)_PCL(0)**	**M_GMA(0.2)_PCL(0.2)**	**M_GMA(0.1)_PCL(0.3)**
3 days	17.694±0.813	21.875±0.826	20.278±0.685	19.136±0.817
	SCORE	4.181	2.583	1.442
7 days	19.650±0.809	23.321±0.522	22.458±0.780	24.400±0.913
	SCORE	3.671	2.808	4.750
15 days	20.030±0.751	23.733±0.696	21.147±0.619	20.400±1.087
	SCORE	3.703	1.117	0 (0.370)

According to the standard guidelines, at 3 and 15 days M_GMA(0.5)_PCL(0) samples scored as "*slight irritant"*, and at 7 days, both M_GMA(0.5)_PCL(0) and M_GMA(0.1)_PCL(0.3) scored as "*slight irritant"*. All other samples scored as *"non irritant"*.

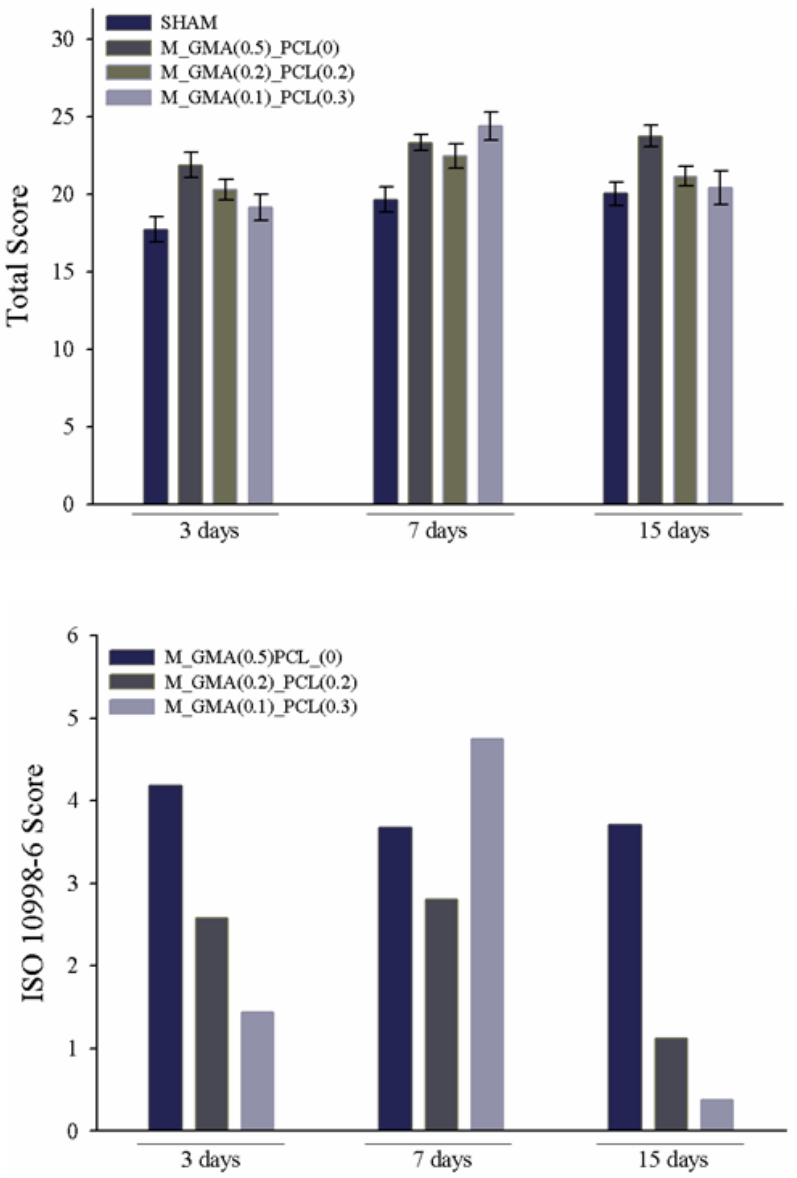

Figure 3.6 Histological scores of subcutaneous implantation of M_GMA(0.5)_PCL(0), M_GMA(0.2)_PCL(0.2) and M_GMA(0.1)_PCL(0.3) membranes.

The calculated scores show that membranes with PCL_IEMA are considered to be *"non irritant"*. This result is very promising since ideally, after implantation, the biomaterial should not induce a severe immune response, which increase the probability of rejection. Figure 3.7 presents the histological analysis of the subcutaneous implantations of the membranes.

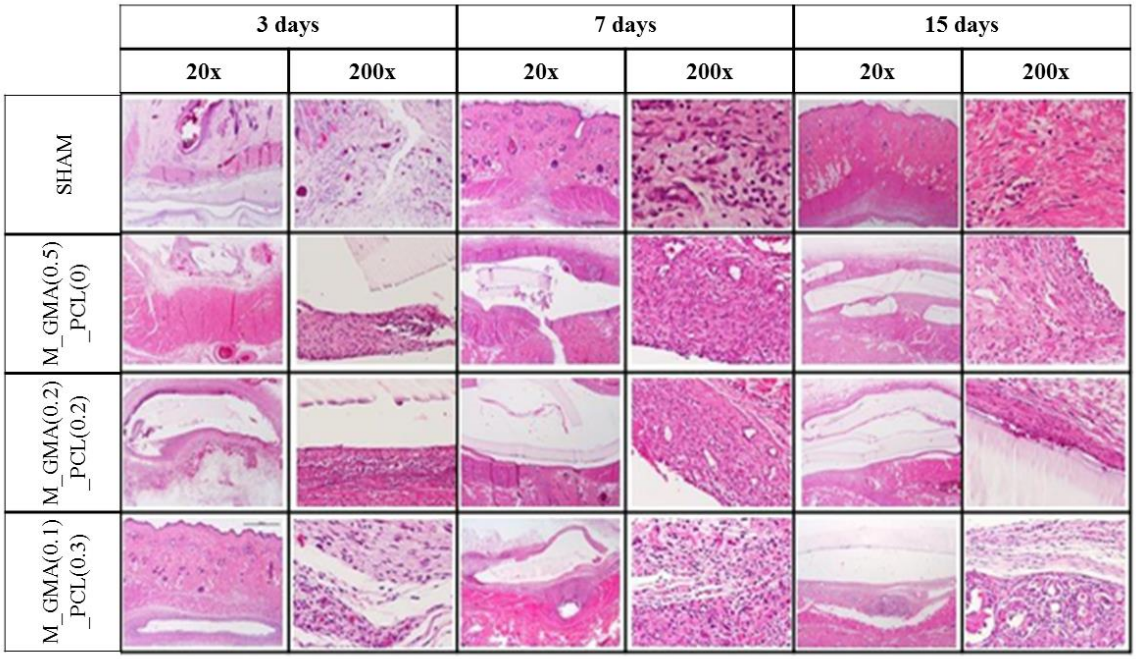

Figure 3.7 Histological analysis of subcutaneous implantation of membranes. Samples were stained with hematoxylin-Eosin (H&E) for accurate evaluation using a Nikon microscope (Nikon Eclipse E600) equipped with ×2, ×4, ×10 and ×40 objectives and coupled with a photo camera (Nikon Digital Sight DS-5M) equipped with a lens (Nikon PLAN UW 2X/0.06).

According to these results, the tested samples are suitable for implantation. To reinforce this claim, systemic effects were evaluated in all the animals tested through necropsy examination. Thorough microscopic analysis was performed for several organs after 15 days of implantation. Figure 3.7 presents the histological analysis of tissue derived from liver, pancreas, heart, spleen and lung.

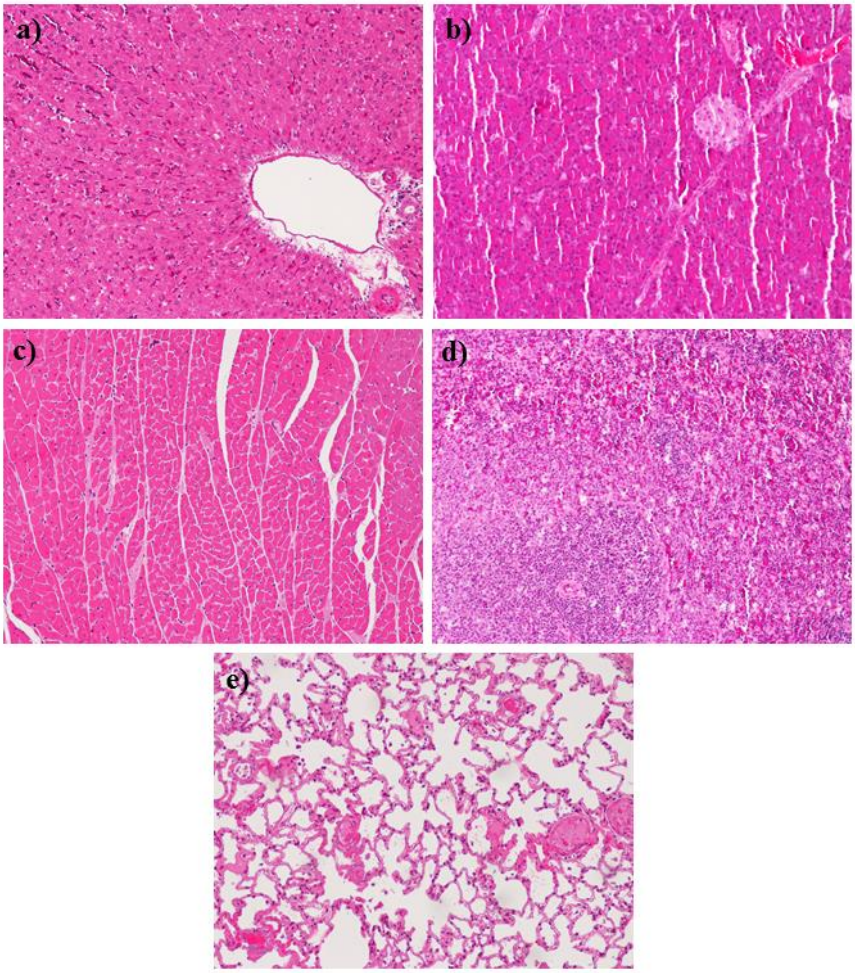

Figure 3.8 Histological analysis of the tissue of the following organs: a) liver; b) pancreas; c) Heart; d) Spleen and e) Lung. Tissues were stained with hematoxylin-Eosin (H&E) for accurate evaluation using a Nikon microscope (Nikon Eclipse E600) equipped with ×2, ×4, ×10 and ×40 objectives and coupled with a photo camera (Nikon Digital Sight DS-5M) equipped with a lens (Nikon PLAN UW 2X/0.06).

In resemblance to the results obtained for the tissue around the implant, the tissues images presented in Figure 3.8 maintained their normal cellular architecture. The internal organs presented their normal topography, relation and morphological features without any signs of necrosis, congestion, or abnormal accumulations.

These facts lead to the conclusion that not only the materials do not trigger a severe immune response, but also, their degradation products do not interfere with the homeostasis of the principal organs tissues.

3.5 CONCLUSIONS

The object of this work was to study the *in vitro* and *in vivo* behavior of dextran-based membranes. The cell viability and cytocompatibility assessment was performed during 7 days. After this time, cells achieved their confluency, leading to a decrease in its activity due to the lack of available surface. The membranes M_GMA(0.1)_PCL(0.3), M_IEMA(0.2)_PCL(0.2) and M_IEMA(0.1)_PCL(0.3) showed the higher cell viability and metabolic rates after 7 days of incubation. In order to reinforce these results, the $[Ca^{2+}]_i$ was measured by an epifluorescense technique using the Fura-2AM probe. The obtained values confirm the presence of viable cells not entering in apoptosis. The subcutaneous implants in rats were carried out for 15 days with evaluation of cell count and biological reaction after 3, 7, ad 15 days. Upon the end of the test M_GMA(0.5)_PCL(0) showed a cell count which corresponds to a score of 3.703, leading to the classification of "*slight irritant*". Nevertheless, even better results were achieved with membranes M_GMA(0.2)_PCL(0.2) and M_GMA(0.1)_PCL(0.3) which obtained scores corresponding to the classification of "*non-irritant*". Additionally, histological analysis was conducted in the tissue surrounding the implants and tissue from different organs revealing no signs of inflammation, fibrosis or necrosis in any sample.

This work confirms that these materials are good candidates for the preparation of medical devices for peripheral nerve regeneration / reconstruction.

3.6 REFERENCES

1. Gärtner, A.; Pereira, T.; Armada-da-Silva, P.; Amado, S.; Veloso, A.; Amorim, I.; Ribeiro, J.; Santos, J.; Bárcia, R.; Cruz, P., Effects of umbilical cord tissue mesenchymal stem cells (UCX®) on rat sciatic nerve regeneration after neurotmesis injuries. *Journal of stem cells & regenerative medicine* **2014,** *10,* 14.

2. Carriel, V.; Garzón, I.; Campos, A.; Cornelissen, M.; Alaminos, M., Differential expression of GAP-43 and neurofilament during peripheral nerve regeneration through bio-artificial conduits. *Journal of Tissue Engineering and Regenerative Medicine* **2017,** *11,* 553-563.

3. Sulaiman, W.; Gordon, T., Neurobiology of peripheral nerve injury, regeneration, and functional recovery: from bench top research to bedside application. *The Ochsner Journal* **2013,** *13,* 100-108.

4. Gu, X.; Ding, F.; Williams, D. F., Neural tissue engineering options for peripheral nerve regeneration. *Biomaterials* **2014,** *35*, 6143-6156.

5. Leary, R. J.; Kinde, I.; Diehl, F.; Schmidt, K.; Clouser, C.; Duncan, C.; Antipova, A.; Lee, C.; McKernan, K.; Francisco, M., Development of personalized tumor biomarkers using massively parallel sequencing. *Science translational medicine* **2010,** *2*, 20ra14-20ra14.

6. Liu, H.; Lv, P.; Zhu, Y.; Wu, H.; Zhang, K.; Xu, F.; Zheng, L.; Zhao, J., Salidroside promotes peripheral nerve regeneration based on tissue engineering strategy using Schwann cells and PLGA: *in vitro* and in *vivo*. *Scientific Reports* **2017,** *7*.

7. Kolar, M. K.; Itte, V. N.; Kingham, P. J.; Novikov, L. N.; Wiberg, M.; Kelk, P., The neurotrophic effects of different human dental mesenchymal stem cells. *Scientific Reports* **2017,** *7*, 12605.

8. Pinho, A. C.; Fonseca, A. C.; Serra, A. C.; Santos, J. D.; Coelho, J. F., Peripheral Nerve Regeneration: Current Status and New Strategies Using Polymeric Materials. *Advanced healthcare materials* **2016**.

9. Szafulera, K.; Wach, R. A.; Olejnik, A. K.; Rosiak, J. M.; Ulański, P., Radiation synthesis of biocompatible hydrogels of dextran methacrylate. *Radiation Physics and Chemistry* **2018,** *142*, 115-120.

10. Janczewska, M.; Jung, P.; Ciach, T., Biodegradable dextran-based nanoparticles as a potential anticancer drug carrier. *Inżynieria i Aparatura Chemiczna* **2014**, 251--252.

11. Balakrishnan, B.; Soman, D.; Payanam, U.; Laurent, A.; Labarre, D.; Jayakrishnan, A., A novel injectable tissue adhesive based on oxidized dextran and chitosan. *Acta Biomaterialia* **2017,** *53*, 343-354.

12. Simoes, M.; Gärtner, A.; Shirosaki, Y.; da Costa, R. G.; Cortez, P.; Gartner, F.; Santos, J.; Lopes, M.; Geuna, S.; Varejão, A., *In vitro* and *in vivo* chitosan membranes testing for peripheral nerve reconstruction. *Acta medica portuguesa* **2011,** *24*, 43-52.

13. Geuna, S.; Raimondo, S.; Fregnan, F.; Haastert-Talini, K.; Grothe, C., *In vitro* models for peripheral nerve regeneration. *European Journal of Neuroscience* **2016,** *43*, 287-296.

14. Al Madhoun, A.; Al-Mulla, F.; Ali, H.; Atari, M.; Akhter, N.; AlKandari, S.; Atizado, V. L., Defined three-dimensional culture conditions mediate efficient induction of definitive endoderm lineage from human umbilical cord Wharton's jelly mesenchymal stem cells. *Stem Cell Research & Therapy* **2016,** *7*, 165.

15. Oppliger, B.; Joerger-Messerli, M. S.; Simillion, C.; Mueller, M.; Surbek, D. V.; Schoeberlein, A., Mesenchymal stromal cells from umbilical cord Wharton's jelly trigger oligodendroglial differentiation in neural progenitor cells through cell-to-cell contact. *Cytotherapy* **2017**.

16. Shalaby, S. M.; Amal, S.; Ahmed, F. E.; Shaban, S. F.; Wahdan, R. A.; Kandel, W. A.; Senger, M. S., Combined Wharton's jelly derived mesenchymal stem cells and nerve guidance conduit: A potential promising therapy for peripheral nerve injuries. *The International Journal of Biochemistry & Cell Biology* **2017,** *86*, 67-76.

17. Martin-Piedra, M. A.; Garzon, I.; Oliveira, A. C.; Alfonso-Rodriguez, C. A.; Sanchez-Quevedo, M. C.; Campos, A.; Alaminos, M., Average cell viability levels of human dental pulp stem cells: an accurate combinatorial index for quality control in tissue engineering. *Cytotherapy* **2013,** *15*, 507-518.

18. Gronthos, S.; Mankani, M.; Brahim, J.; Robey, P. G.; Shi, S., Postnatal human dental pulp stem cells (DPSCs) *in vitro* and *in vivo*. *Proceedings of the National Academy of Sciences* **2000,** *97*, 13625-13630.

19. Spiller, K. L.; Anfang, R. R.; Spiller, K. J.; Ng, J.; Nakazawa, K. R.; Daulton, J. W.; Vunjak-Novakovic, G., The role of macrophage phenotype in vascularization of tissue engineering scaffolds. *Biomaterials* **2014,** *35*, 4477-4488.

20. Koyama, S.; Endo, M.; Kim, Y.-A.; Hayashi, T.; Yanagisawa, T.; Osaka, K.; Koyama, H.; Haniu, H.; Kuroiwa, N., Role of systemic T-cells and histopathological aspects after subcutaneous implantation of various carbon nanotubes in mice. *Carbon* **2006,** *44*, 1079-1092.

21. Deliormanlı, A. M.; Liu, X.; Rahaman, M. N., Evaluation of borate bioactive glass scaffolds with different pore sizes in a rat subcutaneous implantation model. *Journal of Biomaterials Applications* **2014,** *28*, 643-653.

22. Zhang, L.; Cao, Z.; Bai, T.; Carr, L.; Ella-Menye, J.-R.; Irvin, C.; Ratner, B. D.; Jiang, S., Zwitterionic hydrogels implanted in mice resist the foreign-body reaction. *Nature Biotechnology* **2013,** *31*, 553-556.

23. Fisher, S. K.; Domask, L. M.; Roland, R. M., Muscarinic receptor regulation of cytoplasmic Ca2+ concentrations in human SK-N-SH neuroblastoma cells: Ca2+ requirements for phospholipase C activation. *Molecular Pharmacology* **1989,** *35*, 195-204.

24. Grynkiewicz, G.; Poenie, M.; Tsien, R. Y., A new generation of Ca2+ indicators with greatly improved fluorescence properties. *Journal of Biological Chemistry* **1985,** *260*, 3440-3450.

25. Hald, A., *Statistical theory with engineering applications.* John Wiley & Sons: New York, **1952**; p 783.

26. Lichvarova, L.; Jašková, K.; Lacinova, L., NGF-induced neurite outgrowth in PC12 cells is independent of calcium entry through L-type calcium channels. *General Physiology and Biophysics* **2012,** *31*, 473.

27. Takeshita, M.; Banno, Y.; Nakamura, M.; Otsuka, M.; Teramachi, H.; Tsuchiya, T.; Itoh, Y., The pivotal role of intracellular calcium in oxaliplatin-induced inhibition of neurite outgrowth but not cell death in differentiated PC12 cells. *Chemical research in toxicology* **2011,** *24*, 1845-1852.

28. Zhaleh, H.; Azadbakht, M.; Pour, A. B., Effects of extracellular calcium concentration on neurite outgrowth in PC12 cells by staurosporine. *Neuroscience letters* **2011,** *498*, 1-5.

29. Trump, B.; Berezesky, I., Calcium-mediated cell injury and cell death. *The FASEB Journal* **1995,** *9*, 219-228.

30. Rodrigues, J.; Luís, A.; Lobato, J.; Pinto, M.; Lopes, M.; Freitas, M.; Geuna, S.; Santos, J.; Maurício, A., Determination of the intracellular Ca2+ concentration in the N1E-115 neuronal cell line in perspective of its use for peripheric nerve regeneration. *Bio-medical materials and engineering* **2005,** *15*, 455-465.

31. Zhang, W.; Sgdsg, F.; Ling, J.; Lin, Z.; Gao, Y.; Mao, X.; Jian, Y., Odontogenic differentiation of vascular endothelial growth factor-transfected human dental pulp stem cells *in vitro*. *Molecular Medicine Reports* **2014,** *10*, 1899-1906.

32. Silva, D. M.; Caseiro, A. R.; Amorim, I.; Pereira, I.; Faria, F.; Pereira, T.; Santos, J. D.; Gama, F. M.; Maurício, A. C., Inflammatory response to dextrin-based hydrogel associated with human mesenchymal stem cells, urinary bladder matrix and Bonelike® granules in rat subcutaneous implants. *Biomedical Materials* **2016,** *11*, 065004.

Chapter 4: **PREPARATION OF DEXTRAN BASED TUBES, FOR APPLICATION IN PERIPHERAL NERVE REGENERATION**

4.1 ABSTRACT

In the cases where natural end-to-end regeneration of injured nerves is not feasible due to the gap length a surgery is needed in order to correct the lesion by creating conditions to promote the growth or join of the two nerve ends. Although, nerve autograph presents several important issues (e.g site morbidity), it stills considered the "gold standard" treatment for these cases.[1] As alternative, polymeric nerve guide tubes have been proposed for bridging longer gaps. In this work, hollow tubes using dextran based materials were prepared and characterized. A PCL based co-macromonomer was added to the formulations to tailor the properties of the tubes. The tubes were obtained by photocrosslinking under UV light using quartz molds.

The morphology of both inner and outer surfaces of the tubes was studied through SEM. The images obtained revealed a relatively smooth surface, suggesting a highly compact structure. The permeability of the tubes was varied using D-mannitol as porogenic agent during photocrosslinking.

Swelling capacity tests revealed percentages of swelling in a range between 40-60% without visible constriction of the inner diameter of the tubes. *In vitro* hydrolytic degradation tests carried out in phosphate buffered saline solution (PBS, pH=7.4), at 37 ºC, showed that after six months the tubes maintain their structural integrity.

Tensile strength tests showed that materials present a visco-elastic behavior. The elongation at break was around 60% for maximum loads between 2.2-2.4N. The ability to handle suturing was proved since no cracks appeared once the tube was perforated by the suture needle.

The tubes presented a set of characteristics in what concerns swelling capacity, degradation rate and suture handling, which suggest that they could be considered interesting materials to be used in peripheral nerve regeneration.

4.2 INTRODUCTION

Peripheral nerve injuries are quite common in Europe and can be a consequence of industrial or motor vehicle accidents, tumor damage, neurosurgery side effects, among other causes.[2] Although the peripheral nerve system has the ability to regenerate by itself without external aid, often this process is incomplete. Consequently, both motor and

sensory nerves cannot fully recover their function, which may result in permanent disability.[3] To improve this process of regeneration, many alternatives have been studied. Nevertheless, the nerve autograph is still nowadays, the gold standard because it presents the most promising results for larger gaps (>10cm).[4,5] However, this technique presents important disadvantages as site morbidity and the need of extra surgeries. In order to circumvent these issues artificial conduits or nerve guides based on polymeric materials have been proposed.[6]

With respect to synthetic polymers, both non-biodegradable and biodegradable materials have been used. The main problem associated to non-biodegradable polymers is the difficulty in clearance of the material by the body even when the nerve is fully recovered, increasing the possibility of nerve compression during the regeneration process[7]. This fact leads to need of a second surgery to remove the material due to excess of scar tissue.[8] For this reason biodegradable polymers as poly (glycolic acid) (PGA), poly (lactic-co-glycolic acid) (PLGA), poly (ε-caprolactone) (PCL) and poly (DL-lactide-co-caprolactone) (P(DLLA-co-CL)) are preferred due to natural elimination by the body. However, since the majority are polyesters, their degradation led to the acidification of the surrounding tissues.[9,10] In the case of PCL and its conjugates, another difficulty concerns its very slow degradability rate in biological conditions.[11,12]

Natural polymers such as collagen[13,14], chitosan[15-19], alginate[20,21], poly(3-hydroxybutyrate) (PHB)[6,22] and poly(2-hydroxybutyrate-co-hydroxyvalerate) (PHBV)[23,24] have good biocompatibility but poor mechanical properties, which have driven researchers to find strategies to overcome this issue[2], such as: combination with synthetic polymers[14,19,23] and creation of crosslinked materials.[15,16] As an example, chitosan is frequently combined with synthetic polymers as PLA.[19] The nerve conduits prepared were biodegradable, permeable and provided a suitable mechanical support for nerve regeneration. However, the observed axon regeneration was inferior to the autograph approach.[19]

FDA has approved several products mostly made of collagen and PCL. The most used ones are nerve conduits as NeuraGen® made of Collagen Type I and Neurolac® composed by P(DLLA-co-CL). Unfortunately, their use is limited to nerve gaps between 18-20mm.[25] Also, their degradation ratios are not appropriate being too fast, in the case of the collagen based materials (4-8 months), or too slow in the case of Neurolac® (16 months).[26] Due to the aforementioned limitations, their global performance is considered satisfactory but stills inferior compared with the nerve autographs.[26]

Dextran is a biocompatible material approved by FDA, which is already used as core material of several biomedical formulations as hydrogels and nanoparticles for drug delivery[27-31].

To the best of our knowledge, this is the first study involving the preparation of dextran-based nerve guide conduits/tubes. In this work, nerve guide tubes were prepared using dextran based formulations with the addition of a PCL based co-macromonomer in order to tailor the final properties of the tube. The morphology of the inner and outer surfaces of the tubes was assessed by scanning electron microscopy (SEM). The swelling capacity and hydrolytic degradation ratio were also determined. The mechanical properties were evaluated after tensile strength tests.

4.3 EXPERIMENTAL SECTION

4.3.1 Materials

Dextran (Mw=70000 g/mol), D-mannitol, 1-vinyl-2-pyrrolidinone (NVP), lysozyme and PBS tablets were purchased from Sigma Aldrich (St. Louis, Missouri, USA). Glycidyl methacrylate (GMA) and triethylamine (TEA), was purchased from Acros Organics (Geel, Belgium). 4-Dimethylaminopyridine (DMAP), 2-Isocyanatoethyl Methacrylate (IEMA) were acquired from TCI Europe (Zwijndrecht, Belgium) and dimethyl sulfoxide (DMSO) from Fisher Scientific (Hampton, New Hampshire, USA). Dibutyltin dilaurate was purchased from Fluka (St. Louis, Missouri, USA). Tetrahydrofuran (THF) was obtained from VWR (Radnor, Pennsylvania, USA) and *n*-hexane was obtained from José Manuel Gomes dos Santos, Lda (Odivelas, Portugal). Poly(ε-caprolactone) diol (Capa^{TM} 2054; Mw=550 g/mol) was kindly offered by Perstorp (Warrington, UK). Irgacure 2959® was gently supplied by Ciba Specialty Chemicals (Basel, Switzerland). Sodium azide was purchased from Panreac (Barcelona, Spain).

4.3.2 Preparation of the tubes

The synthesis procedures and characterization of the precursors that were used in formulations for the preparation of the tubes, were already described in Sections 2.3.2, 2.4.1 and 2.4.2 of the Chapter 2 of this thesis.

Dextran modified with GMA and PCL-dimethacrylate were dissolved in DMSO, using the formulations presented in Table 4.1. After the complete dissolution of the precursors, the photoinitiator Irgacure 2959® (0.5% w/w relatively to the amount of modified dextran and PCL-dimethacrylate which corresponds to 0.0025g) was added. Also, in some formulations, besides Irgacure 2959®, triethylamine (TEA) and N-Vinylpyrrolidone (NVP) (in catalytic amounts) were also added aiming to reduce the photocrosslinking time.[32]

For the formulations showing most promising results, D-mannitol was added to the mixture in order to create porous within the structure. The amounts tested were 20%, 35% and 50%wt of the tube formulation which translates in 0.08, 0.14 and 0.2g of material. D-Mannitol was added to the formulation after the solubilization of the precursors, followed by the addition of Irgacure 2959. The solution was placed into a mold composed of a quartz tube with a stainless steel rod inside. In order to achieve the same dimensions as commercial product Neurolac® (innerD=2.5mm; outerD=1.5mm), two quartz tubes (6 and 7mm outerD) combined with two different stainless steel rods (1.5 and 2.5mm diameter) were tested. The solutions were placed between the quartz tube and the stainless steel rod. A scheme of the mold is presented in Figure 4.1.

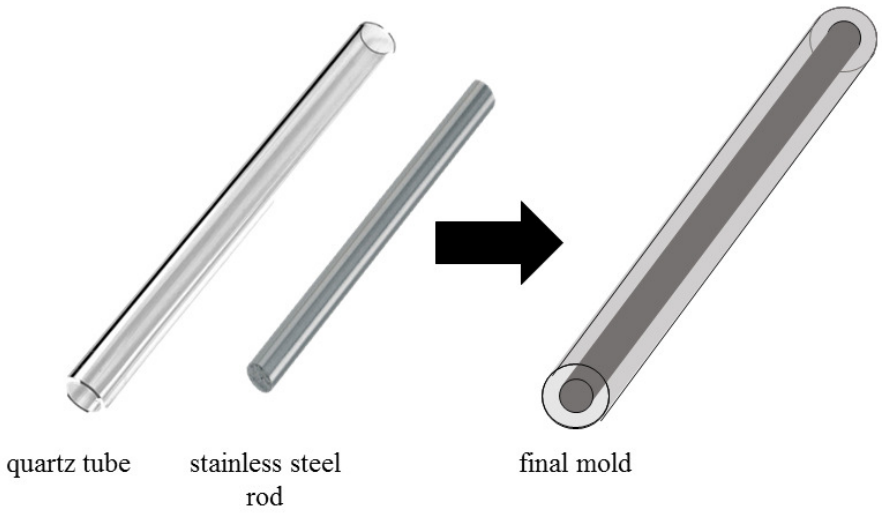

Figure 4.1 Mold used for tube preparation.

The mold with solutions was left to photocrosslink in a UV chamber (Model BS-02, from Dr. Gröbel, UV-Electronik GmbH, with a wavelength of 280 nm), for 20 minutes. After that time, the material was demolded and left in absorbent paper for 2 days to eliminate the excess DMSO. Then, tubes were washed with Milli-Q water in order to remove the DMSO. In the case of the formulations with D-mannitol, after the polymerization, the resulting tubes were immersed in distilled water and left in an oven at 37ºC for 3 days, to remove D-mannitol. Then, these tubes were washed with Milli-Q water for 7 days.

The tubes were dried under vacuum, at 40ºC. After the drying process, segments of tubes with 1cm were cut for characterization.

Table 4.1 Formulation for the preparation of tubes.

Designation	Modified Dextran	PCL_IEMA	DMSO	TEA/NVP	D-Mann
T_GMA24(0.2)_PCL(0.2)	0.2g P_LMW_GMA24	0.2g	2mL	----	----
T_GMA24(0.2)_PCL(0.2)_2	0.2g P_LMW_GMA24	0.2g	2mL	✓	----
T_GMA24(0.2)_PCL(0.2)_3	0.2g P_LMW_GMA24	0.2g	1mL	----	----
T_GMA24(0.2)_PCL(0.2)_4	0.2g P_LMW_GMA24	0.2g	1mL	✓	----
T_GMA8(0.2)_PCL(0.2)	0.2g P_LMW_GMA8	0.2g	2mL	----	----
T_GMA8(0.2)_PCL(0.2)_2	0.2g P_LMW_GMA8	0.2g	2mL	✓	----
T_GMA8(0.2)_PCL(0.2)_3	0.2g P_LMW_GMA8	0.2g	1mL	----	----
T_GMA8(0.2)_PCL(0.2)_4	0.2g P_LMW_GMA8	0.2g	1mL	✓	----
T_GMA24(0.1)_PCL(0.3)	0.1g P_LMW_GMA24	0.3g	2mL	----	----
T_GMA24(0.1)_PCL(0.3)_2	0.1g P_LMW_GMA24	0.3g	2mL	✓	----
T_GMA24(0.1)_PCL(0.3)_3	0.1g P_LMW_GMA24	0.3g	1mL	----	----
T_GMA24(0.1)_PCL(0.3)_4	0.1g P_LMW_GMA24	0.3g	1mL	✓	----
T_GMA8(0.1)_PCL(0.3)	0.1g P_LMW_GMA8	0.3g	2mL	----	----
T_GMA8(0.1)_PCL(0.3)_M20	0.1g P_LMW_GMA8	0.3g	2mL	----	0.08g
T_GMA8(0.1)_PCL(0.3)_M35	0.1g P_LMW_GMA8	0.3g	2mL	----	0.14g
T_GMA8(0.1)_PCL(0.3)_M50	0.1g P_LMW_GMA8	0.3g	2mL	----	0.20g
T_GMA8(0.1)_PCL(0.3)_2	0.1g P_LMW_GMA8	0.3g	2mL	✓	----
T_GMA8(0.1)_PCL(0.3)_3	0.1g P_LMW_GMA8	0.3g	1mL	----	----
T_GMA8(0.1)_PCL(0.3)_4	0.1g P_LMW_GMA8	0.3g	1mL	✓	----

4.3.3 Characterization Techniques

Shrinkage Studies

The differences between the dimensions of the tubes in the dry and wet state were evaluated through the percentage of shrinkage. The dimensions evaluated were the length of the tube

and both inner and outer diameter. The equation used to calculate this parameter is presented in equation 4.1.

$$\%\ Shrinkage = \frac{Wet\ dimension - Dry\ dimension}{Wet\ dimension} \times 100 \qquad \textbf{eq 4.1}$$

The dry dimension is related to the measurements done after drying the tubes under vacuum and wet dimension is the measurement done after water wash.

Scanning Electron Microscopy

Scanning electron microcopies of the surface and transversal cut of the prepared tubes were obtained using a *JOEL XL30* equipment, with Energy Dispersive Spectrometry system (EDS) from *EDAX*. The observations were conducted with a beam acceleration voltage of 10kV. All samples were coated with a thin layer of gold, using the sputtering technique. Samples were coated for 60 seconds with the help of an EDWARDS EXC 120 sputtering equipment, with a power source Huttinger PFG 1500 DC. The sputtering conditions were: P=0,11KW; V=1000V and I=1,83 A.

Swelling Capacity

The swelling capacity of tubes (L x ID x OD: 10 mm x 1.5 mm x 2.5 mm) was measured in PBS (pH=7.4), at 37 ºC. Dried samples with a known dried weight were immersed in 5mL of PBS until the swelling equilibrium was achieved. At predetermined times, the samples were taken out from the PBS, and the surface water gently blotted using a filter paper. The swollen samples were then weighted and the swelling capacity was calculated using the equation 4.2

$$Swelling\ Capacity\ (\%) = \frac{W_s - W_d}{W_d} \times 100 \qquad \textbf{eq 4.2}$$

Where W_s is the weight of the swollen samples and W_d is the weight of the dried samples before the immersion in PBS. The measurements were conducted in triplicate.

In vitro hydrolytic degradation

In vitro hydrolytic degradation tests were performed in PBS (pH=7.4, 0.01M) with 2%wt of sodium azide. Dried tubes with 1cm length, 1.50mm inner diameter and 2.50mm outer diameter with known weight were immersed in the PBS solution, at 37ºC, during 30 days. At predetermined times, the tubes were removed from PBS and rinsed three times with distilled water. Then, the tubes were dried in two step process: first the samples were dried under vacuum at room temperature for a week, and then dried at 50ºC until the stabilization of their weight.

The degree of degradation was calculated according to the equation 4.3

$$Weight\ Loss\ (\%) = \frac{W_0 - W_t}{W_0} \times 100 \qquad \textbf{eq 4.3}$$

Where W_0 is the initial weight of the dry sample before immersion, and W_t is the dry sample weight after incubation for *t* days. The measurements were carried out in triplicate.

Tensile tests

All tubes used in the tensile tests were hydrated in PBS (pH=7.4, 0.01M) overnight to reach the maximum swelling capacity, in an attempt to mimic biologic conditions. The equipment used was the Autograph AG-X from Shimadzu with a maximum load of 5kN. The tests were performed at three different displacement rates (0.03, 0.08, 0.15mm/s). The tests were stopped when the force achieved the value of 1N. For the rupture test, a test speed of 0.08mm/s (5mm/min) was used[33]. The length of the section tested was 2.5mm. Data collection and analysis was performed in Trapezium X software.

Preliminary Suture Test

The ability of the tubes to be sutured without cracking was evaluated using a 7/0 monofilament nylon. Each tube was left to hydrate for 1 hour in PBS (pH=7.4, 0.01M). After that time, the tube was successively punctured to mimic the suture with the nerve.

4.4 RESULTS AND DISCUSSION

Taking into consideration the results of swelling capacity, *in vitro* and *in vivo* degradation and performance, obtained in Chapter 2 and Chapter 3 of the present work, the following materials were considered for the tube preparation: M_LMW_GMA8(0.2)_PCL(0.2); M_LMW_GMA24(0.2)_PCL(0.2); M_LMW_GMA8(0.1)_PCL(0.3) and M_LMW_GMA24(0.1)_PCL(0.3). During this work, some modifications and optimizations were made to the previously described formulations. In addition, new materials were used to achieve the tube conformation during the photocrosslinking. The next subsections intend to describe these changes.

Formulations

The precursors used for the preparation of the tubes were P_LMW_GMA8 and P_LMW_GMA24. Briefly, the only difference between them is the degree of substitution (DS) which is around 31-34% for P_LMW_GMA8 and 44-48% for P_LMW_GMA24. PCL was modified with IEMA and added as a co-macromonomer, as previously reported.

Based on previously results, Irgacure 2959® was used as photoinitiatior. In certain experiments (table 4.1), catalytic amounts of TEA and NVP were added.

The porosity and permeability of tubes for this application are particular important.[34] A permeable tube can allow the exchange of nutrients, which have a positive effect on nerve regrowth.[35] For this reason, D-mannitol was used as porogenic agent due to previously reported promising results of the addition of this compound in the case of hydrogels for stem cell differentiation.[36]

Materials used in the mold for photocrosslinking

Since the radiation used was UV light, quartz was used for the external tube material, to enhance the penetration of the radiation. With this type of material it is possible to reach, the complete polymerization of the formulation in 20 min compared with 2 hours if glass molds are used.

To create a lumen inside the tubes, a stainless steel rod was added to the mold. This material was chosen based on its ability to avoid the formation of passive layers on its surface and consequent oxidation. Furthermore, to facilitate the demolding process after crosslinking,

the rod was polished using four different sandpapers (200, 800, 1200 and 2000). With this process, the surface of the rod became smoother and with a horizontal line pattern. Figure 4.2 illustrates the final mold.

Figure 4.2 Mold used for tube conformation: Stainless steel rod inside of a quartz tube.

Purification of the samples

After completing the crosslinking stage, samples were demolded from the quartz tube. Then, they were put in water to remove the DMSO of the structure. Nevertheless, once the tubes were immersed in water, cracks started to appear on their surface. After several attempts to avoid this problem, we concluded that it may be the sudden solvent change (DMSO to water) that was responsible for the appearance of the cracks. Hence tubes were first left to rest in absorbent paper for 2 days to allow DMSO to get out from structure and then start the contact with water to complete eliminate the DMSO. After that procedure, no more cracks were observed, with the exception of some formulations based on P_LMW_GMA24. This phenomenon may be attributed to quick migration of DMSO from the structure of the tube.

4.4.1 Optimization of the dimensions of the tubes

It is reported that the dimensions of the commercial product *Neurolac*® are ideal for the implantation on the rat sciatic nerve.[37] This arises from the fact that *Neurolac*® has been successfully used in *in vivo* models presenting no limitations concerning dimensions.[37] Also, this product is FDA approved and commercially available, being the only reported disadvantages related to the degradability. For this reason, in this work, the prepared tubes had the same dimensions as *Neurolac*® (1.5 mm for inner diameter with a wall thickness of 1mm in the dry state). Due to hydrophilic nature of dextran relevant changes of dimensions between the dry state and wet state could be observed. These variations were studied for tubes using different formulations.

Two quartz tubes, with inner diameter of 4mm and 5mm were tested with two stainless steel rods with diameter of 1.5mm and 2.5mm, respectively. A scheme of the combined components of the molds tested in presented in Figure 4.3.

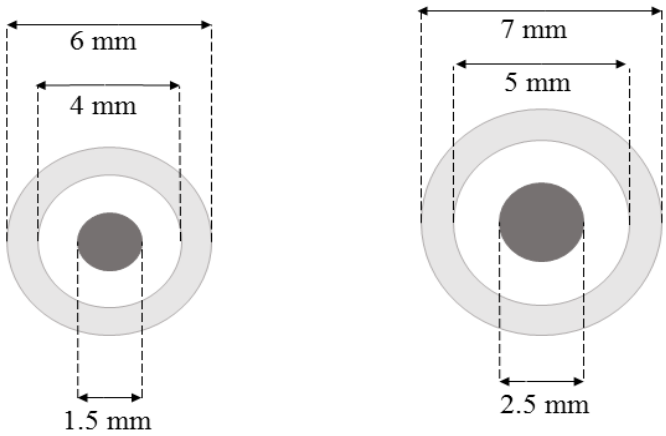

Figure 4.3 Scheme of the view from the top of molds used with the dimensions of the components.

Several attempts with changes in reaction parameters such as kind of photoinitiator, type and time of irradiation, inner mold material and relative dimensions of the mold components were performed. The best results were obtained for the quartz tube with 5mm of inner diameter with a 2.5mm diameter stainless-steel rod.

The shrinkage percentages were obtained through the difference between the value of the measure obtained in wet state and dry state for tubes prepared (Table 4.1) with the 2.5 mm rod (Table 4.2).

Table 4.2 Shrinkage percentage of the prepared tubes with the mold with a 2.5 mm rod where L refers to length, ID is related to inner diameter and OD is outer diameter.

	Wet tube (mm)			Dry tube (mm)			Shrinkage (%)		
Designation	**L**	**ID**	**OD**	**L**	**ID**	**OD**	**L**	**ID**	**OD**
T_GMA24(0.2)_PCL(0.2)	65.0	2.5	5.0	35.0	1.0	2.6	46.2	60.0	48.0
T_GMA24(0.2)_PCL(0.2)_2	48.0	2.5	5.0	29.0	1.3	2.8	39.6	47.2	44.6
T_GMA24(0.2)_PCL(0.2)_3	22.0	2.5	5.0	15.0	1.1	2.7	31.8	58.0	46.2
T_GMA24(0.2)_PCL(0.2)_4	26.0	2.5	5.0	16.0	1.1	2.7	38.5	55.2	45.4
T_GMA8(0.2)_PCL(0.2)	63.0	2.5	5.0	35.0	1.1	2.6	44.4	56.0	47.4
T_GMA8(0.2)_PCL(0.2)_2	64.0	2.5	5.0	37.0	1.2	2.8	42.2	53.2	45.0
T_GMA8(0.2)_PCL(0.2)_3	33.0	2.5	5.0	20.0	1.2	3.1	39.4	51.2	38.4
T_GMA8(0.2)_PCL(0.2)_4	68.0	2.5	5.0	45.0	1.4	3.2	33.8	46.0	35.6
T_GMA24(0.1)_PCL(0.3)	52.0	2.5	5.0	28.0	1.1	2.6	46.2	56.4	47.4
T_GMA24(0.1)_PCL(0.3)_2	64.0	2.5	5.0	16.0	1.1	2.7	75.0	54.4	46.8
T_GMA24(0.1)_PCL(0.3)_3	60.0	2.5	5.0	38.0	1.3	3.1	36.7	48.4	38.2
T_GMA24(0.1)_PCL(0.3)_4	74.0	2.5	5.0	50.0	1.4	3.2	32.4	44.8	36.0
T_GMA8(0.1)_PCL(0.3)	70.0	2.5	5.0	36.0	1.4	2.6	48.6	44.4	48.8
T_GMA8(0.1)_PCL(0.3)_2	82.5	2.5	5.0	45.0	1.12	2.6	45.5	54.0	47.8
T_GMA8(0.1)_PCL(0.3)_3	78.0	2.5	5.0	50.0	1.3	3.1	35.9	46.4	39.0
T_GMA8(0.1)_PCL(0.3)_4	55.0	2.5	5.0	36.0	1.4	3.2	34.6	44.4	37.0

For composition of formulation, see table 4.1

It was concluded that the tubes with closer dimensions to expected ones (ID=1.5mm; OD=2.5 mm in the dry state) were T_GMA8(0.1)_PCL(0.3) and T_GMA8(0.1)_PCL(0.3)_2. These tubes present shrinkage percentages around 50%. Both tubes were quite similar with no visual cracking. Moreover, in comparison with the tubes

resulting from the other formulations, these two proved to be much more flexible and are more transparent. It is also worth to note that the demolding process of these tubes was also smoother and easier.

As indicated in Table 4.1, the only difference between these two formulations is the incorporation of the TEA/NVP system. In literature, it is reported that TEA (a co-initiator) is typically combined with NVP in order to accelerate the polymerization process.[38] Also, some studies show promising results using this system with visible light, for scaffolds with peptides and in contact with cells.[32,39] In our case, no changes in the polymerization time or quality of final products were observed. Subsequently, the tube chosen for being characterized was T_GMA8(0.1)_PCL(0.3). Figure 4.4 presents a photo of the tube.

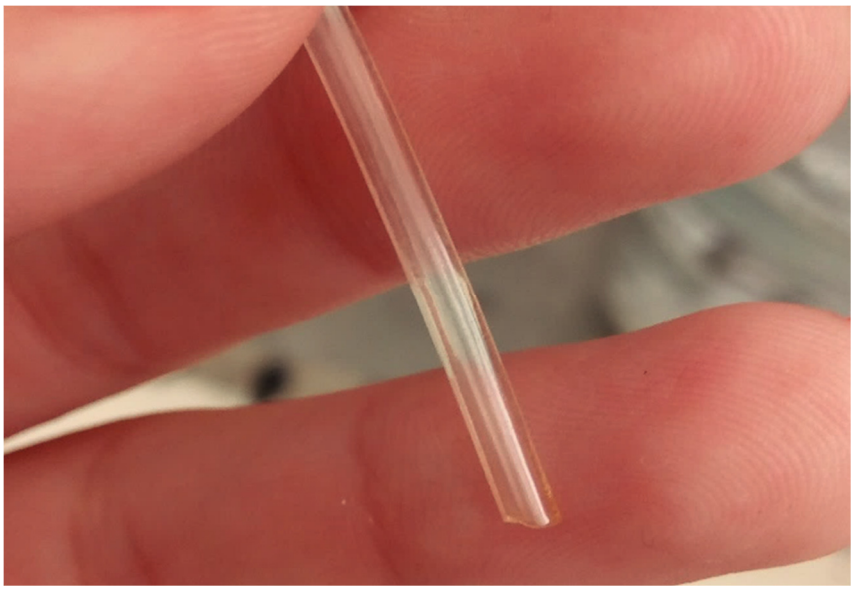

Figure 4.4 Tube T_GMA8(0.1)_PCL(0.3).

In the following sections, only the characterization of T_GMA8(0.1)_PCL(0.3) will be presented due to the aforementioned reasons. D-mannitol was only added to this mixture.

4.4.2 Morphology of the tubes

The microstructure of the prepared tubes with formulation T_GMA8(0.1)_PCL(0.3) was evaluated with scanning electron microscopy (Figure 4.5).

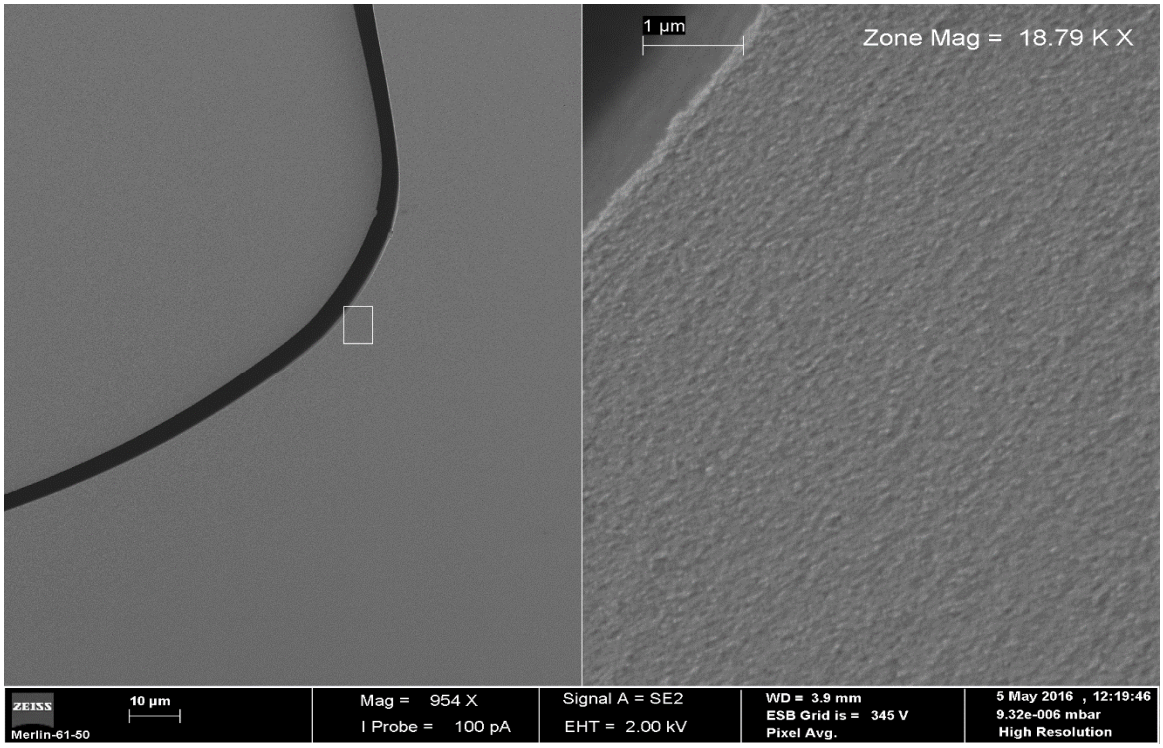

Figure 4.5 Micrograph of the surface of the tube T_GMA8(0.1)_PCL(0.3). Magnification 954x(right) and 1879x (left).

The micrographies presented in Figure 4.5 suggest that the outer surface of T_GMA8(0.1)_PCL(0.3) is smooth showing no pores or small cracks along the structure. Besides, in the micrograph of the left, with higher magnification, it can be observed that the pattern of the surface is quite regular. Therefore, the surfaces can be considered to be compact with no accentuated roughness. In order to get porous surfaces D-mannitol was incorporated into formulation of T_GMA8(0.1)_PCL(0.3) in different amounts (20%, 35% and 50% w). Figure 4.6 presents the micrographs obtained for the corresponding tubes.

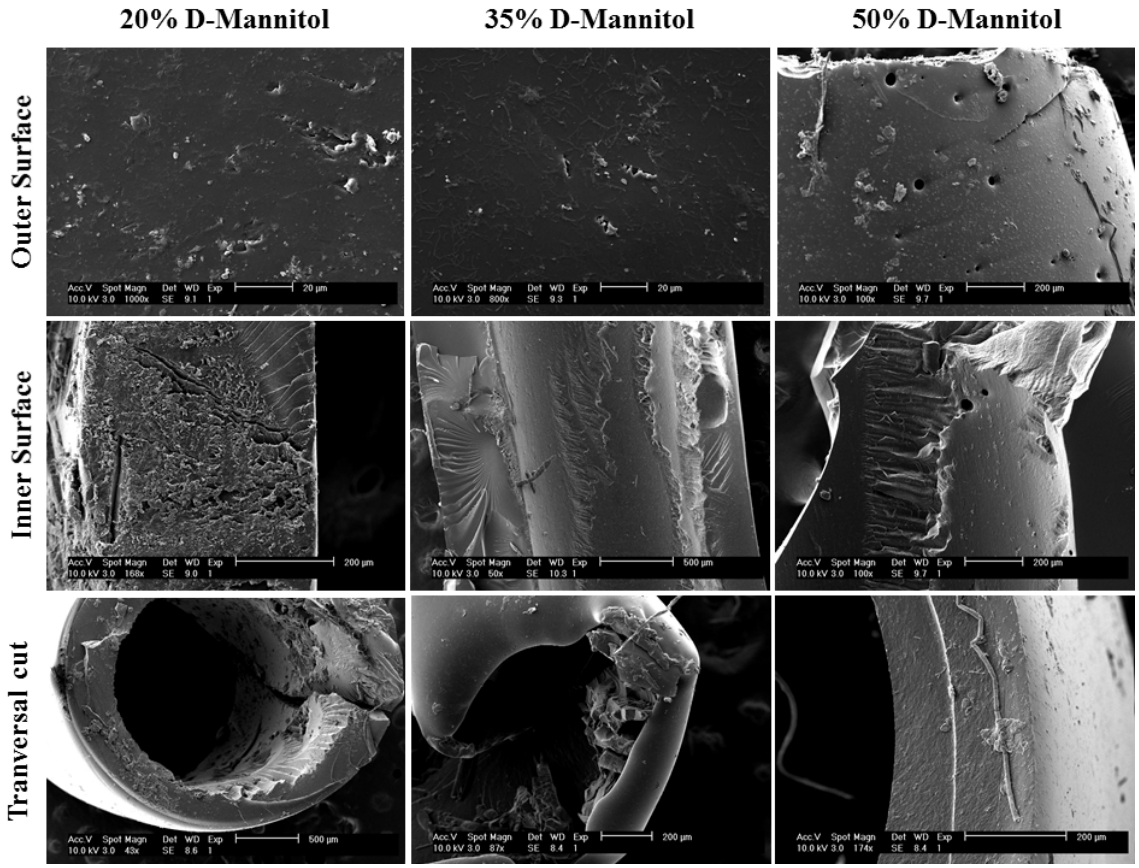

Figure 4.6 Micrographs of T_GMA8(0.1)_PCL(0.3) with different amounts (% wt) of D-Mannitol.

The micrographies presented in Figure 4.6 clearly reveal that the only formulation where it is possible to observe the existence of pores is the one with 50% wt D-mannitol. The size of these pores varies between 20-100µm. However, pores do not seem to cross the tube section, as desired. Nevertheless, these pores could be preferential sites of degradation, which can enhance the permeability of the tube over time. With the increase of permeability, nutrients and oxygen may be exchanged between the lumen of the tube and the media. Thus, the drainage of nerve wound exudates will be also facilitated.

In order to evaluate the performance of another porogenic agent, sodium chloride and sodium carbonate were also tested. The first one was impossible to solubilize in the mixture, and therefore, it was not possible to prepare tubes. Regarding sodium carbonate, the amount used was 35% wt. The quantity of 20%wt was not tested because, in the case of D-mannitol, no pores were observed. In addition, it was not possible to prepare the formulation with 50% wt of sodium carbonate because it was not possible to achieve complete solubilization. The micrographs obtained are shown in Figure 4.7.

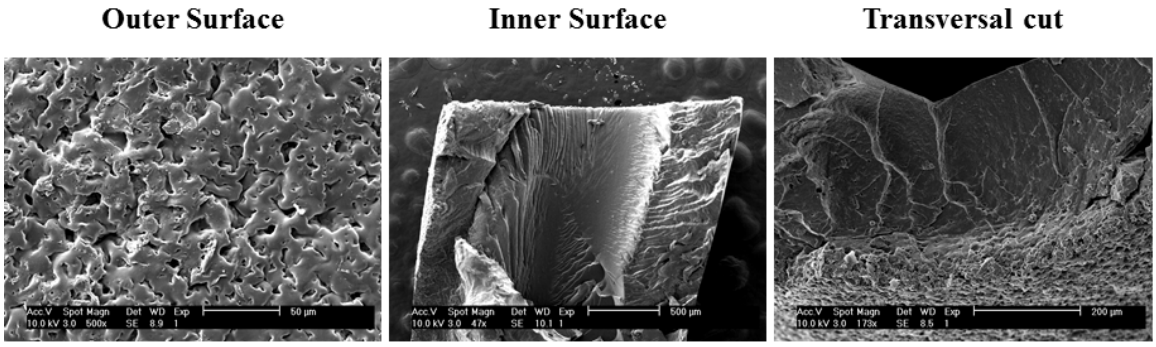

Figure 4.7 Micrographs obtained for T_GMA8(0.1)_PCL(0.3) with 35% wt of sodium carbonate.

The micrograph of the outer surface of the tube suggests that the structure has higher porosity, in comparison to the result obtained with D-Mannitol. However, the pore size measured is around 10-20µm, which can be too small for the exchange of compounds from the inside of the tube towards the outside. Moreover, the inner surface seems to be more compact than the outer surface. This could indicate that pores are mostly located in the outer surface of the tube. This fact is confirmed by the transversal cut where it is possible to observe that the pores are mostly situated in the outer surface, and gradually disappear towards the inner surface.

As mentioned before, the porosity and permeability of tubes for peripheral nerve regeneration, although controversial, are quite important. It is reported that permeable tubes allow the exchange of nutrients and oxygen, allow the drainage of the tube and also, allow the vascularization inside the tube.[40] All these factors have shown to have an important role on the enhancement of nerve regeneration.[40] Yet, bigger pores may allow the infiltration of fibrous tissue, which could jeopardize the regeneration process.[35] In our work, it would be desirable to have interconnective pores which crossed the tube structure. Unfortunately, with both porogenic agents, it was not possible to achieve that kind pores. For D-mannitol, some pores in the structure can be seen, most of them with sizes between 10-30µm, which are reported to be preferential as they not allow the infiltration of fibrous tissue. On the contrary, for sodium carbonate, the structure presents many pores that are not evenly distributed over the structure. This may be due to the position in which the tube is constructed. The tubes were crosslinked horizontally, and therefore, a higher amount of sodium carbonate may have deposit in the side that was faced down during the polymerization. Therefore, the presence of pores starts to decrease from that side to the top

of the tube. Due to this inconsistency, the tube with 50% wt of D-mannitol was considered to be more appropriate for the final application.

From this point of the work, the tubes that will be characterized in further studies are T_GMA8(0.1)_PCL(0.3) and T_GMA8(0.1)_PCL(0.3) with 50% wt of D-Mannitol, which will receive the designation of T_GMA8(0.1)_PCL(0.3)_M50.

In order to measure the degree of porosity of T_GMA8(0.1)_PCL(0.3)_M50 and compare with T_GMA8(0.1)_PCL(0.3), mercury porosimetry was performed. Both tubes were subject to 3 independent experiments. The plots obtained by this technique are presented in Figure C1.

The degree of porosity calculated for the porous tube was almost the same (*ca.* 3%) as the value obtained for the normal tube (approximately 2-3% degree of porosity). However, SEM micrographs show clearly that T_GMA8(0.1)_PCL(0.3) has no pores, in contrast with the porous tube. The reason for these values may be in the fact that before measurements, all tubes had to be dried. During this stage, the pore structure could have collapsed, resulting in a denser structure than the original one. Since no conclusions were taken from this technique, it was not possible to quantity the degree of porosity of T_GMA8(0.1)_PCL(0.3)_M(50).

4.4.3 Swelling Capacity of the tubes

Swelling capacity of both T_GMA8(0.1)_PCL(0.3) and T_GMA8(0.1)_PCL(0.3)_M50 was evaluated in PBS (pH=7.4), at 37ºC. The evaluation of the swelling capacity of the tubes is critical for using these materials in regenerative medicine. If significant changes in the dimensions of the tube occur, nerve constriction could occur, which have a negative effect on the regeneration process. Figure 4.8 presents the results of swelling capacity of T_GMA8(0.1)_PCL(0.3) and T_GMA8(0.1)_PCL(0.3)_M50.

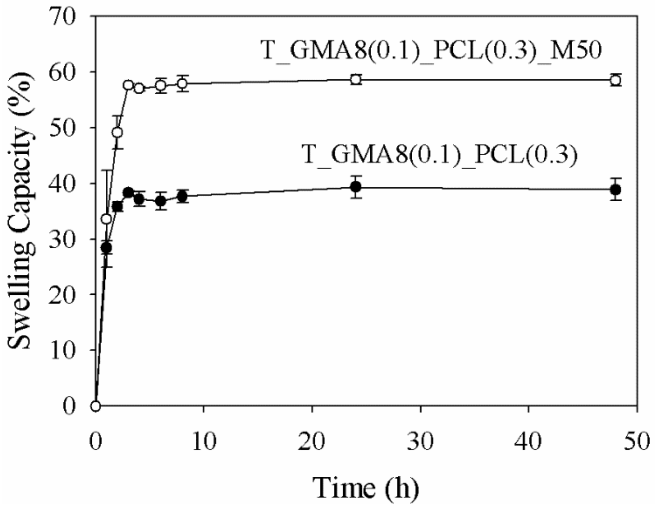

Figure 4.8 Swelling Capacity of the tube T_GMA8(0.1)_PCL(0.3) and T_GMA8(0.1)_PCL(0.3)_M50.

The results show that the swelling capacity of the tubes stabilizes approximately after 4-5 hours of immersion. T_GMA8(0.1)_PCL(0.3) presents a swelling capacity around 40%, while the value obtained for T_GMA8(0.1)_PCL(0.3)_M50 is *ca.* 60%. This difference was expected since it is known that porous structures have more ability to swell in comparison with more compact structures.[41] Since the degree of porosity of the porous tube could not be assessed, the difference in the swelling capacity may not be only attributed to the presence of pores. One of the parameters that directly influence the swelling capacity is the crosslinking density.[42,43] Furthermore, the use of a porogenic agent could affect the crosslinking process, leading to a different crosslinked structure, which results in a structure with more free space between chains.[36] With the increase of free space, the ability to swell of the final material also increases. The combination of these two facts may have influenced the swelling capacity of the tubes.

On the other hand, T_GMA8(0.1)_PCL(0.3) presents lower swelling capacity (40%) when compared with the previous membranes prepared in Chapter2 (over 50% for M_GMA8(0.1)_PCL(0.3) formulation). This result can indicate that the conformation of the materials has influence in their interaction with the surrounded media.[44]

In order to evaluate the influence of the immersion on PBS would have in the final inner diameter of the tubes, pictures were taken after this experiment, in dark light. Figure 4.9 shows the pictures taken before and after swelling capacity measurements.

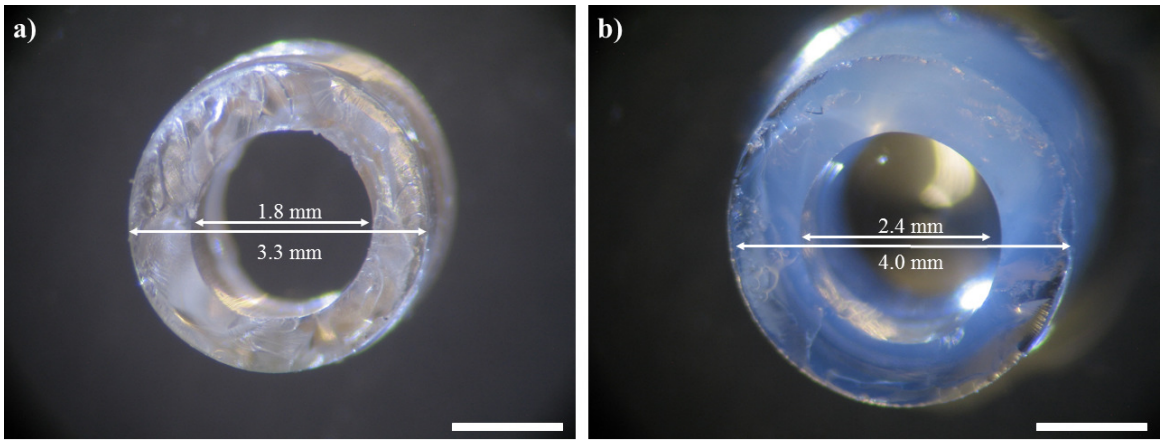

Figure 4.9 Dark light images of T_GMA8(0.1)_PCL(0.3)_M50: a) before swelling; b) after swelling. Scale bar: 1.0 mm.

In the dark light images is clear that the dimension of the inner diameter of tube is not compromised after swelling equilibrium is achieved. Likewise, the inner diameter increases, which will be useful for implantation purposes. An ideal swelling capacity value for these kind of biomedical devices is not defined. In turn, it is reported that swelling should be limited, in order to avoid nerve constriction. [45,46] In our case, since the lumen does not compress, this result is very relevant.

4.4.4 *In Vitro* hydrolytic degradation of tubes

The *in vitro* hydrolytic degradation of the tubes, under simulated physiological conditions (PBS, pH=7.4, 37ºC) was studied. Figure 4.10 presents the weight loss profiles of the tubes.

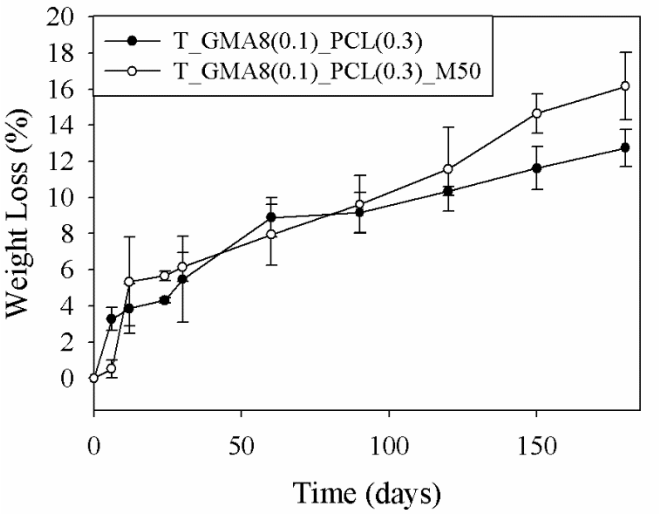

Figure 4.10 Weight Loss of T_GMA8(0.1)_PCL(0.3) and T_GMA8(0.1)_PCL(0.3)_M50.

Figure 4.10 shows that after 180 days, it is possible to see that T_GMA8(0.1)_PCL(0.3) lost around 16% of its mass, and T_GMA8(0.1)_PCL(0.3)_M50 lost around 13%. Both profiles indicate that both tubes can degrade consecutively with no significant alterations on the degradation rates until 100 days. After that, a different profile is observed, showing T_GMA8(0.1)_PCL(0.3)_M50 higher degradation. These results are in agreement with the previous values obtained for swelling capacity.[47,48,49] In this case, since swelling capacity measurements indicated that T_GMA8(0.1)_PCL(0.3)_M50 had a less crosslinking structure, it was expected that it would have a faster degradation rate in comparison with T_GMA8(0.1)_PCL(0.3). Additionally, the existence of pores facilitates the degradation of the tube, since they represent preferential sites of degradation.

This is an excellent indicator since for the final application, tubes should degrade along with the regeneration of the nerve. With a smoother process, the possibility of rejection by the body decreases.[50]

4.4.5 Mechanical tests

The mechanical properties of T_GMA8(0.1)_PCL(0.3) and T_GMA8(0.1)_PCL(0.3)_M50 were assessed by tensile strength evaluation.

Both tubes were left to swell overnight before tests. The mechanical tests were carried out at three stretching rates, until a maximum load of 1N. Ultimate tensile strength, elongation

at break and calculation of Young Modulus were made for 0.08mm/s stretching rate until tube fracture. These results are shown in Figure 4.11.

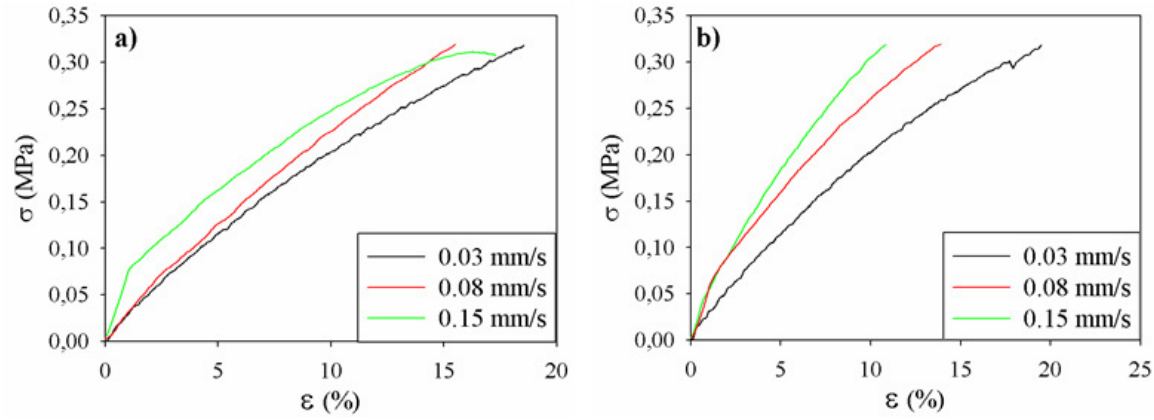

Figure 4.11 Stress-strain behavior of a) T_GMA8(0.1)_PCL(0.3); and b) T_GMA8(0.1)_PCL(0.3)_M50 with three different test speed.

Figure 4.11 shows that with the increase of the rate of the applied load, both tubes display a variation of the Young's modulus. This behavior was already expected since it is reported in literature that this parameter is dependent of the test speed.[51] This dependency arises from the fact that the deformation of a polymer, during a tensile test, is controlled by the entanglements of the network chains.[52] For higher rates, the network has less time to reorganize their uncrosslinked segments, which will result in higher resistance to deformation that is translated in higher Young modulus' values. On the other hand, for lower test speed, the chains have more time to reorganize the network before entering in the plastic domain. Additionally, a polymers' deformation is affected by the energy expended during plastic deformation, which is mostly dissipated as heat.[53] Regarding higher speeds, this influence is even more accentuated due to its association with adiabatic drawing.[54] This means that concerning these conditions, the dissipation of heat is lower compared with lower speeds, which, in contrary, are associated with isotherm drawing.[54] Hence, for higher speeds, as the energy is not so effectively dissipated, there is the need of higher load to achieve the same strain rates verified for lower speeds. Consequently, with the decrease of test speeds, polymers present a more elastic behavior, leading to lower Young modulus values.

To evaluate the fracture behavior of the tubes, the tensile tests were performed with a loading rate of 0.08 mm/s. The tests were only interrupted by the fracture of the tube. The results obtained are shown in Figure 4.12.

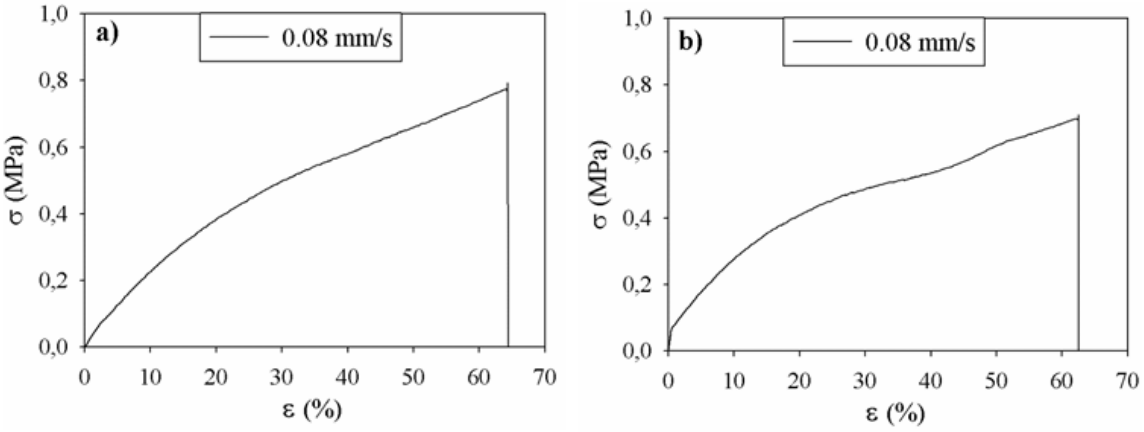

Figure 4.12 Stress-strain behavior until fracture at 0.08 mm/s of a) T_GMA8(0.1)_PCL(0.3); and b) T_GMA8(0.1)_PCL(0.3)_M50.

The stress-strain curve of both tubes shown that regarding the elongation at break, they present values higher than 60%. Moreover, the maximum stress that both tubes can handle before fracture is quite similar, being their values between 0.64-0.67MPa. Table 4.3 presents the values calculated for both tubes.

Table 4.3 Calculated mechanical properties of T_GMA8(0.1)_PCL(0.3) and T_GMA8(0.1)_PCL(0.3)_M50

	Ultimate tensile strength (MPa)	**Elongation at break (%)**
T_GMA8(0.1)_PCL(0.3)	0.64 ± 0.14	63.36 ± 1.38
T_GMA8(0.1)_PCL(0.3)_M50	0.65 ± 0.07	65.74 ± 4.35

Table 4.3 shows that in what concerns the values at fracture, both tubes present very similar results. Actually, the results of elongation at break are very close to the one reported in literature, for an intact human nerve (≈ 61%).[46] The ultimate tensile strength obtained, in

turn, is lower than the reported for the same nerve.[46] However, the human nerve values were obtained in a test with a displacement rate of 0.05mm/s, which means that these values should be evaluated critically. These results are promising since high elongation at break helps the tube to withstand the mechanical forces from adjacent muscles.[15]

For T_GMA8(0.1)_PCL(0.3)_M50, in the middle of the plastic domain curve, there is a zone where the curve does not increase consistently, which means that for achieving that for specific elongation, less stress was needed. This might be related to some relaxation of the tube, where the polymer network could rearrange its chains in order to absorb the stress more efficiently.

On the other hand, for very lower stress values (until 2% elongation) the tubes present distinct behaviors (Figure 4.13). In what concerns the porous tube (b), an initial slope corresponding to an apparent elastic phase can be observed followed by the beginning of the plastic domain. From the non porous tube (a) it is not possible to identify a clear elastic zone. For this reason, and in order to evaluate the tensile stress and the Young modulus, the derivative of the corresponding curves was also calculated (Figure 4.13).

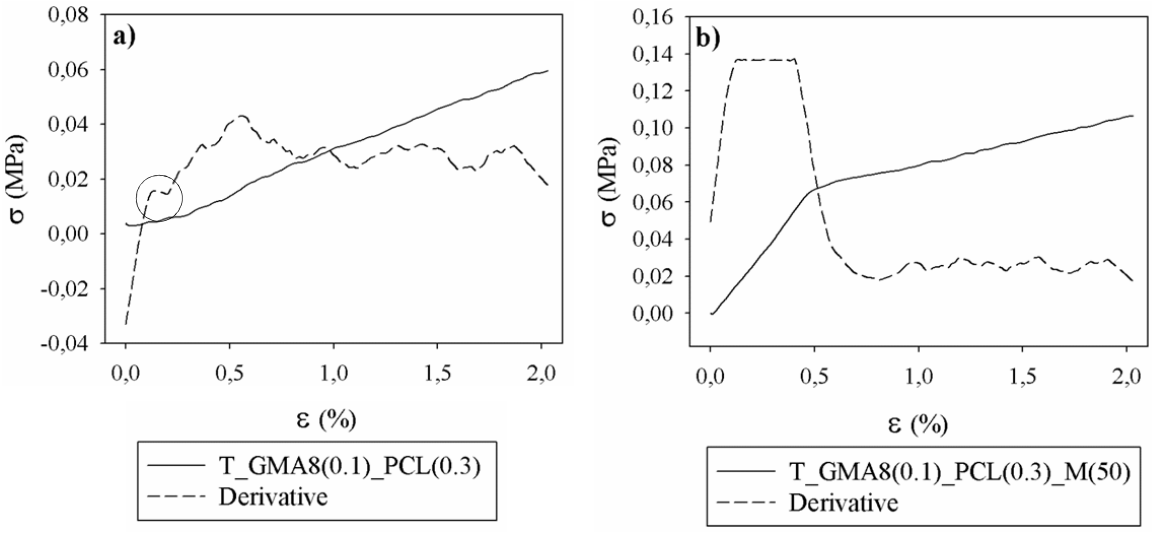

Figure 4.13 Stress/strain curves and respective derivatives of a) T_GMA8(0.1)_PCL(0.3); and b) T_GMA8(0.1)_PCL(0.3)_M50.

In the case of T_GMA8(0.1)_PCL(0.3)_M50, the linear elastic region is easily identified by the constant values of the derivative. For T_GMA8(0.1)_PCL(0.3), the derivative do not show constant values and hence it is not possible to clearly identify the corresponding elastic domain. For this analysis it will be important consider that the tubes were analyzed

in their hydrated forms which could give to materials singular characteristics due to the plastifying effect of the water molecules. These results are derived from several replications and not from a single experiment. When the stress is applied, there are no chains to unroll, which causes the early break of them, with the cleavage of the bonds that have less bond energy. For this reason, it would be expected that both tubes presented similar elastic domains profiles. However, the porous tube clearly presents a region, which corresponds to elastic deformation. The higher elastic region of T_GMA8(0.1)_PCL(0.3)_M50 may be related to its less crosslinked structure, discussed in the previous section (4.4.5 Swelling Capacity).

For this reason, only for the porous tube, the Young Modulus was calculated with the derivative method. The non-porous material present a small region at the beginning of the stress-strain curve (marked in Figure 4.13 a)), that could be considered to have elastic behavior and 2 point were considered for the calculation the Young Modulus using the secant approximation. For comparison purposes, same points were considered for the porous material. The two points selected correspond to 0.11% and 0.17% of elongation, for both tubes. Table 4.4 present the values of Young modulus calculated with both methods.

Table 4.4 Calculated Young Modulus of T_GMA8(0.1)_PCL(0.3) and T_GMA8(0.1)_PCL(0.3)_M50 with the derivative method and secant method.

	Young Modulus (MPa)	
	Derivative Method	Secant Method
T_GMA8(0.1)_PCL(0.3)	------	0.12 ± 0.10
T_GMA8(0.1)_PCL(0.3)_M50	0.14 ± 0.05	0.13 ± 0.05

With the method of secant, it was possible to calculate and compare the Young modulus of both tubes. The values obtained are quite similar, which suggests that, in this case, the presence of porosity does not affect the mechanical properties of the tubes.

In the context of the application of these tubes, it is important that the mechanical properties of the nerve guide conduit does not overmatch the nerve.[55] Generally, it is difficult to compare the values of the tensile strength tests obtained from the literature. This problem arises from the fact that there are no conventions or ISO Norms, for testing small cylinders with an open lumen. In our study, the observed values for the Young modulus are significantly lower than the ones reported in the literature for human tibial nerve (15.87MPa for a measure rate of 0.05mm/s).[56] Furthermore, in the literature, there are already some studies concerning tubes prepared with crosslinked chitosan where it was possible to obtain Young Modulus' values between 3-16MPa showing promising results when tested *in vitro*.[15,57] Although the calculated Young Modulus (table 4.4) are lower than the cited references in literature, it is also important to analyze the maximal loading which a nerve can handle. It is known that a rat sciatic nerve only supports 5-30% strain before starting to break.[58] Additionally, the nerve can only handle a maximal load between 1-2N with 0.05mm/s rate.[58] In our work, both tubes presented values of maximum loading between 2.2-2.4N for a dispersion rate of 0.08mm/s, which means that it could provide good protection for the growing nerve. Therefore, these results are very promising since the load values match the one obtained for the nerve.

Another structural aspect that is very important for peripheral nerve regeneration is the ability of the tubes, to handle suturing.[55,59,60] Since during implantation the tubes are sutured to both nerve stumps it is extremely important that they can bear the handling and suturing.[61 61] For this reason, it is desirable that the tube not break or crack. Furthermore, during the recovery time, they should be flexible enough to accommodate the movements of the patient. To address this parameter, both tubes were sutured with a needle to verify if they would resist to the perforation. Figure 4.14 shows the sutured tube.

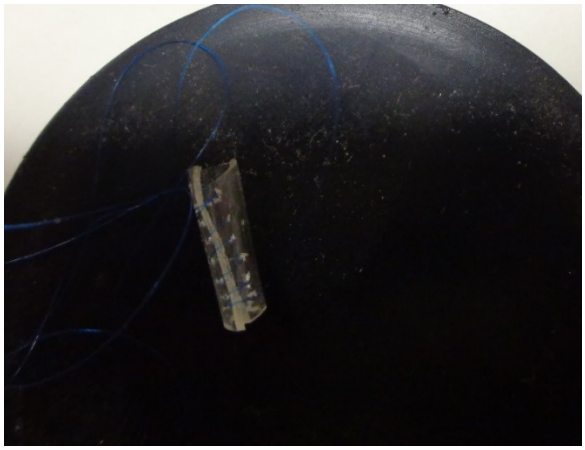

Figure 4.14 Suturing tests performed in tube.

As it can be observed in Figure 4.14, the wet tubes were sutured longitudinally and in both extremities. No cracks were visible in any perforation made. The needle trespassed easily the tube walls showing the easiness of the process. For this reason, it can be assumed that these tubes have the proper ability to handle suturing. This means that both tubes are very promising for implantation *in vivo*.

4.5 CONCLUSIONS

The aim of this work was to prepare dextran-based nerve guide tubes, which could be applied in peripheral nerve regeneration. This goal was successful achieved and transparent tubes were characterized giving promising results. The tubes were projected to have the same dimensions as the commercial product Neurolac®. Due to shrinkage during the tube fabrication, different sizes of mold were studied and also different formulations for the materials were tested. In order to create pores in the tube structure, D-mannitol was used as porogenic agent and added to the formulation T_GMA8(0.1)_PCL(0.3). These pores can be preferential sites of degradation, which can be good for increasing permeability of the tube. SEM micrographies showed that most of the pores are in a size range suitable for this application. In what concerns to swelling capacity, both, porous and non-porous tubes, showed values under 60%, being the non-porous tube only 40%. This is a very promising result in what concerns the behavior on the tube once it is implanted. With the help of dark light microscopy images, it could be seen that the inner diameter of the tubes was never compromised during swelling, which avoid any constriction of nerves during application.

Regarding degradation rates of tubes, the hydrolytic study revealed that after 180 days, the tubes still maintain their structural integrity and only lost between 12-16% of their initial weight.

Mechanical tests revealed that the Young modulus is influenced by the stretching rate. Besides, both tubes present a visco-elastic behavior, showing an elastic domain for the initial loads, from where it was possible to calculate the Young modulus. Although the values obtained are significantly lower than the ones reported in literature, both tubes can handle the maximum loads described for the rat sciatic nerve. Furthermore, it was proved that the prepared tubes can handle suturing without cracking or breaking, which is an important characteristic for implantation processes. Based on the results obtained by the present characterization, it is possible to state that these tubes can be considered good candidates for the implantation *in vivo*, to bridge a nerve sciatic gap.

4.6 REFERENCES

1. Wang, G.-W.; Yang, H.; Wu, W.-F.; Zhang, P.; Wang, J.-Y., Design and optimization of a biodegradable porous zein conduit using microtubes as a guide for rat sciatic nerve defect repair. *Biomaterials* **2017,** *131*, 145-159.

2. Pinho, A. C.; Fonseca, A. C.; Serra, A. C.; Santos, J. D.; Coelho, J. F. J., Peripheral Nerve Regeneration: Current Status and New Strategies Using Polymeric Materials. *Advanced Healthcare Materials* **2016,** *5*, 2732-2744.

3. Lim, E.-M. F.; Nakanishi, S. T.; Hoghooghi, V.; Eaton, S. E. A.; Palmer, A. L.; Frederick, A.; Stratton, J. A.; Stykel, M. G.; Whelan, P. J.; Zochodne, D. W.; Biernaskie, J.; Ousman, S. S., AlphaB-crystallin regulates remyelination after peripheral nerve injury. *Proceedings of the National Academy of Sciences* **2017,** *114*, E1707-E1716.

4. Tuft, B. W.; Xu, L.; White, S. P.; Seline, A. E.; Erwood, A. M.; Hansen, M. R.; Guymon, C. A., Neural Pathfinding on Uni- and Multidirectional Photopolymerized Micropatterns. *ACS Applied Materials & Interfaces* **2014,** *6*, 11265-11276.

5. Poggetti, A.; Battistini, P.; Parchi, P.; Novelli, M.; Raffa, S.; Cecchini, M.; Nucci, A.; Lisanti, M., How to Direct the Neuronal Growth Process in Peripheral Nerve Regeneration:

Future Strategies for Nanosurfaces Scaffold and Magnetic Nanoparticles. *Surgical technology international* **2017,** *30*.

6. Schaakxs, D.; Kalbermatten, D. F.; Pralong, E.; Raffoul, W.; Wiberg, M.; Kingham, P. J., Poly-3-hydroxybutyrate strips seeded with regenerative cells are effective promoters of peripheral nerve repair. *Journal of Tissue Engineering and Regenerative Medicine* **2017,** *11*, 812-821.

7. Goulart, C. O.; Lopes, F. R. P.; Monte, Z. O.; Dantas, S. V.; Souto, A.; Oliveira, J. T.; Almeida, F. M.; Tonda-Turo, C.; Pereira, C. C.; Borges, C. P., Evaluation of biodegradable polymer conduits–poly (l-lactic acid)–for guiding sciatic nerve regeneration in mice. *Methods* **2016,** *99*, 28-36.

8. Luo, L.; Gan, L.; Liu, Y.; Tian, W.; Tong, Z.; Wang, X.; Huselstein, C.; Chen, Y., Construction of nerve guide conduits from cellulose/soy protein composite membranes combined with Schwann cells and pyrroloquinoline quinone for the repair of peripheral nerve defect. *Biochemical and Biophysical Research Communications* **2015,** *457*, 507-513.

9. Karp, J. M.; Shoichet, M. S.; Davies, J. E., Bone formation on two-dimensional poly(DL-lactide-co-glycolide) (PLGA) films and three-dimensional PLGA tissue engineering scaffolds *in vitro*. *Journal of Biomedical Materials Research Part A* **2003,** *64A*, 388-396.

10. Li, H.; Chang, J., pH-compensation effect of bioactive inorganic fillers on the degradation of PLGA. *Composites Science and Technology* **2005,** *65*, 2226-2232.

11. Peng, H.; Ling, J.; Liu, J.; Zhu, N.; Ni, X.; Shen, Z., Controlled enzymatic degradation of poly(ε-caprolactone)-based copolymers in the presence of porcine pancreatic lipase. *Polymer Degradation and Stability* **2010,** *95*, 643-650.

12. Zheng, R.; Duan, H.; Xue, J.; Liu, Y.; Feng, B.; Zhao, S.; Zhu, Y.; Liu, Y.; He, A.; Zhang, W.; Liu, W.; Cao, Y.; Zhou, G., The influence of Gelatin/PCL ratio and 3-D construct shape of electrospun membranes on cartilage regeneration. *Biomaterials* **2014,** *35*, 152-164.

13. Fujimaki, H.; Uchida, K.; Inoue, G.; Miyagi, M.; Nemoto, N.; Saku, T.; Isobe, Y.; Inage, K.; Matsushita, O.; Yagishita, S., Oriented collagen tubes combined with basic

fibroblast growth factor promote peripheral nerve regeneration in a 15 mm sciatic nerve defect rat model. *Journal of Biomedical Materials Research Part A* **2017,** *105*, 8-14.

14. Suzuki, H.; Araki, K.; Matsui, T.; Tomifuji, M.; Yamashita, T.; Kobayashi, Y.; Shiotani, A., Value of a novel PGA-collagen tube on recurrent laryngeal nerve regeneration in a rat model. *The Laryngoscope* **2016,** *126*.

15. Lu, G.; Kong, L.; Sheng, B.; Wang, G.; Gong, Y.; Zhang, X., Degradation of covalently cross-linked carboxymethyl chitosan and its potential application for peripheral nerve regeneration. *European Polymer Journal* **2007,** *43*, 3807-3818.

16. Fregnan, F.; Ciglieri, E.; Tos, P.; Crosio, A.; Ciardelli, G.; Ruini, F.; Tonda-Turo, C.; Geuna, S.; Raimondo, S., Chitosan crosslinked flat scaffolds for peripheral nerve regeneration. *Biomedical Materials* **2016,** *11*, 045010.

17. Meyer, C.; Wrobel, S.; Raimondo, S.; Rochkind, S.; Heimann, C.; Shahar, A.; Ziv-Polat, O.; Geuna, S.; Grothe, C.; Haastert-Talini, K., Peripheral nerve regeneration through hydrogel-enriched chitosan conduits containing engineered schwann cells for drug delivery. *Cell transplantation* **2016,** *25*, 159-182.

18. Shapira, Y.; Tolmasov, M.; Nissan, M.; Reider, E.; Koren, A.; Biron, T.; Bitan, Y.; Livnat, M.; Ronchi, G.; Geuna, S., Comparison of results between chitosan hollow tube and autologous nerve graft in reconstruction of peripheral nerve defect: An experimental study. *Microsurgery* **2016,** *36*, 664-671.

19. Xie, F.; Li, Q. F.; Gu, B.; Liu, K.; Shen, G. X., *In vitro* and *in vivo* evaluation of a biodegradable chitosan–PLA composite peripheral nerve guide conduit material. *Microsurgery* **2008,** *28*, 471-479.

20. Shahriari, D.; Koffler, J.; Lynam, D. A.; Tuszynski, M. H.; Sakamoto, J. S., Characterizing the degradation of alginate hydrogel for use in multilumen scaffolds for spinal cord repair. *Journal of Biomedical Materials Research Part A* **2016,** *104*, 611-619.

21. Suzuki, Y.; Ishikawa, N.; Tanihara, M.; Saito, S., Nontubulation Repair of Peripheral Nerve Gap Using Heparin/Alginate Gel Combined with b-FGF. *Plastic and Reconstructive Surgery Global Open* **2016,** *4*, e600.

22. Young, R.; Terenghi, G.; Wiberg, M., Poly-3-hydroxybutyrate (PHB): a resorbable conduit for long-gap repair in peripheral nerves. *British Journal of Plastic Surgery* **2002,** *55*, 235-240.

23. Biazar, E.; Keshel, S. H., Chitosan–cross-linked nanofibrous PHBV nerve guide for rat sciatic nerve regeneration across a defect bridge. *ASAIO Journal* **2013,** *59*, 651-659.

24. Biazar, E.; Heidari Keshel, S., A nanofibrous PHBV tube with Schwann cell as artificial nerve graft contributing to Rat sciatic nerve regeneration across a 30-mm defect bridge. *Cell Ccommunication & Adhesion* **2013,** *20*, 41-49.

25. Pabari, A.; Yang, S. Y.; Seifalian, A. M.; Mosahebi, A., Modern surgical management of peripheral nerve gap. *Journal of Plastic Reconstruction & Aesthetic Surgery* **2010,** *63*, 1941-1948.

26. Kehoe, S.; Zhang, X. F.; Boyd, D., FDA approved guidance conduits and wraps for peripheral nerve injury: A review of materials and efficacy. *Injury* **2012,** *43*, 553-572.

27. Hoffman, A. S., Hydrogels for biomedical applications. *Advanced Drug Delivery Reviews* **2012,** *64*, 18-23.

28. Pescosolido, L.; Vermonden, T.; Malda, J.; Censi, R.; Dhert, W. J.; Alhaique, F.; Hennink, W. E.; Matricardi, P., In situ forming IPN hydrogels of calcium alginate and dextran-HEMA for biomedical applications. *Acta Biomaterialia* **2011,** *7*, 1627-1633.

29. Remya, N.; Syama, S.; Sabareeswaran, A.; Mohanan, P., Toxicity, toxicokinetics and biodistribution of dextran stabilized Iron oxide Nanoparticles for biomedical applications. *International Journal of Pharmaceutics* **2016,** *511*, 586-598.

30. Szafulera, K.; Wach, R. A.; Olejnik, A. K.; Rosiak, J. M.; Ulański, P., Radiation synthesis of biocompatible hydrogels of dextran methacrylate. *Radiation Physics and Chemistry* **2017**.

31. Banerjee, A.; Bandopadhyay, R., Use of dextran nanoparticle: A paradigm shift in bacterial exopolysaccharide based biomedical applications. *International Journal of Biological Macromolecules* **2016,** *87*, 295-301.

32. Bahney, C. S.; Lujan, T. J.; Hsu, C. W.; Bottlang, M.; West, J. L.; Johnstone, B., Visible light photoinitiation of mesenchymal stem cell-laden bioresponsive hydrogels. *European Cells & Materials* **2011,** *22*, 43-55.

33. Ameri Bafghi, R.; Biazar, E., Development of oriented nanofibrous silk guide for repair of nerve defects. *International Journal of Polymeric Materials and Polymeric Biomaterials* **2016,** *65*, 91-95.

34. Arslantunali, D.; Dursun, T.; Yucel, D.; Hasirci, N.; Hasirci, V., Peripheral nerve conduits: technology update. *Medical Devices* **2014,** *7*, 405-424.

35. Bhatnagar, D.; Bushman, J. S.; Murthy, N. S.; Merolli, A.; Kaplan, H. M.; Kohn, J., Fibrin glue as a stabilization strategy in peripheral nerve repair when using porous nerve guidance conduits. *Journal of Materials Science: Materials in Medicine* **2017,** *28*, 79.

36. Li, H.; Wijekoon, A.; Leipzig, N. D., 3D differentiation of neural stem cells in macroporous photopolymerizable hydrogel scaffolds. *PLoS One* **2012,** *7*, e48824.

37. Luis, A. L.; Rodrigues, J. M.; Amado, S.; Veloso, A. P.; Armada-Da-silva, P. A. S.; Raimondo, S.; Fregnan, F.; Ferreira, A. J.; Lopes, M. A.; Santos, J. D.; Geuna, S.; Varejão, A. S. P.; Maurício, A. C., PLGA 90/10 and caprolactone biodegradable nerve guides for the reconstruction of the rat sciatic nerve. *Microsurgery* **2007,** *27*, 125-137.

38. Hao, Y.; Lin, C.-C., Degradable thiol-acrylate hydrogels as tunable matrices for three-dimensional hepatic culture. *Journal of Biomedical Materials Research Part A* **2014,** *102*, 3813-3827.

39. Michael, V. T.; Sonja, S.; Jeffery, C. L.; Georgia, P., Effective tuning of ligand incorporation and mechanical properties in visible light photopolymerized poly(ethylene glycol) diacrylate hydrogels dictates cell adhesion and proliferation. *Biomedical Materials* **2013,** *8*, 025001.

40. Oh, S. H.; Kim, J. R.; Kwon, G. B.; Namgung, U.; Song, K. S.; Lee, J. H., Effect of surface pore structure of nerve guide conduit on peripheral nerve regeneration. *Tissue Engineering Part C: Methods* **2013,** *19*, 233-243.

41. Zhao, Y.; Su, H.; Fang, L.; Tan, T., Superabsorbent hydrogels from poly (aspartic acid) with salt-, temperature-and pH-responsiveness properties. *Polymer* **2005,** *46*, 5368-5376.

42. Koetting, M. C.; Guido, J. F.; Gupta, M.; Zhang, A.; Peppas, N. A., pH-responsive and enzymatically-responsive hydrogel microparticles for the oral delivery of therapeutic proteins: Effects of protein size, crosslinking density, and hydrogel degradation on protein delivery. *Journal of Controlled Release* **2016,** *221*, 18-25.

43. Javni, I.; Hong, D. P.; Petrović, Z. S., Soy-based polyurethanes by nonisocyanate route. *Journal of Applied Polymer Science* **2008,** *108*, 3867-3875.

44. Castner, D. G.; Ratner, B. D., Biomedical surface science: Foundations to frontiers. *Surface Science* **2002,** *500*, 28-60.

45. de Ruiter, G. C.; Malessy, M. J.; Yaszemski, M. J.; Windebank, A. J.; Spinner, R. J., Designing ideal conduits for peripheral nerve repair. *Neurosurgical focus* **2009,** *26*, E5.

46. Chiono, V.; Tonda-Turo, C., Trends in the design of nerve guidance channels in peripheral nerve tissue engineering. *Progress in Neurobiology* **2015,** *131*, 87-104.

47. Rahmat, M.; Ghasemi, I.; Karrabi, M.; Azizi, H.; Zandi, M.; Riahinezhad, M., Silane crosslinking of poly (lactic acid): The effect of simultaneous hydrolytic degradation. *Express Polymer Letters* **2015,** *9*.

48. Browning, M.; Cereceres, S.; Luong, P.; Cosgriff-Hernandez, E., Determination of the *in vivo* degradation mechanism of PEGDA hydrogels. *Journal of Biomedical Materials Research Part A* **2014,** *102*, 4244-4251.

49. Holloway, J. L.; Ma, H.; Rai, R.; Burdick, J. A., Modulating hydrogel crosslink density and degradation to control bone morphogenetic protein delivery and *in vivo* bone formation. *Journal of Controlled Release* **2014,** *191*, 63-70.

50. Yildirimer, L.; Seifalian, A. M., Three-dimensional biomaterial degradation—Material choice, design and extrinsic factor considerations. *Biotechnology advances* **2014,** *32*, 984-999.

51. Mulliken, A.; Boyce, M., Mechanics of the rate-dependent elastic–plastic deformation of glassy polymers from low to high strain rates. *International journal of solids and structures* **2006,** *43*, 1331-1356.

52. Baley, C., Analysis of the flax fibres tensile behaviour and analysis of the tensile stiffness increase. *Composites Part A: Applied Science and Manufacturing* **2002,** *33*, 939-948.

53. Sahin, S.; Yayla, P., Effects of testing parameters on the mechanical properties of polypropylene random copolymer. *Polymer Testing* **2005,** *24*, 613-619.

54. Dasari, A.; Misra, R. D. K., On the strain rate sensitivity of high density polyethylene and polypropylenes. *Materials Science and Engineering: A* **2003,** *358*, 356-371.

55. Nectow, A. R.; Marra, K. G.; Kaplan, D. L., Biomaterials for the development of peripheral nerve guidance conduits. *Tissue Engineering Part B: Reviews* **2012,** *18*, 40-50.

56. Dumont, C. E.; Born, W., Stimulation of neurite outgrowth in a human nerve scaffold designed for peripheral nerve reconstruction. *Journal of Biomedical Materials Research Part B: Applied Biomaterials* **2005,** *73B*, 194-202.

57. Wang, A.; Ao, Q.; Wei, Y.; Gong, K.; Liu, X.; Zhao, N.; Gong, Y.; Zhang, X., Physical properties and biocompatibility of a porous chitosan-based fiber-reinforced conduit for nerve regeneration. *Biotechnology Letters* **2007,** *29*, 1697-1702.

58. Hinuber, C.; Chwalek, K.; Pan-Montojo, F. J.; Nitschke, M.; Vogel, R.; Brunig, H.; Heinrich, G.; Werner, C., Hierarchically structured nerve guidance channels based on poly-3-hydroxybutyrate enhance oriented axonal outgrowth. *Acta Biomaterialia* **2014,** *10*, 2086-2095.

59. Shahriari, D.; Shibayama, M.; Lynam, D. A.; Wolf, K. J.; Kubota, G.; Koffler, J. Y.; Tuszynski, M. H.; Campana, W. M.; Sakamoto, J. S., Peripheral nerve growth within a hydrogel microchannel scaffold supported by a kink-resistant conduit. *Journal of Biomedical Materials Research Part A* **2017,** *105*, 3392-3399.

60. Borschel, G. H.; Kia, K. F.; Kuzon, W. M., Jr.; Dennis, R. G., Mechanical properties of acellular peripheral nerve. *Journal of Surgical Research* **2003,** *114*, 133-139.

61. Ciardelli, G.; Chiono, V., Materials for peripheral nerve regeneration. *Macromolecular Bioscience* **2006,** *6*, 13-26.

Chapter 5: **NOVEL DEXTRAN-BASED TUBE-GUIDES FOR THE REGENERATION OF THE RAT SCIATIC NERVE AFTER NEUROTMESIS INJURY**

5.1 ABSTRACT

Peripheral nerve injury can result in the discontinuity of axons and consequent denervation.[1] As a result, nerve loses its function, which can result in posterior muscle weakness, and deficient sensorial function (sense of anesthesia).[2] Therefore, reconstruction of peripheral nerves after injury by means of tube-guides has been extensively studied.[3] The use of polymeric tube-guides is one of the approaches presenting the most promising results and allowing the addition of cellular systems and growth factors.

This study intends to evaluate the *in vivo* performance of previously prepared dextran-based tube-guides in a sciatic nerve neurotmesis model in rats. Two types of nerve tube-guides were implanted being the only difference between them, the structure porosity. The evaluation testes were carried out for 20 weeks after the neurotmesis injury and nerve reconstruction surgery, with functional measurements taken at different time points. Twelve animals were divided into two groups. The Group 1 received the normal tube - T_GMA(0.1)_PCL(0.3), while Group 2 received T_GMA(0.1)_PCL(0.3)_M50 tube. In what concerns functional recovery, Extensor Postural Thrust (EPT), Withdrawal Latency Reflex (WLR) and Static Sciatic index (SSI) were measured and evaluated. The results obtained for EPT and WRL showed no significant difference between the animals which received the two tubes ($P<0.05$). However, the results obtained for T_GMA(0.1)_PCL(0.3)_M50 indicated higher functional and sensorial recovery. In addition, the results obtained are very close to the ones reported in literature for the commercial product Neurolac®.[4] Regarding the SSI, the differences between the results obtained from both nerve tube-guides were statistically different ($P>0.05$), with Group 2 presenting the closer results to a healthy behavior. This work suggests that the use of the prepared dextran-based nerve tube-guides have a positive effect on the regeneration of the peripheral nerve, after a neurotmesis injury.

5.2 INTRODUCTION

Tubulization techniques have been proposed as good alternatives to enhance nerve regeneration after injury. The scope of this technique relies on the use of a hollow tube, which is sutured to both nerve ends to guide the newly formed axons from distal to proximal stump. Biocompatible polymeric materials, due to their characteristics, have been used for the preparation of this particular type of medical device. Since the final application implies *in vivo* implantation, there is the need of finding appropriate animal models, which deliver outputs that can be correlated in order to evaluate the morphological, and above all, the functional recovery of the nerve. In this sense, recovering process after neurotmesis (complete physiological and anatomical transection of a nerve[5]) of the rat sciatic nerve is one of the most common models used. The main reasons supporting this preference are related to its easiness and the fact that it is relatively well studied by several reports in literature.[6] In addition, by studying the sciatic nerve, the recovery of motor and sensory function can be assessed at the same time, since it has both functions.[7,8] Although the rat is the most common animal used, other animal models as dog[9-13] and rabbit[14,15] sciatic nerve are also reported. The length of the nerve gap can be variable, but in general, the most studied length is 10 mm, which is already considered to be unsuitable for direct repair considering the rat model.

As aforementioned, polymeric materials are being used for the preparation of nerve guide tubes. In this sense, natural polymers and biodegradable synthetic polymers single used or combined, have shown the most promising results. Relatively to natural polymers, the most reported ones are collagen and chitosan. In a comparative study of the performance of a collagen tube and a silicone tube in a neurotmesis of the rat sciatic nerve, the first one revealed enhanced axonal regeneration, Schwann cell association and revascularization.[16] Collagen is often combined with synthetic polymers in order to overcome its limitations regarding the lack of mechanical properties. In a case report, a 30-year old woman received a PGA-collagen based nerve guide tube for the bridging of a lingual nerve.[17] After one year, the sensory function was successfully achieved.[17] FDA approved a collagen tube-guide named NeuraGen®, which is already available commercially. In a study regarding 126 patients, NeuraGen® was used to bridge nerve gaps revealing a percentage of sensory recovery in a range between 35-45%.[18] The main disadvantages associated to this product are the high degradation time (36-48 months) and their use are limited to nerve gaps no longer than 2-3cm.[19] Regarding chitosan,

progesterone impregnated chitosan tube-guides have been studied in the bridging of a 5 mm sciatic nerve gap in rats.[20] The results showed that after 180 days, the recovered kinematic function was comparable to healthy animals.[20] In another study, chitosan was combined with silk fibroin for the preparation of nerve guide tubes to bridge a 10mm gap of rat sciatic nerve.[21] At the end of the experiment, restoration of nerve continuity was observed.[21] Chitosan is also generally combined with other materials, namely alginate[22] and poly(3-hydroxybutyrate-co-hydroxyvalerate) (PHBV)[23], among others, for the preparation of devices for peripheral nerve regeneration.

Among the reported synthetic polymers, the most tested in *in vivo* trials are poly(glycolic acid) (PGA), poly(lactic acid-co-glycolic acid) (PLGA), and poly(ε-caprolactone) (PCL). Very often, these polymers are added to formulations with natural polymers in order to combine the best properties of both materials. The bridging of an 80mm gap in the left peroneal nerve in dogs was conducted with PGA-collagen based nerve guide tubes achieving interesting results. After 6 months of implantation, no marked difficulty was found in the gait movement.[24] However, after 12 months, the new nerve fibers were still smaller and covered by thinner myelin sheaths in comparison with normal nerves.[24] Similar nerve guide tubes were also tested in 10 patients for the recovery of digital nerves, revealing improved recovery of the sensorial function in comparison with end-to-end repair.[25] Another human study involving 136 patients which received PGA tubes had similar results showing better sensorial outcome than direct repair of the nerve.[26]

The use of PLGA for the preparation of nerve guide conduits tests *in vivo* is also quite common. In a report of PLGA tube-guides seeded with olfactory ensheathing cells, for the bridging of a 15mm gap in rat sciatic nerve showed, after 6 weeks, improvement of the nerve conduction velocity.[27] PLGA tubes were also compared with commercial product Neurolac® in a neurotmesis of the sciatic nerve model during 20 weeks. Results showed no significant differences between the number of regenerated nerve fibers between the materials, indicating that both materials are comparable.[4] PLGA/PCL nerve tube-guides prepared by electrospinning technique were also tested in a neurotmesis of the sciatic nerve model allowing the establishment of the neuronal function.[28]

Despite of the slow degradation rate of PCL, this polymer has also been reported for this application. A comparative study between a PCL nerve tube-guides with a PCL-collagen tube was conducted in a 10mm buccal nerve defect in rats. The results show that the incorporation of collagen improved neurite extension.[29] In another approach, PCL was combined with PEG and tested in a 10mm defect gap, revealing enhanced regeneration

behavior in comparison with a single PCL tube.[30] Additionally, Food and Drug Administration (FDA) approved a PCL copolymer based nerve guide conduit (P(DLLA-*co*-CL)), which has the commercial name of Neurolac®. Despite the extensive studies, synthetic polymers present limitations in what concerns their biodegradability ratio. For this reason, the combination of synthetic and natural polymers is a promising approach in which the final product could benefit from the advantages that both types of materials bring.

The present study aims to evaluate the *in vivo* performance of dextran-based nerve tube-guides, previously prepared. The *in vivo* assessment was conducted through a neurotmesis injury induced in the sciatic nerve of rats, with a gap length of approximately 10mm. Functional recovery was evaluated by means of Extensor Postural Thrust (EPT), Withdrawal Reflex Latency (WRL) and Static Sciatic Index (SSI).

5.3 EXPERIMENTAL SECTION

5.3.1 Materials

Dextran (Mw=70000 g/mol) and D-Mannitol were purchased from Sigma Aldrich (St. Louis, Missouri, USA). Glycidyl methacrylate (GMA) was purchased from Acros Organics (Geel, Belgium). 4-Dimethylaminopyridine (DMAP), 2-Isocyanatoethyl Methacrylate (IEMA) were acquired from TCI Europe (Zwijndrecht, Bélgica) and dimethyl sulfoxide (DMSO) from Fisher Scientific (Hampton, New Hampshire, USA). Dibutyltin dilaurate was purchased from Fluka (St. Louis, Missouri, USA). Tetrahydrofuran (THF) was obtained from VWR (Radnor, Pennsylvania, USA) and *n*-hexane was obtained from José Manuel Gomes dos Santos, Lda (Odivelas, Portugal). Poly(ε-caprolactone) diol (Capa™ 2054; Mw=550 g/mol) was kindly offered by Perstorp (Warrington, UK). Irgacure 2959® was gently supplied by Ciba Specialty Chemicals (Basel, Switzerland). Adult male Sasco Sprague Dawley rats (twelve) were supplied by Charles River Laboratories (Barcelona, Spain). Animal cages (Makrolon type 4) were purchased from Tecniplast (VA, Italy).

5.3.2 Preparation of the nerve tube-guides

The preparation of the tubes was already described in section 4.3.2 of Chapter 4.

Table 5.1 resumes the composition and nomenclature of the tubes used in this Chapter.

Table 5.1 Composition of the tubes.

Tubes	**Composition**		
Designation	**Modified dextran**	**PCL-IEMA**	**D-Mannitol**
T_GMA(0.1)_PCL(0.3)	0.1g P_LMW_GMA8*	0.3g	------
T_GMA(0.1)_PCL(0.3)_M50	0.1g P_LMW_GMA8*	0.3g	0.2g

*8 - corresponds to 8h – time of reaction between dextran and GMA

5.3.3 Surgical Procedure

Adult male Sasco Sprague Dawley rats, weighting 300-350g, were divided into two groups of six animals each. The first group (Group 1) received T_GMA(0.1)_PCL(0.3) guide tube, while the second group (Group 2) received the T_GMA(0.1)_PCL(0.3)_M50. All animals were housed in a temperature- and humidity-controlled room with 12-12h light/dark cycles, two animals per cage. Normal cage activities were allowed, under standard laboratory conditions. The animals were fed with standard chow and water *ad libitum*. Pain and discomfort were minimized by taken the adequate measures taking in consideration human endpoints for animal suffering and distress. Before entering the experience, animals were housed for two weeks.

For surgery, rats were placed prone under sterile conditions. The skin from the clipped lateral right thigh was scrubbed with antiseptic solution, in a routine fashion. Surgeries were conducted under an M-650 operating microscope (Leica Microsystems, Wetzlar, Germany). The anesthesia used was constituted by ketamine 9mg/100g; xylazine 1.25mg/100g; atropine 0.025mg/100 body weight, and was applied intramuscularly. Under the effect of anesthesia, a skin incision extending from the greater trochanter to the

midhalf distally was made. Then, a muscle-splitting incision was performed to expose the sciatic nerve of the animal. After the immobilization, with the help of straight microsurgical scissors, a transection (neurotmesis) was induced. The nerve was injured immediately above the terminal nerve ramification. In both groups, the proximal and distal stumps were inserted 3 mm into the nerve guide tubes (T_GMA(0.1)_PCL(0.3) and T_GMA(0.1)_PCL(0.3)_M50), and held in place with two epineural sutures using 7/0 monofilament nylon. The nerve gap between the two stumps was 10 mm. Figure 5.1. illustrates the nerve tube-guides sutured to both nerve stumps.

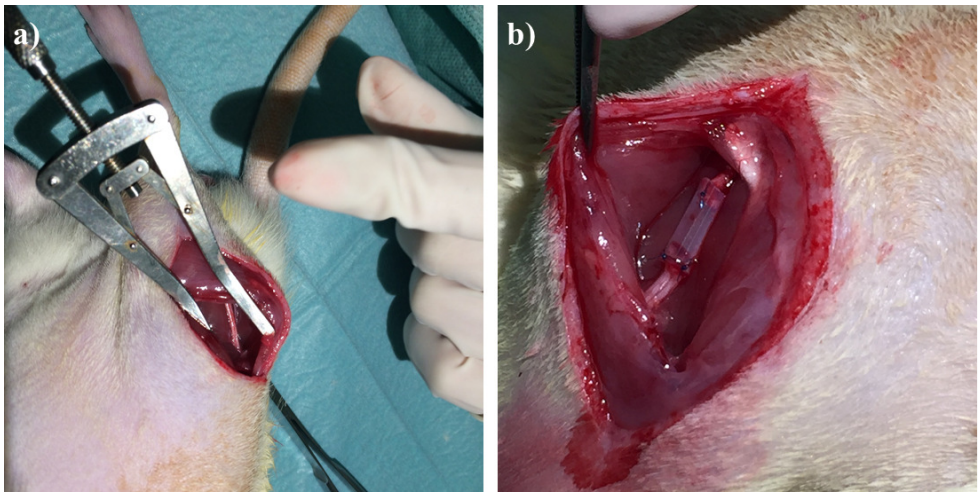

Figure 5.1 Surgical procedure: a) rat sciatic nerve; b) rat sciatic nerve sutured to the prepared nerve guide conduit.

The opposite leg and sciatic nerve were left intact in both groups, and were considered to be the control for normal nerves. A deterrent substance was applied to the right foot of the animals, in order to prevent autotomy.[31,32] All procedures were conducted with the approval of the Veterinary Authorities of Portugal in accordance with the European Communities Council Directive of November 1986 (86/609/EEC).

5.3.4 Functional Assessment

The individual body weight of each animal was determined using a digital balance. All measurements were taken prior to each functional analysis evaluation. The arithmetic mean of the weight of each animal in each week was considered for the descriptive

statistics. All animals were tested during a period of 20 weeks. Measurements were taken every 2 weeks since week 1 until the last week (week 20).

Evaluation of motor performance

The motor performance was assessed by the conduction of Extensor Postural Thrust (EPT).[33,34] For the registration of the EPT test results, the body of the rat, with the exception of the hind limbs, is wrapped in a surgical towel. The animal is then supported and lowered by the operator towards the platform of a digital balance. With the approximation to the platform, the animal is allowed to establish visual contact with the platform. Then the animal will anticipate the contact with the platform by extending the hind limb. This contact is made by the distal metatarsus and digits. The weight (force), in grams, applied to the digital platform balance (model TM 560; Gibertini, Milan, Italy) was recorded for both experimental (EEPT) and normal (NEPT) members. Measurements were repeated three times, and the value considered is the mean average between them. The EEPT and NEPT were integrated in equation eq 5.1., to obtain the percentage of functional deficit, as reported by Koka *et al*.[35] Figure 5.2 illustrates the EPT test.

$$\%Motor\ deficit = \frac{NEPT-EEPT}{NEPT} \times 100 \qquad \textbf{eq. 5.1}$$

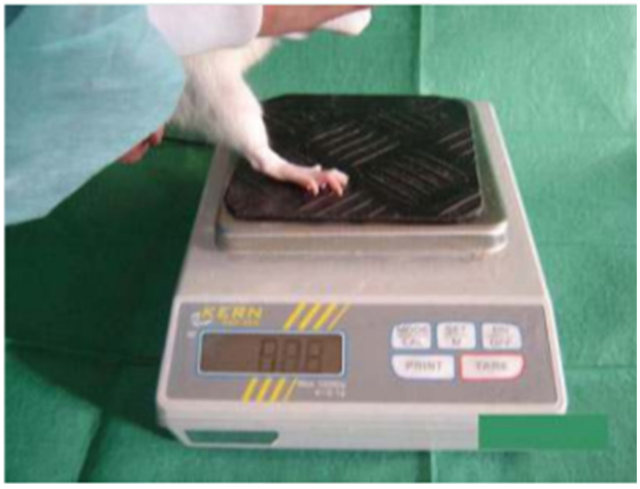

Figure 5.2 Extensor Postural Thrust (EPT) test.[4]

Evaluation of the nociceptive function

The nociceptive function was assessed by the evaluation of the withdrawal Reflex Latency (WRL). The nociceptive withdrawal reflex (WRL) was evaluated by the hotplate test modified as described by Masters *et al*.[36] The animal is wrapped in a surgical towel above its waist. Then, it is positioned to stand with the affected hind paw on a hot plate at 56ºC (model 35-D, IITC Life Science Instruments, Woodland Hill, CA). WRL is defined as the time elapsed from the onset of hotplate contact to withdrawal of the hind paw. This period of time is measured with a stopwatch. Normal rats withdraw their paws from the hotplate within 4.3s or less.[37] The limbs subjected to the experiment were tested three times, with an interval of 2 min between consecutive tests to prevent sensitization. The final result is presented as the average of those three measurements.[38,39] If the withdrawal of the paw did not occur after 12s, the heat stimuli was removed, and the test interrupt, to prevent tissue damage. In these cases, the animal was assigned the maximal WRL of 12s. Figure 5.3 represents the WRL test.

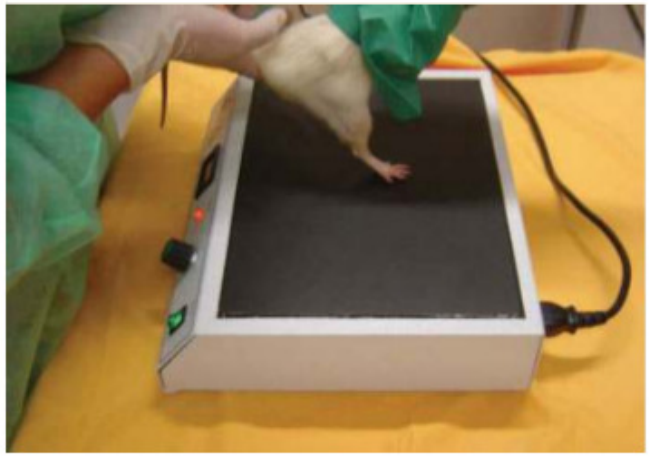

Figure 5.3 Withdrawal Reflex Latency (WRL) test.[4]

Sciatic functional index and static sciatic index

Sciatic functional index (SFI) is measured by testing the animals in a confined walkway (42cm long and 8.2cm wide), with white paper placed on the floor a dark shelter in the end, as previously described.[4] Figure 5.4 illustrates the walkway corridor.

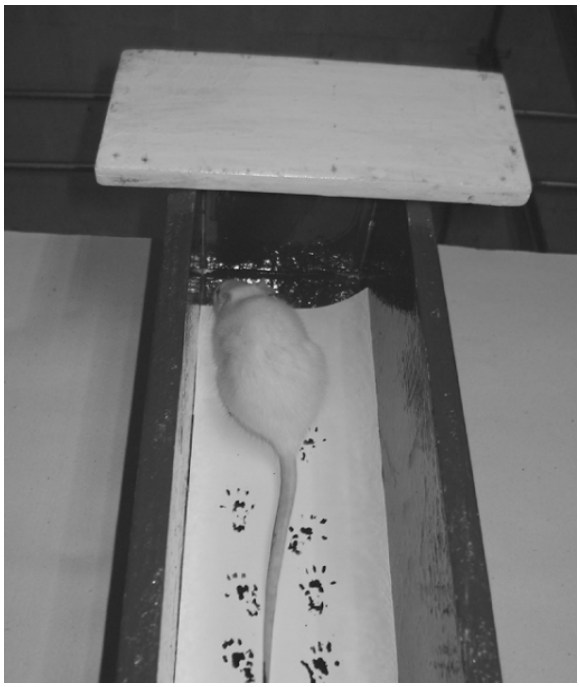

Figure 5.4 Walkway corridor used for the SFI tests.[40]

Briefly, the hind paws of the animals were pressed down onto a finger paint soaked sponge not toxic and appropriate to these measurements. Then, they were allowed to walk along the corridor to mark their footprints on the paper. Since this procedure is not simple, often, many walks were needed in order to obtain a clear mark. The walking tracks were recorded postoperatively at week 1, 3, 5, 7, 9, 14, 16, 18 and finally 20. The measurements taken to the footprints were: (i) the print length (PL) which is the distance from the heel to the third toe; (ii) the toe spread (TS), corresponding to the distance from the first toe to the fifth; and (iii) the intermediary toe spread (ITS), referent to the distance from the second to the fourth toe. Figure 5.5 presents a scheme of the measurements taken.

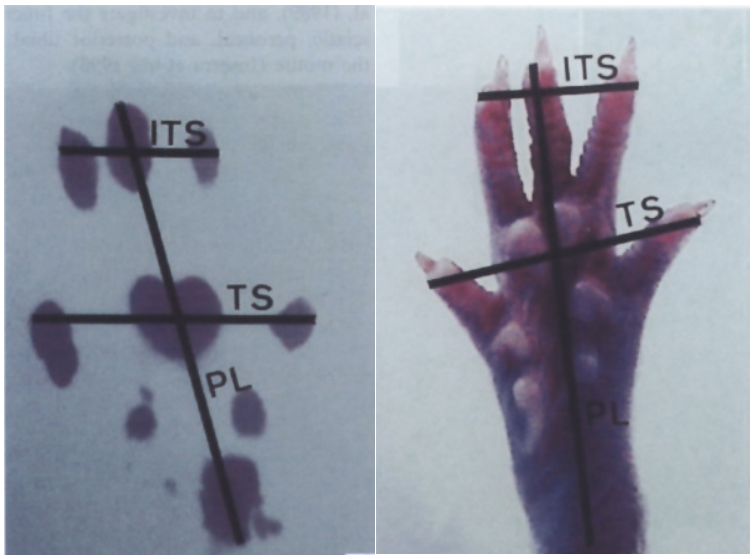

Figure 5.5 Scheme of the footprint measurements.

In the static sciatic index (SSI), the same measurements to the footprints were taken with the exception of the print length. For this test, the measurements were acquired just by the standing of the animals, and not during a walk. All footprints were obtained at least during four occasional rest periods. For both SFI and SSI, all measurements were taken from both normal (N) and experimental (E) sides. Four steps were analyzed per animal and their prints were chosen based on their clarity. The mean distances of the three different measurements taken were used to calculate the following factors:

$$Toe\ spread\ factor\ (TSF) = \frac{ETS-NTS}{NTS} \qquad \textbf{eq. 5.2}$$

$$Intermediate\ toe\ spread\ factor\ (ITSF) = \frac{EITS-NITS}{NITS} \qquad \textbf{eq. 5.3}$$

$$Print\ length\ factor\ (PLF) = \frac{EPL-NPL}{NPL} \qquad \textbf{eq. 5.4}$$

Where capital letter N stands for normal, and E to experimental.
All measurements were taken from both dynamic and static analysis.

Then the SFI was calculated with the following equation, as previously described[41]:

$$SFI = -38.3\left(\frac{EPL-NPL}{NPL}\right) + 109.5\left(\frac{ETS-NTS}{NTS}\right) + 13.3\left(\frac{EIT-NIT}{NIT}\right) - 8.8 \qquad \textbf{eq. 5.5}$$

SSI is calculated using the static factors only, not considering the PLF.[42] The following equation was used for its calculation[43]:

$$SSI = (108.44 \times TSF) + (31.85 \times ITSF) - 5.49 \qquad \textbf{eq. 5.6}$$

For both SFI and SS, an index score of 0 is considered normal while and index of -100 is translated into total impairment. In the cases where the footprints were not measurable, it was attributed an index score of -100.[44] In each walking track, a single observer analyzed three footprints. The average of measurements was used in SFI calculations.

5.3.5 Statistical Analysis

Statistical analysis was performed using the GraphPad Prism version 6.00 for Mac OS X, GraphPad Software, La Jolla California USA. All data were presented as mean value. The statistical analysis of the weight of the animals was assessed by Student's t test.[45,46] The given *P* values correspond to errors of the second kind ($P<0.05$).[45] For the functional assessment tests, differences were statistically evaluated by performing two-way analysis of variance (ANOVA)[47,48] test, using a mixed model taking into consideration the time and the different biomaterials tested. Pair wise comparisons between groups were conducted by *post hoc* Tukey HSD[49,50]. Differences were considered statistically significant at $P\leq0.05$.

5.4 RESULTS AND DISCUSSION

Prior to the first analysis, one of the rats died (G2/R3), which is common in experiments using living animals. Therefore, this fact may not be correlated to the implantation of the prepared medical device. For this reason, Group 1 (with T_GMA(0.1)_PCL(0.3)), includes six animals, while Group 2 (with T_GMA(0.1)_PCL(0.3)_M50), has a population of five animals.

5.4.1 Body Weight Measurement

Table 5.2 shows the weight of the animals at each time point and the calculated mean value.

Table 5.2 Weight measurements taken after each time point.

	Weight (g)								
	Week								
Group/Rat	**1**	**3**	**5**	**7**	**9**	**14**	**16**	**18**	**20**
G1/R1	396	425	435	465	495	505	563	580	538
G1/R2	385	430	440	425	458	538	517	528	536
G1/R3	413	475	495	543	547	597	620	630	630
G1/R4	374	405	391	446	460	450	530	535	534
G1/R5	352	395	410	433	454	487	512	534	543
G1/R6	340	405	422	452	478	524	560	560	508
G2/R1	356	395	420	424	450	482	502	408	512
G2/R2	381	416	433	447	465	502	526	535	546
G2/R4	363	390	400	423	445	500	537	527	535
G2/R5	341	432	401	454	475	505	512	545	550
G2/R6	331	360	368	377	390	417	430	440	498
Mean value	**366.55**	**411.64**	**419.55**	**444.45**	**465.18**	**500.64**	**528.09**	**529.27**	**539.09**

Table 5.2 shows that the weight of all animals increase during the time of the experiment. Figure 5.6 plots the mean weight and standard deviation (SD) values of each group, over the 20 weeks of follow-up.

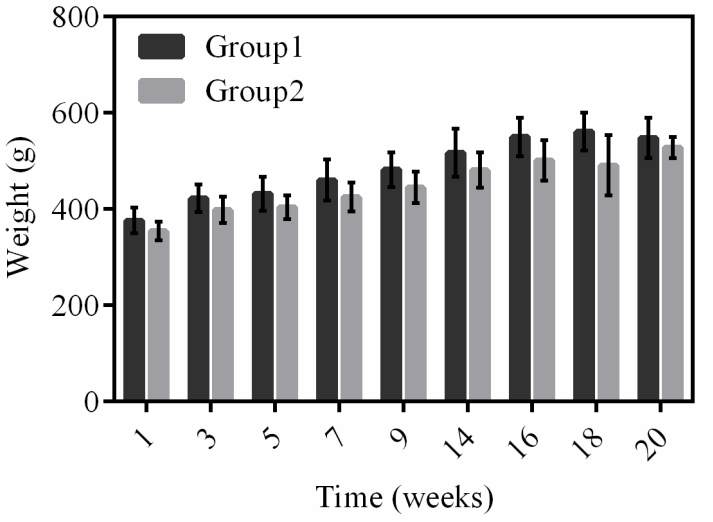

Figure 5.6 Mean animal weight values and standard deviation, for each time point during the experiment.

The weight measured for Group 1 is consistently higher than the measurements taken for Group 2. In order to understand if these results represent a tendency, linear regression was traced for both experimental groups. Figure 5.7 presents the linear regression of the mean values taken.

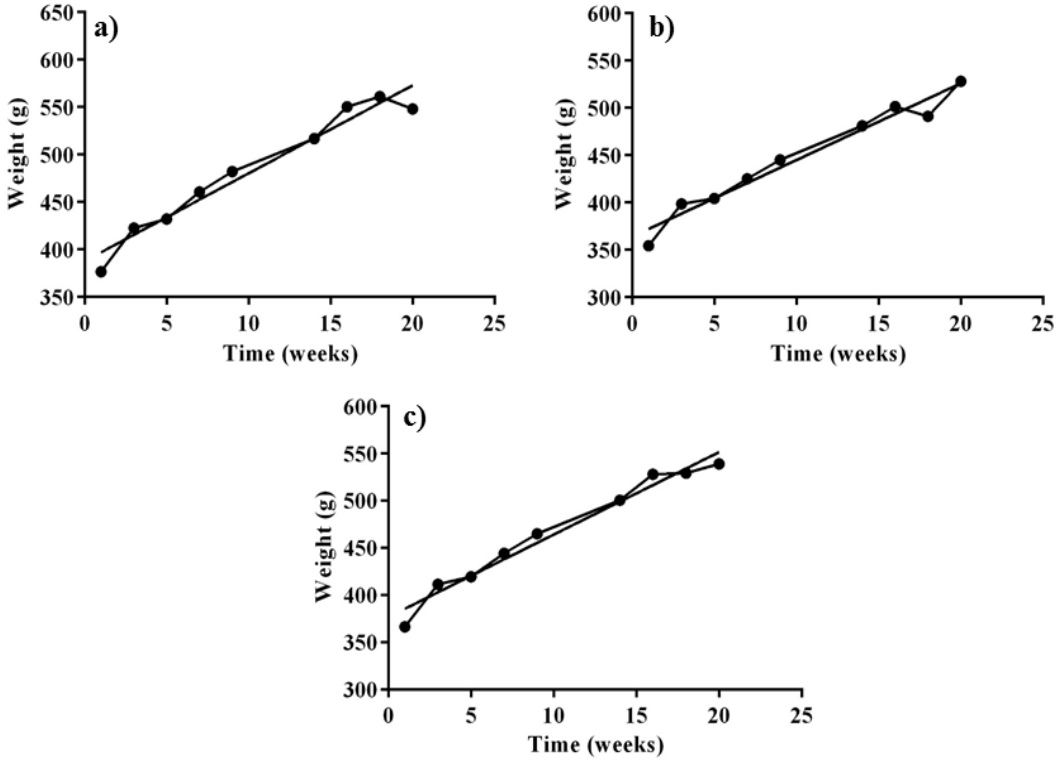

Figure 5.7 Linear regression of the weight mean values at each time point: a) Group 1; b) Group 2; c) All animals.

The linear regression confirms that the mean weight of the animals increases over time. Student's *t*-test was performed to compare both biomaterials. It is accepted the null hypothesis of *t*-test since the *p-value* (0.234) is higher than 0.05 ($P>0.05$). Thus, there are no statistically significant differences in the weight of the animals that received different nerve guide tubes, although, on average, the animals from Group 1 had a higher final weight. This may be a consequence in the decrease in movement by the animals subsequent to the nerve injury.

5.4.2 Motor performance

The extensor postural test (EPT) provides a quantitative measurement of functional recovery.[35] It aims to analyze the motor recovery of the nerve/limb by recording the weight applied by the limb on a digital scale. The percentages of motor deficit, calculated with eq. 5.1, are presented in Table 5.3.

Table 5.3 Percentage of motor deficit obtained for all animals of both Group 1 and Group 2. All values are presented as mean value.

	Motor Deficit (%)								
	Week								
Group/Rat	**1**	**3**	**5**	**7**	**9**	**14**	**16**	**18**	**20**
G1/R1	73	94	91	50	8	67	93	70	63
G1/R2	78	89	68	84	51	66	-9	28	68
G1/R3	66	94	81	88	15	75	76	43	77
G1/R4	72	86	78	77	62	67	80	41	65
G1/R5	79	83	63	61	15	76	67	43	62
G1/R6	54	97	48	97	17	25	69	45	60
Mean value	**70**	**90**	**71**	**76**	**28**	**62**	**63**	**45**	**66**
G2/R1	90	98	41	65	35	80	55	69	71
G2/R2	77	88	90	85	48	60	68	69	49
G2/R4	72	94	86	92	50	62	70	77	77
G2/R5	88	91	77	90	46	71	61	57	63
G2/R6	85	92	83	26	59	44	-8	88	57
Mean value	**82**	**92**	**75**	**72**	**48**	**63**	**49**	**72**	**63**

The results obtained present higher dispersion, which was expected, due to the fact that the tests are performed for living animals and, despite of the efforts in order to maintain the test conditions, animals' daily behavior may vary.

At week-1 and week-3 post surgery, the percentage of motor deficit obtained were higher in comparison to the values obtained for the next weeks. These results were expected since during these period after neurotmesis, a Wallerian degeneration occurs, which is fundamental for the prior regenerative process. During the subsequent weeks, the percentage of motor deficit decreases, which indicates that the nerve is regenerating over time. However, this decrease is not linear. In order to understand if these values have the tendency to decrease over time, linear regression was traced for both groups. (Figure 5.8)

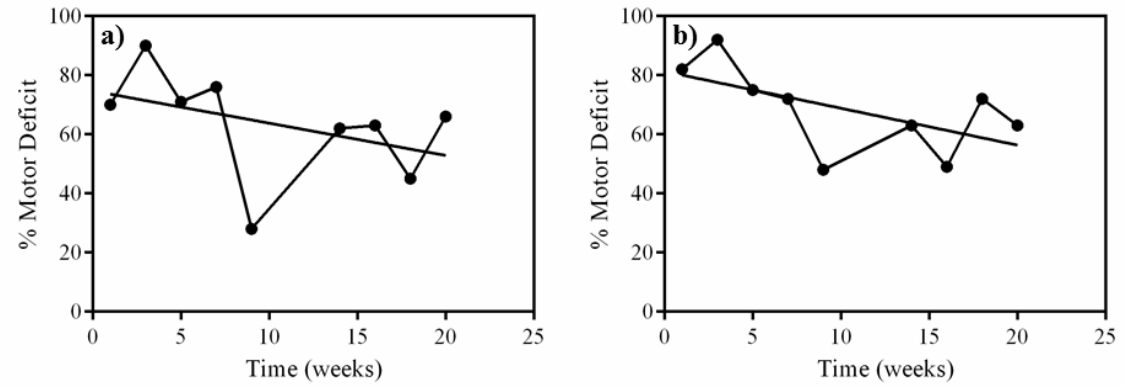

Figure 5.8 Linear regression of the percentage of motor deficit: a) Group 1; b) Group 2. The results as presented as mean value.

Despite the oscillating values resulting from the difficulty in ensuring equal movements of the animals during limb extension, linear regression traces show a general tendency for a decrease in the percentage of motor deficit value in both groups. Thus, an improvement in the percentage of motor recovery over the weeks is observed. Statistical analysis shown that there are no significant differences between the results obtained for Group 1 in comparison with Group 2 ($P>0.05$). Therefore, the type of tube-guide implanted did not influence, significantly, the recovery of motor function. However, two way ANOVA showed significant differences over time. *Post hoc* analysis of all results show that after week 9 post implantation, the decrease in the percentage of motor deficit begins to be significantly different ($P<0.0001$). This might indicate that the regeneration of the nerve was faster and more efficient after this time point.

EPT measurements of commercial product Neurolac®, taken in similar conditions to this work, has been reported.[4] After 20 weeks, the mean value obtained for the percentage of motor deficit was 53%.[4] This means that 47% of motor function recovery was fulfilled. In the present work, the nerve guide tube which presented the most close value to Neurolac® was T_GMA(0.1)_PCL(0.3)_M50 (Group 2), achieving 63% of motor deficit after 20 weeks and subsequently, 37% of motor function recovery. Although there are no statistical difference, the results suggest that porous structure of the tube may have a positive effect in the recovery of the motor function.

5.4.3 Nociceptive function

The nociceptive information (relative to the sensorial perception of pain) is carried to the central nervous system from several neurological pathways. It is evaluated through the withdrawal reflex, obtained with the use of painful stimuli. In this work, this stimuli was achieved by thermal stimulation. In this sense, the withdrawal reflex latency (WRL) is defined as the time elapsed (in seconds) from the onset of hotplate contact to withdrawal of the hind paw. The measurements taken to each animal are presented in Table 5.4.

Table 5.4 WRL values obtained for all animals at each time point. Values are presented as mean value.

	WRL (s)								
	Week								
Group/Rat	**1**	**3**	**5**	**7**	**9**	**14**	**16**	**18**	**20**
G1/R1	12.00	9.33	10.00	2.67	12.00	11.00	6.67	6.33	9.67
G1/R2	12.00	10.33	11.67	4.00	2.67	7.33	5.67	5.67	9.33
G1/R3	12.00	8.00	9.00	8.00	6.00	6.67	9.33	5.00	9.33
G1/R4	12.00	12.00	11.33	10.67	11.33	12.00	7.33	8.00	9.33
G1/R5	12.00	9.33	3.00	4.33	9.00	12.00	9.33	3.33	6.00
G1/R6	12.00	12.00	9.67	4.33	12.00	10.33	7.33	6.67	3.67
Mean value	**12.00**	**10.17**	**9.11**	**5.67**	**8.83**	**9.89**	**7.61**	**5.83**	**7.89**
G2/R1	12.00	8.33	12.00	9.00	2.33	10.67	5.33	9.33	6.00
G2/R2	12.00	10.33	11.00	11.33	2.67	12.00	10.00	2.00	5.67
G2/R4	12.00	8.00	5.00	12.00	8.33	3.33	6.00	6.67	5.67
G2/R5	12.00	7.67	7.00	8.00	7.00	12.00	8.67	8.67	5.00
G2/R6	12.00	12.00	10.67	4.00	5.67	10.33	4.33	2.00	3.67
Mean value	**12.00**	**9.27**	**9.13**	**8.87**	**5.20**	**9.67**	**6.87**	**5.73**	**5.20**

At week-1 post-surgery, none of the animals were able to respond to the heat stimuli within the time established. To protect animals from burning, after 12s, the tests were interrupted. In the subsequent time points, the WRL values oscillate, which was expected. At week-20, although mean values are never below the value considered normal for a rat with nerve integrity (4.3s or less)[51,52], for Group 2 the obtained value was very close to normal (5.20s). On the other hand, Group 1 present a mean value of 7.89s after 20 weeks, which suggests that for this group, the recovery of sensorial function was less efficient. Linear regression traces of both groups are presented in Figure 5.9.

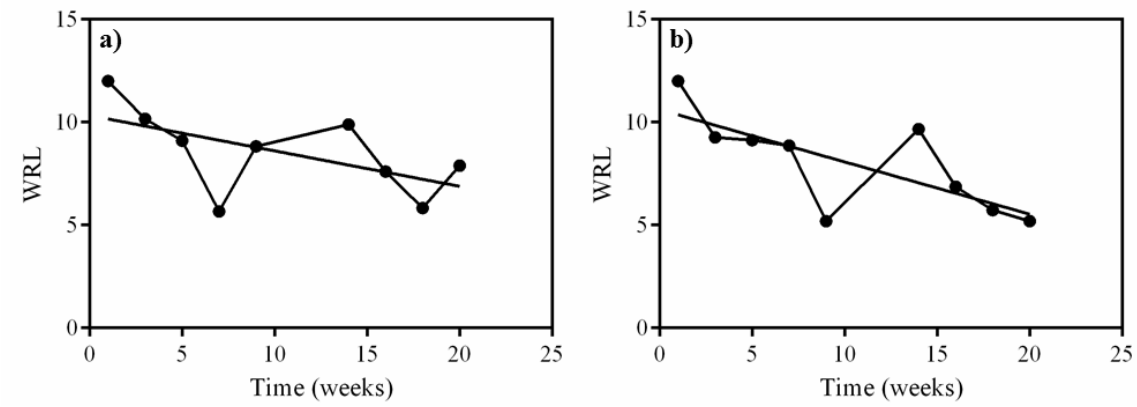

Figure 5.9 Linear regression of WRL mean values at each time point: a) Group 1; b) Group 2. All values obtained are presented as mean value.

The linear regression lines demonstrate a tendency of decrease of WRL over time. This means that an improvement in the sensorial function was observed. Despite the oscillating values, at week-20 all animals took less time to respond to the stimuli, in comparison with the first time point. Two way ANOVA statistical analysis showed no statistically significant differences in the WRL values of the animals that received different biomaterials (P>0.05). Regarding the differences over time, *Post hoc* analysis revealed that significant differences started to appear after 7 weeks for Group 1, and after 9 weeks for Group 2.

Although there are no statistical significance in the difference between both groups, on average, the animals that received T_GMA(0.1)_PCL(0.3)_M50 (Group 2) present lower WRL values, suggesting superior sensory recovery over Group 1. Similarly, to what was verified for motor recovery, the presence of pores seems to enhance the function recovery of the regenerated nerve. Reported experiments on commercial product Neurolac®, show fully sensorial recovery after 20 weeks, based on the WRL value.[4] In this work, rats of Group 2 almost achieved that WRL mean value, presenting the most promising results since they are closer to the healthy ones.

5.4.4 Sciatic functional index (SFI) and static sciatic index (SSI)

In order to evaluate the degree of functional recovery during gait movement, a SFI was developed in which an evaluation of the animal´s footprint is performed with three parameters: print length (PL), intermediate toe spread (ITS), and toe spread (TS).

However, for the experimental member it was very difficult to obtain clear footprints during gait movement. In addition, the PL value may vary considerably depending on the gait velocity, which difficult its analysis. For those reasons, for the experimental member, the Static sciatic index (SSI) was recorded instead of the sciatic functional index, since it provided more clear and reliable results. Therefore, only the SSI could be calculated for both members allowing the comparison of the obtained results. Both normal and experimental (injured) members were evaluated. Whenever possible, the footprint measurements were taken during gait movement. The calculated SSI (eq. 5.6) is presented in table 5.5.

Table 5.5 SSI values obtained for all animals at each time point. Values are presented as mean value.

	SSI								
	Week								
Group/Rat	**1**	**3**	**5**	**7**	**9**	**14**	**16**	**18**	**20**
G1/R1	-58.93	-61.59	-0.26	-41.62	-61.43	-22.51	-70.60	-65.16	-78.23
G1/R2	-50.76	-35.25	-50.99	-62.16	-37.18	-43.82	-55.33	-34.95	40.23
G1/R3	-54.92	-47.09	-61.29	-64.37	-76.49	-59.12	-37.98	-38.51	-61.69
G1/R4	-52.30	-66.81	-88.45	-35.54	-63.40	-27.56	-17.71	-19.04	-44.29
G1/R5	-58.06	-63.66	-52.28	-9.83	-45.20	-16.13	-62.73	-55.33	-50.39
G1/R6	-24.62	--	--	--	--	--	--	--	--
Mean value	**-49.93**	**-54.88**	**-50.65**	**-42.70**	**-56.74**	**-33.83**	**-48.87**	**-42.60**	**-38.87**
G2/R1	-31.80	-63.99	7.74	-29.05	-43.81	-19.47	-62.84	-43.41	-34.14
G2/R2	-44.70	-47.65	-51.16	-55.73	-35.28	-30.30	-51.65	21.25	7.00
G2/R4	-21.74	-58.42	-60.81	-50.09	-58.34	-45.16	-44.45	-46.49	-4.75
G2/R5	-14.06	-41.95	5.35	-37.15	-44.76	-14.10	-53.91	-9.33	-44.59
G2/R6	-34.28	-79.86	-23.28	-28.94	-31.44	-57.78	-22.76	-30.19	13.73
Mean value	**-29.31**	**-58.38**	**-24.43**	**-40.19**	**-42.73**	**-33.36**	**-47.12**	**-21.63**	**-12.55**

It is possible to observe that the average of SSI at each time point is always higher for Group 2. Since these values are closer to the normal value (0), this group was the one achieving the best results. The worst results for both groups were obtained for week-3 after surgery. Here, the SSI values are quite similar, surpassing -50. After this week, the SSI values start to increase, although not consistently. This means that after this time, the footprints of both experimental and normal sides left by animals started to be more similar, meaning that functional recovery was being accomplished. However, SSI values are very oscillating, which difficult their analysis. For this reason, a linear regression was traced for both Groups in order to understand if there is a tendency in the values. The linear regression is plotted in Figure 5.10.

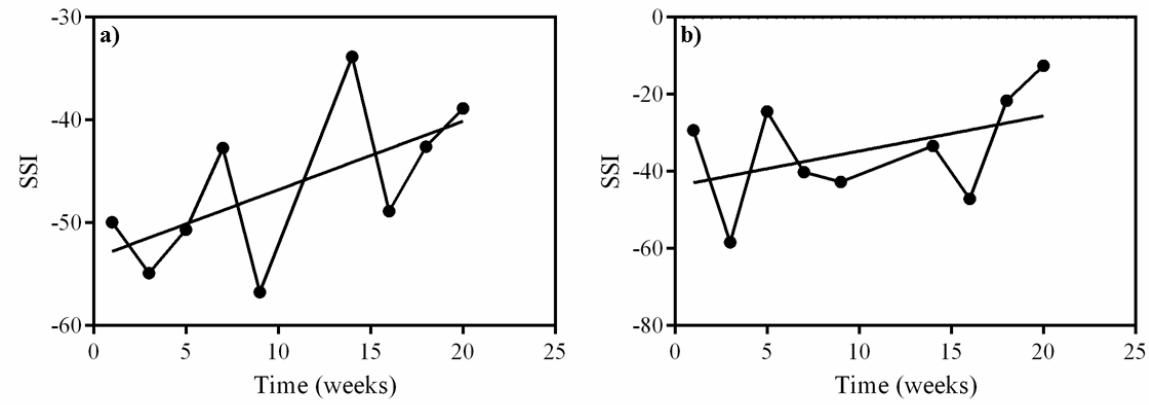

Figure 5.10 Linear regression of SSI mean values at each time point: a) Group 1; b) Group 2. All values obtained are presented as mean value.

Linear regression traces show that for both groups there are a tendency for the mean values of SSI to increase over time. This means that functional recovery was consistently achieved. Also, animals that received both nerve guide conduits show superior SSI at the end of the experiment comparing with the first week after surgery. Contrary to what was verified in the previous functional analysis measurements, two way ANOVA statistical analysis showed that there are significant statistical differences between the SSI values of the animals that received different biomaterials (P= 0.0108, P<0.05). This means that the porosity of the T_GMA(0.1)_PCL(0.3) material seems to be beneficial for the recovery of the animal as their experimental footprints became more similar to normal footprints. In addition, regarding the differences over time, *Post hoc* analysis revealed that the main difference concerning the time, in the footprint for Group 2, occurred at

week-20 after surgery (P<0.05). No significant differences were found over time for Group 1.

Unfortunately, it was not possible to find SSI values for commercial Neurolac® in the literature. However, in comparison with other nerve tube-guides prepared with PLGA[33,53], tested in similar conditions, the results obtained for T_GMA(0.1)_PCL(0.3)_M50 stood as the reported values are sited around -30. In this work, after 20 weeks post-surgery, the obtained mean SSI value is *ca.* -12, which is quite close to the normal value (0). This means that T_GMA(0.1)_PCL(0.3)_M50 enhanced functional recovery of the experimental hind paws as animals were able to produce footprints closer to normal.

5.5 CONCLUSIONS

The main goal of this work was to study the *in vivo* performance of dextran-based nerve conduits in a sciatic nerve neurotmesis model in rats. Two nerve guide conduits were tested, being the only structural difference between them, the existence of porosity. Twelve animals were divided into two groups and each group received a different nerve guide tube-guide. Group 1 received the normal T_GMA(0.1)_PCL(0.3) and Group 2 received T_GMA(0.1)_PCL(0.3)_M50. The tests were performed for a 20 weeks of follow up. The evolution of the weight of animals was assessed at each time point of the follow-up period. All animals presented an increase of their weight, which can be related to the loss of movements. The functional analysis assessed by EPT tests showed no significant differences between different groups meaning that the materials have the same performance. Despite of this fact, T_GMA(0.1)_PCL(0.3)_M50 showed superior percentage of motor recovery. Concerning the nociceptive function, the WRL results revealed no statistical difference between the two experimental groups. Nevertheless, Group 2 presented a mean WRL value of *ca.* 5 s, which is close to the normal value (around 4.3 s), suggesting that it has a better sensory recovery than Group 1.

The major differences between the two groups were seen in the SSI tests. Animals that received T_GMA(0.1)_PCL(0.3)_M50 presented SSI values, after 20 weeks, of -12, which is close to the normal value (0). This means that the footprints of the experimental and normal paw left by these animals are quite similar. This can be correlated with functional recovery. The score obtained (-12) are quite superior to other values obtained

for PLGA tubes, reported in literature (around -30). The inclusion of porosity in the tubes structure seem to have a positive effect on the nerve regeneration.
Further investigation might be conducted to study in detail the benefits of porosity in the recovery of the nerve in the prepared materials. Moreover, the prepared materials presented very promising results for their use in the preparation of medical devices for regenerative medicine, more specifically, peripheral nerve regeneration.

5.6 REFERENCES

1. Navarro, X.; Vivó, M.; Valero-Cabré, A., Neural plasticity after peripheral nerve injury and regeneration. *Progress in Neurobiology* **2007,** *82*, 163-201.

2. Hsu, H.-Y.; Kuo, L.-C.; Kuan, T.-S.; Yang, H.-C.; Su, F.-C.; Chiu, H.-Y.; Shieh, S.-J., Determining the functional sensibility of the hand in patients with peripheral nerve repair: Feasibility of using a novel manual tactile test for monitoring the progression of nerve regeneration. *Journal of Hand Therapy* **2017,** *30*, 65-73.

3. Bozkurt, A.; Claeys, K. G.; Schrading, S.; Rödler, J. V.; Altinova, H.; Schulz, J. B.; Weis, J.; Pallua, N.; Neerven, S. G., Clinical and biometrical 12-month follow-up in patients after reconstruction of the sural nerve biopsy defect by the collagen-based nerve guide Neuromaix. *European Journal of Medical Research* **2017,** *22*, 34.

4. Luis, A. L.; Rodrigues, J. M.; Amado, S.; Veloso, A. P.; Armada-Da-silva, P. A.; Raimondo, S.; Fregnan, F.; Ferreira, A. J.; Lopes, M. A.; Santos, J. D., PLGA 90/10 and caprolactone biodegradable nerve guides for the reconstruction of the rat sciatic nerve. *Microsurgery* **2007,** *27*, 125-137.

5. Rigoni, M.; Montecucco, C., Animal models for studying motor axon terminal paralysis and recovery. *Journal of Neurochemistry* **2017**.

6. Meek, M.; Den Dunnen, W.; Schakenraad, J.; Robinson, P., Long-term evaluation of functional nerve recovery after reconstruction with a thin-walled biodegradable poly(DL-Lactide-ε-caprolactone) nerve guide, using walking track analysis and electrostimulation tests. *Microsurgery* **1999,** *19*, 247-253.

7. Varejão, A. S.; Melo-Pinto, P.; Meek, M. F.; Filipe, V. M.; Bulas-Cruz, J., Methods for the experimental functional assessment of rat sciatic nerve regeneration. *Neurological Research* **2004,** *26*, 186-194.

8. Ganguly, A.; McEwen, C.; Troy, E. L.; Colburn, R. W.; Caggiano, A. O.; Schallert, T. J.; Parry, T. J., Recovery of sensorimotor function following sciatic nerve injury across multiple rat strains. *Journal of Neuroscience Methods* **2017,** *275*, 25-32.

9. Yao, Y.; Cui, Y.; Zhao, Y.; Xiao, Z.; Li, X.; Han, S.; Chen, B.; Fang, Y.; Wang, P.; Pan, J., Efect of longitudinally oriented collagen conduit combined with nerve growth factor on nerve regeneration after dog sciatic nerve injury. *Journal of Biomedical Materials Research Part B: Applied Biomaterials* **2017**.

10. Xue, C.; Zhu, H.; Tan, D.; Ren, H.; Gu, X.; Zhao, Y.; Zhang, P.; Sun, Z.; Yang, Y.; Gu, J., Electrospun silk fibroin based neural scaffold for bridging a long sciatic nerve gap in dogs. *Journal of Tissue Engineering and Regenerative Medicine* **2017**.

11. Wang, X.; Hu, W.; Cao, Y.; Yao, J.; Wu, J.; Gu, X., Dog sciatic nerve regeneration across a 30-mm defect bridged by a chitosan/PGA artificial nerve graft. *Brain* **2005,** *128*, 1897-1910.

12. Ding, F.; Wu, J.; Yang, Y.; Hu, W.; Zhu, Q.; Tang, X.; Liu, J.; Gu, X., Use of tissue-engineered nerve grafts consisting of a chitosan/poly (lactic-co-glycolic acid)-based scaffold included with bone marrow mesenchymal cells for bridging 50-mm dog sciatic nerve gaps. *Tissue Engineering Part A* **2010,** *16*, 3779-3790.

13. Xue, C.; Hu, N.; Gu, Y.; Yang, Y.; Liu, Y.; Liu, J.; Ding, F.; Gu, X., Joint use of a chitosan/PLGA scaffold and MSCs to bridge an extra large gap in dog sciatic nerve. *Neurorehabilitation and Neural Repair* **2012,** *26*, 96-106.

14. Chávez-Delgado, M.; Gomez-Pinedo, U.; Feria-Velasco, A.; Huerta-Viera, M.; Castro Castañeda, S.; López-Dellamary Toral, F.; Parducz, A.; Anda, L. D.; Mora-Galindo, J.; García-Estrada, J., Ultrastructural analysis of guided nerve regeneration using progesterone-and pregnenolone-loaded chitosan prostheses. *Journal of Biomedical Materials Research Part B: Applied Biomaterials* **2005,** *74*, 589-600.

15. Lee, D.-Y.; Choi, B.-H.; Park, J.-H.; Zhu, S.-J.; Kim, B.-Y.; Huh, J.-Y.; Lee, S.-H.; Jung, J.-H.; Kim, S.-H., Nerve regeneration with the use of a poly (l-lactide-co-glycolic acid)-coated collagen tube filled with collagen gel. *Journal of Cranio-Maxillofacial Surgery* **2006,** *34*, 50-56.

16. Kemp, S. W.; Syed, S.; Walsh, S. K.; Zochodne, D. W.; Midha, R., Collagen nerve conduits promote enhanced axonal regeneration, schwann cell association, and neovascularization compared to silicone conduits. *Tissue Engineering Part A* **2009,** *15*, 1975-1988.

17. Seo, K.; Inada, Y.; Terumitsu, M.; Nakamura, T.; Horiuchi, K.; Inada, I.; Someya, G., One year outcome of damaged lingual nerve repair using a PGA-collagen tube: a case report. *Journal of Oral and Maxillofacial Surgery* **2008,** *66*, 1481-1484.

18. Wangensteen, K. J.; Kalliainen, L. K., Collagen Tube Conduits in Peripheral Nerve Repair: A Retrospective Analysis. *HAND* **2010,** *5*, 273-277.

19. Kehoe, S.; Zhang, X.; Boyd, D., FDA approved guidance conduits and wraps for peripheral nerve injury: a review of materials and efficacy. *Injury* **2012,** *43*, 553-572.

20. Sarabia-Estrada, R.; Bañuelos-Pineda, J.; Carrasco, L. P. O.; Jiménez-Vallejo, S.; Jiménez-Estrada, I.; Rivas-Celis, E.; Dueñas-Jiménez, J. M.; Dueñas-Jiménez, S. H., Aberrant gastrocnemius muscle innervation by tibial nerve afferents after implantation of chitosan tubes impregnated with progesterone favored locomotion recovery in rats with transected sciatic nerve. *Journal of Neurosurgery* **2015,** *123*, 270-282.

21. Wei, Y.; Gong, K.; Zheng, Z.; Wang, A.; Ao, Q.; Gong, Y.; Zhang, X., Chitosan/silk fibroin-based tissue-engineered graft seeded with adipose-derived stem cells enhances nerve regeneration in a rat model. *Journal of Materials Science: Materials in Medicine* **2011,** *22*, 1947-1964.

22. Pfister, L. A.; Alther, E.; Papaloïzos, M.; Merkle, H. P.; Gander, B., Controlled nerve growth factor release from multi-ply alginate/chitosan-based nerve conduits. *European Journal of Pharmaceutics and Biopharmaceutics* **2008,** *69*, 563-572.

23. Biazar, E.; Keshel, S. H., Chitosan–cross-linked nanofibrous PHBV nerve guide for rat sciatic nerve regeneration across a defect bridge. *ASAIO Journal* **2013,** *59*, 651-659.

24. Matsumoto, K.; Ohnishi, K.; Sekine, T.; Ueda, H.; Yamamoto, Y.; Kiyotani, T.; Nakamura, T.; Endo, K.; Shimizu, Y., Use of a newly developed artificial nerve conduit to assist peripheral nerve regeneration across a long gap in dogs. *ASAIO Journal* **2000,** *46*, 415-420.

25. Seo, K.; Terumitsu, M.; Inada, Y.; Nakamura, T.; Shigeno, K.; Tanaka, Y., Prognosis After Surgical Treatment of Trigeminal Neuropathy with a PGA-c Tube: Report of 10 Cases. *Pain Medicine* **2016,** *17*, 2360-2368.

26. Weber, R. A.; Breidenbach, W. C.; Brown, R. E.; Jabaley, M. E.; Mass, D. P., A Randomized Prospective Study of Polyglycolic Acid Conduits for Digital Nerve Reconstruction in Humans. *Plastic and Reconstructive Surgery* **2000,** *106*, 1036-1045.

27. Tan, C. W.; Ng, M. H.; Ohnmar, H.; Lokanathan, Y.; Nur-Hidayah, H.; Roohi, S. A.; Ruszymah, B. H. I.; Nor-Hazla, M. H.; Shalimar, A.; Naicker, A. S., Sciatic nerve repair with tissue engineered nerve: Olfactory ensheathing cells seeded poly(lactic-co-glygolic acid) conduit in an animal model. *Indian Journal of Orthopaedics* **2013,** *47*, 547-552.

28. Panseri, S.; Cunha, C.; Lowery, J.; Del Carro, U.; Taraballi, F.; Amadio, S.; Vescovi, A.; Gelain, F., Electrospun micro-and nanofiber tubes for functional nervous regeneration in sciatic nerve transections. *BMC biotechnology* **2008,** *8*, 39.

29. Kannan, R. Y.; Salacinski, H. J.; Butler, P. E. M.; Seifalian, A. M., Artificial nerve conduits in peripheral-nerve repair. *Biotechnology and Applied Biochemistry* **2005,** *41*, 193-200.

30. Niu, Y.; Chen, K. C.; He, T.; Yu, W.; Huang, S.; Xu, K., Scaffolds from block polyurethanes based on poly(ε-caprolactone) (PCL) and poly(ethylene glycol) (PEG) for peripheral nerve regeneration. *Biomaterials* **2014,** *35*, 4266-4277.

31. Kerns, J. M.; Braverman, B.; Mathew, A.; Lucchinetti, C.; Ivankovich, A. D., A comparison of cryoprobe and crush lesions in the rat sciatic nerve. *Pain* **1991,** *47*, 31-39.

32. Sporel-Özakat, R.; Edwards, P.; Hepgul, K.; Savas, A.; Gispen, W., A simple method for reducing autotomy in rats after peripheral nerve lesions. *Journal of Neuroscience Methods* **1991,** *36*, 263-265.

33. Luís, A. L.; Rodrigues, J. M.; Geuna, S.; Amado, S.; Shirosaki, Y.; Lee, J. M.; Fregnan, F.; Lopes, M. A.; Veloso, A. P.; Ferreira, A. J., Use of PLGA 90: 10 scaffolds enriched with *in vitro*–differentiated neural cells for repairing rat sciatic nerve defects. *Tissue Engineering Part A* **2008,** *14*, 979-993.

34. Gärtner, A.; Pereira, T.; Armada-da-Silva, P.; Amorim, I.; Gomes, R.; Ribeiro, J.; Franca, M.; Lopes, C.; Porto, B.; Sousa, R., Use of poly (DL-lactide-ε-caprolactone) membranes and mesenchymal stem cells from the Wharton's jelly of the umbilical cord for promoting nerve regeneration in axonotmesis: *In vitro* and *in vivo* analysis. *Differentiation* **2012,** *84*, 355-365.

35. Koka, R.; Hadlock, T. A., Quantification of functional recovery following rat sciatic nerve transection. *Experimental neurology* **2001,** *168*, 192-195.

36. Masters, D. B.; Berde, C. B.; Dutta, S. K.; Griggs, C. T.; Hu, D.; Kupsky, W.; Langer, R., Prolonged regional nerve blockade by controlled release of local anesthetic from a biodegradable polymer matrix. *Anesthesiology* **1993,** *79*, 340-346.

37. Hu, D.; Hu, R.; Berde, C. B., Neurologic evaluation of infant and adult rats before and after sciatic nerve blockade. *Anesthesiology: The Journal of the American Society of Anesthesiologists* **1997,** *86*, 957-965.

38. Campbell, J. N., Nerve lesions and the generation of pain. *Muscle & Nerve* **2001,** *24*, 1261-1273.

39. Shir, Y.; Zeltser, R.; Vatine, J.-J.; Carmi, G.; Belfer, I.; Zangen, A.; Overstreet, D.; Raber, P.; Seltzer, Z. e., Correlation of intact sensibility and neuropathic pain-related behaviors in eight inbred and outbred rat strains and selection lines. *Pain* **2001,** *90*, 75-82.

40. Wong, K.-H.; Naidu, M.; David, P.; Abdulla, M. A.; Abdullah, N.; Kuppusamy, U. R.; Sabaratnam, V., Peripheral nerve regeneration following crush injury to rat peroneal nerve by aqueous extract of medicinal mushroom Hericium erinaceus (Bull.: Fr) Pers.(Aphyllophoromycetideae). *Evidence-based Complementary and Alternative Medicine* **2011,** *2011*.

41. Bain, J.; Mackinnon, S.; Hunter, D., Functional evaluation of complete sciatic, peroneal, and posterior tibial nerve lesions in the rat. *Plastic and Reconstructive Surgery* **1989,** *83*, 129-136.

42. Tao, J.; Hu, Y.; Wang, S.; Zhang, J.; Liu, X.; Gou, Z.; Cheng, H.; Liu, Q.; Zhang, Q.; You, S., A 3D-engineered porous conduit for peripheral nerve repair. *Scientific Reports* **2017,** *7*.

43. Xie, H.; Yang, W.; Chen, J.; Zhang, J.; Lu, X.; Zhao, X.; Huang, K.; Li, H.; Chang, P.; Wang, Z., A silk sericin/silicone nerve guidance conduit promotes regeneration of a transected sciatic nerve. *Advanced Healthcare Materials* **2015,** *4*, 2195-2205.

44. Dijkstra, J. R.; Meek, M. F.; Robinson, P. H.; Gramsbergen, A., Methods to evaluate functional nerve recovery in adult rats: walking track analysis, video analysis and the withdrawal reflex. *Journal of Neuroscience Methods* **2000,** *96*, 89-96.

45. Hald, A., *Statistical theory with engineering applications.* John Wiley & Sons: New York, **1952**; p 783.

46. Harris, D. C., *Exploring Chemical Analysis*. W. H. Freeman and Company: New York, **1997**.

47. Sokal, R.; Rohlf, F. J., *Biometry - The principles and practice of statistic in biological research*. 4th ed.; San Francisco, **1981**; p 915.

48. Clarke, K.; Warwick, R., Similarity-based testing for community pattern: the two-way layout with no replication. *Marine Biology* **1994,** *118*, 167-176.

49. Keppel, G.; Wickens, T., Simultaneous comparisons and the control of type I errors. *Design and analysis: A researcher's handbook. 4th ed. Upper Saddle River (NJ): Pearson Prentice Hall. p* **2004**, 111-130.

50. Ruxton, G. D.; Beauchamp, G., Time for some a priori thinking about post hoc testing. *Behavioral Ecology* **2008,** *19*, 690-693.

51. Pedrosa, S. S.; Caseiro, A. R.; Santos, J. D.; Maurício, A. C., Scaffolds for Peripheral Nerve Regeneration, the importance of i*n vitro* and *in vivo* studies for the development of

cell-based therapies and biomaterials: State of the Art. In *Scaffolds in Tissue Engineering-Materials, Technologies and Clinical Applications*, InTech: 2017.

52. Wu, Y.-H.; Liang, H.-W.; Chen, W.-S.; Lai, J.-S.; Luh, J.-J.; Chong, F.-C., Electrophysiological and functional effects of shock waves on the sciatic nerve of rats. *Ultrasound in Medicine & Biology* **2008,** *34*, 1688-1696.

53. Liu, H.; Lv, P.; Zhu, Y.; Wu, H.; Zhang, K.; Xu, F.; Zheng, L.; Zhao, J., Salidroside promotes peripheral nerve regeneration based on tissue engineering strategy using Schwann cells and PLGA: *in vitro* and *in vivo*. *Scientific Reports* **2017,** *7*.

Chapter 6. **FINAL REMARKS**

6.1 CONCLUSIONS

Since last century, peripheral nerve degeneration and regeneration have been extensively studied. The demand of new strategies to enhance the nerve regeneration and avoid permanent disability increased in the last decades. The tubulization approach has been by far, the one presenting best results more comparable to nerve autogragh. In this sense, polymeric materials have been proposed as good materials for the preparation of tubular devices for this application, due to the possibility of structure manipulation and easily tailoring their final properties. Among the materials studied, dextran, a biocompatible polysaccharide already used in several biomedical devices and approved by FDA, has never been proposed as core material of nerve guide conduits.

In this work, novel dextran based nerve guide tubes were prepared by a photocrosslinking technique, proving to be good alternatives to commercial products.

Dextrans with different molecular weights were modified with GMA (with different degrees of substitution) and IEMA, in order to introduce double bonds in its network. A PCL derivative with terminal double bonds was also prepared. Different formulations were prepared varying the content of these three components. Photocrosslinking using Irgacure2959® with different reaction conditions were carried out. The final formulations were conformed into a membrane shape and then characterized for their thermal-mechanical properties. The relation between swelling capacity with PCL_IEMA content in the formulations, was established. *In vitro* hydrolytic degradation ratio revealed that PCL_IEMA retards the degradation ratio of the membranes over time. Additionally, membranes were able to maintain their structural integrity during the test (Chapter 2).

Taking into consideration the results obtained in Chapter 2, cytotoxicity tests were conducted membranes using human dental pulp stem cells (hDPSCs) for 7 days (Chapter 3). After this period, membranes with PCL_IEMA showed the highest cell viability and metabolic rates. Intracellular concentration of calcium ions of adherent cells was measured revealing that all membranes constitute a suitable substrate for these cells (Chapter 3).

Chapter 3 describes the study of membranes implantation in mice. Evaluation of cell count and biological reaction revealed that M_GMA(0.2)_PCL(0.2) and M_GMA(0.1)_PCL(0.3) received a score that corresponds to the classification of “non-irritant”. Histological analysis performed in different organs after the implantation time showed no signs of

inflammation, fibrosis or necrosis. The *in vitro* and *in vivo* preliminary tests reinforced that the modified dextran originate membranes that were appropriate for regenerative medicine.

In Chapter 4, the conformation into tube shape was successfully achieved. Shrinkage studies were related to dextran structure and final tube dimensions were similar to the commercial product Neurolac®. To enhance the permeability of the tube, D-Mannitol was added as porogenic agent, creating pores with a size range between 10-20μm. Swelling capacity of tubes were lower than the values obtained for the membranes. Dark light imaging revealed that swelling do not change tube inner diameter a very important result taking into account a possible nerve constriction. *In vitro* hydrolytic degradation showed that after 180 days all tubes were able to maintain their structural integrity, with mass loss values in a range between 12-16%. The mechanical properties of the tubes were also evaluated, revealing that tubes are able to sustain the tension and elongation that a healthy nerve can support. In addition, both tubes can handle suturing without cracking.

Finally, tubes prepared and characterized in Chapter 4, were used in a nerve sciatic nerve neurotmesis model (Chapter 5). The *in vivo* tests were performed for 20 weeks. Two groups of 6 rats were divided and each group received the non porous tube (Group 1) and the porous tube (Group 2). After this time, functional analysis was assessed by EPT, WRL and SSI. These tests revealed that concerning motor deficit, both groups had similar results showing 40% of recovery. Group 2 revealed better sensory recovery than Group 1, supported by the WRL tests. Furthermore, SSI tests showed that footprints acquired for Group 2 present a score value close to the healthy one. This means that porosity may have a positive influence in the regeneration of the nerve. The results obtained by the *in vivo* tests suggest that these devices can be used in regenerative medicine, namely, peripheral nerve regeneration.

To sum up, this PhD work allowed the development of novel dextran based hollow tubes, which are biocompatible, biodegradable and non toxic for living tissues. The obtained results showed that these materials can have a positive influence in the enhancement in the regeneration process of an injured nerve.

6.2 FUTURE WORK

The results presented in this PhD thesis constitute a new approach in the preparation of biomedical devices for regenerative medicine, namely, peripheral nerve regeneration. Among several possibilities to enhance the final performance of the prepared devices, the following topics are considered to be of particular relevance:

- To continue the optimization of the base formulations will be of interest (e.g., ratios and degree of modification of the co-macromonomer PCL_IEMA) in order to enhance the final mechanical properties and fine tune the degradation ratio of the nerve guide conduits.

- To continue the optimization of the porosity of the nerve guide tubes by the use of new porogenic agents, in order to be able to tailor and enhance the final permeability of the nerve guide conduit. Furthermore, it would be interesting to test the performance of nerve guide conduits with different degrees of porosity with variation of the pore size.

- To evaluate the ability of nerve regeneration involved cells (e.g. Schwann Cells, neurotrophic factors) to adhere and proliferate on the surface of the prepared nerve guide conduits, in order to enhance the regeneration process.

- To evaluate the performance of the nerve guide conduits in a neurotmesis model with kinematic and morphological analysis.

ANNEXES

ANNEX A

Supporting information for:

Chapter 2: **Preparation of novel dextran based membranes for application in regenerative medicine**

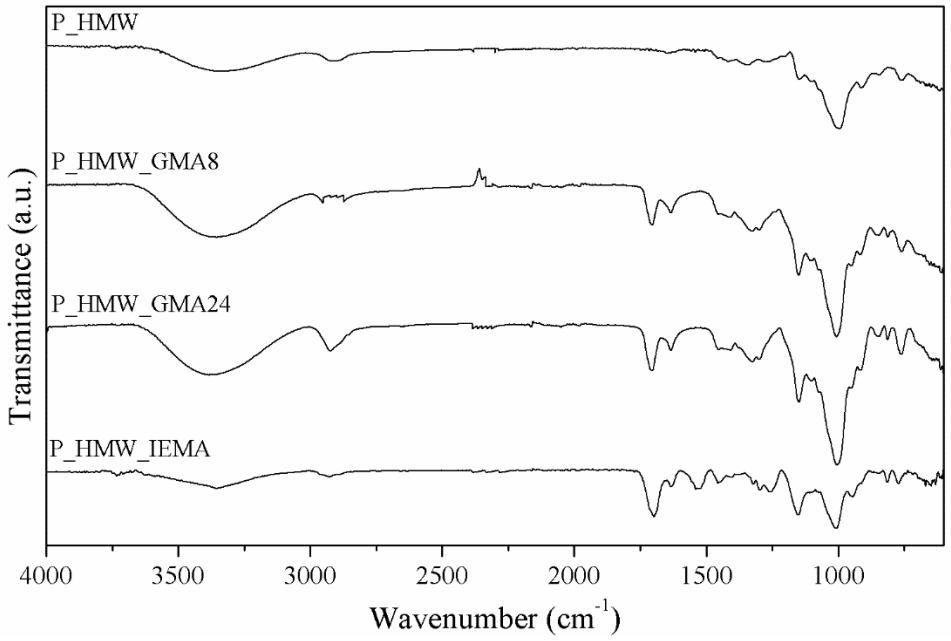

Figure A.1 FTIR spectra of high molecular weight dextran and respective products of modification.

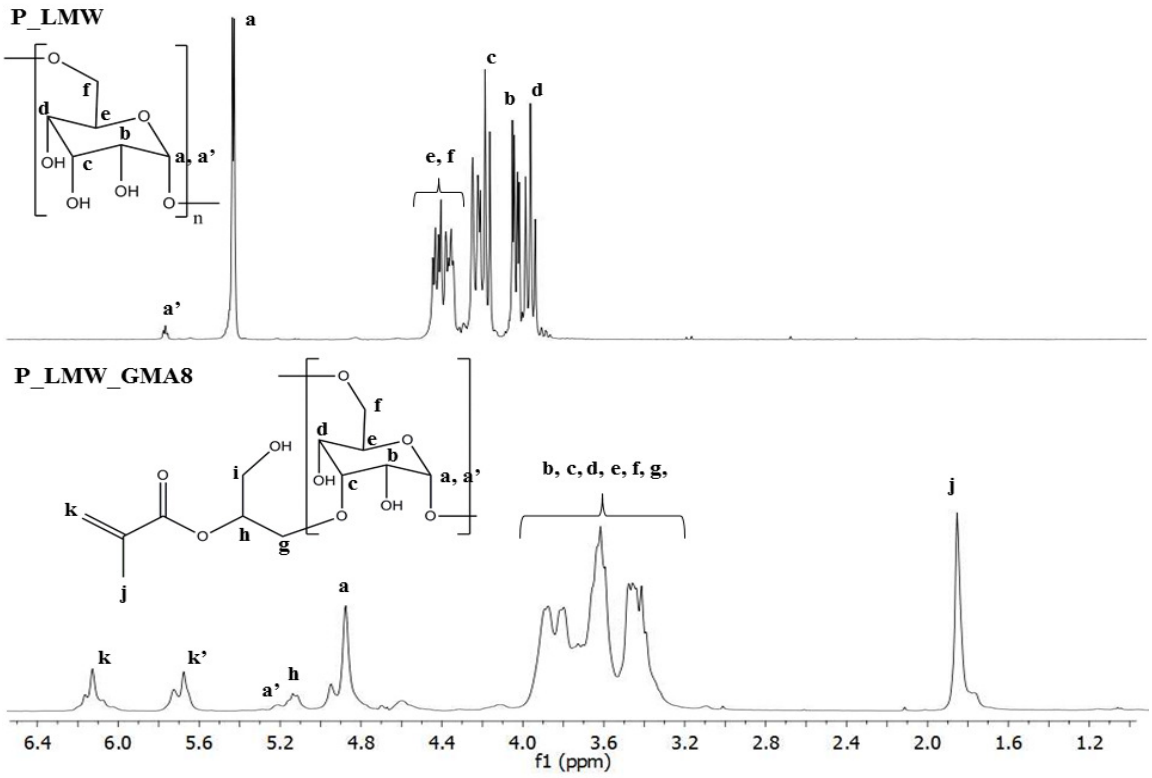

Figure A.2 ^{1}H NMR spectra of P_LMW and P_LMW_GMA8.

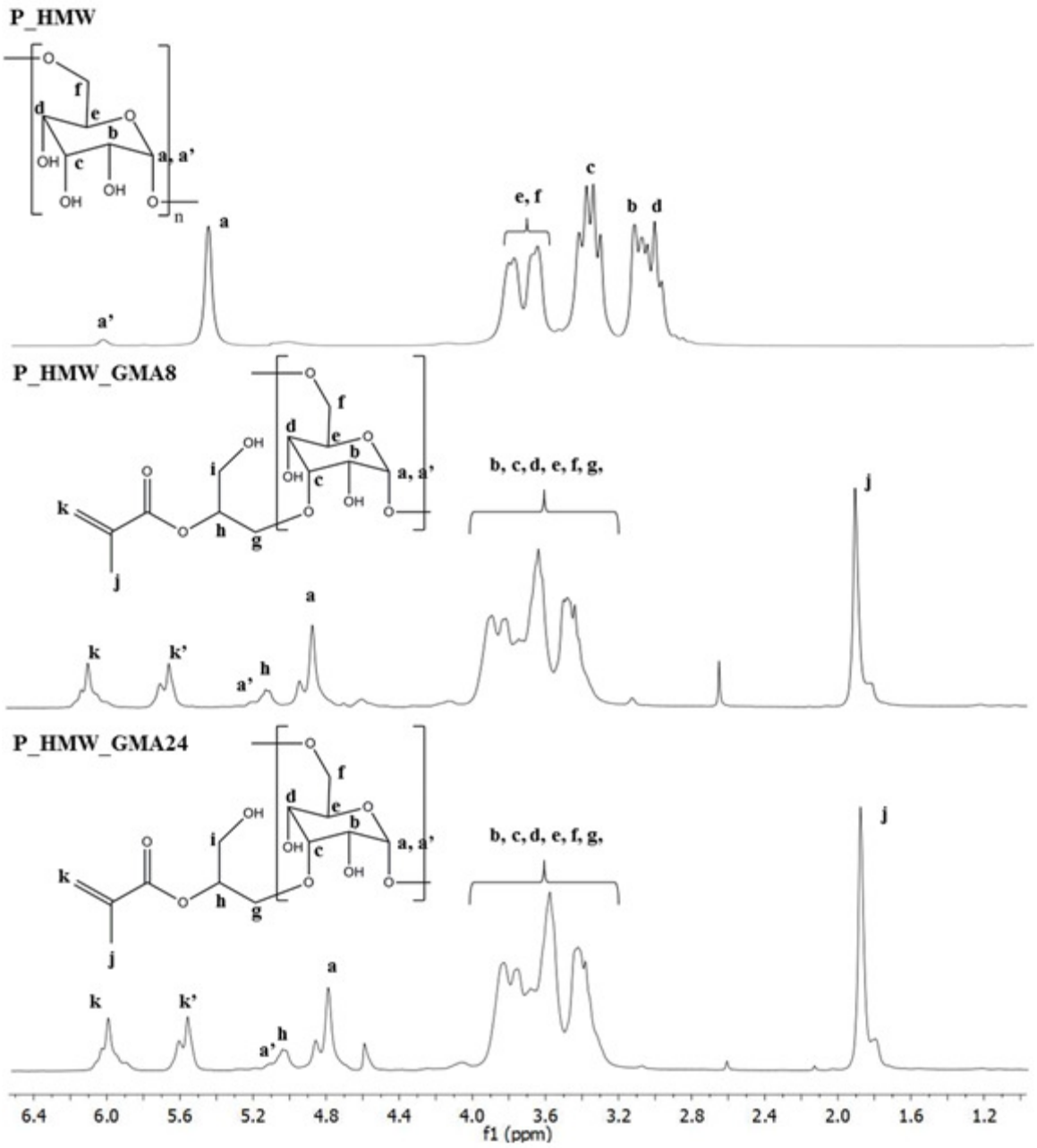

Figure A.3 ^{1}H NMR spectra of P_HMW, P_HMW_GMA8 and P_HMW_GMA24.

$$\%GMA = \frac{n(GMA)}{n(GMA) + n(Dex)} \times 100 = \frac{\int k/_2}{\int k/_2 + \int a/_1} \times 100$$

Equation A.1 Equation for the calculation of the degree of substitution of GMA.

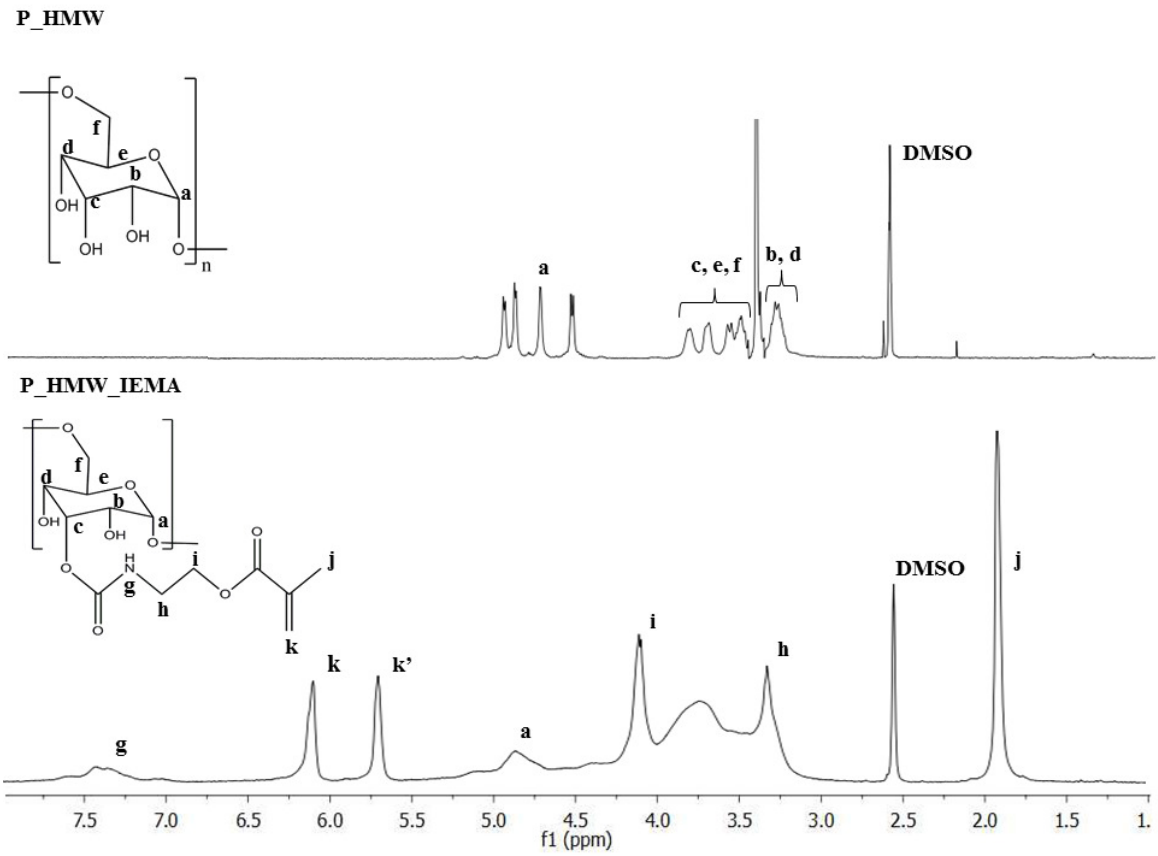

Figure A.4 ^{1}H NMR spectra of P_HMW and P_HMW_IEMA

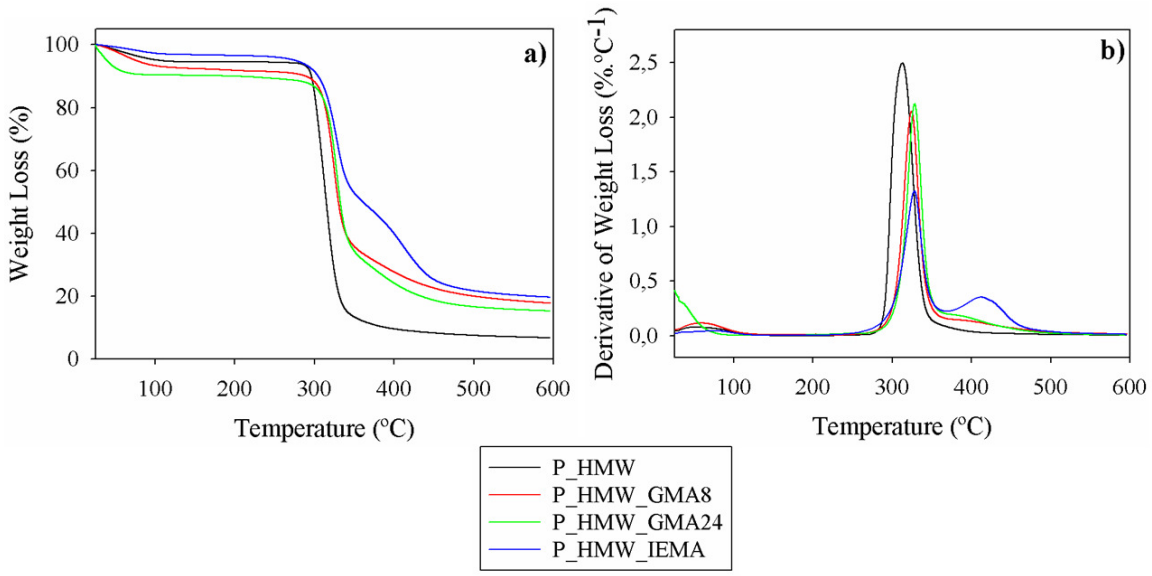

Figure A.5 Thermoanalytical curves of dextran, P_HMW_GMA and P_HMW_IEMA: a) TG, and b) DTG.

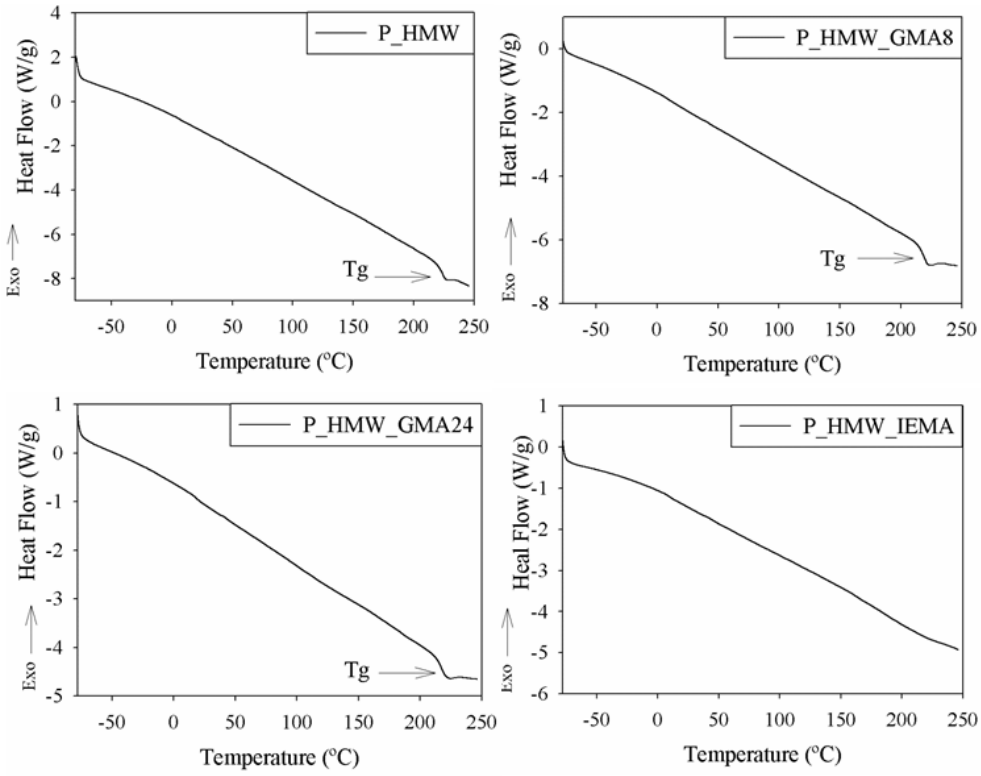

Figure A.6 Heat flow curves of P_HMW and its modifications.

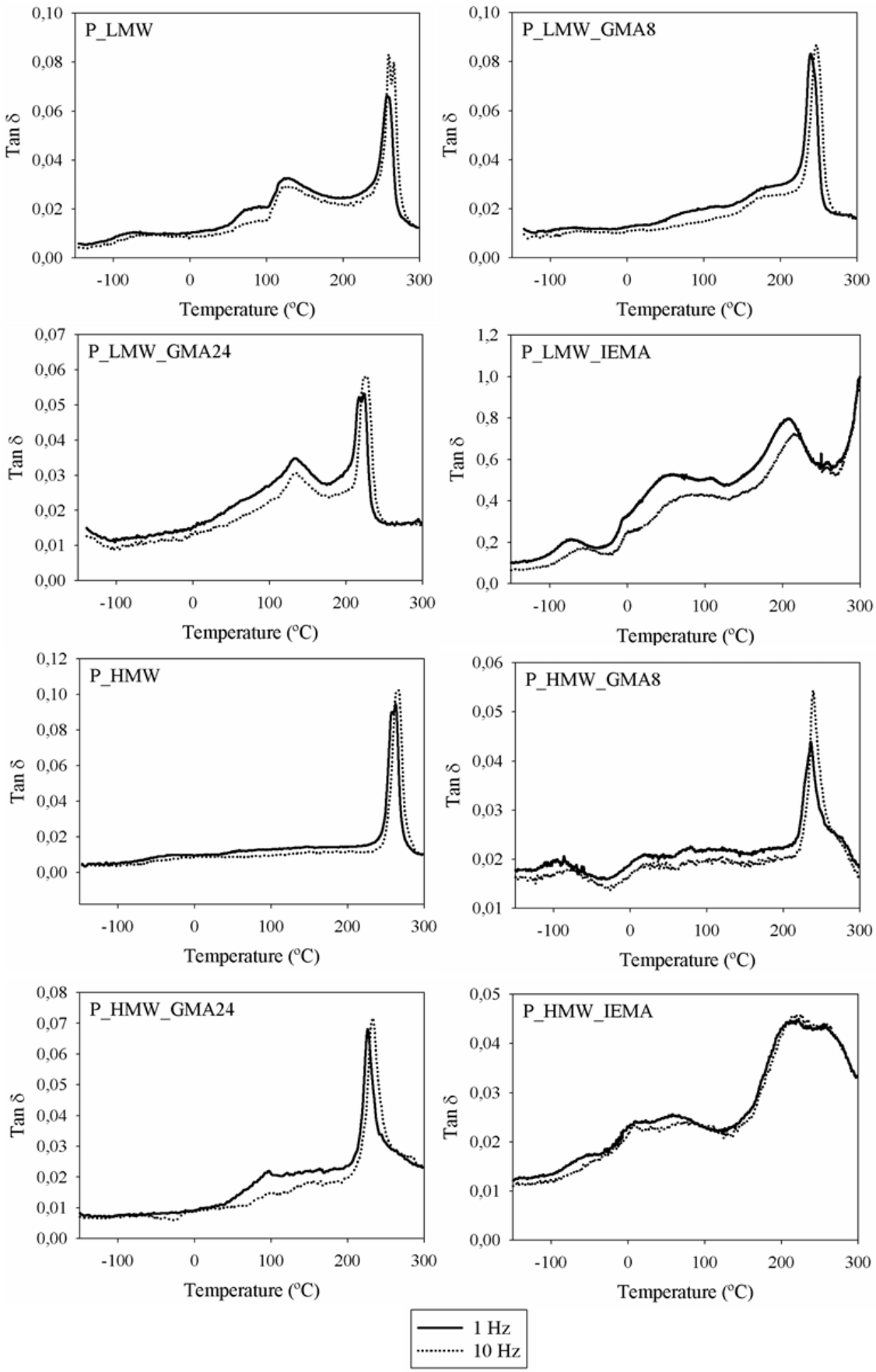

Figure A.7 DMTA multifrequency traces of dextran and its modifications.

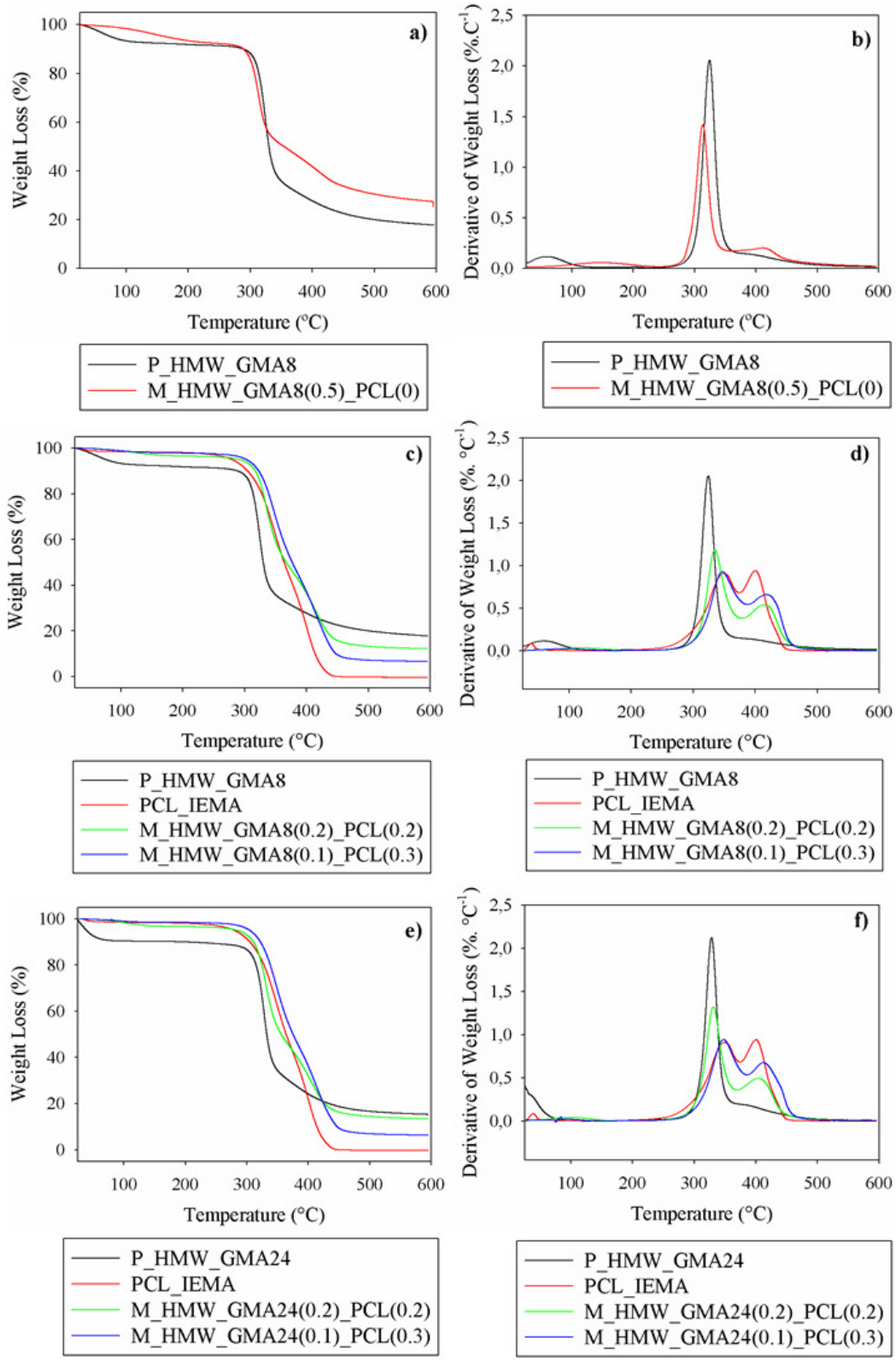

Figure A.8 Thermogravimetric curves of membranes prepared with P_HMW: a), c), e) Weight Loss(%); b), d), f) Derivative of Weight Loss(%.C^{-1})

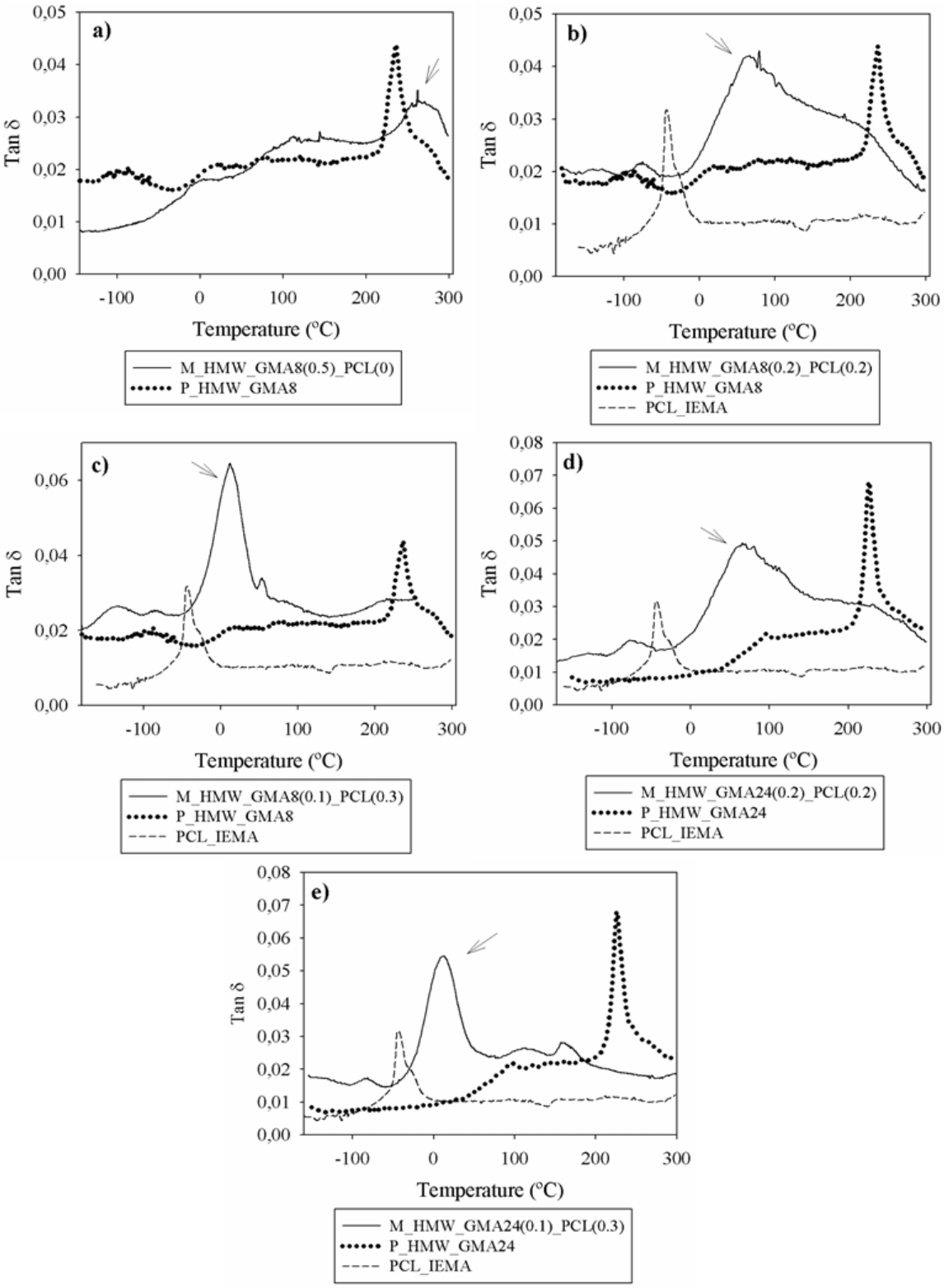

Figure A.9 DMTA traces of the membranes prepared with P_HMW: a)M_HMW_GMA8(0.5)_PCL(0); b)M_HMW_GMA8(0.2)_PCL(0.2); c)M_HMW_GMA8(0.1)_PCL(0.3); d)M_HMW_GMA24(0.2)_PCL(0.1); e)M_HMW_GMA24(0.1)_PCL(0.3). The arrows indicate the peak corresponding to the glass transition of the membranes.

ANNEX B

Supporting information for:

Chapter 3: **Cytocompatibility evaluation using hDPSCs and biocompatibility evaluation by ISO 10-998-6 score – Membranes.**

Table B.1 Detailed cell count after 3, 7 and 15 days post-implantation.

	3 days post-implantation				7 days post-implantation				15 days post-implantation			
	SHAM	M_GMA(0.5)_PCL(0)	M_GMA(0.2)_PCL(0.2)	M_GMA(0.1)_PCL(0.3)	SHAM	M_GMA(0.5)_PCL(0)	M_GMA(0.2)_PCL(0.2)	M_GMA(0.1)_PCL(0.3)	SHAM	M_GMA(0.5)_PCL(0)	M_GMA(0.2)_PCL(0.2)	M_GMA(0.1)_PCL(0.3)
Polymorphonuclear	1.333±0.169	2.063±0.193	1.667±0.243	1.318±0.166	1.300±0.179	2.643±0.106	2.250±0.150	1.950±0.211	0.970±0.154	2.167±0.192	1.765±0.169	1.200±0.249
Lymphocytes	2.306±0.137	2.125±0.180	2.944±0.056	2.409±0.157	2.550±0.135	2.393±0.094	2.375±0.145	2.550±0.153	2.697±0.111	2.667±0.100	2.500±0.114	2.900±0.100
Plasma cells	1.056±0.149	1.500±0.158	1.056±0.056	1.182±0.156	1.150±0.167	0.750±0.083	0.750±0.124	2.150±0.131	1.000±0.131	0.667±0.111	0.706±0.079	1.400±0.306
Macrophages	2.556±0.116	2.813±0.136	3.000±0.000	2.500±0.171	2.600±0.169	3.000±0.051	3.125±0.069	2.750±0.123	2.788±0.084	3.000±0.048	2.647±0.102	1.900±0.277
Giant cells	0.056±0.039	0.313±0.198	0.000±0.000	0.273±0.117	0.300±0.128	0.679±0.137	0.667±0.177	0.050±0.050	0.303±0.119	1.067±0.179	0.500±0.154	0.000±0.000
Necrosis	0.139±0.058	0.563±0.203	0.389±0.216	0.045±0.045	0.050±0.050	0.000±0.000	0.042±0.042	0.450±0.153	0.091±0.051	0.000±0.000	0.059±0.041	0.000±0.000
Sub-total (x2)	14.889±0.791	18.750±0.750	18.111±0.766	15.455±0.769	15.900±0.774	18.929±0.509	18.417±0.732	19.800±0.694	15.697±0.680	19.133±0.619	16.353±0.550	14.800±1.162
Vascularization	2.167±0.189	2.438±0.241	2.111±0.301	2.318±0.179	2.350±0.196	3.000±0.051	2.750±0.138	3.150±0.167	3.121±0.113	2.833±0.136	2.882±0.082	3.700±0.153
Fibrosis	0.639±0.099	0.125±0.085	0.056±0.056	1.364±0.124	1.400±0.134	1.393±0.094	1.292±0.095	1.450±0.135	1.212±0.136	1.767±0.124	1.912±0.107	1.900±0.277
Fatty infiltrate	0.000±0.000	0.563±0.563	0.000±0.000	0.000±0.000	0.000±0.000	0.000±0.000	0.000±0.000	0.000±0.000	0.000±0.000	0.000±0.000	0.000±0.000	0.000±0.000
Sub-total	2.806±0.198	3.125±0.632	2.167±0.305	3.682±0.222	3.750±0.239	4.393±0.119	4.042±0.195	4.600±0.275	4.333±0.161	4.600±0.228	4.794±0.1551	5.600±0.400
TOTAL	17.694±0.813	21.875±0.826	20.278±0.685	19.136±0.817	19.650±0.809	23.321±0.522	22.458±0.780	24.400±0.913	20.030±0.751	23.733±0.696	21.147±0.619	20.400±1.087

ANNEX C

Supporting information for:

Chapter 4: **Preparation of dextran based tubes, for application in peripheral nerve regeneration.**

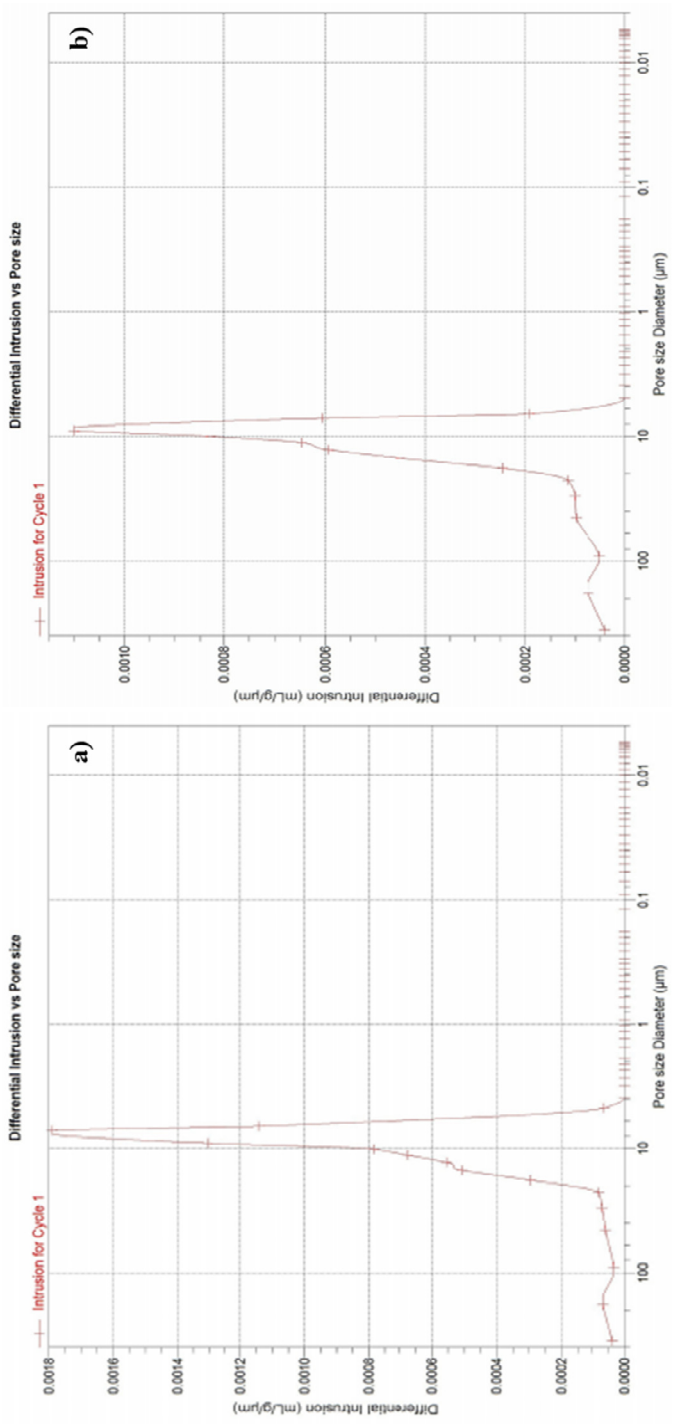

Figure C.1 Mercury porosimetry of a) T_GMA8(0.1)_PCL(0.3); and b) T_GMA8(0.1)_PCL(0.3)_M50.